Investigating Epileptiform Activity Associated with Slow Wave Sleep

Leonie Cunnington

Institute of Neuroscience
Faculty of Medical Sciences
Newcastle University

Submitted in accordance with the requirements for the degree of
Doctor of Philosophy
June 2013

Abstract

The characteristic EEG trait of patients with nocturnal idiopathic epilepsies during childhood is the spike and wave discharge. Cognitive dysfunction is prevalent among these patients and is thought to be linked to disturbances in memory consolidation processes that normally occur during slow wave sleep. Several genetic mutations of nicotinic receptor subunits have been linked to these disorders. However, there is little known about the underlying mechanisms or the spatiotemporal characteristics of this epileptiform activity within the neocortex.

This thesis presents a rat *in vitro* model of the epileptiform activity synonymous with nocturnal childhood epilepsies, that allows for pharmacological manipulation of receptor subunits linked to these disorders. The application of DTC [10μM], a non-selective, competitive nicotinic acetylcholine receptor antagonist, to an *in vitro* model of the cortical delta rhythm induced two individual forms of paroxysm events - wave discharges and the conventional spike and wave discharges.

Pharmacological manipulation of this model suggest that the epileptiform activity is mediated by excitatory currents which is consistent with the use of glutamate antagonists as anticonvulsants. A blanket blockade of inhibition by a $GABA_A$ antagonist resulted in severe discharges, hence hugely increasing excitatory response. Only partial disinhibition is suggested to be required to generate epileptiform activity as nicotinic acetylcholine receptors and 5-HT_3 receptors are located on dendrite targeting interneurons. Mapping of unit activity revealed the difference between the two paroxysm events was recruitment of superficial layers with simultaneous paroxysm events in delta frequency-generating Layer V pyramidal cells.

It is proposed that the hyperexcitability responsible for the generation of the spike component of a spike and wave discharge is mediated by the lack of excitatory tone in 5-HT_3 and nicotinic acetylecholine receptor expressing inhibitory interneuron subtypes. The disinhibition, spike generation and disruption of interplay between deep and superficial layers of the neocortex is thought to be associated with synaptic plastic changes.

To Simon

Acknowledgements

Throughout the course of my PhD I have had the privilege to be supported and influenced by some amazing people. The support of those mentioned below, as well as many others, has been invaluable over the last 5 years of my academic career.

Firstly, I would like to thank my supervisors Prof.Miles Whittington and Dr.Alton Horsfall who have guided me through the ups and downs of my PhD. I am incredibly grateful to Miles for the endless patience necessary to teach an electrical engineer about the delicacies of neurobiology, as well as his abundance of knowledge, encouragement and enthusiasm towards the research, as without it I would have been lost. To Alton I want to say thank you for encouraging me during the second year of my undergraduate course to apply for a PhD, it may not have been solely dedicated to engineering but it gave me the best of both worlds. I also want to thank him for all of his help and advice during my PhD, particularly when the majority of it was so alien a topic.

I would like to thank several other academics who made this PhD possible. I would like to thank my assessor Dr Fiona Le Beau for her constructive criticisms but also for introducing me to the field of electrophysiology during my MRes. I would also like to thank Dr Christopher Adams for being my sounding board for many crazy fabrication ideas as well as my guide through the two worlds of electrophysiology and fabrication processes.

I would like to thank my friends for their support and acceptance of me during my PhD, particularly during the writing of this thesis as I know I wasn't much fun to be around. Special mentions to Claire (who understood me completely), Rupert (for all the clean room training you provided as well as many comedy moments) and Henrik (my matlab guru).

I would like to thank my family - my parents, Vanessa and David, my sister Char-

lotte, my brother Andrew and my nephew Lucas, for encouraging me through my many years of education and at such a distance from you all. My new family, Gill and Mark, and Stuart and Alena for your support and encouragement.

Finally I want to say a huge thank you to my fiancee Simon, as without his constant support, love and 'bullying' I may not have made it here. He has helped me through many tough decisions during my PhD and I am so grateful for his encouragement and guidance when things got tough, and for having the amazing ability to look for the silver lining in every situation whilst putting a smile on my face. With both of our PhD's now complete, I look forward to exploring our next challenge together ....

Contents

List of Figures

List of Tables

List of Abbreviations

μ_n	Electron Mobility ($cm^2V^{-1}s^{-1}$)
μ_p	Hole Mobility ($cm^2V^{-1}s^{-1}$)
μV	micro Volts
ρ	resistivity (Ωcm)
σ	Conductance (S)
5-HT	Serotonin
ACh	Acetylcholine
AChRs	Acetylcholine receptors
ACSF	Artificial Cerebrospinal Fluid
ADNFLE	Autosomal dominant nocturnal frontal lobe epilepsy
ANOVA	Analysis of Variance
AP	Action Potential
ATP	Adenosine triphosphate
BCB	Benzocyclobutene
BECTS	Benign epilepsy of childhood with centrotemporal spikes
Ca^{+2}	Calcium
CAE	Childhood absence epilepsy
cAMP	cyclic adenosine monophosphate

CNS	central nervous system
CO_2	Carbon Dioxide
CSWS	Continuous spike and waves during sleep
CTS	Centro-temporal spikes
CTZ	Cyclothiazide
CVD	chemical vapour deposition
DA	Dopamine
DRIE	Deep reactive ion etching
DRN	Dorsal raphe nucleus
DRS	Deep Regular Spiking
DTC	d-tubocurarine
EEG	electroencephalography
EPSPs	Excitatory postsynaptic potentials
ESES	Electrical Status Epilepticus during Sleep
FXS	Fragile X syndrome
GABA	γ-aminobutyric acid
GAERS	Genetic absence epilepsy rat from Strasbourg
His	Histamine
Hz	Herz
I_h	hyperpolarisation-activated cation current
I_T	low threshold Ca^{2+} current
IB	Intrinsic Bursting
ICP	Inductively coupled plasma
IPSC	inhibitory postsynaptic current
IPSPs	Inhibitory postsynaptic potentials

LC	locus coeruleus
LFP	Local field potential
LGS	Lennox-Gastaut syndrome
LKS	Landau Kleffner Syndrome
LTP	Long term potentiation
mAChR	muscarinic acetylcholine receptor
mGluR	metabotropic glutamate receptor
NA	Noradrenaline
nAChR	nicotinic acetylcholine receptor
NAM	negative allosteric modulator
NMDA	N-Methyl-D-aspartate
NREM	Non Rapid Eye Movement
PAM	positive allosteric modulator
PD	Parkinson's Disease
PGO	ponto-geniculo-occipital
PI	Polyimide
PNS	Peripheral nervous system
PPT	pedunculopontine
REM	Rapid Eye Movement
RIE	reactive ion etching
RS	Regular Spiking
RTT	Rett Syndrome
SEM	Standard error of the mean
SiC	Silicon Carbide
SRS	Superficial Regular Spiking

SWD	Slow Wave Discharge
SWS	Slow-wave sleep
TC	Thalamo-Cortical
TMN	tuberomammillary nucleus
UEA	Utah Electrode Array
VLPO	ventrolateral preoptic
vPAG	ventral periaqueductal grey
VTA	ventgral tegmental area
WAG/Rij	Wistar albino Glaxo rat from Rijswilk
WD	Wave Discharge

Publications

Carracedo LM, Kjeldsen H, Cunnington L, Jenkins A, Schofield I, Cunningham MO, Traub RD and Whittington MA. (2013) A neocortical delta rhythm facilitates reciprocal interlaminar interactions via nested theta rhythms. *Journal of Neuroscience*

Chapter 1

General Introduction

This thesis details work conducted with the aim to better comprehend the neurobiological and electrophysiological mechanisms related to electroencephalography recordings of epileptiform activity present in nocturnal childhood epilepsies.

Chapter 1 presents a detailed introduction and literature review of the knowledge and previous work of many in relevant fields relating to sleep, learning and childhood nocturnal epilepsies. Firstly, a brief history of sleep is presented with the theories which have been popular through the years, as to why mammals sleep and the mechanisms of this process. Following this, the current research into the neurobiology of sleep is detailed concentrating on the role of neuromodulators as this knowledge will be utilised during pharmacological experiments and later discussions. The next section briefly covers electroencephalography (EEG) and how it can be utilised to study sleep and sleep disorders. Due to the output of the EEG, as well as the electrophysiological recording methods that are utilised within this thesis, a greater understanding of the neural oscillations is necessary. Hence frequencies up to 100Hz, which are related to sleep, are subsequently detailed. The next section describes our current understanding of how sleep links to learning and memory processes. This is of particular interest as within the subsequent section, there is considerable evidence presented of a link between childhood nocturnal epilepsies and the epileptiform activity present during sleep and learning disabilities. The aims, objectives and outline of this thesis conclude this chapter.

1.1 History of Sleep

Every human, animal and plant goes through a form of sleep/wake cycle every day of their life. However, it is thought that sleep did not occur in the earliest forms of life approximately 600 million years ago but had to evolve. It is thought that slow wave

sleep (SWS) was not present in mammals until 180 million years ago, which is 70 million years after mammal-like reptiles had evolved [Thorpy and Yager, 2001]. When 'sleep' is thought of today, it includes both a dreaming state, also known as Rapid Eye Movement (REM) sleep and a non-dream state, slow wave sleep. However, it is thought that it took another 50 million years of evolution for REM to appear in sleep cycles. In these first instances of sleep, it is most likely that a polyphasic sleep pattern existed, i.e. many short naps throughout the light/dark cycle as this is still what most animals follow everyday. However, with the evolution of primates came a biphasic sleep pattern which consists of a core sleep period of approximately 6 hours and a short sleep, or nap at mid day lasting approximately 30 minutes (figure 1.1). This is a similar pattern to what early man, i.e. Homo erectus (from Asia, Africa and Europe) and Neanderthals (from Europe and Asia), would have also followed. It wasn't until 10,000 BC that monophasic sleep patterns were thought to have developed in man where only one long period of sleep is needed during the daily light/dark cycle as shown in figure 1.1 [Thorpy and Yager, 2001].

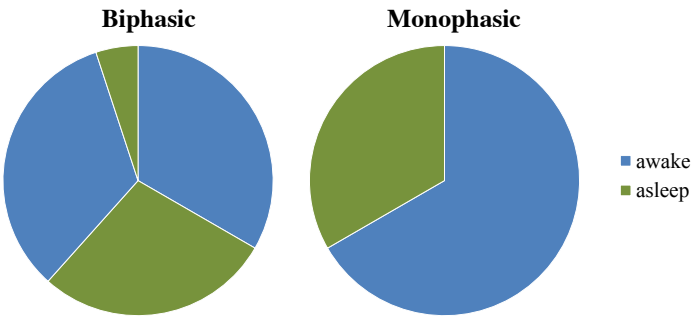

Figure 1.1: Biphasic and Monophasic sleep patterns

In ancient times, many civilisations believed in gods and goddess of sleep and dreaming and would pray to them and give sacrifice if they were having trouble sleeping. In ancient Egypt, the people prayed to Bes, the god of relaxation and sleep, and Imhotep, the god of healing, medicine, learning and sleep. In ancient Rome, the people worshipped Cuba, the goddess of children's sleep, and Somnus, the god of sleep and dreams. Even from this early point in history, people believed there was a link between health and sleep. However, until relatively recently very little was known about how sleep is generated and why it is so important for health. As a consequence perhaps, treatment of these early sleep disorders was mainly through plants, oils, minerals and animal substances that were ingested, inhaled or given as suppositories or enemas. Opium, also known as laudanum, has been used to treat sleep disorders like insomnia as far back as the Sumerian age [Aggrawal, 1995].

Until the start of the 20th Century there were four main sleep theories:

- Vascular (mechanical, anemic, congestive)
- Neural (Histological)
- Chemical (Humoral)
- Behavioural (psychological, biological)

Vascular Theory

In ancient Greece during the fifth century, Alcmaeon believed that sleep was due to blood filling the brain, whilst waking was associated with the return of blood to the rest of the body [Diels and Kranz, 1952]. Hippocrates, on the other hand, believed sleep was caused by the blood leaving the limbs and collecting in the center of the body [Chadwick and Mann, 1978]. Albrecht von Haller (1708-77) and Hermann Boerhaave (1667-1738) agreed with Alcmaeon's theory and that the increased blood flow to the head resulted in increased pressure on the brain, thereby inducing sleep [Thorpy and Yager, 2001]. However, Johann Friedrich Blumenbach (1752-1840) was the first to observe the brain of a sleeping subject in 1795 where he noted that the brain was pale during sleep, which was contrary to the earlier vascular theories [Blumenbach, 1828].

The congestive theory of sleep became the most popular during the first half of the 19th Century. Johannes Evangelistica Purkinje (1787-1869), a neuroanatomist and professor of physiology and pathology at Breslau, proposed that the brain pathways (corona radiata) become compressed by blood congestion of the cell masses of the brain (basal ganglia), hereby severing neural transmission and inducing sleep [Wagner, 1844]. However this congestive theory was finally contradicted in 1863 by John Hughlings Jackson (1853-1911), an outstanding clinical neurologist, through observing the decreased blood flow in the retinal arteries during sleep [Thorpy and Yager, 2001]. The most popular alternative to the congestion theory was that sleep was due to insufficient blood flow to the brain (anaemia), which was believed by many scientists, including Alexander Fleming and Sir Leonard Erskine Hill. In 1896, Hill reported that there was no change in cerebral blood pressure during sleep. He believed that the brain did not become either anaemic or congested during sleep which lead to the vascular theory being discredited [Hill, 1866].

Neural Theory

In 1875, the first clear picture of a nerve cell and it's processes were demonstrated by Camillo Golgi (1843-1926) [Culebras, 2005]. This research was extended by many others resulting in the discovery of neurons, axons and dendrites in the cortex. During the

1890's several scientists believed that during sleep there was a partial paralysis of the neuron prolongations preventing communication between cells. Ramon Y Cajal (1852-1934) believed that signal alteration by neuroglia could explain sleep as well as the effect of hypnotic medications through inhibition [Hill, 1866]. This research later led to the theories based upon synaptic transmission of neurotransmitters which became the prominent neural explanation for changes in sleep and wakefulness, as described in more detail later in this chapter.

Chemical Theory

The chemical theories were based on Aristotle's theory that sleep was due to the effect of fumes in the blood present after eating [Culebras, 2005]. The popular chemical theory was that sleep was linked to the oxygen levels in the body and brain. This theory led to several others on the accumulation of toxic substances, which included cholesterol and other toxic waste products. In 1895, Raymond Emil Du Bois (1818-1896) proposed that sleep was the result of carbon dioxide (CO_2) toxicity [Culebras, 2005]. He believed that small amounts of CO_2 during wakefulness led to sleep and that large amounts of CO_2 during sleep evoked wakefulness [Du Bois, 1895]. These chemical theories remained popular until the end of the 19th century. It is interesting to note that CO_2 and neurochemicals such as hormones and transmitters are now recognised as very much involved in generating and modulating sleep, as will be discussed later.

Behavioural Theories

Based upon the previous work of Rolando and Flourens in which they discovered that removing part of the cortex induced a sleep-like state, Charles Edouard Brown-Sequard (1817-94) proposed that sleep was due to an inhibitory reflex [Brown-Sequard, 1889]. This was expanded upon by Heubel (1876), of Kiev University who proposed that sleep was due to the loss of peripheral stimuli [Heubel, 1876]. Several researchers believed that there was a specific organ of sleep. Initially this was thought to be the thyroid, however this was disproved when insomnia wasn't induced with thyroid removal. The Choroid plexus was also considered as the sleep organ by Jonathon Osbourne in 1849 [Osborne, 1849]. Although the main focus during the second half of the 19th Century was the cause of sleep, important contributions were also made to sleep disorder medicine, particularly sleep apnea, nocturnal epilepsy, narcolepsy and insomnia.

1.2 Neurobiology of Sleep

It has been suggested that consciousness can be considered in terms of neural correlates, such that neural diseases and drugs that can mimic or alleviate the symptoms can provide insight into the mechanisms of consciousness [Perry et al., 1999]. From the work of Morruzzi and Magoun, it has been demonstrated that there are two ascending pathways in the brain which are thought to dominate in mediating arousal and wakefulness, the cholinergic and monoaminergic pathways [Aldrich, 1999, Krahn et al., 2009]. These networks are responsible for the perception of sensory stimuli, the sense of consciousness and the inhibition of sleep.

The cholinergic system is thought to be the most important neuromodulatory neurotransmitter system in the brain [Perry et al., 1999]. It originates in neurons of the basal forebrain and the pedunculopontine (PPT) nuclei which project to the reticular and relay nuclei of the thalamus. These nuclei projections open the gateway to the cerebral cortex for peripheral sensory input. 90% of brainstem projections to the thalamus are cholinergic which is of interest due to the importance of the thalamus and its projections to the cortex in conscious awareness [Perry et al., 1999]. During REM sleep, cortical activation is present as it is during wakefulness [Krahn et al., 2009]. The monoaminergic system consists of many ascending axons which are linked to monoaminergic neurotransmitters, as shown in figure 1.2. Stimulation of the neurons listed in figure 1.2 activates the cerebral cortex thereby allowing the flow of information from the thalamus. These neurons are also known to inhibit the ventrolateral preoptic (VLPO) nuceli, the primary generator of non rapid eye movement (NREM) sleep. The VLPO is believed to be important in the control of circadian rhythms. The cortical activity seen during wakefulness and REM sleep remains present in the absence of monoaminergic neuromodulator activity, i.e serotonergic and noradrenergic whilst in the presence of cholinergic activity, hence it has been suggested that the ascending cholinergic system alone has the ability to keep the brain in an active state [Buzsáki et al., 1988]. Whereas, during SWS or NREM sleep, where consciousness is absent or tremendously altered, there is a large amount of inhibition in the thalamic and cortical neurons due to a decrease in excitatory projections from the thalamus [Delacour, 1997].

A number of other neuromodulatory systems are also linked to modulation of the sleep/wake cycle: glutamate released by thalamic and cortical projection neurons as well as by neurons of the mesencephalic reticular formation [Delacour, 1997]; acetylcholine by neurons in the basal forebrain and the PPT; noradrenaline by neurons in the locus ceruleus; serotonin by neurons in the raphe nucleus; and histamine by neurons in the hypothalamus.

γ-aminobutyric acid (GABA) which is released by interneurons is also thought to be involved in the loop between the reticularis nucleus of the thalamus and the other thalamic nuclei [Delacour, 1997]. All of which will be considered in greater detail within the following sections.

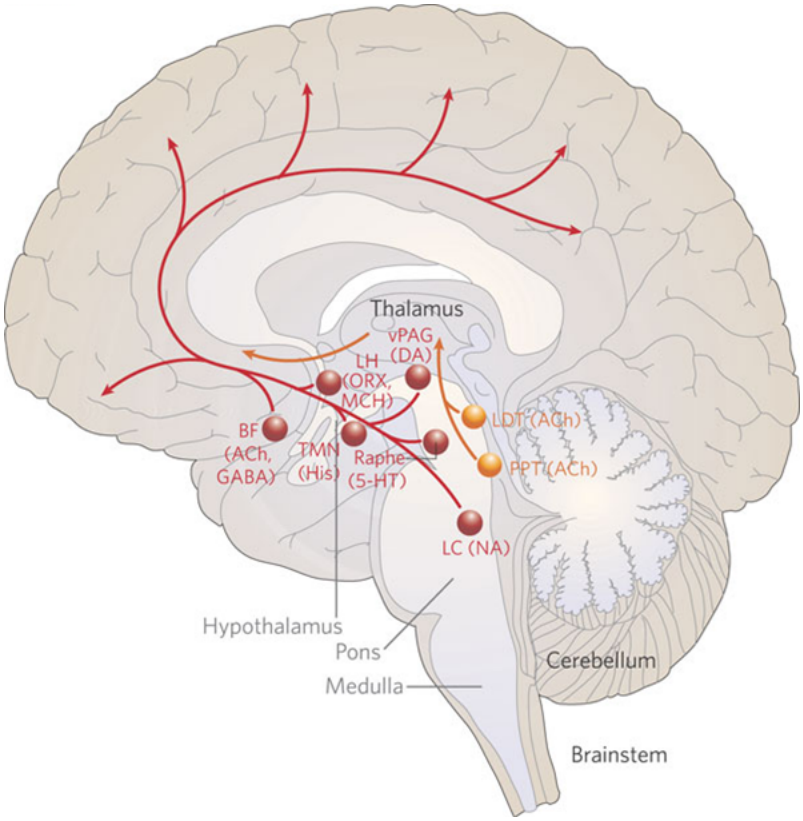

Figure 1.2: **A schematic drawing depicting some of the key pathways of the ascending arousal system.** The yellow path depicts the group of cholinergic cells which aid in thalamocortical transmission, whilst the red path indicated the regions of the cortex activated by signals from monoaminergic mediated neurons, particularly histamine, dopamine, serotonin and acetylcholine. Other neuromodulators which are also thought to contribute to the signalling of this pathway are GABA and acetylcholine. This network of pathways is thought to be 'essential for the binding of multiple aspects of sensory experience into a single framework of consciousness [Jones, 1998]. *Adapted from [Saper et al., 2005].*

1.2.1 Neuromodulators associated with Sleep

Acetylcholine

Acetylcholine (ACh) is a neurotransmitter found in the central and peripheral nervous system. It is known be a principle component of the ascending reticular activating system and hence plays a large role in the regulation of sleep and wakefulness [Thorpy and Yager,

2001]. The two major groups of ascending cholinergic neurons are located in the pontomedencephalic tegmentum and the basal forebrain. Along with the other neurons that make up the reticular formation, the pontomedencephalic tegmentum neurons project to the thalamus, the hypothalamus and the basal forebrain. From the thalamus, they project to a diffuse area of the cerebral cortex which allows for widespread signal transmission and activation. The maximum release of ACh into the thalamus is associated with fast cortical activity during wakefulness and REM sleep. ACh depolarizes and excites thalamocortical neurons which stimulates the fast cortical activity of arousal and REM whilst inhibiting the slow wave activity of NREM sleep. The fast cortical activity particularly occurs in the gamma frequency range (30-80Hz). The basal forebrain neurons provide connections to the hippocampus and the cortex. Hence these neurons have the capacity to stimulate ubiquitous cortical activity. When acetylcholine receptors (AChRs) are agonised using nicotine and muscarine, cortical activation is elicited, whereas when they are antagonised, the fast cortical activity associated with sleep is diminished [Stickgold and Walker, 2009a]. For example, Atropine, a muscarinic AChR antagonist, produces slow wave activity in the cortex. ACh has subsequently been perceived to stimulate cortical activity during REM sleep. From this, the cholinergic systems are known to play an important role in REM sleep and arousal.

In a review by Crunelli and Hughes (2010), *in vitro* sleep rhythm studies in rats, mice ferrets and cats were compared to similar animals in *in vivo* sleep studies. These studies reported that the morphology of the local field potential activity was similar in amplitude, however the activity was slower during *in vitro* experiments. This was also seen during cellular activity of thalamic reticular nuclei neurons. Whereas the cellular activity of thalamocortical neurons was very similar during both *in vivo* and *in vitro* studies. To achieve the slow wave oscillation observed during sleep, the *in vivo* studies used various anaesthetics to mimic sleep. However, during *in vitro* studies, it is not possible to use an anaesthetic, instead modifications must be made to the calcium (Ca^{+2}) concentration of the perfused solution [Rigas and Castro-Alamancos, 2007, Shu et al., 2003] or the addition of the cholinergic agonist, carbachol is needed [Lorincz et al., 2007, Lorincz et al., 2008, Cunningham et al., 2006] to evoke similar rhythms to those seen during SWS sleep and under anaesthesia. Of particular interest is the use of Carbachol to induce the slow oscillations observed during sleep. This is due to the presence of some cholinergic mediated action being needed to induce sleep, as although high levels of ACh are seen during waking states, a very low level is present during SWS, hence the need to apply a small concentration of an AChR agonist.

ACh plays a large role in memory processes. Muscarinic-AChR antagonists have been

shown to decrease memory consolidation whilst both short and long term memory processes are enhanced by ACh. Long term potentiation is enhanced by ACh [Stickgold and Walker, 2009a]. It also stimulates theta frequency oscillations which in turn, also enhances long term potentiation and neuronal plasticity. In recent studies [Granon et al., 1995] [Chan et al., 2007], nicotinic AChRs (nAChRs) have also been linked to memory processes, particularly α_7 and $\alpha_4\beta_2$, which area involved in working and reference memory and solely working memory respectively. It is well known that consolidation of procedural memories are enhanced during REM sleep whilst declarative memories are consolidated during SWS (see section 1.6). Thus, it is likely that nAChRs play a role in both NREM and REM sleep.

In reviews penned by Delacour (1997) and Baars (1998), it has been shown that ACh is greatly involved in attentional processes and conscious awareness. Cortical ACh is currently thought to have many roles: affects discriminatory processes; increases signal-noise ratios; regulates the cortical processing of sensory inputs; controls the response to stimuli and rates their level of significance; and limits the conscious stream [Perry and Perry, 1995, Warburton and Rusted, 1993, Perry et al., 1999, Delacour, 1997]. During slow-wave sleep (SWS), these characteristics are reversed. The amplitude and signal-to-noise ratio of sensory responses are decreased [Livingstone and Hubel, 1981], and spike trains become randomised between interspike intervals: large populations of neurons burst simultaneously. As stated by Delacour (1997), 'this temporal structure introduces distortions in information transmission'. Modulation of the levels of cortical ACh may have an adverse impact on these roles, similar to the behaviour of patients with autism-spectrum disorders. ACh level modulation may also have an impact on learning and memory processes, as previously described.

AChRs, both muscarinic and nicotinic, are membrane proteins and are composed of a mixture of five subunits: alpha (α), beta (β), delta (δ), epsilon (ϵ) and gamma (γ)(as shown in figure 1.3). So far, 12 nicotinic-AChR (nAChR) (α_2 - α_{10} and β_2 - β_4) and 5 muscarinic-AChR (mAChR) subunits (α_1, β_2, δ, ϵ and γ) have been identified [Marini and Guerrini, 2007]. Neuronal nAChRs are part of the family of excitatory ligand-gated ion channels [Karlin, 2002] and have a very similar structure to the inhibitory ligand-gated channels which consist of glycine and $GABA_A$ receptors. α_7, α_8 (only found in avian species), α_9 and α_{10} (only when co-expressed with the α_9 subunit [Baker et al., 2004]) subunits are distinguished by their ability to form robust homomeric receptors in the absence of a β subunit. Each of these homomeric receptors has five binding sites. It is not known how many of these sites need to be occupied by an agonist to open the channel, however occupancy of only one binding site by an antagonist is needed to block

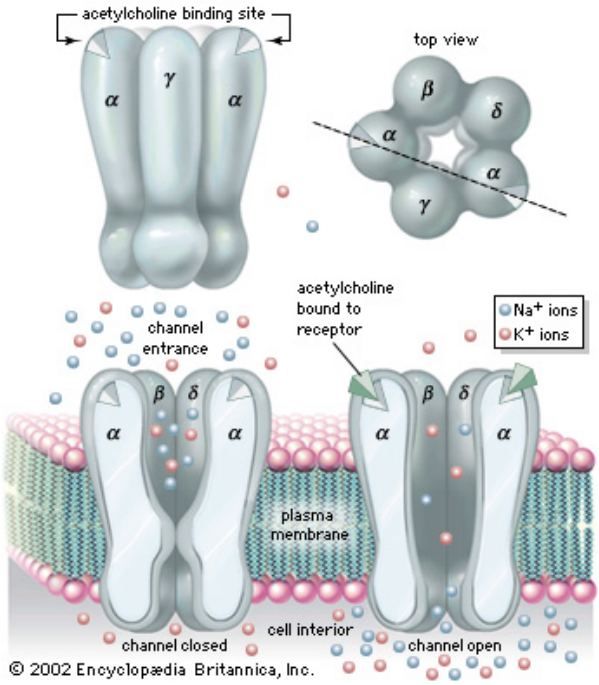

Figure 1.3: The nAChR is a ligand-gated ion channel. Five subunits surround central pore which allows for the diffusion of sodium (Na^+) and potassium (K^+) ions through the membrane. [Encyclopedia-Britannica,]

the channel from opening [Palma et al., 1996]. The remaining α and β subunits group to form heteromeric receptors, i.e. $\alpha_4\beta_2$, $\alpha_3\beta_2$ and $\alpha_3\beta_4$. Of all of the nAChR subtypes, α_4, α_7 and β_2 are the most ubiquitous in the mammalian central nervous system (CNS) with $\alpha_4\beta_2*$ (where $*$ indicates the possible inclusion of unspecified subunits) and α_7 nAChRs having a complementary distribution [Wonnacott and Barik, 2007].

Neuronal nAChRs are highly expressed in the hippocampus, neocortex, thalamus and midbrain neurons. nAChRs as previously stated, have been linked to memory processes, therefore it is unsurprising that the hippocampus contains large numbers of nAChRs. Whole-cell recordings have shown that these receptors are present on hippocampal GABAergic interneurons as well as pyramidal cells in both the hippocampus and the neocortex. Studies have indicated that most hippocampal interneurons possess α_7 containing nAChRs [Alkondon et al., 1997, Ji and Dani, 2000] whereas the nicotinic currents evoked by subpopulations of neocortical interneurons are thought to be mediated by non-α_7 nAChRs. Neuronal presynaptic nAChRs have been shown to modulate the release of many different neurotransmitters within the brain, although they are also known to exist on somatodendritic regions and in perisynaptic or extra synaptic locations [Wonnacott and Barik, 2007]. The thalamus plays a key role in passing sensory and motor information to the cortex. Additionally, abnormalities in the thalamo-cortical circuitry can result in epileptic episodes or seizures [Raggenbass and Bertrand, 2002]. $\alpha_4\beta_2$ nAChRs are highly expressed in the thalamus, hence they are thought to have a role in thalamo-cortical circuitry. Activation of the β_2 containing nAChRs can result in an increase in GABA release from axon terminals thereby effecting the inhibitory synap-

tic transmission in the thalamus. Mutations of the genes that encode the α_4 or the β_2 receptors can result in some forms of autosomal dominant nocturnal frontal lobe epilepsy (ADNFLE, covered in greater detail in section 1.7.2).

The majority of neurons of the substantia nigra and ventral segmental area (VTA) of the midbrain have been shown to possess β_2 containing nAChRs, whereas α_7 containing nAChRs are thought to be present in less than half of those neurons [Klink et al., 2001]. The activation of somatic nAChRs in VTA neurons is thought to contribute to the release of dopamine in the nucleus accumbens, however other mechanisms are also thought to contribute, some of which are considered in the next section.

Dopamine

Dopamine (DA) is a catecholamine neurotransmitter and is produced in several regions of the brain, including the VTA and the substantia nigra. DA neurons starting in the VTA are proposed to be involved in arousal and maintenance of wakefulness unlike the nigrostriatal system which generally do not play a direct role in sleep and wakefulness [Aldrich, 1999]. The depletion of DA is involved in the pathophysiology of Parkinson's disease (PD), whereas hyperdopaminergia is thought to play a part in generating endophenotypes linked to schizophrenia. Due to the sleep disturbances seen in both schizophrenia and PD, DA is considered to play a major role in regulating the sleep-wake cycle [Dzirasa et al., 2006].

DA has been shown to have an important role in controlling REM sleep. Electrophysiological results have revealed an increase in bursting activity in the VTA DA neurons during REM sleep. DA levels are also elevated in the prefrontal region during this stage of REM sleep. Work by Sakai (1991) suggests that DA may directly regulate the activity of REM active neurons located in the peri-Locus Coereleus alpha, likely through adrenergic α_2 receptors. Work by Lu *et al* (2006) has exposed a previously unclassified group of wake-active DA neurons in the ventral periaqueductal grey (vPAG) that may provide the long-sought ascending dopaminergic waking influence [Stickgold and Walker, 2009b]. These vPAG DA neurons have been mistaken for dopaminergic neurons that originate in VTA (A10 DA neurons) over the years, however anatomical and physiological characteristics of the vPAG neurons now suggest that these cells form their own distinct neuronal poulation. vPAG DA neurons are considered important when discussing sleep as they project to the VLPO, which as stated previously, is a critical sleep-promoting center of the brain. Although it is not yet understood how DA influences sleep and arousal, it is most likely that due to the inhibition of VLPO sleep active neurons and the activation of the basal forebrain and monoaminergic systems.

As with ACh, DA is generally considered to promote wakefulness and inhibit SWS. Lena *et al* (2005) demonstrated that in rat *in vivo* studies, extracellular DA levels in the prefrontal cortex and the nucleus accumbens are greater during both wakefulness and REM sleep, in comparison to SWS. DA receptors can be grouped into two distinctive groups, D_1-like and D_2-like receptors [Beaulieu and Gainetdinov, 2011]. The D_1-like receptors consist of the D_1 and D_5 receptors [Tiberi et al., 1996], whereas the D_2 subfamily comprises of D_2, D_3 and D_4 receptors [Andersen et al., 1990]. The D_1 subfamily are coupled to the G_s protein and increase the intracellular levels of cyclic adenosine monophosphate (cAMP) by activating adenylate cyclase. The D_1 receptor is a postsynaptic receptor and is the most ubiquitous DA receptor in the CNS [Monti and Monti, 2007]. Although the D_3-D_5 receptors are found in much lower levels than the D_1 and D_2 receptors, DA binds to them with nanomolar or submicromolar affinity constants compared to the micromolar ranges needed for D_1 and D_2 receptors. In the rodent brain, D_1 receptors are richly expressed in the caudate-putamen, the nucleus accumbens and the olfactory tubercle [Murrin and Zeng, 1990]. In lower levels they are also expressed in other brain regions such as the cerebral cortex, the thalamus and hypothalamus [Lachowicz and Sibley, 1997]. D_1 and $GABA_A$ (see below for more detail) receptors are generally present in the same areas of the brain [Le Moine and Gaspar, 1998]. It is well established that the activation of D_1 receptors plays a large role in the inhibition of GABAergic transmission an GABA neurotransmitter release [Eder et al., 2003, Fuxe et al., 1998, Liu et al., 2000].

The D_5 receptor is also a postsynaptic receptor. Expression of the D_5 receptor is moderate in the hippocampus, hypothalamus and olfactory tubercule, however no mRNA expression has been reported in brainstem structures [Monti and Monti, 2007]. The D_2 subfamily are G_i/G_o coupled, and decrease the cellular concentrations of cAMP by inhibition of adenylate cyclase [Beaulieu and Gainetdinov, 2011]. The highest expression of D_2 receptors are found in the same areas as D_1 receptors. They are also expressed in the cerebral cortex, the basal forebrain, the hypothalamus and the rhombencephalon [Monti and Monti, 2007]. D_2 receptors are also present on neuron cell bodies. Unlike, the previous DA receptors, D_3 and D_4 receptors are present at much lower levels in the rodent brain. D_3 receptors are mainly expressed in the Islands of Calleja and the nucleus accumbens with lower levels present in the cerebral cortex, hippocampus, amygdala and hypothalamus. However, no cells expressing the D_3 receptor mRNA have been found in the brainstem structures involved in the regulation of sleep and wakefulness [Monti and Monti, 2007]. Lastly, D_4 receptors are expressed in the frontal cortex, the hippocampus and the hypothalamus.

During a study to understand how pharmacological manipulations could effect the state of awareness, Monti *et al* (1990) found that the antagonism of the DA D_1-like receptor in the rodent increased SWS and reduced wakefulness and REM sleep. SCH23390 has also been demonstrated to produce sedation in the monkey and rabbit [Ongini et al., 1985]. Whereas, SKF 38393, a selective DA D_1 receptor agonist significantly increases wakefulness and reduced SWS and REM sleep [Monti et al., 1990]. A double blind clinical study by Eder *et al* (2003) characterized the effect of the D_1 receptor antagonist NNC-687 on sleep variables in healthy young men between 21 and 27 years. The D_1 antagonist was shown to significantly increase the length of the first NREM sleep period. Wakefulness and REM sleep were unaffected. The stimulation of adenylate cyclase, which is coupled to the D_1 receptor, depolarises neurons ascending to the thalamus, hypothalamus and basal forebrain and neurons descending to the dorsal raphe nucleus and locus coeruleus. The activation of these neuronal groups results in the stimulation of cortical activation [Aloe et al., 2005]. Several studies by Monti *et al* published in 1988, have shown that the systemic administration of D_2 receptor agonists (apomorphine ($D_1 > D_2$), bromocriptine ($D_2 > D_1$), pergolide ($D_2 > D_1$) [Monti et al., 1988a] or quinpirole ($D_2 > D_3$)) into rodents induce biphasic effects. Low doses reduce wakefulness and increase SWS and REM sleep which has been related to the predominant activation of the D_2 autoreceptor, whilst large doses induce the opposite effect (increase wakefulness and decrease SWS and REM sleep) which has been related to the predominant facilitation of the D_2 postsynaptic receptor [Monti and Monti, 2007].

Serotonin

Serotonin (5-HT) and sleep research have had a varied relationship over the years. After some initial research in 1955, it was thought that 5-HT was the principal sleep neurotransmitter due to its inhibiting effects on the mesencephalic reticular formation and the locus coeruleus (LC) [Jouvet, 1999]. Both of which, in 1973, were thought to be the two putative waking centres of the brain. However, in 1976 it was observed that the electrical activity of dorsal raphe nuclei neurons (DRN, 5-HT neurons) increased during wakefulness, decreased during slow-wave sleep and totally disappear during REM sleep [Lydic and Biebuyck, 1988]. Thereby showing that there was a complex relationship between 5-HT liberation and sleep. More recent research postulates that the liberation of 5-HT during wakefulness may lead to a cascade of postsynaptic genomic events which will trigger sleep onset [Jouvet, 1999]. As of yet, the full relationship between 5-HT and sleep is unknown and the role of the raphe nuclei remains elusive.

5-HT receptors are G protein coupled receptors and ligand gated ion channels found in the central and peripheral nervous system. They mediate both excitatory and inhibitory

neurotransmission of many neurotransmitters, including glutamate, GABA, dopamine, noradrenaline and acetylcholine. There are 7 different classes of 5-HT receptors, designated 5-HT_{1-7}. The 5-HT_1, 5-HT_2, 5-HT_3 and 5-HT_5 classes are made up on five (5-$HT_{1A-B-D-E-F}$), three (5-HT_{2A-B-C}) and two (5-HT_{3A-B} and 5-HT_{5A-B}) subtypes respectively, whereas the remaining classes are currently known to have only one subtype each [Monti, 2011]. All, bar the 5-HT_3 receptor subtypes, are G protein coupled receptors. 5-HT_1 [Monti and Jantos, 1992], 5-HT_2 [Dugovic et al., 1989], 5-HT_3 [Ponzoni et al., 1993] and 5-HT_7 [Hedlund et al., 2005] have all been linked to sleep processes.

5-HT_{1A} receptors are located on the soma and dendrites of 5-HT neurons, at postsynaptic sites and non-5-HT cells of the DRN [Monti, 2011]. Most of the DRN cells are GABAergic interneurons. Whilst the 5-HT_{1B} receptors are thought to be located at presynaptic (5-HT axon terminals) and postsynaptic (outside the DRN) sites. As with 5-HT_{1A}, the 5-HT_{1B} receptor has been characterized in the DRN where it is expressed in non-5-HT neurons [Clark et al., 2006]. Systemic administration of the 5-HT_{1A} agonist, 8-OH-DPAT has been shown to increase waking whilst reducing REM sleep. Within SWS there was a delayed increase of highly synchronized sleep which Bjorvatn *et al* (1997) classified as SWS-2. Another agonist, ipsapiron is also known to increase SWS in both rats [Tissier et al., 1993] and humans [Seifritz et al., 1996]. Hence it is postulated that 5-HT_{1A} receptors may facilitate sleep or sleep characteristics in at least some central nervous system areas [Ursin, 2002]. A study by Boutrel *et al* (1999) reported 5-HT_{1B} knock-out mice display larger amounts of REM sleep than their wild-type equivalent whereas no significant change is seen in wakefulness or SWS. Systemic administration of CP-94253, a selective 5-HT_{1B} agonist, significantly increased waking activity whilst reducing SWS and REM sleep in the rat [Monti et al., 1995]. Hence it is thought that the activation of the 5-HT_{1B} receptor promotes the occurrence of waking activity and negatively effects REM sleep.

5-HT_2 receptors are located postsynaptically in many different brain region, the cortex, thalamus and substantia nigra to name a few. Selective 5-HT_2 agonists, specifically 5-HT_2A and 5-HT_2C, are known to increase wakefulness and decrease SWS and REM sleep [Dugovic, 1993]. Whereas, the 5-HT_2 receptor antagonist ritanserin is known to promote sleep in both humans [Idzikowski et al., 1986] and rats [Dugovic and Wauquier, 1987], hence this would imply that the 5-HT_2 receptor plays a role in waking activity. However, in cats, ritanserin is known to reduce sleep [Sommerfelt and Ursin, 1993]. A rodent study by Borbely *et al* (1988) showed that the power spectral data indicated that the sleep resulting from the antagonist administration was different from natural sleep. Work by Steriade *et al* (1993), suggests that the arousing effect of 5-HT_2 receptor may

be mediated by the thalamic reticular nucleus and the sleep spindle generating cells of the cortex and reticular nucleus. Hence it is thought that serotonin acting on thalamic 5-HT_2 receptors may play a role in spike activity and waking.

In 1992, Adrien (1992) proposed that the 5-HT_3 receptor did not play a major role in sleep or wakefulness. However, in 1993, Ponzoni *et al* reported that the injection of the selective 5-HT_3 agonist m-choloro-phenylbiguanide (m-CPBG) into the lateral ventricle or the bilateral injection into the nucleus accumbens increases waking and decreases SWS. REM sleep remained unchanged during the latter described injection. However, the effect of the 5-HT_3 agonist can be blocked by the selective 5-HT_3 antagonist MDL 72222 [Ponzoni et al., 1993,Ponzoni et al., 1995]. Ponzoni *et al* also reported that the systemic administration of MDL 72222 and another antagonist, ondansetron, significantly increased SWS and/or REM sleep, respectively. Ponzoni speculated that the effects seen due to the stimulation of the 5-HT_3 receptors are linked to the increased release of other neurotransmitters, particularly dopamine [Ponzoni et al., 1995]. The 5-HT_3 receptor is a member of the superfamily of ligand-gated ion channels, a family that also include the neuronal nicotinic acetylcholine receptors (nAChRs), as well as the inhibitory neurotransmitter receptors for GABA [Maricq et al., 1991]. The 5-HT_3 and nAChRs share similar attributes, particularly the α_7 nAChR subunit [Eisele et al., 1993], i.e. topological organisation, and activation and desensitisation reactions. As such, both the 5-HT_3 receptor and nAChRs are inhibited by nanomolar concentrations of d-tubocurarine (DTC) in a competitive fashion [Yan et al., 1999]. Chimeras containing the amino-terminal domain of the α_7 nAChR and the carboxyl-terminal of the 5-HT_3 receptor form functional ligand-gated channels with ligand specificities characteristic of AChRs and the permeability of 5-HT_3 receptors [Eisele et al., 1993]. The work by Eisel *et al* (1993) would suggest that 5-HT_3 and AChRs have similar structures and signal transduction mechanisms [Yan et al., 1999]. The study conducted by Yan *et al* (1999) suggested that the ligand binding domain of the 5-HT_3 receptor is formed by multiple parts of the extracellular domain that are similar to regions of the AChR known to be involved in ligand binding.

Hedlund *et al* (2005) studied the changes in sleep state of 5-HT_7 receptor knockout mice. The knockout mice spent less time in REM sleep during the light period than their wild-type counterparts. However, no different was seen in either group with respect to waking activity and SWS duration. A rodent pharmacological study [Monti et al., 2008], has tentatively proposed that the activation of projection GABAergic neurons in the DRN resulting from a selective 5-HT_7 receptor agonist, LP-44, may be responsible for the inhibition of cholinergic cells in the laterodorsal and pedunculopontine tegmental nuclei and the decrease in REM sleep [Monti, 2011].

Histamine

Histamine (His) is a naturally occurring substance that is released during tissue damage as well as acting as a neurotransmitter. Histominergic neurons are found exclusively in the tuberomammillary nucleus (TMN) in the posterior hypothalamus with their axons extending throughout the CNS. Histaminergic neurons' are active during wakefulness but are inactive during sleep, which is thought to be due to the suppression of histaminergic neurons' firing by high firing GABAergic inputs from the VLPO area [Tabarean et al., 2007].

All aminergic nuclei cause excitatory projections, however the mechanisms for these excitations vary. Nicotinic receptor-mediated cholinergic activity desensitizes histaminergic neurons through the α7-type receptors [Uteshev et al., 2002] and it is thought that this action represents a sensor for the central waking actions of nicotine [Haas et al., 2008]. No muscarinic receptor-mediated effects, as of yet, have been noted in vitro. Noradenaline does not have a direct effect on histaminergic neurons however it is known to control GABAergic input via α2-type receptors hence controlling the inhibition of inhibitory postsynaptic currents (IPSCs). See below for a more comprehensive introduction to role of acetylcholine in sleep. Dopamine is known to excite histaminergic neurons through an as yet undefined mechanism. Serotonin depolarises and hence excites the histamine neurons via the activation of the Na^+ - Ca^{2+} exchange [Eriksson et al., 2001]. Histamine neurons may also be involved in CO_2 mediated arousal [Johnson et al., 2005].

Of the four histamine receptors known, three are widely expressed in the brain (H_1-H_3) whilst H_4 receptors are predominantly found in the peripheral tissues, such as blood, spleen, lungs and livers. H_1 receptors occur throughout the CNS with a high density in areas involved with arousal and waking, i.e. thalamus [Soria-Jasso et al., 1997], cortex [Reiner and Kamondi, 1994] and aminergic nuclei [Stickgold and Walker, 2009c]. H_1 receptor antagonists, antihistamines are prescribed for allergies and are widely known for their sedative properties. This suggests that histamine is involves in sleep-wake regulation particularly H_1 receptors [Haas and Panula, 2003]. Experiments were undertaken with H_1 receptor knock-out mice, however no significant changes were observed in the sleep-wake pattern but the waking response usually seen with H_3 receptor antagonists had been eliminated. Activation of H_2 receptors blocks Ca^{2+} activated K^+ conductance which is responsible for the firing and long-lasting after-hyperpolarization after action potentials. H_3 receptors are located on the TMN cell body, dendrites and axon. They are also present on many nonhistaminergic varicosities, such as those containing glutamate, acetylcholine, dopamine, noradrenaline, serotonin, GABA and various peptides [Stickgold and Walker, 2009c]. Histamine is known to depress the glutamatergic perforant

pathway by 30% in rats. It also suppresses the glutamatergic corticostriatal and the dopaminergic nigrostriatal pathways.

Noradrenaline

Noradrenaline (NA), also known as Norepinephrine, is a catecholamine with multiple roles throughout the central and peripheral nervous system, as a hormone and a neurotransmitter. Noradrenaline was once thought to enhance sleep however, it is now considered to be an important agent in the activation of wakefulness [Thorpy and Yager, 2001]. The noradrenergic neurons of the LC are nearly always active during wakefulness, becoming less active during NREM sleep and are practically silent during REM sleep. It is probable that NA works in conjunction with acetylcholine to produce wakefulness, however lesions of the LC have not led to substantial changes in the amount of waking as may be expected from previous research [Aston-Jones et al., 2007].

Noradrenaline is a receptor ligand to either α_1, α_2 or β-adrenergic receptors. The activation of α_2 results in the decrease in intracellular Ca^{2+} resulting in the inhibition of neurotransmitter release. According to Jones (2009), NA promotes waking by inhibiting sleep-promoting GABAergic neurons in the preoptic are and basal forebrain which express α_2 adrenergic receptors. These GABAergic neurons discharge during SWS and REM sleep in a complimentary manner to the NA LC neurons.

1.3 Sleep Electrophysiology

The discovery of brain electrical activity in 1875 by Richard Caton was a major turning point in the study of sleep. Caton revealed the action potentials in the brains of cats, rabbits and monkeys. This discovery went largely unrecognised until 1929 when electrical signals were recorded from the human brain by Berger, a German physician. These recordings were called *electroencephalograms* (EEG), which aided in the demonstration of fundamentally different electrographic signatures associated with sleep and wakefulness. Figure 1.4 depicts an early EEG of general excitatory states [Penfield et al., 1942]. The development of electroencephalography has led to increasingly sophisticated studies of brain function and brain activity [Aldrich, 1999]. In 1937, the EEG was used to determine different sleep states resulting in Alfred L. Loomis, E. Newton Harvey and Garret Hobart classifying five different stages of sleep. Rapid eye movement (REM) sleep was first characterised as dreaming sleep in 1953 by Eugene Aserinsky and Nathaniel Kleitman, who demonstrated the presence of rapid eye movements during a dream stage of sleep. However, in 1957 this discovery was furthered by the discovery of a recurring pattern of REM and NREM sleep during overnight EEG monitoring by Kleitman and

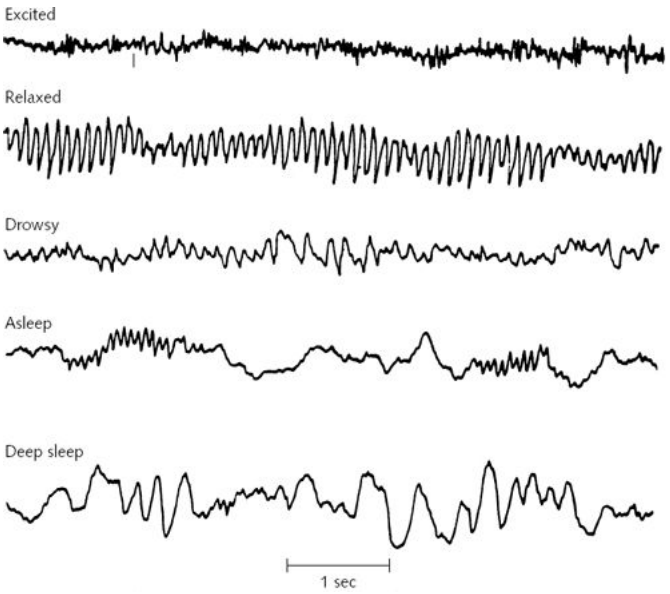

Figure 1.4: An early EEG. Effect of general excitatory states. Normal electroencephalograms as varied by conditions of generalized excitation, relaxation, drowsiness, light sleep, and deep sleep. *Taken from [Penfield et al., 1942].*

William Dement.

An EEG signal is a measurement of currents that flow during synaptic events, predominantly in the dendrites of many pyramidal neurons in the cerebral cortex [Sanei and Chambers, 2007]. When the neurons are activated either via an excitatory or inhibitory input, synaptic currents are induced within the dendrites. An electric field is generated by the spatially separated voltage differences in the neurophil caused by this current which is detectable from the scalp via EEG electrodes (figure 1.5). Scalp electrodes detect signals from only the most superficial layers of the brain (i.e. cerebral cortex) due to the attenuating effect of electrically inactive tissues between the signal origin and the EEG electrode.

When discussing EEG activity, rhythms are often introduced as they are perhaps the single most prominent feature detectable with EEG electrodes. Rhythmicity can be local to a single neuron, regional involving several neighbouring neuronal circuits or remote involving neuronal circuits which span many brain structures [Misulis and Head, 2003]. EEG rhythms are typically classified into seven frequency bands. These rhythms and their relationship to *in vitro* studies will be covered in more detail in section 1.5.2. Signals are then further characterised by amplitude and morphology. Frequency refers to how many successive peaks or troughs occur in one second and is measured in Hertz (Hz). Amplitude refers to the magnitude change in electrical potential of peaks and troughs and is measured in micro volts (μV). Morphology refers to the shape of the particular EEG wave or group of waves, reflecting both their frequency and amplitude [Stickgold and Walker, 2009e].

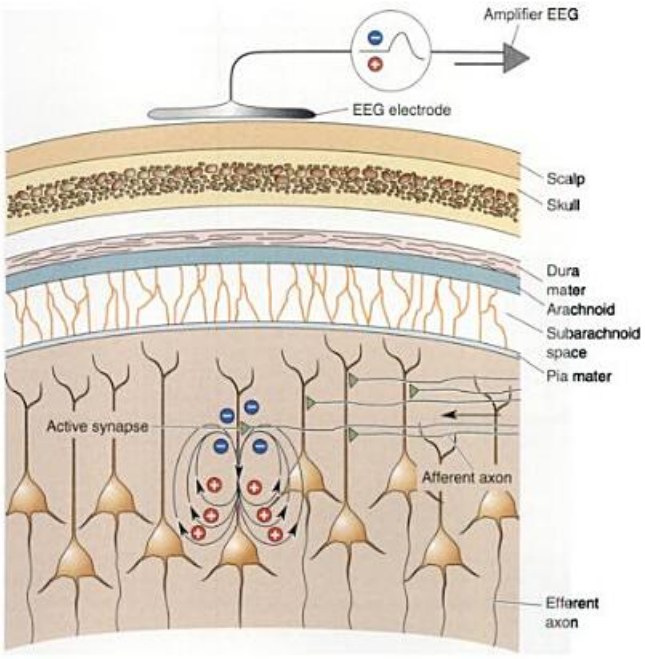

Figure 1.5: Pyramidal cell dendrites extend through many cortical layers. When a large collection of cells simultaneously undergoes a similar excitatory or inhibitory activity, the resulting local field potential (the average signal from this group of cells) is detected by the EEG electrode recording on the scalp. This signal needs to be substantial enough to pass through several layers of non-neural tissue. *Adapted from [Bear et al., 2006].*

The position of the electrodes in standard EEG monitoring sessions results in even coverage across the scalp which allows for the majority of the cortex to be mapped (figure 1.6a) due to the penetrating nature of the dendrites of the deep layer pyramidal cells. When epileptologists discuss such conditions as Benign Epilepsy of Childhood with Centro-Temporal spikes (see section 1.7.2) or Frontal Lobe epilepsy, they often refer to the EEG which will show abnormalities in the central and temporal regions, for the former, and as suggested in the frontal regions for the latter. Topographical maps can be used as a visual aid when analysing results (figure 1.6b).

1.4 Stages of Sleep

The invention of the EEG allowed scientists to study sleep in ways that were not previously possible. Further studies of human sleep have demonstrated that sleep progresses through a number of stages during which different traces are displayed. As mentioned above, there are two main types of sleep. These are introduced in more detail here:

1. **Non-REM Sleep (NREM).** This is also known as Delta sleep, Slow wave sleep (SWS) or Quiet Sleep.

2. **Rapid Eye Movement (REM) Sleep.** This is also known as active sleep or paradoxical sleep.

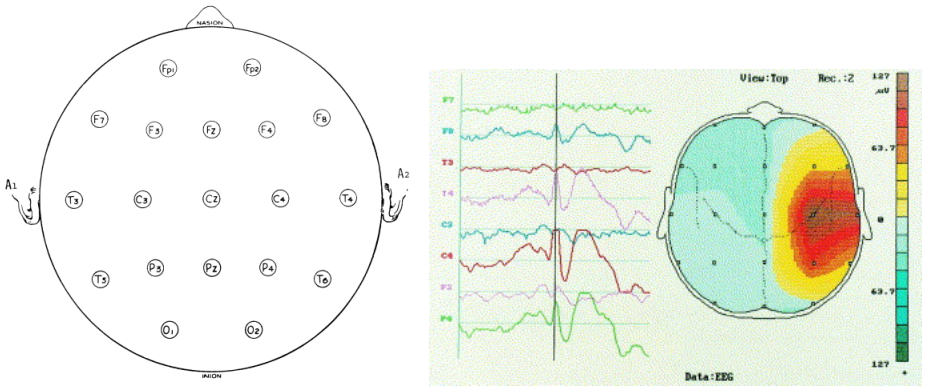

(a) (b)

Figure 1.6: **a). Standard 10-20 electrode placement system.** A - auricle (or ear), C - central, F - frontal, T - temporal, P - parietal, O - occipital, Cz - central vertex, z - midline. *Adapted from [Hughes, 1994].* **b). Topographic map** showing activity in right centro-temporal region in a 9-year old boy with Benign Epilepsy in Childhood with Centro-Temporal Spikes. *Adapted from [Tsai and Hung, 1998].*

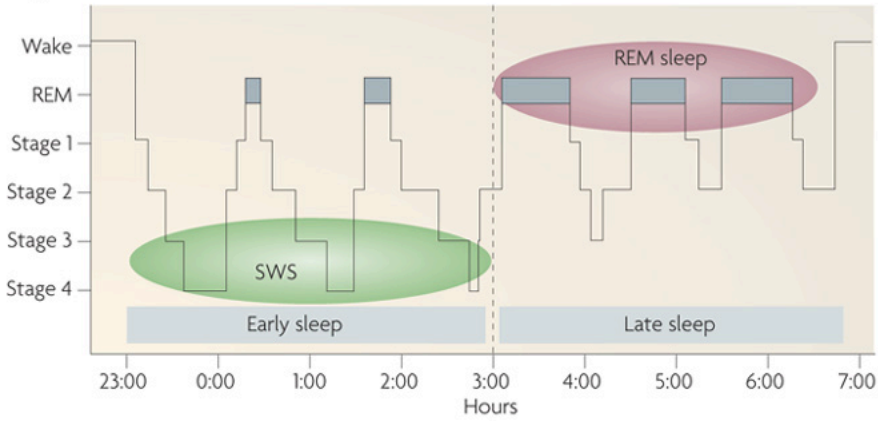

Figure 1.7: **Architecture of sleep in a healthy adult.** This is a simplified depiction of a normal healthy adult during the different stages of sleep over the course of a night. In humans, the first part of the night (early sleep) is characterised by high amounts of slow wave sleep, whereas the latter half of the night is predominantly REM sleep. *Adapted from [Diekelmann and Born, 2010].*

1.4.1 NREM sleep

Non-rapid eye movement sleep is made up of four sleep stages, stages 1 and 2 are the lighter stages of sleep, and stages 3 and 4 which are described as SWS. These sleep stages show distinct EEG characteristics which are depicted in figure 1.8. Unlike REM sleep, there is usually little or no eye movement during these stages. Stage 1 type sleep is seen throughout the night thanks to the cyclic nature of sleep. It is initially characterised by a theta rhythm replacing the awake alpha rhythm (see stage 1 in figure 1.8). Stage 2 type sleep sees no eye movement and the absence of dreams. EEG recordings typically show sleep spindles and K-complexes (see stage 2 in figure 1.8). The K-complex can occur spontaneously or can also be evoked by sensory stimulation, however the functional meaning of the K-complex remains unknown [Gennaro et al., 2000]. It has been shown that K-complexes are the result of a synchronized cortical network that causes both excitatory and inhibitory actions on cortical neurons, hence creating a slow wave oscillation (0.5-0.9Hz and 1-4Hz) which spreads through the cortex [Amzica and Steriade, 1997]. Stages 3 and 4 form SWS which is characterised by the presence of specific oscillations and neuromodulator activity. The most common field potential oscillations observed during SWS are slow oscillations (delta rhythms) and spindles (see stages 3 and 4 in figure 1.8). The delta rhythms recorded come from dipoles originating in the neocortex with a peak frequency of ∼0.8Hz [Molle et al., 2002]. However, there are multiple possible sources of this activity, including locally generated networks (purely neocortical) and distributed networks (thalamocortical [Steriade, 2003]). The origins of delta rhythms are dealt with in more detail in section 1.10. These oscillations synchronize the neuronal activity into down states of widespread hyperpolarization and subsequent up states of depolarisation and increased neuronal firing [Diekelmann and Born, 2010]. Spindle activity refers to the ∼10-15Hz oscillations observed in human sleep in both stage 2 and SWS. It may be present in low voltage background EEG, superimposed on delta waves, or temporally locked to a K complex [Gennaro and Ferrara, 2003]. During SWS, levels of ACh are decreased compared to both REM and wakefulness.

1.4.2 REM sleep

The majority of REM sleep occurs within the latter half of the night as shown in figure 1.7. REM is characterised by the presence of ponto-geniculo-occipital (PGO) waves, theta activity and specific neuromodulator levels. PGO waves are phasic electrical burst of neural activity which originate in the Pons and propagate to the lateral geniculate nucleus in the hypothalamus and finally end in the occipital primary visual cortex, hence the name. All of these cortical regions are involved in eye movement and visual processing.

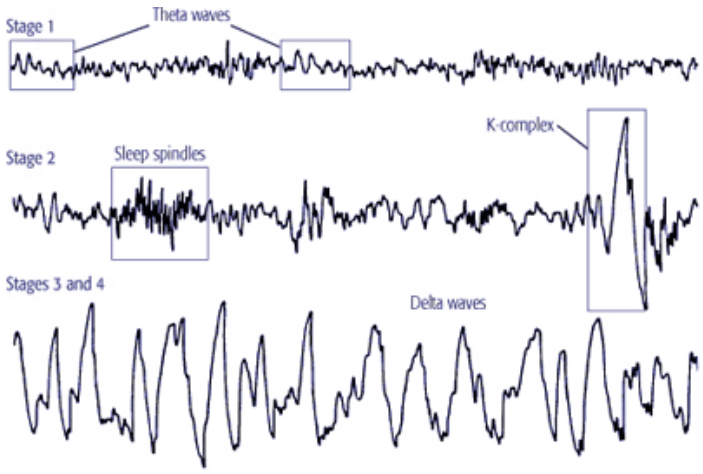

Figure 1.8: Stages of NREM sleep.

These rhythms have been observed in rats and cats however are not reliably identified in humans. Theta oscillations (4-8Hz) are predominantly seen in the hippocampus during REM sleep. Cholinergic activity during REM sleep is similar or higher than the levels seen during wakefulness. Levels of both NA and 5-HT are at a minimum during REM, as previously discussed in section 1.2.1. Figure 1.9 shows a typical EEG recorded in a healthy person during REM sleep.

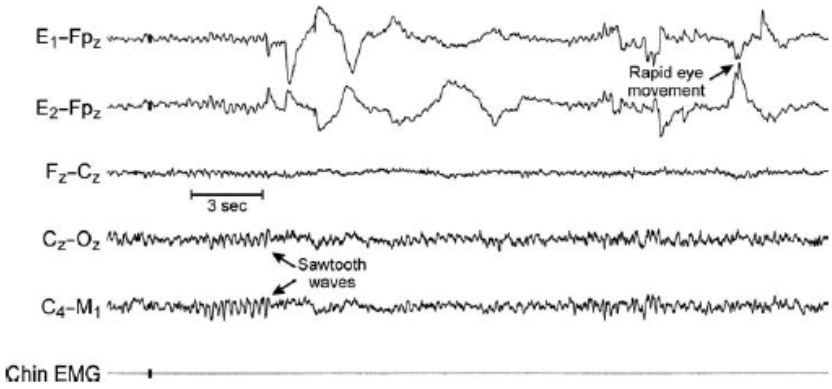

Figure 1.9: **REM Sleep.** REM stage shows low voltage and mixed frequency of EEG, sawtooth wave pattern (2-6Hz sharply contoured or serrated waves over the central area) is often present. *Taken from [Krahn et al., 2009]*

1.5 Neuronal Oscillations

1.5.1 Oscillations *in vivo*

The cerebral cortex is a dynamic system with the characteristics of a small world network [Watts and Strogatz, 1998]. However, work by Kaiser *et al* (2010) has shown that a hierarchical approach may be another method to understanding dynamic neural networks. "Hierarchy" can be classified in several different ways and can be applied to topological, temporal, spatial as well as functional properties of neural networks [Kaiser et al., 2010]. Large networks of widely dispersed neurons are often involved in cognitive and executive processes. These networks have many signals circulating through them and it is thought that internal mechanisms control the selective routing of these signals. Singer (2009) proposed that in order for a neuron to convey two messages simultaneously, it would need to exploit two parallel independent coding strategies. The first encoded message is in the discharge frequency of the neurons, also called the rate code. It is proposed that the second encoded message is contained in the precise timing relationships between individual spikes of distributed neurons (temporal code) [Singer, 2009]. It is further proposed that these precise timing relations are established either by the timing of external events (stimulus locking) or by internal timing mechanisms.

1.5.2 Classification of oscillations during sleep-wake cycle

Oscillatory patterns of neuronal responses are often studied in neuroelectrophysiology. These oscillations are rarely detectable at the single cell level due to the tendency of individual cells not to generate outputs on every oscillation cycle but they are easily observed when large populations of neurons are recorded simultaneously (i.e. with EEG scalp electrodes). Experimentally this can either be achieved through multi unit recordings or recordings of the local field potential [Singer, 2009], hence it is also referred to as the population code. Work has shown that patterns of oscillation are often (though not exclusively) generated by the chemical and electrical inputs to inhibitory interneurons. Resulting inhibitory signals are passed to pyramidal cells which cause them to stop discharging when inhibition is strongest and instead discharge at the relatively depolarised peaks between inhibitory events, causing firing synchrony in a local population. Oscillations can be synchronised over large distances due to mutual coupling of the oscillatory networks via long-range excitatory cortico-cortical connections [Singer, 2009]. These oscillations have been separated into different groups dependent on the frequency they oscillate at. These are: slow wave oscillations (<1Hz), delta (1-4Hz); theta (5-7Hz); alpha (8-12Hz); beta (13-27Hz); gamma (30 - 80Hz); and ripples (>80Hz) (see figure 1.10 for a more detailed breakdown). Many *in vitro* studies use the change in oscillatory pat-

tern as an indicator for the effect a drug has on cells in a network. For example, when any N-Methyl-D-aspartate (NMDA) antagonist (Ketamine, DAP5 etc.) is bath applied gamma frequency patterns are altered, which may be associated with cognitive disorders, like Schizophrenia [Uhlhaas et al., 2008].

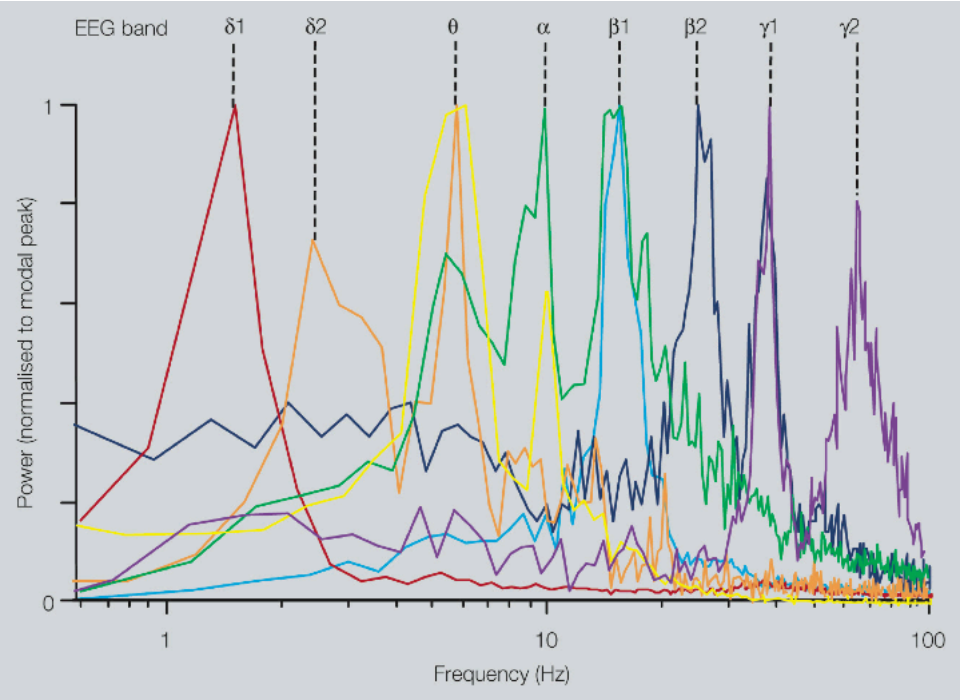

Figure 1.10: Multiple modal peak frequencies of persistent rhythms generated in isolated neocortex *it vitro.* (*Taken from [Roopun et al., 2008]*).

Ripples (>80Hz)

High frequency oscillations are known as ripples or 'high gamma' waves. The ripples frequency band is generally considered to span from 80-250Hz whilst fast ripples are categorised as any rhythm greater than 250Hz. Ripples can be observed in both normal and pathologic brain processes [Bagshaw et al., 2009] whereas fast ripples are generally only identified in epilepsy patients and animal models [Staba et al., 2002]. Previous studies have shown that ripples are present during all stages of sleep, predominantly during SWS [Bagshaw et al., 2009, Grenier and Steriade, 2001]. However, these ripples, which originate from the interaction between inhibitory interneurons and pyramidal cells in CA1 of the hippocampus, are generally superimposed on hippocampal sharp waves (fast depolarising events) [Diekelmann and Born, 2010]. Sharp waves are described as large-amplitude local field potentials which occur irregularly in the CA1 region of the hippocampus during a state of minimal interaction, i.e. SWS or immobility [Buzsáki et al.,

1983]. Hippocampal sharp wave-ripples are present during the re-activation of hippocampal pathways which were previously active during the preceding wakefulness [Wilson and McNaughton, 1994]. Previous prefrontal cortex studies have found temporal correlations during SWS between hippocampal ripples and spindle activity (see below for more detail) which are thought to reflect the co-activation of hippocampal and neocortical pathways [Siapas and Wilson, 1998]. Sirota *et al* (2003) also discovered a similar correlation of neuronal discharges between the hippocampus and the somatosensory cortex. Due to the simultaneous activation of the hippocampal and neocortical regions, this relationship is thought to be part of an important process in memory consolidation [Rauchs et al., 2005, Wilson and McNaughton, 1994, Siapas and Wilson, 1998].

Fast ripples in the epileptic brain are thought to reflect action potential population bursts of synchronously discharging neuronal clusters [Bragin et al., 2002].There is considerable evidence for linking fast ripples with seizure onset in epilepsy patients [Grenier et al., 2003]. Grenier *et al* (2003) also demonstrated that neocortical ripples are not only associated with paroxysmal events such as spikes, but are also present at their onset. This supports work by Bragin *et al* (2002), in which they state that the synchronization of clusters of high interconnected neurons result in epileptiform bursts which eventually lead to seizure activity.

Gamma Frequency Oscillations (30-80Hz)

Gamma frequency oscillations are generally considered to span from 30 to 80Hz, however they are often broken down into low (30-40Hz) and high (60-100Hz) as shown in figure 1.10. Previous *in vitro* and *in vivo* studies have shown that there is a relationship between slow wave sleep rhythms (delta oscillations) and gamma oscillations [Compte et al., 2008, Steriade et al., 1996, Mena-Segovia et al., 2008, Isomura et al., 2006]. These studies have shown that gamma oscillations preferentially occur during the 'UP' state, characterized by rhythmic cycles of synaptically mediated depolarization, of the slow wave and disappear during the 'DOWN' state, the hyperpolarizing phase [Valderrama et al., 2012]. Several EEG studies have previously reported the lack of significant phasic gamma activity observed during SWS [Fell et al., 2002, Molle et al., 2002], however this is thought to be due to the spatial limitations of EEG and that gamma oscillations are generally phase-locked over short distance but rapidly lose this synchronization over distance. Valderrama *et al* (2012) have since reported on gamma activity during SWS via the use of intracranial recordings which allow the analysis of short-range spatially coherent activities that are not easily available with scalp recordings. These findings are supported by work from the same group when using multi-electrode arrays in human cortex during SWS [Le Van Quyen et al., 2010]. It has been suggested [Isomura et al.,

2006] that gamma activity during the 'UP' state may aid in the transfer of previously coded information via parahippocampal pathways [Le Van Quyen et al., 2010] whilst activity during the 'DOWN' state may relate to a hippocampal replay and modification of intrahippocampal and entorhinal cortical connectivity [Valderrama et al., 2012].

Beta Frequency Oscillations (12-25Hz)

The beta frequency range can be broken down into two individual ranges, sigma or spindle (12-16Hz) and beta (16-25Hz) as shown in figure 1.10. Spindle oscillations as well as other faster oscillations are grouped by slow wave oscillations (<1Hz). As stated previously in section 1.4, sleep spindles characterise Stage 2 sleep, although spindle density generally increases through the night [Fogel and Smith, 2011]. The spindle frequency range itself can be split into two further ranges: slow (∼12-14Hz) and fast (∼14-16). Slow spindles are generally observed in the frontal regions of the brain, whereas fast spindles are seen in the posterior regions. These two frequency bands are thought to originate from separate generators [Merica, 2000]. However, De Gennaro and Ferrara (2003) have argued that instead of two spindle ranges there is in fact one spindle range and an anterior peak of alpha activity. Beta rhythms are generally linked to muscle contractions and movement however they are observed during SWS although on a much smaller magnitude than spindle frequencies [Molle et al., 2002].

Alpha Frequency Oscillations (8-12Hz)

There are three types of alpha rhythm observed during the wake-sleep cycle. The first presents during the relaxed mental state whilst the eyes are closed, but the subject is not asleep or tired. This oscillation is centred over the occipital lobe and tends to dissipate during drowsiness and stage 1 of sleep to be replaced by theta oscillations. The second presents during REM sleep in the frontal-central region of the brain [Roth et al., 1999]. The third occurs in SWS and spreads across the brain in a anterior-posterior gradient [Pivik and Harman, 1995]. Alpha activity during or superimposed on delta rhythms during SWS tends to be present when a patient is complaining of non-restorative sleep and is generally observed in individuals with sleeping disorders, like narcolepsy and sleep apnea [Jaimchariyatam et al., 2011].

Theta Frequency Oscillations (4-8Hz)

Theta oscillations are most commonly seen in the hippocampus, and is particularly strong in the CA1 region of this structure. Theta oscillations are consistently present during the initial stages of Stage 1 sleep and throughout REM sleep [Jouvet, 1969] whilst also being associated with locomotor activity [Vanderwolf, 1969]. It has been proposed [Cantero

et al., 2003] that theta oscillations might serve as an arousal mechanism for the transition from sleep to wake. Although theta in the hippocampus has been greatly studied, it does occur in other regions of the mammalian brain including the entorhinal cortex [Mitchell and Ranck, 1980]. Unlike during rodent studies, the theta rhythm seen in humans during REM sleep is composed of short 1 second bursts of activity and during transitions to wakefulness [Cantero et al., 2003]. It has been widely suggested that theta oscillations enhance the formation of long-term memories by aiding with long-term potentiation process [Huerta and Lisman, 1996, Holscher et al., 1997]. Cantero *et al* (2003) demonstrated during subdural EEG studies, a lack of functional coupling between the hippocampal theta rhythm and the neocortical theta rhythm which strongly suggests that the human rhythms have evolved from those observed in animal models and are now independent and state-dependent rhythms. Very little theta rhythm activity is observed during SWS in either the hippocampus or neocortical regions.

Delta Frequency Oscillations (1-4Hz)

Delta frequency oscillations are high amplitude rhythms and are usually associated with SWS. The presence of these rhythms on an EEG aid in characterising stages 3 and 4 of NREM sleep. There are two types of delta rhythms observed *in vivo*: the stereotyped clock-like delta rhythm; and a cortical delta rhythm which continues after extensive thalamectomy [Stickgold and Walker, 2009f].

The clock-like corticothalamic delta rhythm is generated intrinsically by the interplay of I_T and I_h currents in thalamocortical (TC) neurons [Stickgold and Walker, 2009g]. The I_T current is a low threshold Ca^{2+} current [Llinas, 1988] and the I_h current is a cation current that is activated upon hyperpolarisation of thalamic relay neurons [McCormick and Pape, 1990]. The corticothalamic delta activity can be synchronised by corticothalamic volleys that activate the thalamic relay neurons. This in turn hyperpolarises the TC neurons to a suitable membrane potential and results in delta rhythm generation [Steriade et al., 1991]. Hence, the cortical neurons firing simultaneously result in exciting the relay neurons, which occurs during the depolarisation of the slow oscillation, and hyperpolarising the TC neurons. This activity is then transferred back to the cortex, hence completing the loop and shaping the delta rhythm [Steriade, 2006, Crunelli and Hughes, 2010]. Steriade *et al* (1991) found that low cholinergic tone maintains the corticothalamic delta rhythm, hence maintaining deep sleep. They found that the delta rhythm is suppressed during the transition from deep sleep to wakefulness or REM sleep and is predominantly due to the stimulation of cholinergic projections from the brain stem. Therefore, elevated levels of ACh are thought to be deterimental to the generation of the corticothalamic delta rhythm [Steriade et al., 1991].

The cortical delta rhythm has been associated with noisy brain states during deep sleep, i.e. sleep states where delta rhythms are co-expressed with numerous other higher frequency bands like theta and gamma. Such a situation is also seen, albeit with lower delta power, during wakeful states [Lakatos et al., 2005]. As stated in the previous subsections, the cortical delta rhythm acts as a carrier for higher frequency oscillations and is also thought to be linked to synaptic plasticity [Aeschbach, 2009]. However, little is currently known about the cellular mechanisms mediating cortical delta oscillation. Amzica and Steriade (1998), however, proposed that cortical delta may be driven by the discharge of intrinsically bursting neurons. Carracedo (2010) found that the application of a cholinergic agonist and a D1-like receptor antagonist evoked delta frequency oscillations during *in vitro* experiments, similar to those seen *in vivo*.

Slow-wave Oscillations (<1Hz)

During NREM sleep the majority of cortical neurons have rhythmic fluctuations in membrane potential, from a hyperpolarised state of silence to a depolarised state of intense firing [Steriade et al., 1993c]. Intracellular recordings have shown that this activity was present in almost all cortical neurons and the spiking activity could be phase-linked to the <1Hz oscillation [Steriade et al., 1993c]. The slow wave oscillation is believed to originate in the cortex as it continues after extensive thalamectomy [Steriade et al., 1993b] as well as existing in cortical *in vitro* slice preparations [Sanchez-Vives and McCormick, 2000]. One of the proposed mechanisms for the origin of slow wave oscillations is linked to the spontaneous activity of layer V cortical neurons [Sanchez-Vives and McCormick, 2000]. Sanchez-Vives and McCormick (2000) proved that it was possible to generate persistent slow wave oscillations *in vitro* by providing a bath medium that mimicked the ionic composition of interstitial fluid *in situ*. The slow oscillation manifested in regular spiking, intrinsically bursting and chattering pyramidal neurons as well as fast spiking interneurons, which fired in phase with the local field. From it's origin in layer V, the rhythm propagated to layer VI after a short delay, and then onto layers II/III after a further delay. The rhythm was abolished after the blockade of non-NMDA glutamatergic ionotropic receptors. The blockade of NMDA receptors also blocked or greatly reduced the slow wave oscillation. Hence glutamatergic transmission was needed to generate the rhythm.

1.5.3 Pharmacology of *in vitro* delta oscillations

As stated previously, research by Carracedo (2010) demonstrated that cortical delta rhythms could be evoked in acute brain slices through the perfusion of the cholinergic

agonist, carbachol and the DA D1-like receptor antagonist SCH23390. It is this *in vitro* model that is used as the main model from which to induce sleep-related pathological activity in this thesis.

Induction of delta oscillation through cholinergic agonists

ACh is known to play an important role in the sleep-wake cycle as detailed in section 1.2.1. Cholinergic transmission is typically reduced during SWS compared to wakefulness and REM sleep, however it is not completely stopped. Replicating the low, but not 'zero' cholinergic tone characteristic of SWS via the application of a cholinergic agonist is sufficient to evoke delta oscillations *in vitro* [Carracedo, 2010]. Some cholinergic mediated action needs to be induced as, although high levels of ACh are seen during waking states, a very low level is present during SWS. Hence the model determined by Carracedo (2010) needed the application of a small concentration [4μM] of the AChR agonist, Carbachol. Once the delta rhythm is stable, it continues to increase in amplitude whilst slowing in frequency over several hours, as is generally observed in stages of NREM sleep during *in vivo* studies throughout the night.

Effect of Dopamine on cholinergic transmission

As with ACh, DA acts to promote wakefulness and REM sleep and inhibits SWS as was demonstrated by the extracellular studies carried out by Lena *et al* (2005). Rodent *in vivo* studies have shown that antagonism of dopaminergic transmission by the dopamine D1-like receptor antagonist SCH23390 increased SWS and reduced wakefulness and REM sleep [Monti et al., 1990]. Monti *et al* (1990) also proposed that the activity of the cholinergic pathways were enhanced by DA release. However, the manipulation of dopaminergic transmission alone is not sufficient to evoke cortical oscillations in the isolated brain slice. Di Cara *et al* (2007) demonstrated that the use of the D1-like receptor antagonist SCH23390, reduced extracellular ACh levels in the frontal cortex and the hippocampus. Whereas an increase in ACh levels were reported during the perfusion of the D1 agonist SKF38393 [Del Arco et al., 2007]. This therefore suggests that DA can mediate ACh levels, which when paired together more closely mimic the neurobiological properties of sleep; thus, reproducing a more accurate model of delta oscillations during SWS.

1.6 Sleep, Memory and Learning

There are many theories for the purpose of sleep. The most modern theories include: brain detoxification [Inoue et al., 1995]; tissue restoration [Smith, 1985]; immune control;

energy conservation [Benington and Heller, 1995] and memory consolidation [Diekelmann and Born, 2010,Born et al., 2006,Walker, 2008,Siegel, 2001]. With regards to this thesis, the most relevant theory is that of memory consolidation. Memory consolidation can be distinguished as three specific processes: Synaptic consolidation, which occurs within the first few hours after learning [Dudai, 2004]; Systems consolidation, which occurs over a larger amount of time, generally weeks or years, as the memories become independent of the hippocampus [Roediger et al., 2007]; and reconsolidation, where consolidated memories can become labile again during the reactivation of the specific memory pathway [Tronson and Taylor, 2007].

The notion that sleep has had an important role in memory and hence learning, has been around for over 200 years. This has become more specific over the last 15 years with concentration on sleep dependent memory processing. As detailed in the previous section, sleep can be simply broken down into two states, REM and NREM. NREM sleep itself can be broken down into different stages, as previously shown, however when discussing memory consolidation, we refer to stages 3 and 4, where slow-wave sleep (SWS) is observed. Likewise, memory is not considered to be a single phenomenon either but can also be roughly separated into two memory types: declarative (episodic) memory and non-declarative (procedural) memory. Declarative memories are accessible to conscious recollection. These include facts and episodes like learning vocabulary or recalling events. Procedural memories are those that involve skills, habits or actions that result from repeated practice and are not necessarily available for conscious recollection. For example, tying your shoes or riding a bike and once practised, they require no conscious effort.

In humans, SWS is known to dominate the early part of the nocturnal sleep cycle and REM to dominate the later part. Several studies have shown that declarative memories are consolidated during SWS and that procedural memories are consolidated during REM sleep [Diekelmann and Born, 2010]. These studies support the 'dual process hypothesis' where SWS and REM sleep facilitate different processes [Hobson and Pace-Schott, 2002]. A study by Plihal and Born (1997), reported that deprivation of SWS in the first quarter of sleep selectively impairs performance on declarative memory task such as paired-word associates. While deprivation of REM during the last quarter of sleep impairs performance on procedural memory tasks, like mirror drawing. Whereas, other studies that support the 'sequential hypothesis' have shown that SWS can improve procedural memories and vice versa, REM can also improve declarative memories [Rauchs et al., 2004,Huber et al., 2004,Rauchs et al., 2005]. The 'sequential hypothesis' follows the theory that all stages of sleep are needed to consolidate a memory in a complementary and

sequential manner [Hobson and Pace-Schott, 2002]. As previously stated, consolidation refers to the process of transforming the newly acquired and easily altered memories that have been encoded during wakefulness, into substantial representations which become absorbed into the network of existing long term memories. This consolidation process essentially involves reviewing the new memories within the neural networks that were used to encode them initially [Diekelmann and Born, 2010]. This occurs most efficiently during sleep to ensure no crossover between the encoded memory and the consolidated memory, and without the possibility of hallucination occurring during consolidation [McClelland et al., 1995]. The reactivation of the encoded pathways generally occurs during SWS and only in a minority of recorded neurons. During SWS, these reactivations (the re-firing of neurons which were previously active during the initial encoding of the memory [Wilson and McNaughton, 1994]) usually occur in the same order that they were originally experienced in [Foster and Wilson, 2006], albeit on a condensed timescale [Nadasdy et al., 1999].

1.7 Sleep and Epilepsy

Sleep can be disturbed due to a variety of reasons, from change in temperature to sleeping disorders like sleep apnea, however during this thesis, the most relevant and interesting are epileptic seizures. Seizures occur when there is a misfiring of the synchronous rhythms of the brain and the physical manifestation of a seizure can vary. They can manifest as tonic or clonic movements, where tonic movements typically last less than 60 seconds during which muscle tone of exterior muscles is increased while clonic movements are convulsions. A seizure will also cause an alteration of mental state. The large amplitude, hypersynchronous patterns of electrical activity associated with seizures can be observed through the use of EEG, which assists in the classification of the epilepsy. As previously stated, synchrony of the network is needed for the EEG to detect the signal, hence many cells must undergo a similar disruption simultaneously. There are two distinctive periods of neural activity with regards to epilepsy: ictal and interictal paroxysmal activity. Ictal activity relates to the presence of an electrographic seizure during an EEG recording, whilst interictal paroxysmal activity relates to the time between seizures when epileptiform activity continues to be detected, but only as brief, transient events. It is simple to differentiate between the two states as interictal events do not associate with overt epileptic activity. They can even be detected in patients with no history of epilepsy.

1.7.1 Paroxysmal patterns

There are many different interictal paroxysmal patterns that consist of several components. The first is a single random spike. According to IFSECN (1974)(International Federation of Electroencephalography and Clinical Neurophysiology), a spike is a transient, clearly distinguished from the background activity, with a pointed peak and a duration from 20 to under 70msec while the amplitude is variable [Niedermeyer and da Silva, 2004a]. The appearance of these spikes does not always suggest a hidden or overt paroxysmal event. Other questions need to be asked to distinguish the possible reason of the spike. These investigations should include the wave morphology, the patients age, whether they are in a state of sleep or wakefulness and the location of spike occurrence. Wave morphology can be used as an indicator of epilepsy, however the size of the spikes does not always correlate with the size of the seizure. For example, Rolandic spikes in children aged between 4 and 10 years are very prominent although the seizure disorder is usually benign (i.e. seizures do not occur). There are many types of spikes that are linked to age, for example spikes of an epileptic newborn may seem similar to those observed in an elderly patient but with very different diagnoses. The level of awareness of the patient, as stated previously, is very important as spikes may occur in any state of awareness. However each different state may relate differently to the spikes. The location of the spikes can help denote which seizure disorder the patient may have. The types of spikes described below are each observed at a different location while all relate to forms of seizure disorders.

Occipital spikes

Occipital spikes, also known as spikes and waves, predominantly show as an age-dependent, EEG-defined, benign focal epilepsy manifesting as autonomic symptoms followed by brief or prolonged partial motor seizures in younger children [Nass and Gross, 2001]. Older children present with visual symptoms and headaches. However, occipital spikes are not always benign. Nass *et al* (2001) reported that they also present in some children with autism or autistic regression. These children exhibit severe language and behaviour deficits. This probably results from the occipital maximal spike fields extending to posterior temporal and parietal regions, as both are involved in language acquisition and cognitive development. Occipital spikes, as the names suggests are detected in the occipital region of the brain. This localised detection is only observed during interictal EEGs during wakefulness however these spike wave complexes are detectable in other cortical regions during sleep (i.e. central, temporal and frontal) [Caraballo et al., 2007].

Centro-temporal spikes

Centro-temporal spikes are usually classified as high amplitude focal sharp wave discharges in the central and temporal regions, and are either bilateral or unilateral [Smith, 2005]. Dalla Bernardina *et al* (2002) described the typical paroxysm as a focal negative diphasic slow spike of medium to high voltage generally over 100μV, followed by a slow wave located in the rolandic or centrotemporal regions with possible diffusion to surrounding areas. Centro-temporal spikes (CTS) are not limited to children with epilepsy, they have also been documented to occur in healthy children. Of the 3726 healthy children aged between 6 and 13 years of age who participated in a meta study, Cavazzuti *et al* (1980) found that mid temporal spikes were present in 50 (1.34%) of the children whilst centroparietal spikes were recorded in 27 (0.72%). It is thought that the presence of CTS spikes in healthy children suggests a genetic predisposition to epilepsy if no neurological deficit or history of CNS problems are present [Niedermeyer and da Silva, 2004a]. A 2005 study conducted by Berroya *et al* reported that the mean spike frequency in sleep (45.6 per minute) was twice that during drowsiness, which was greater than twice the mean spike frequency during wakefulness (33 children that had recordings taken during wakefulness, drowsiness and sleep). This study also found that during drowsiness and sleep, the main effect was the increase in spike frequency rather than the spike location or the number of foci detected and that little difference in morphology was detected between the three states of awareness [Berroya et al., 2005]. Greater detail of the centrotemporal spikes present in epileptic disorders is given in section 1.7.2, particularly Benign Epilepsy of childhood with centrotemporal spikes (BECTS). Epilepsies with CTS are generally considered to be at the lower end of the spectrum of those epilepsies that present with paroxysm patterns [Loddenkemper et al., 2011]. The more severe manifestations of spike wave patterns in epilepsy are present in continuous spike and waves during sleep which is detailed below.

Continuous spike and waves during sleep

Continuous spikes and waves during sleep (CSWS) is an age-dependant epileptic encephalopathy which only occurs in children and presents with neurocognitive regression, seizures and displays an EEG component of usually generalised (near)-continuous spike and wave complexes during a significant portion of REM sleep, which can also be known as electrical status epilepticus during sleep (ESES) [Loddenkemper et al., 2011]. Generally, CSWS is considered to be the syndrome and ESES, the EEG pattern observed in patients with CSWS; however it is common for the two names to be used interchangeably. For this thesis, ESES will be used to describe the EEG pattern and CSWS will be used to describe the syndrome.

Loddenkemper *et al* (2011), stated that the ESES pattern can be defined as:

- The presence or the increase in amplitude of epileptiform discharges during sleep [Bureau, 1995, Tassinari et al., 2000]
- Near-continuous, bilateral, or occasionally lateralised slow spikes and waves [Bureau, 1995, Tassinari et al., 2000]
- Occurrence during a significant proportion of SWS, with the range varies dependent on study from 25 to 85% [Bureau, 1995, Tassinari et al., 2000, Yasuhara et al., 1991]

As with CTS, the more frequency locations of epileptiform activity during wakefulness are frontotemporal and centrotemporal regions, however it has also been proposed that to be classed as ESES epileptiform activity should not be present during wakefulness [Hughes, 1994]. As is also seen with CTS and Occipital spikes, during sleep the focal epileptiform discharges disperse and spiking becomes more generalised and more frequent, typically with the maximum being detected in the frontal or central region [Loddenkemper et al., 2011] as shown in Figure 1.11. However, during REM sleep the ESES pattern disappears [Bureau, 1995]. These generalised spike wave discharges (SWD) occur at a 1.5-2Hz rate. Although there has been instances where the typical SWD is devoid of the slow wave, leaving only the spike to be present [Michelucci et al., 1987]. The occurrence of the SWDs is generally partnered with the decrease in neurophysiological functions including the absence of new learning. Similar encephalographic properties are observed in patients with Lennox Gastaut Syndrome as well as the neurological deficits. This is described in more detail in the following subsection. ESES is generally considered to eventually be a self-limiting pattern that steadily disappears around 11 years of age which is on average 3-4 years after onset [Morikawa et al., 1995].

Many of the above spike and spike-related epileptiform patterns are associated with a range of neurological disorders. Some of the more prominent examples of which are introduced in the next section.

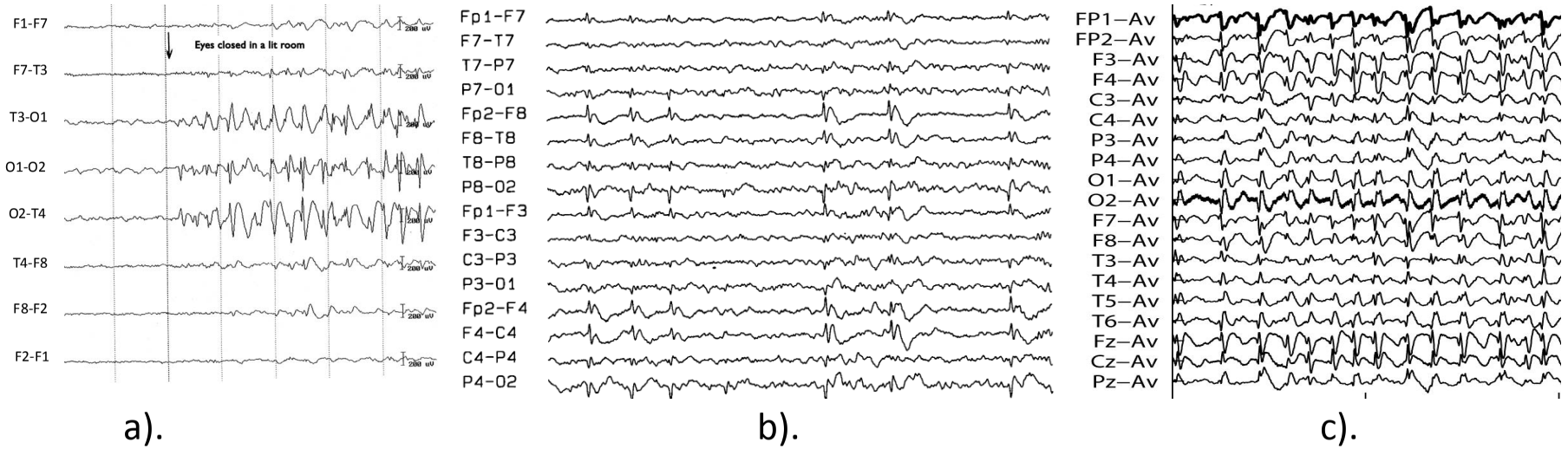

Figure 1.11: **Comparison of examples of Paroxysmal events. a).** Occipital spikes [Caraballo et al., 2008], **b).** Centrotemporal spikes [Pan et al., 2004], **c).** Electrical Status Epilepticus during Sleep [Bölsterli et al., 2011].

1.7.2 Epilepsies and Neurological Disorders

The EEG pattern of the above spike wave variants are associated with many types of epilepsies and neurological disorders as briefly outlined previously. Here, detailed examples of several such disorders are introduced:

Benign epilepsy of childhood with centrotemporal spikes

Benign epilepsy of childhood with centrotemporal spikes (BECTS), or Benign Rolandic Epilepsy is the most common idiopathic childhood epilepsy syndrome. It is called 'benign' because it generally has a good outcome - nearly all children with it will outgrow it during puberty. BECTS is first discerned between the ages of 3 and 13 years and commonly stops spontaneously around the age of 16. The syndrome is defined by: brief, simple, partial, hemifacial motor seizures frequently having associated somatosensory symptoms [Neubauer et al., 1998]. Nocturnal seizures often become generalized and are the most frequent form of seizure in this syndrome. Despite its the benign nature in terms of epilepsy, BECTS can be accompanied by specific cognitive disorders and low academic achievement [Pinton et al., 2006]. Pinton *et al* (2006) observed that of a group of 18 children with BECTS, IQ, verbal functions and memory were all considered normal for their age, however drawing and visuo-spatial skills, attention and visuo-spatial memory were significantly lower than would be normal for their age group. Reading, numeracy and spelling ability were all significantly delayed by one or more academic years in over 50% of the test subjects.

The EEG characteristic of BECTS are blunt, high-voltage shaped centrotemporal spikes often followed by slow waves as shown in figure 1.11b (also shown in figure 1.6b). Centrotemporal spikes, unlike BECTS itself, have been reported to follow an autosomal dominant path of inheritance with incomplete penetrance and age dependency and as such may be used to indicate an increased risk of developing BECTS [Neubauer, 2000]. Evidence for genetic linkage in BECTS has been found in the q14 region of chromosome 15, which is the location of the neuronal AChR α7 subunit (CHRNA7) [Neubauer et al., 1998]. Mount *et al* (1999) , discovered that the gene of a cation-chloride cotransporter (KCC4) is also located on chromosome 15q14. Cation-chloride co-transporters play a major role in controlling $GABA_A$ and glycine receptor mediated responses whilst also showing close interactions with glutamatergic signalling [Blaesse et al., 2009]. This relationship with glutamergic signalling may result in the transformation of normal delta oscillations into a tonically activated pattern during both waking and dreaming sleep [Steriade, 1994]. There is also evidence that there is no linkage to chromosome locations 6p21 (EJM1) [Whitehouse et al., 1993], the fragile X site 20q13 (EBN1) and

8q24 (EBN2) [Neubauer et al., 1997]. This is considered important as these locations have previously been linked to other epileptic disorders with similar nocturnal spike wave EEG traits (see below), suggesting a multiplicity of primary pathologies may converge to generate such spike and wave patterns.

Fragile X syndrome

Fragile X syndrome (FXS) is the most common cause of inherited retardation affecting ∼1 in 4,000 males and 1 in 8,000 females [Berry-Kravis, 2002]. Clinical features of FXS include: moderate to severe mental retardation; dysmorphic facial features; post pubertal macro-orchidism; behavioural abnormalities and seizures. Seizures are present in 10-20% of individuals with full mutation FXS and typically of the complex partial type [Porri and Korff, 2010]. The EEG trait of FXS is sudden bursting (paroxysmal) discharges of EEG spikes, mainly localised in the central or centro-temporal regions, with higher prevalence during sleep (i.e. rather similar to BECTS above). Porri *et al*'s (2010) EEG research revealed slow background activity with left fronto-temporal and bilateral occipital spikes during sleep. The morphology of these spikes were also similar to those seen in BECTS [Musumecia et al., 1991, Musumeci et al., 1999].

Evidence suggests that dysregulation of the metabolic glutamate receptor arising from absence of the *FMR1* protein, results in the activation of a voltage-gated inward current with a net increase in the excitability of neuronal circuits [Hagerman and Stafstrom, 2009]. This inward current may be the cellular basis for epileptogenic behaviour induced by activation of the metabotropic glutamate receptor 5 subtype [Bianchi et al., 2009]. The dysregulation of glutaminergic neurons in FXS can disrupt the normal actions of inhibitory GABAergic neurons. Hence, further increasing neuronal hyperexcitability by the downregulation of GABA receptor subunits and altering enzyme expression linked to the metabolism of GABA [D'Hulst et al., 2009].

Lennox-Gastaut syndrome

Lennox-Gastaut syndrome (LGS) is a form of childhood-onset epilepsy that appears between the ages of 2 and 6 years of age and is very difficult to treat. LGS occurs in between 1-5 children in every 100 who present with epilepsy, thus being the most common cause of intractable childhood epilepsy. Unlike other epilepsies, many forms of seizures can occur in LGS. The most commonly occurring seizure types are: tonic, which typically lasts less than 60 seconds during which muscle tone of exterior muscles is increased, 90% of which occur nocturnally. Atypical absences are also prevalent in this syndrome. As with other epilepsies, slow (1-2.5Hz) spike wave complexes (mostly around 2/sec) can be

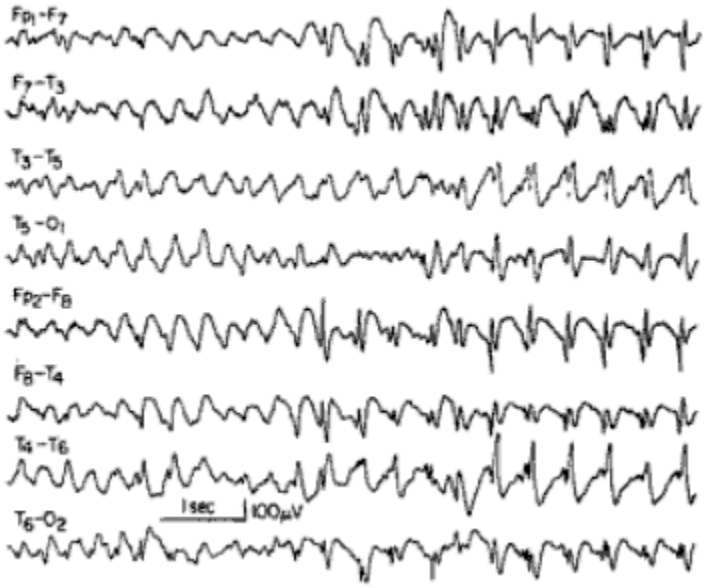

Figure 1.12: Generalised slow spike wave complexes (mostly around 2/sec) in a child with severe epileptic seizure disorder (Lennox Gastaut syndrome). *Taken from [Niedermeyer and da Silva, 2004a].*

observed using an EEG as shown in figure 1.12. [Siddiqui et al., 2007]. Clinical trials are currently being undertaken by Foletti *et al* (Institution de Lavigny, Switzerland) to explore the positive effects of melatonin administration to adults with LGS. Foletti *et al* have hypothesized that melatonin can reduce the epileptic activity observed via EEG during sleep whilst also stabilizing the structure of sleep. This hypothesis is supported by research from Peled *et al* (2001) who suggest that melatonin decreases seizure activity, particularly nocturnal seizures, in children with intractable epilepsy. There are several preliminary reports that indicate that melatonin possesses anti-epileptic properties attributed to its potent free radical scavenging properties [Peled et al., 2001, Kabuto et al., 1998]. Studies have shown that approximately 50% of those with LGS show no neurological deficit nor any evidence of brain disease [Gastaut and Gastaut, 1976, Zimmerman et al., 1977]. The remaining 50% show a wide variety of infantile brain lesions, which are usually linked to neurological deficits such as forms of cerebral palsy [Niedermeyer and da Silva, 2004b]. Mental retardation ranges from the most extreme to the slightest amount. There is a direct correlation between the age of onset and the level of mental retardation, however no mental retardation may be seen in those that present after the age of 10.

Rett Syndrome

Rett Syndrome (RTT), originally known as cerebroatrophic hyperammonemia, is a neurodevelopmental disorder of the grey matter of the brain that almost exclusively affects females. It is considered to be one of the most common causes of complex disability in girls [Smeets et al., 2011]. Originally characterized by Andreas Rett in 1954 and published in 1966, however it was only internationally recognised in 1983 after a Swedish

clinical study led by Bengt Hagberg [Hagberg et al., 1983] shared Rett's findings. As the syndrome progresses, the child can lose purposeful use of their hands which then leads onto apraxia. Most girls with RTT also have a varying degree of speech absence and generally display autistic-like behaviours. The dyspraxia and short attention span of these girls along with their lack of interest in play make it very difficult to gauge their developmental progress [Smeets et al., 2011]. EEG abnormalities are almost always seen. Spikes are common over the central regions, particularly during sleep. These spike wave complexes are similar to those seen in BECTS: centro-temporal spikes. However, unlike in BECTS, there have been cases where these CTS have been blocked or attenuated by passive finger movements [Niedermeyer and Sakkubai, 1990]. In 1999, it was discovered that a mutation of the *MECP2* gene, located at the Xq28 site on the X chromosome, was responsible for Rett syndrome [Amir et al., 1999]. Hence, RTT was the first neurodevelopmental disorder related to a defective transcription of methylated DNA [Smeets et al., 2011].

Childhood absence epilepsy

Childhood absence epilepsy (CAE) is an idiopathic generalised epilepsy characterised by absence seizures. These show as a loss of awareness accompanied by bilateral, symmetrical, 2.5-4Hz spike and wave complexes in the EEG [Everett et al., 2007, Cerminara et al., 2012]. CAE is first observed in school-going children. They typically have 10-200 episodes a day brought on by hyperpnea, an abnormal increase in the rate and depth of breathing [Fehrenbach et al., 2007], in the form of absences and atypical absences [Siddiqui et al., 2007]. Children with CAE were thought to outgrow their disorder with little lasting effect to behaviour and cognitive ability, however recent studies have shown this not to be the case [Pavone et al., 2001, Caplan et al., 2008]. Caplan *et al* (2008) reported that when a cohort to 69 children aged 9.6 years were compared against an age and gender matched control group, 25% had subtle cognitive deficits, 43% linguistic difficulties, 61% a psychiatric diagnosis and 30% clinically relevant child behaviour checklist scores.

Everett *et al* (2007), have provided genetic evidence to indicate that *CACNG3* is a susceptibility locus for CAE. The *CACNG3* gene encodes the voltage-dependent calcium channel γ_3 subunit, thus mutations in this gene cause increased channel activity resulting in increased neuronal excitability. Cerminara *et al* (2012), have recently reported on rare cases where the child suffered from both CAE and BECTS. While these are two distinct epileptic conditions, recent observations in animal models suggest that they would be pathophysiologically related and that genetic links could play a large role [Cerminara et al., 2012].

Landau-Kleffner syndrome

Landau Kleffner Syndrome (LKS) is also referred to as 'children with midtemporal spikes, progressive aphasia and seizures' [Niedermeyer and da Silva, 2004b]. LKS is the most studied form of syndrome associated with CSWS. LKS is found in children approximately 5 years old. Speech patterns and vocabulary deteriorate and eventually become limited to a few words. Inter-ictal EEG shows SWDs, predominantly over the left midtemporal region, but generalised spike-wave bursts do occur with these discharges becoming attenuated during non-REM sleep [Metz-Lutz and Filippini, 2006].

In a high proportion of children with LKS, phonological short term memory is impaired and is linked to one-ear extinction involving the channel on the opposite side of the head that the SWDs are observed on during an active epileptic period [Metz-Lutz and Filippini, 2006]. Other cognitive deficits observed in LKS include: verbal and non-verbal short term memory and loss of language. A recent study by Lesca *et al* (2012), proposed that there are several genomic regions or genes (*ATP13A4, CDH9, CNTNAP2, CTNNA3, DIAPH3, GRIN2A, MDGA2, SHANK3*) that are linked to LKS. Most importantly these genes or regions are also associated with autism disorders or involved in speech or language impairment.

Autosomal dominant nocturnal frontal lobe epilepsy

Autosomal dominant nocturnal frontal lobe epilepsy (ADNFLE) is a dominantly inherited disorder with high pentrance (70-80%) characterised by clusters of short motor seizures during SWS. These seizures vary from simple arousal from sleep to dramatic hyperkinetic events and only a minority experience these seizures during wakefulness [Kurahashi and Hirose, 2002]. Interictal EEG recordings are usually normal however 12-65% of patients have frontal lobe epileptiform abnormalities, mainly during sleep [Panayiotopoulos, 2008, Olandi et al., 1998]. These abnormalities are generally not seen in succession, like those observed in BECTS (figure 1.11b) instead they are single occurrences. Picard *et al* (2009) reported reduced intellect in 45% of 11 subjects. Executive tasks were particularly affected. In cases of severe ADNFLE, there is approximately a 25% [Derry et al., 2008] chance of a degree of mental retardation in comparison to typical affected individuals who measure as normal intelligence.

Gene mutations relating to ADNFLE are rare, however several mutations have been identified in different families in the genes encoding subunits of neuronal nAChRs: α_4 (CHRNA4) [Marini and Guerrini, 2007, Steinlein et al., 1995] and β_2 (CHRNB2) [Siddiqui et al., 2007]. In the families that show no linkage to the previous genes, they

show strong linkage to chromosome 15 (15q24) near α_3 (CHRNA3), α_5 (CHRNA5), β_4 (CHRNB4) [Marini and Guerrini, 2007, De-Fusco et al., 2000]. Picard *et al* (2006) recently performed a positron emission tomography (PET) study in a group of ADNFLE patients with known mutations and showed significant regional changes in brain nAChRs density. Such findings point towards an over activated cholinergic pathway ascending from the brainstem [Picard et al., 2006]. An additional finding of this study was a decrease of receptor density in the prefrontal cortex, which was hypothesized to reflect progressive neuronal loss caused by seizure activity [Picard et al., 2006]. Steinlein *et al* (2012) suggested that nAChR may be responsible for the increased risk for major neurological systems such as mental retardation and marked cognitive deficits.

1.7.3 Learning disabilities and Epilepsy

As previously discussed in Section 1.6, memory consolidation is thought to occur during sleep, particularly SWS and REM. Over the past 10 years, there have been many papers published discussing how the disruption of sleep may have a negative effect on the cognitive development of individuals with epilepsy [Parisi et al., 2010]. The data discussed in these papers are mainly related to nocturnal EEG epileptiform activity, such as those observed in childhood nocturnal epilepsy syndromes. As has been briefly described, cognitive dysfunction is prevalent in most childhood epileptic disorders, whether they are malignant or benign. Table 1.1 summarises the previously detailed syndromes and the cognitive dysfunction observed in affected individuals.

In patients with epilepsy it is common for the polysomnogram to show elevated states of sleep fragmentation and a greater proportion of wakefulness and light sleep. This is paired with a decrease in stages 3 and 4 (SWS) and REM [Touchon et al., 1991] in which memory consolidation occurs. However, it has also been documented that SWDs during interictal activity may also result in marked sleep instability [Parisi et al., 2010]. These epileptic bursts are known to elicit arousal, whether by physiologic movement, muscle jerk or an epileptic attack [Parrino et al., 2006]. Parisi *et al* (2010) proposed that if nocturnal epileptiform activity regularly occurs in a specific area involved in learning, it may hinder neuroplasticity processes. This theory is supported by the impairment of language skills in LKS following persistent left frontotemporal epileptiform activity, and the impairment on executive tasks observed in ADNFLE [Picard et al., 2009]. Interestingly, a transient version of this effect was documented by Aarts *et al* in 1984. A study of 46 participants with subclinical EEG discharges were asked to perform two short term memory tests, one verbal and one non-verbal. When discharges were present, performance was disrupted in comparison to when the discharges were not present (the control). Therefore if this dis-

ruption were to occur during the consolidation process during sleep, particularly SWS, it is proposed that there will be a long term effect on memory and hence, learning. Holmes and Lenck-Santini's work corroborates this theory. In a 2006 paper, they suggested that:

> "Interictal spikes can result in transitory cognitive impairment with the type of deficit dependent on where in the cortex the spike arises. We suggest that interictal spikes, particularly if frequent and widespread, can impair cognitive abilities, through interference with waking learning and memory, and memory consolidation during sleep."

Syndrome	**Cognitive Dysfunction**	**EEG trait**	**Gene Mutation**
Benign Epilepsy of Childhood with Centro-Temporal Spikes	visuo-spatial skills visuo-spatial memory drawing attention literacy numeracy	CTS	*CHRNA7* *KCC4*
Fragile X syndrome	moderate to severe mental retardation	CTS OS during sleep	*FMR1*
Lennox-Gastaut syndrome	range of mental retardation in 50% none when onset over 10 years	generalised slow SWC	-
Rett syndrome	dyspraxia attention autistic-like behaviour	CTS	*MECP2*
Childhood Absence Epilepsy	below average IQ language attention (visual, verbal and non-verbal) thinking visuo-spatial skills memory (verbal and non-verbal)	bilateral, generalised slow SWC	*CACNG3*
Landau-Kleffner Syndrome	Language Short term memory (verbal and non-verbal)	CSWS SWC	-
Autosomal Dominant Nocturnal Frontal Lobe Epilepsy	executive tasks	frontal SWC	*CHRNA4* *CHRNB2* *CHRNA3* *CHRNA5* *CHRNB4*

Table 1.1: Summary table of the previously described neurological and epileptic disorders related to abnormal EEG. CTS - Centro-Temporal Spikes, OC - Occipital Spikes, SWC - Spike Wave Complexes.

1.8 Aims and Objectives

This chapter has reviewed and outlined the current understanding of the neurobiology of sleep, epileptic and neurological disorders related to sleep and the physiological functions. Sleep has been studied extensively using EEG and both *in vivo* and, fairly recently, *in vitro*. As has the pathophysiology of epilepsy and neurological disorders related to sleep. However, the mechanisms behind the EEG traits observed in these disorders is currently lacking. The aims of this thesis are therefore as follows:

- To establish an *in vitro* model of the SWD observed in both childhood epilepsies and neurological disorders related to sleep.
- To elucidate the pharmacological properties of the SWD
- To study the activity of individual neurons during delta rhythms interspersed with SWDs and establish the contribution of specific types of neuron to the phenomenon in order to determine the cellular basis of the pathology and the interactions between local neuronal populations in superficial and deep layers of the neocortex.
- Finally, to design a method of improving the current *in vitro* recording methods to allow for better understanding of the interactions between local neuronal populations.

1.9 Thesis Outline

Chapter 2 details the methods and procedures followed during experiment preparation, the equipment and recording techniques employed in the accruement of data and the analytical procedures exercised to both the online data and post hoc data.

Chapter 3 details the nature of seizure discharges associated with sleep by referring to clinical data and studies. Once an understanding is achieved of the epileptiforms present within nocturnal epilepsies then an *in vitro* model can be investigated.

Chapter 4 presents work carried out with the aim of understanding the competitive, non-selective nicotinic acetylcholine receptor antagonist, d-tubocurarine also known as DTC. The chapter presents the results from extracellular studies, including laminar profiles and epileptiform activity from the somatosensory region of the rodent cortex. The chapter concludes in a discussion on the possible mechanisms of DTC and it's inducement of epileptiform activity.

Chapter 5 focusses on the research conducted to understand which receptor subunits are responsible for an increase in power of delta frequency oscillations and the inducement of epileptiform activity similar to that present in EEG recordings of nocturnal childhood epilepsies.

Chapter 6 presents a number of intracellular recording studies designed to uncover the neuronal subtypes and their input and output characteristics during DTC-induced epileptiform activity. This chapter also utilised the spatiotemperal recording capabilities of multichannel electrode arrays.

Chapter 7 details some of the current recording methods available in electrophysiology. This background information then supports the work and research presented with the aim of fabricating a solid state electrode array for intracellular recordings. A mechanical efficacy study and an electrical efficacy study are detailed in this chapter.

Chapter 8 summaries the aims and outcomes from each individual chapter. It also briefly details the Future work which could follow this thesis.

Chapter 2

Electrophysiological Methodology

2.1 Animal Provision

The majority of slices used in the course of this thesis were taken from young adult male Wistar rats, aged between 2 months and 4 months old, weighing >150grams. These were supplied by Charles River (Margate, UK). Adult male C57 mice were also supplied by Charles River. Animals were maintained on a 24-hour light dark cycle with free access to food and water with environmental enrichment.

2.2 Animal Procedures

All procedures involving animals were carried out in accordance with the UK Animals (Scientific Procedures) Act 1986. Rats and mice were first anaesthetised by brief inhalation of isofluorane at a sufficient concentration to induce light anaethesia within 2 minutes of exposure, typically 3-4mls in a 5 litre bell jar. Animals were removed from the bell jar once the righting reflex had been overcome. Animals were given an intramuscular injection in the gluteal region with 0.3mls ketamine (dose ∼100mg/kg rat, ∼300mg/kg mice, Pfizer, Inc. NY, USA) and 0.3mls of 2% Xylazine (dose ∼10mg/kg, ∼30mg/kg, Animalcare, York, UK). When all responses to noxious stimuli, such as toe pinch and corneal reflexes, had completely subsided, the anterior thoracic wall was removed to expose the heart. A catheter was inserted into the left atrium and was mechanically perfused with ∼50ml of oxygenated sucrose-modified artificial cerebrospinal fluid (sACSF, see Section 2.5) at a rate of approximately 0.6-0.8mls/sec. The right atrium was perforated prior to perfusion to permit exsanguination during the sACSF perfusion. The intracardial perfusion of sACSF was undertaken to improve the viability of neurons [Kuenzi et al., 2000] and [Aghajanian and Rasmussen, 1989].

2.3 Preparation of Cortical slices

The animal's spinal cord was severed and an incision was made along the midline of the headline to expose the skull of the animal. The skull was dissected in the midline along the sagittal suture in a caudal to rostral direction. The skull bones were carefully removed, and the brain cleared of any adherent dura matter. The cerebrum, along with the cerebellum and medulla were extracted from the skull cavity and placed in ice cold oxygenated sACSF. The brain was trimmed of the cerebellum, hindbrain and frontal lobes (figure 2.1).

The caudal side of the tissue block was promptly glued to the plate of the Leica VT1000 microtome (Leica Microsystems, Nussloch GmbH, Germany) and was immersed in ice-

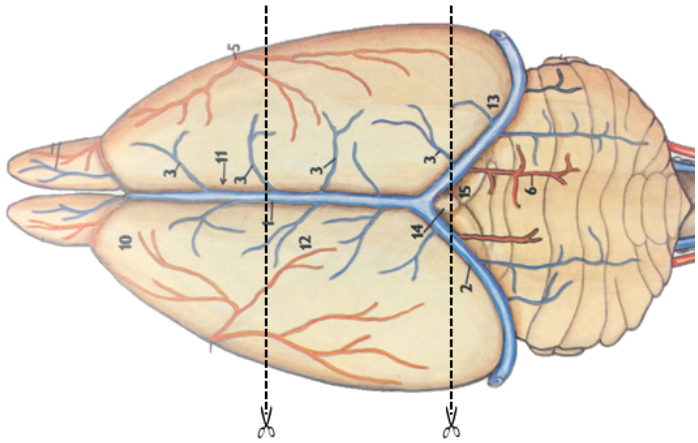

Figure 2.1: Dorsal view of the rat brain [Popesko et al., 1990]

cold oxygenated sACSF. The tissue block was cut in the coronal plane into 450μm thick slices. Individual slices were collected in a petri dish containing oxygenated ice-cold sACSF. Only slices containing the hippocampi were collected to allow for simple location of the primary Somatosensory region. The slices were then dissected coronally along the midline and saggitally, lateral to the lateral posterior thalamic nucleus as shown in figure 2.2.

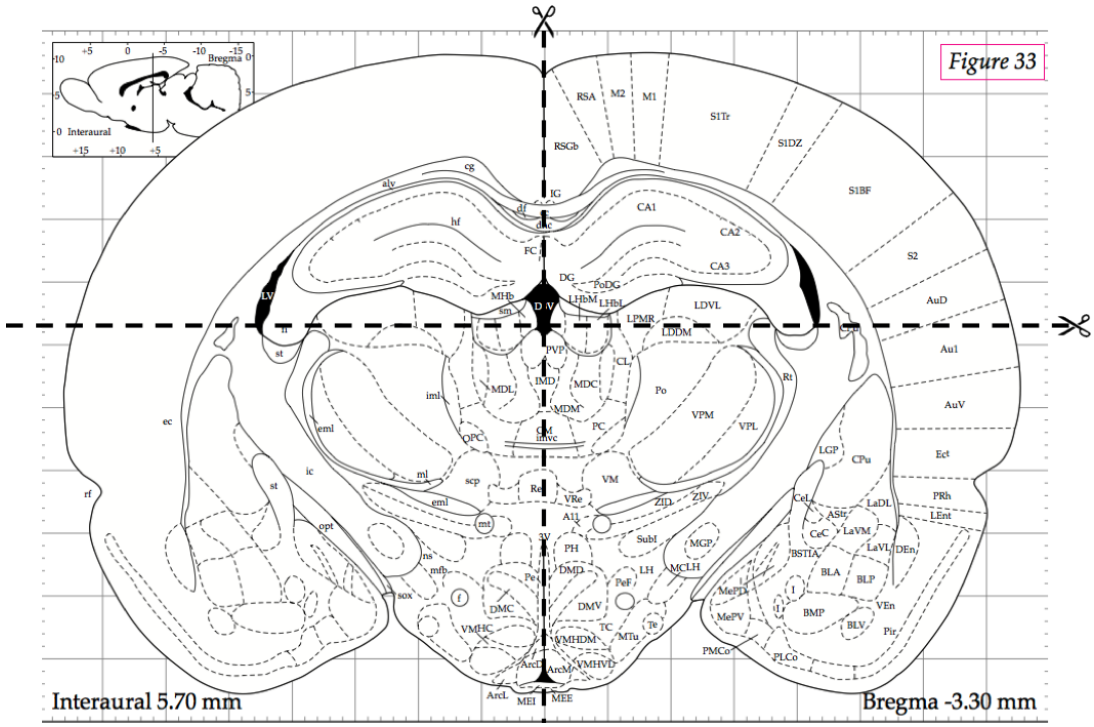

Figure 2.2: Schematic of coronal slice dissection [Paxinos and Watson, 1998]

2.4 Slice Maintenance

After slicing, tissue was relocated to a holding chamber, which maintained slices at room temperature in oxygenated ACSF. After slices had equilibrated for approximately 45 minutes, two slices were transferred to an interface recording chamber for the duration of experiments and were placed on a bilayer of lens cleaning paper. Slices were maintained at ∼32±1°C, at the interface between continuous perfusion of NaCl-based ACSF (see Section 2.5) and 100% humidified carbogen gas (95% O_2/5% CO_2) atmosphere. ACSF was circulated through the chamber using a Gilson Minipuls 2 peristaltic pump (Gilson, Inc. WI, USA) at a rate of 2-3mls/min. Spare slices were stored in a holding chamber at the interface between oxygenated ACSF and humidified carbogen gas at room temperature. The remaining tissue slices maintained in the holding chamber and the slices in the recording chamber remained healthy for approximately 10 hours.

2.5 Drug Stocks and Materials

Sucrose-modified artificial cerebrospinal fluid (sACSF) was composed of [in mM]: sucrose, 252; $NaHCO_2$, 24; KCl, 3; NaH_2PO_4, 1.25; $MgSO_4$, 1;$CaCl_2{\cdot}H_2O$, 1.2; glucose, 10. All salts were obtained from BDH Laboratory Supplies (Poole, UK), except $MgSO_4$, which was obtained from Sigma Aldrich (MO, USA) and $NaHCO_2$ and Sucrose, which were obtained from Fisher Scientific (MA, USA). Artificial cerebrospinal fluid (ASCF) was of an identical composition except sucrose was replaced with an equiomolar concentration [126mM] of NaCl.

In general, stock drug solutions were made by dissolving the drug salt in distilled ultra pure H_2O. Drugs that were insoluble in distilled water were dissolved in dimethylsulfoxide (DMSO; Sigma Aldrich, MO, USA). Drug solutions were added directly to the ACSF reservoir perfusing the bath at known concentrations. In the case of stocks prepared in DMSO, the final DMSO concentration was never above 0.1% v/v. The drugs/chemicals and concentrations at which they were used in the course of this thesis are listed in Table 2.1.

Drug	**Chemical Name**	**Concentration**	**Supplier**
α-Conotoxin AulB		200nM-1μM	Tocris
α-Conotoxin PnlA		1-10μM	Tocris
Atropine	endo-($\pm$)-α-(Hydroxymethyl)benzeneacetic acid 8-methyl-8-azabicyclo[3.2.1]oct-3-yl ester	20μM	Sigma Aldrich
Carbachol (CCh)	(2-Hydroxethyl)trimethylammonium chloride carbamate	4μM	Tocris
Conotoxin Vc1.1 (ACV 1)		200nM-1μM	Tocris
Cyclothiazide (CTZ)	6-Chloro-3,4-dihydro-3-(5-norbornen-2-yl)-2H-1,2,4-benzothiazidiazine-7-sulfonamide-1,1-dioxide	10-20μM	Tocris
D-AP5	D-(-)-2-Amino-5-phosphonopentanoic acid	20μM	Tocris
Dihydro-β-erythroidine hydrobromide (DHβE)	(2S, 13bS)-2-Methoxy-2,3,5,6,8,9,10,13-octahydro-1H, 12H-benzo[i]pyrano[3,4-g]indolizin-12-one hydrobromide	10-20μM	Tocris
DMSO	Dimethylsulfoxide		Sigma Aldrich
MG 624	N,N,N-Triethyl-2-[4-(2-phenylethenyl)ethanaminium iodide	1-10μM	Tocris
Pancuronium dibromide	1,1'-(3α,17β-Dihydroxy-2β,5α-androstan-2β,16β-ylene)bis[1-methylpiperidinium] diacetate dibromide	2-10μM	Tocris
Potassium Acetate (KAc)		$\sim$2M	Sigma Aldrich
SCH23390 Hydrochloride	(R)-(+)-7-Chloro-8-hydroxy-3-methyl-1-phenyl-2,3,4,5-tetrahydro-1H-3-benzazepine hydrochloride	7μM	Tocris
(+)-Tubocurarine chloride (DTC)	2,3,12a,14,15,16,25,25a,-Octahydro-9,19-dihydroxy-18,29-dimethoxy-1,14,14-trimethyl-13H-4,6:21,24-dietheno-8,12-metheno-1H-pyrido[3'.2':14,15][1,11]dioxacycloeicosino[2,3,4-ij]isoquinolinium chloride hydrochloride	2-10μM	Tocris
MDL 72222	Tropanyl3,5-dichlorobenzoate	1-10μM	Tocris
SR 95531 (Gabazine)	6-Imino-3-(4-methoxyphenyl)-1(6H)-pyridazinebutanoic acid hydrobromide	500nM-5μM	Tocris

Table 2.1: Drugs used throughout the duration of this thesis

2.6 Recording Techniques

Micropipettes for extracellular field potential recordings were made from thin wall borosilicate glass capillaries (1.2mm O.D. x 0.94mm I.D.) containing an inner filament (Harvard Apparatus Ltd., Edenbridge, Kent, UK) using a Narishige PP-83 electrode puller (Narishige, Japan). Micropipettes were filled with the same ACSF solution perfusing the recording chamber. The tip resistance of extracellular electrodes ranged between 2-6MΩ.

Sharp microelectrodes for intracellular recording were made from standard wall borosilicate glass capillaries (1.2mm O.D. x 0.69mm I.D.)(Harvard Apparatus Ltd.) containing an inner filament (Harvard Apparatus Ltd.) using a model P-97 Flaming/Brown-type horizontal puller (Sutter Instruments Co., Novato, CA, USA). Sharp microelectrodes were filled with [2M] potassium acetate. The tip resistance of intracellular electrodes was in the range 50-250MΩ. Cells were recorded in standard bridge-mode mode.

Once the slices in the recording chamber had fully equilibrated to 32°C, extracellular electrodes were placed in layer V of the primary somatosensory cortex. Viewing the slices under a microscope allows electrodes to be accurately positioned by the use of a manipulator. Control recordings of activity were taken prior to the addition of pharmacological agents, to ascertain whether later oscillatory activity was an effect of the drugs applied. Electrodes remained in the same position throughout the stabilisation period of the oscillations and then the pharmacological experiments. Carbachol and SCH23390, the main delta-oscillogenic compounds utilised in this thesis, were bath applied to the circulating ACSF and evoked a persistent oscillation. The oscillations evolved over approximately a 2 hour period at which point oscillations were deemed stable when three delta power recordings over 15 minutes varied less than 10%. Once stability had been achieved, pharmacological manipulations or laminar profiles were performed.

For spatial analysis experiments, electrode arrays were used once delta activity had been established and confirmed through the use of glass micro electrode recordings. Multielectrode recordings of local field potentials and unit activity were detected using three dimensional silicon electrode grids, specifically Utah Electrode Arrays (UEAs) (Cyberkinetics Inc, USA). These grids were composed of a 10 x 10 array of 1.5mm long silicon microneedles that projected out from a 4mm x 4mm x0.25mm thick substrate, with each individual electrode having an impedance ranging from 230-370kΩ. UEAs were mounted onto a Teflon head stage holder (Molecular Devices) using epoxy, which were then installed onto a 3D patch manipulator (Scientifica, UK). To ensure that the electrode tips were in the same plane as the surface of the slice in the recording chamber, the electrode

assembly was aligned to the upper surface of the recording chamber in both the x and y axes. The UEA was then located over the are of interest in the slice and lowered onto the surface of the slice to give a penetration of no more than 50μm into the slice.

2.7 Data Acquisition

2.7.1 Glass microelectrode recording

The signals detected from the slices were first amplified by pre-amplifiers present within the headstages. Extracellular signals were recorded in current-clamp mode, band-pass filtered at 0.0005-0.2kHz and amplified by an Axoprobe-1A amplifier (X10 Axon Instruments Inc., Union City, CA, USA). Intracellular recordings were recorded in DC mode and low-pass filtered at 2kHz using an external Brownlee Precision Instrumentation Amplifier (Brownlee Precision Co. CA, USA). 50Hz mains noise was eliminated from the raw signal by adaptive filtering via Humbugs (Quest Scientific Instruments Inc., North Vancover, Canada). Data was subsequently redigitised at 5kHz by an Instrutech ITC-16 A/D board (Instrutech Corp., NY, USA). Data was stored on an Apple Macintosh G4 computer using AxoGraph X software (Axon Instruments) for off-line analysis.

2.7.2 Multi-electrode array recording

Utah electrode arrays were connected to a 128 channel Cerebus digitiser/amplifier following analogue pre-amplification. Data was collected online from the array using Central (Blackrock Microsystems Inc, USA), digitised at 30kHz, and then saved for offline analysis in Neuroexplorer (Nex Technologies, Littleton, USA). The time series data from each channel was saved continuously after filtering (0.1-500Hz) and down sampled to 2kHz. In addition to this data, timestamps for unit data and the digitised template for each detected spike were also saved for *post-hoc* analysis. Spike detection parameters were manually set and performed online during data collection using a combination of threshold crossing and 2-window template matching. Unit time stamps and local field potential (LFP) time series were exported to Matlab (The MathWorks Inc.) for further offline analysis.

2.8 Data Analysis

Data were analysed offline using Axograph X (Axon Instruments Inc., Union City, CA, USA), Minitab 16 (Minitab Inc, USA), Microsoft Excel (Microsoft Corp.), SigmaPlot 11.0 (Systat Software Inc, USA) and Matlab R2011b (The Mathworks Inc., Natick, MA,

USA) software packages. Microsoft PowerPoint (Microsoft Corp.) was used for the presentation of data. The properties of oscillations were defined by several parameters:

- the modal peak frequency of oscillation,
- power of oscillation within a particular frequency band,
- area power of oscillation and
- rhythmicity.

Power spectra of network activity, which quantitatively defines the frequency components of oscillatory activity, were used to assess these oscillatory properties. Power spectra were derived from 60-second epochs of data, whereby a Fast-Fourier Transform algorithm breaks down the oscillation into its constituent sinusoidal waveform components and calculates the power of each waveform. Data is subsequently plotted as a sum of squares of the voltage at a specific frequency, over a range of frequencies (0.3-10Hz).

2.8.1 Analysis of Network Oscillations

Most data presented in Chapters 4 and 5 of this thesis is in the form of individual power spectra. Mean peak frequency and amplitude of oscillation were calculated from pooled data. A systematic analysis of changes in oscillatory activity is undertaken by measuring the power of the oscillations corresponding to a relevant range of frequencies, such as activity in the delta range. The oscillatory power was calculated as the area under the spectra between two specific frequency boundaries. Power in the delta range was calculated between 0.5 and 5Hz.

The rhythmicity of an oscillation was calculated via autocorrelation analysis of a 1 second epoch of extracellular data. An autocorrelation is a measure of how a signal is correlated with itself. The resultant graph generally looks similar to a sinusoidal damping curve, with the strength of the signal being plotted against time. The rhythmicity can be calculated from the autocorrelation by measuring the amplitude of the first side peak on the Y axis. The mean peak frequency can also be determined due to the inverse relationship between time and frequency. Whereas cross-correlation analysis calculates the similarity between two 1 second epoch recordings. If both signals are synchronised, the resultant graph is sinusoidal. Cross correlation was used to measure the synchrony between the oscillatory activity at two recording sites and used to determine the phase-lag between the two sites. The position of the central peak on the Y axis at time 0 determines the synchrony between the two sites whilst the side peak on the X axis is a measure of the phase lag.

Within the confines of this thesis, an epileptiform form is characterised as an anomalous event when compared with the oscillatory activity preceding and following it. When epileptiform activity was detected during a 60 second epoch of extracellular data, each individual occurrence was categorised as either a wave discharge (WD) or a spike wave complex (SWC). A wave discharge had to have an amplitude of $>200\mu$V peak-to-peak, a smooth trace with no spikes interrupting the wave and easily distinguishable from the general LFP activity. The only difference between a wave discharge and a spike wave complex was that, a SWC needed to have a spike present during the wave, the position within the wave was inconsequential. The number of WDs and SWCs was recorded for each 60 second epoch of data. This data could then be used to calculate the incident rate of each epileptiform activity category, the total number of occurrences and the effect of drug concentration on epileptiform activity within the region recorded from.

Spectrograms were produced to understand the frequencies embedded within the epileptiform activity, this would also allow for a categorical difference to be observed between the two epileptiform categories. Using Matlab (Mathworks), an epoch containing epileptiform activity, generally 1 second in length, was extracted from a 60 second recording. It was then filtered using a butterworth, highpass filter using the Matlab *SOSfilt* function (Fs=5kHz, Fstop=4Hz, Fpass=6Hz, Astop=20dB, Apass=1dB). This filtered data was then processed using the Matlab *spec* function to produce a spectrogram with 8192 bins. The maximum and minimum limits for the colourmap for the spectrogram were set to 0.05 and 0.01 respectively. Due to the frequencies of interest in this reasearch, the y axis was always set to 100Hz.

2.8.2 Analysis of Intracellular Activity

Sharp electrode recordings of cells which had a resting membrane potential negatively greater than -50mV and action potentials which were reaching over 0mV were recorded. Electrophysiological characterisation of these cells was achieved using a 0.2nA depolarising or a 0.3nA hyperpolarising current injection step with a duration of approximately 200ms [McCormick et al., 1985]. Figure 2.3 shows examples of the intrinsic characteristics of the cell subtypes studied: Regular spiking (RS) neurons and intrinsic bursting (IB) neurons. Layer V RS cells were defined from the position of impalement in the slice (Layer V) and the slow, accommodating action potentials with slow after hyperpolarisations (AHPs) (Figure 2.3A). The same method was utilised for RS cells in layers II and III (Figure 2.3B). IB cells in Layer V displayed a very different response to the depolarising current injection. Single bursts of activity were seen consisting of multiple APs, in

many cases these were superimposed on a slow depolarising envelope followed by very slow afterhyperpolarisation (Figure 2.3C). Excitatory postsynaptic potentials (EPSPs) were gained by hyperpolarising cells to the point where action potentials no longer fired, typically -75mV with a DC current injection. Inhibitory postsynaptic potentials (IPSPs) were gained by increasing the membrane potential of the cell to -30mV by injecting a positive DC current.

2.8.3 Analysis of Utah Data

Each of the 96 active channels was individually inspected for unit activity using Central software (Blackrock Microsystems Inc. USA). If units were found to be present, these were labeled using different coloured 'windows'. Concurrently, characterisation of these units was attempted, whereby units were initially characterised by their location in the slice, i.e. within the Superficial Layers (Layer I-III) or the Deep layers (Layer IV-VI). This was then developed by noting if the spike rate was regular or bursting, as this information would lead to classifying units as Superficial Regular Spiking (SRS) cells, Deep Regular Spiking (DRS) cells or IB cells. This process was applied for each slice and for each drug concentration.

Unit data was exported to Neuroexplorer where further analysis was applied (spike synchrony analysis (time distance to the nearest spike between pairs of units), spike-spike correlations and spike-field correlations). The numerical outputs of this analysis was exported to Matlab for thresholding and pictorial representation with reference to electrode positions in the slice.

For spike-spike correlations, cross-correlations were performed between each pair of units and connectivity was quantified by extracting the y-axis value of where the central peak intercepted the Y-axis. For spike-field correlations, correlations with continuous variables were preformed between the unit spike rate histograms and the LFPs for each unit and LFP combination. The correlations was similarly quantified, by extracting the intercepting point of the central peak on the Y-axis.

With regards to LFP data recorded via the utah array, maps of the spatial distribution of the activity were produced using MatLab, where they were mapped with reference to electrode positions in the specific Utah grid used. This was the interpolated and illustrated in a two dimensional 'surf' plot with a 'jet' colourmap.

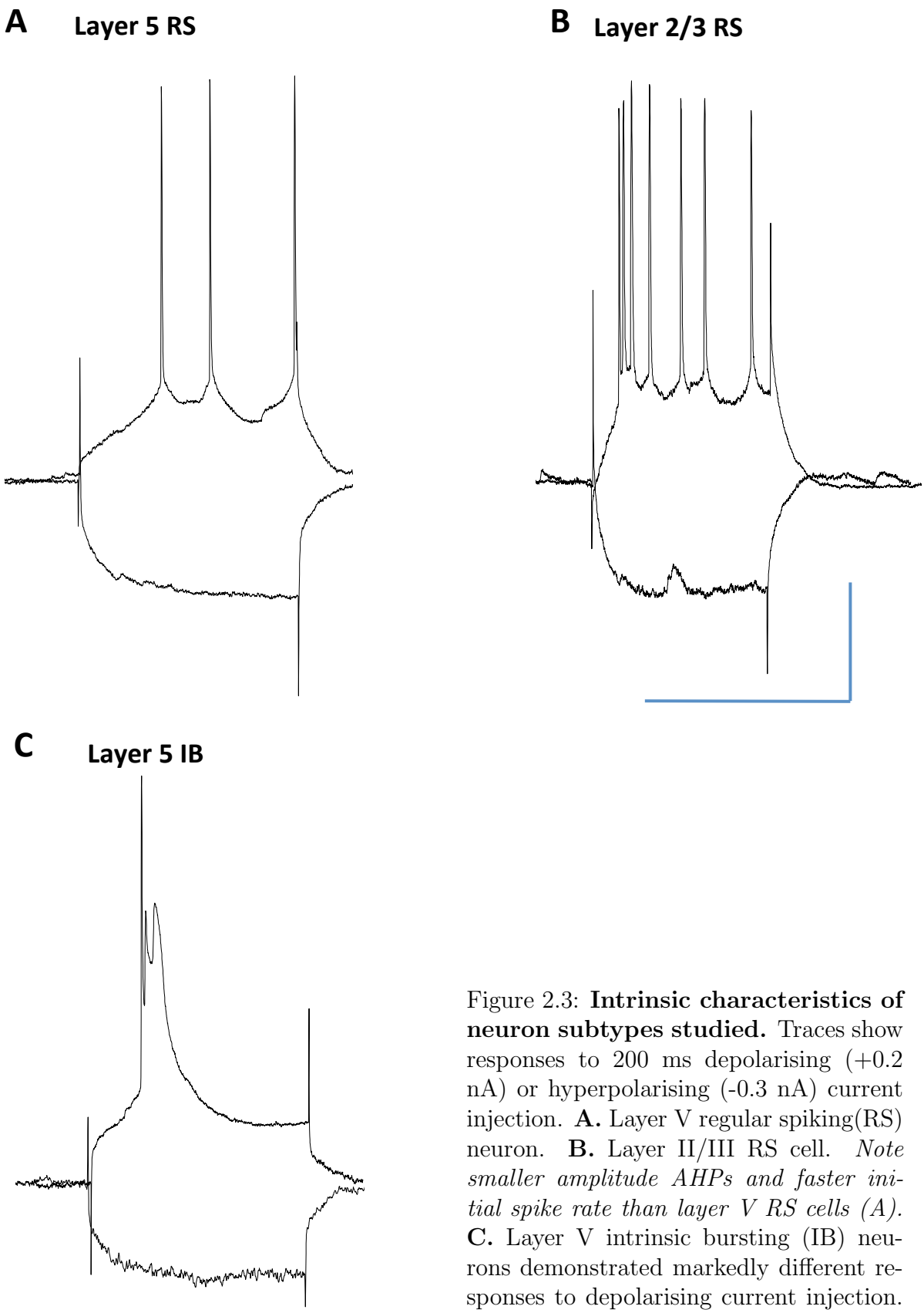

Figure 2.3: **Intrinsic characteristics of neuron subtypes studied.** Traces show responses to 200 ms depolarising (+0.2 nA) or hyperpolarising (-0.3 nA) current injection. **A.** Layer V regular spiking(RS) neuron. **B.** Layer II/III RS cell. *Note smaller amplitude AHPs and faster initial spike rate than layer V RS cells (A).* **C.** Layer V intrinsic bursting (IB) neurons demonstrated markedly different responses to depolarising current injection. Scale bars 200 ms, 20 mV.

2.9 Statistical Analysis of Data

Statistics were calculated on filtered data using SigmaPlot 11 software (Systat Software Inc., San Jose, CA, USA). Data was primarily analysed to determine whether the data was normally distributed. Normally distributed data was presented as mean ± standard error of the mean (S.E.M.). Paired t-tests were also used on the normally distributed data to measure any differences between the mean of before and after a manipulation from the same slice. However, if the data was not from the same slice, an unpaired t-test was used. A One-way Analysis of Variance (ANOVA) test calculates the difference between the means of two or more data sets, and was used to help determine whether any significant changes were seen in the oscillatory response to drug/concentration changes. Alternatively, if the data was not normally distributed it was expressed as a median value with it's interquartile range (displayed as x $\rightarrow$ y). The Mann-Whitney Rank Sum Test provided an alternative to the t-test when handling not normally distributed data, whereby differences in the medians of the two sets of data were compared. Results were deemed statistically significant if $P<0.05$.

Chapter 3

Quantification and modelling of spike and wave discharges

3.1 Introduction

This brief chapter will consider in greater detail the nature of seizure discharges associated with sleep. The aim is provide a clinical reference point to be able to understand the success of the models used in later chapters and to see what can be learnt relating to putative epileptogenic mechanisms.

3.1.1 Detailed features of spike and wave discharges use for detection

Syndromes in which spike and wave discharges are associated with sleep are numerous as previously detailed in chapter 1. Interestingly, despite the obvious nature of these discharges when examining EEG traces 'by-eye', it has proven difficult to automate this process. This may in part be due to the variability between patients and also the variability in the morphology of the discharges associated with sleep (e.g. simple centrotemporal spikes, spike and wave discharges, polyspike and wave discharges and continous spike and wave discharges (CSWS)). This section will concentrate on wave discharges (WD) as a derangement of normal delta rhythms, whilst spike and wave discharges will be considered as themselves as they account for the main form of epileptic activity seen during experiments in this thesis.

The majority of methods that are used for detecting sleep-associated and related absence seizures rely on the two keys features of the discharges - the slow wave and the kinetically faster spike. These are reasonably preserved whether they occur as discrete,

single events or in runs (multiple consecutive events). Clincial data shows epochs of large amplitude (0.1-1mV) spike and wave discharges lasting from approximately 1 second (the duration of a single event), to many minutes [Van Hese et al., 2009]. These components can be separated irrespective of duration and amplitude using spectral analysis, of which there are several variations. Van Hese (2009) used a modified FFT-based algorithm to fairly successfully detect runs of spike and wave complexes. More mathematically sophisticated spectrum-based approaches produce similar results. For instance, spectra derived using complex Morlet wavelets is also able to robustly detect runs of spike and wave discharges [Xanthopoulos et al., 2009]. However, while useful for CSWS-like, long lasting events, these spectrally-based methods do not perform well when looking at single, discrete events.

An alternative to this spectral based approach to detecting sleep-associated seizure-like events, is to use component analysis. Principal component analysis by singular value decomposition has been shown to be particularly useful at removing or enhancing transient events that drastically vary from the mean activity (i.e. artefact removal or spike detection) [Lagerlund et al., 1997]. Simply, the process breaks the overall EEG signal into it's separate components and deals with these separated parts as individual and independent timeseries. The analyst can then recombine a series of components to capture as much of the signal of interest, and as little of the remaining, unwanted activity. The absolute values of each relevant component can then also be combined to create a numerical indicator for event detection. Variations on this theme are known to have yielded good detection results and reinforces the theory that the spike and wave components of the spike and wave complex are indeed separate entities [McKeown et al., 1999]. McKeown *et al* (1999), took data from 5 patients with superficially variable seizure-like events. Using independent component analysis, they found at least two distinct components for the spike or the wave, each with a spatially different localisation. These components were also completely separable from the rest of the signal that described the background, non-seizure related activity.

These different approaches all strongly suggest that the mechanism underlying the spike, and that underlying the wave, have different origins in the brain.

3.1.2 Clinical features suggesting possible mechanisms.

Possible mechanisms related to the construction of an experimental model of sleep-associated seizure-like activity can be better understood through the application of two separate areas of clinical data: Firstly, the pharmacological spectrum of successful treat-

ments. Secondly, the relationship between spike and wave discharges and other brain rhythms with known underlying mechanisms.

Sleep associated epilepsies most often present during childhood. Many conventional antiepileptic drugs do not have the same effect in children as they do in adults, making the approach of the clinician difficult. However, a number of approaches have been shown to have at least partial success, both in alleviating seizures and improving the cognitive performance of the patient. It has been suggested by clinicians that the primary pathology may be linked to the immune system due to the significant improvement in some Landau Kleffner patients with CSWS following immunoglobulin administration. This was even seen in patients who had not responded well to prior attempts with other therapies [Arts et al., 2009]. However, improvement was not always seen, and any connection to immune status remains a mystery. As seen in most epilepsies, those associated with sleep also respond fairly successfully to drugs that boost synaptic inhibition (e.g. see [Veggiotti et al., 2012]). The efficacy of benzodiazapines (clobazam 1mg/kg/day or clonazepam 0.1mg/kg/day) has been established, but they do not work in all patients and can have unwanted cognitive side effects (being profoundly sedative and hypnotic agents). In addition, some classical antiepileptic agents that boost inhibition (e.g. carbamazepine and phenobarbital) actually make the seizures worse, casting doubt on a role for GABAergic system deficits in epileptogenesis during sleep. Ethosuximide, a blocker of T-type calcium channels [Broicher et al., 2007] has been shown to be effective in some spike and wave associated epilepsies, but not specifically those related to sleep [Yasuhara et al., 1991].

Of the most recent antiepileptic drugs, Levetiracetam has proved particularly effective. It has been shown to decrease spike and wave complexes rapidly and reliably [Cavitt and Privitera, 2004]. Interestingly, the drug is unique in that it modulates synaptic vesicle proteins that results in a use-dependent reduction in both excitatory and inhibitory neurotransmitter release [Gillard et al., 2006]. Work by McTague and Cross (2013), has shown that changes in pH provided by the kerogenic diet also appear to be effective, although the reasons for this are currently unknown.

In terms of the relationship between spike and wave complexes and other EEG rhythms, the connection to the delta rhythm is explicit in sleep-associated epilepsies. This would suggest that some aspect of the normal generator mechanisms of the delta rhythm may also underlie the spike and wave complex. Interestingly, observations made during seizure-like events during wakefulness would also suggest this. Delta and slow wave oscillations still dominate the spectrum during wakefulness although they are far smaller

in magnitude. Nevertheless, it has been proposed that derangement of delta rhythms, specifically slowing and increasing in variability period-on-period (polymorphic delta), are a good pre-ictal indicator for spike and wave-like discharges [Tao et al., 2011]. This correlation between delta slowing and spike and wave complexes is also seen in tuberous sclerosis. In this case, both measures are affected by cortical glucose suggesting a metabolic basis of this type of epilepsy [Nishida et al., 2008]. The slowing of sleep-associated rhythms has been shown experimentally to be related to a decrease in glucose concentration [Cunningham et al., 2006]. Cunningham *et al* (2006) demonstrated that slow wave oscillations, and their frequency, were tightly related to the activity of an ATP-sensitive potassium channel. Reducing glucose (the'fuel' for the brain), reduced energy levels in neurons (in terms of ATP concentration), thus causing the potassium channels to open. This is turn resulted in a switch from high frequency activity in the EEG to hyper polarised neurons prone to burst discharges favouring much slower frequencies of activity.

This latter work was performed in animal model *in vitro*, where control and access to specific mechanisms is far greater than in the clinical situation. The use of animal models to sleep-associated epileptiform activity will be introduced in more detail in chapter 4.

3.1.3 Aims

The aim of this chapter was to provide clinical data to directly compare with results from the experimental model detailed in chapters 4-6.

3.2 Methods

Clinical recordings were taken from an inpatient at the Royal Victoria Infirmary (Newcastle upon Tyne). The patient was an 11 year old female with a history of learning impairment from approximately age 4. The patient presented with symptoms of predominantly sleep-associated generalised seizures which has gradually worsened over the year before recordings used here were taken.

Extracranial EEG measurements were taken suing the standard 10-20 electrode placement (see figure 3.1B). Data was collected and digitised using a SynAmps-2 Neuvo long term monitoring system (Compumedics Ltd). Clinical observation used a double-banana montage with data down sampled to 256Hz. Raw, individual channel data was transferred to MatLab using the Biosig suite of programmes (Institute of Science and Technology, Austria), where the data was earth-subtracted and band-stop filtered to remove mains noise (FIR filter, 49.5-50.5Hz, -50dB).

Most automated spike and wave detection routines use the spectral signature of the EEG data (section 3.1.1). Here, we constructed a measure of spike and wave complexes (SWC) by first deriving spectrograms of the filtered data from each channel. Data was Hanning windowed over 1 second epochs, moving along the dataset with as 39ms (10 data point) time-step. The SWC 'magnitude' measure was quantified as the mean power (in mV^2) of the underlying, on-going wave discharge over 10s (see figure 3.2A) multiplied by the power in the band encompassing the spike discharges (in this patient's case, 4-9Hz). This simple analysis allowed separation of SWCs from any changes in underlying delta power and frequency. Spatial maps of SWC magnitude were constructed by arranging each EEG channels 'magnitude' on a 2D grid (see figure 3.2 with respect to the montage placement seen in figure 3.1).

3.3 Results

EEG recordings obtained from the Neurophysiology department revealed a pattern of activity where wakefulness was associated with fairly normal EEG rhythms. However, in one epoch (see figure 3.1A) the patient went from relaxed wakefulness to sleep. The onset of sleep (from visual inspection of videotelemetry) was accompanied by the onset of a large-amplitude, protracted (>10 minutes) non-convulsive, electrographic seizure. Superficial analysis of this activity revealed a typical CSWS-type occurrence of repetitive spike and wave complexes (figure 3.1C). Both spike and wave amplitudes varied considerably across different electrodes, with peak amplitudes being seen on electrodes C3, P3 and T5 (mean maximal amplitude 248±25μV, n=100 events , P3). Marked inversions of the waveform were seen between C3 and more frontal electrodes (e.g. F3) and to a lesser extent across the midline. The ratio between spike and wave occurrence and amplitude appeared to vary across the montage. While waves were seen strongest in electrodes in the left rear quadrant, some position showed very little wave activity but near continuous, low amplitude spikes at approximately 3-7Hz (e.g. Cz and T4). In contrast, on no channels were waves seen without accompanying spikes.

GIven the spectrum-based approaches to spike and wave complex detection, the data was subjected to simple spectrographic analysis (figure 3.2A). This approach clearly demonstrated the relationship between delta frequency activity and the spiking. The near continuous spike and wave complexes yielded a strong spectral line peaking at 1.8±0.2Hz (a slow delta rhythm, see section 3.1), although the magnitude of the peak was variable. In this patient, spikes manifest as transient increases in spectral power peaking between 4 and 10Hz, with a mean peak frequency of 6.5±0.8Hz. Combining the mean

powers in these two bands yielded a spatial map of spike and wave complex magnitude (figure 3.2B). A clear peak in this measure of spike and wave activity was observed along the left temporoparietal axis. This peak was stable during the seizure. The dominance of delta power in this method of quantification yielded low powers in electrodes where the wave component of the spike and wave discharge was of low amplitude or absent (i.e. particularly Cz and T4).

The lateralisation of the spike and wave complexes were examined further by generating spatial maps of the raw, filtered electrode voltages (figure 3.2C). The initial wave positivity was seen on electrodes which loosely correlated with those that were previously giving peak spike and wave magnitudes from above quantification method. However, peak initial positivity was shifted more towards the back of the brain, peaking in electrodes T5, P3 and O1. Interestingly, the peak negativity of each discharge in these electrodes was associated with peak positivity in corresponding contralateral electrode positions, with some positivity also seen in the right frontal area. At the termination of the spike component of the spike and wave discharge, a remarkable midline symmetry was seen. Positive peaks were seen along the entire midline from FPz to Pz and across both temporoparietal axes. This difference in spatial localisation of signal positivity appeared to correlate with a temporal shift in the spike relative to the wave component of each spike and wave discharge across the midline (e.g. compare P3 vs P4 and T5 vs T6 in figure 3.2B). While figure 3.2 shows a single example, the illustrated pattern of spatiotemporal voltage changed was remarkably stereotypes across the 100 spike and wave complexes analysed.

3.4 Discussion

The data presented and superficially analysed in this chapter provides the core features of spike and wave discharges that need to be present for an experimental model of sleep-related spike and wave discharges to be valid. These are:

1. A clear relationship with delta frequency activity: The wave component of each spike and wave discharge should correspond to a large, slow period of delta activity.

2. The spatial localisation of the discharges should correspond with regions generating the largest delta power: In humans this has been shown to be the parietal and frontal areas [Ioannides et al., 2009]. While some studies show that SWCs are of frontal origin during clinical observation and some animal models [Medvedev et al., 1996, Kubota et al., 1997], the patient examined here showed clear parietal dominance. This fits with the general spectrum of epileptiform abnormalities from BECTS through to CSWS and is therefore, a more attractive region on which to

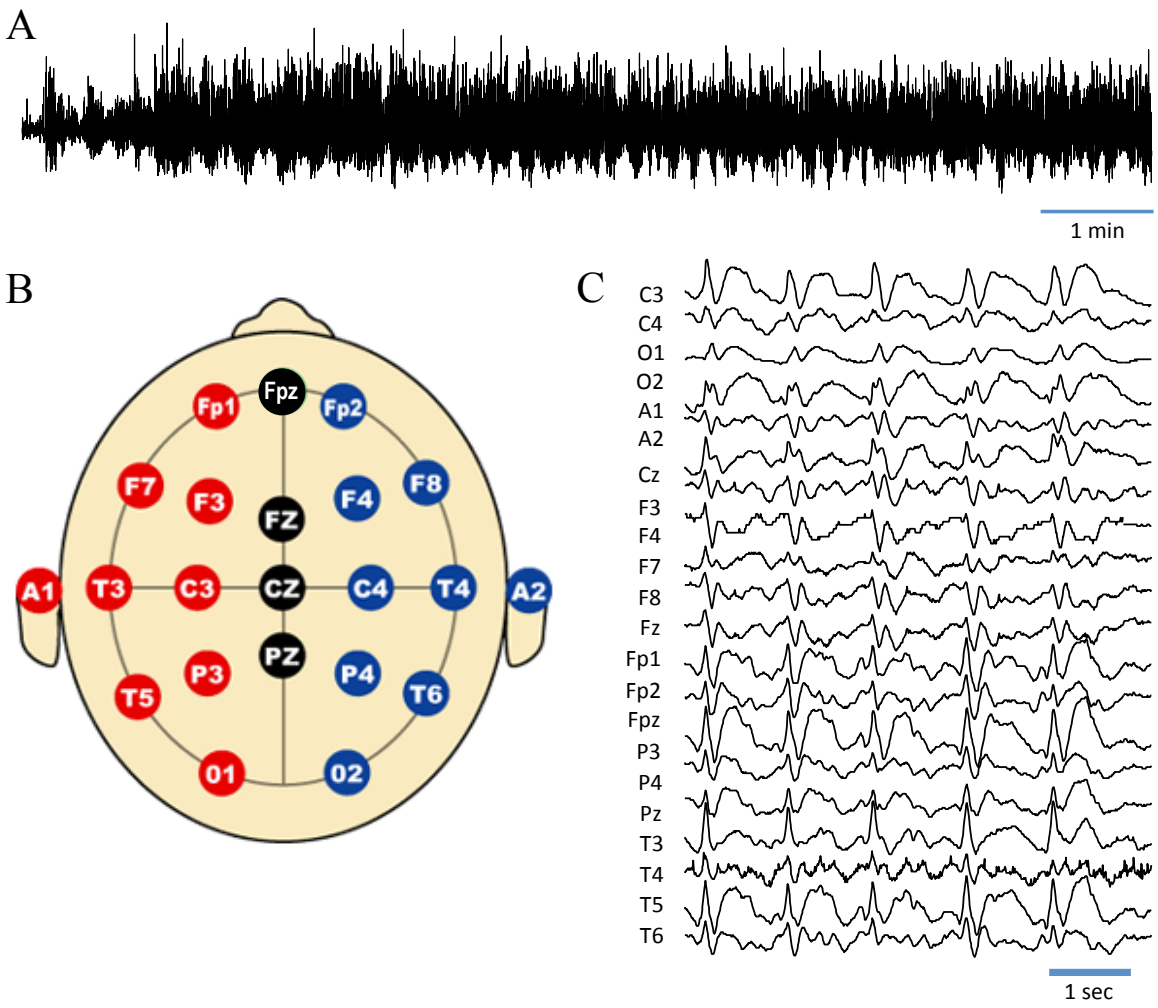

Figure 3.1: **Example spike and wave seizure discharge. A.** A 10 minute recording taken from electrode P3 as the patient progressed from relaxed wakefulness to sleep. Increase in peak-peak amplitude from onset corresponds to the occurrence of near-continuous spike and wave complexes. **B.** Diagram illustrating the placement of the electrodes used, positioned in the standard 10-20 format. **C.** Expanded timescale traces from each electrode depicted in figure B after filtering (see 3.2). Note the dominance of the spike and wave complexes on electrode in the lower right quadrant.

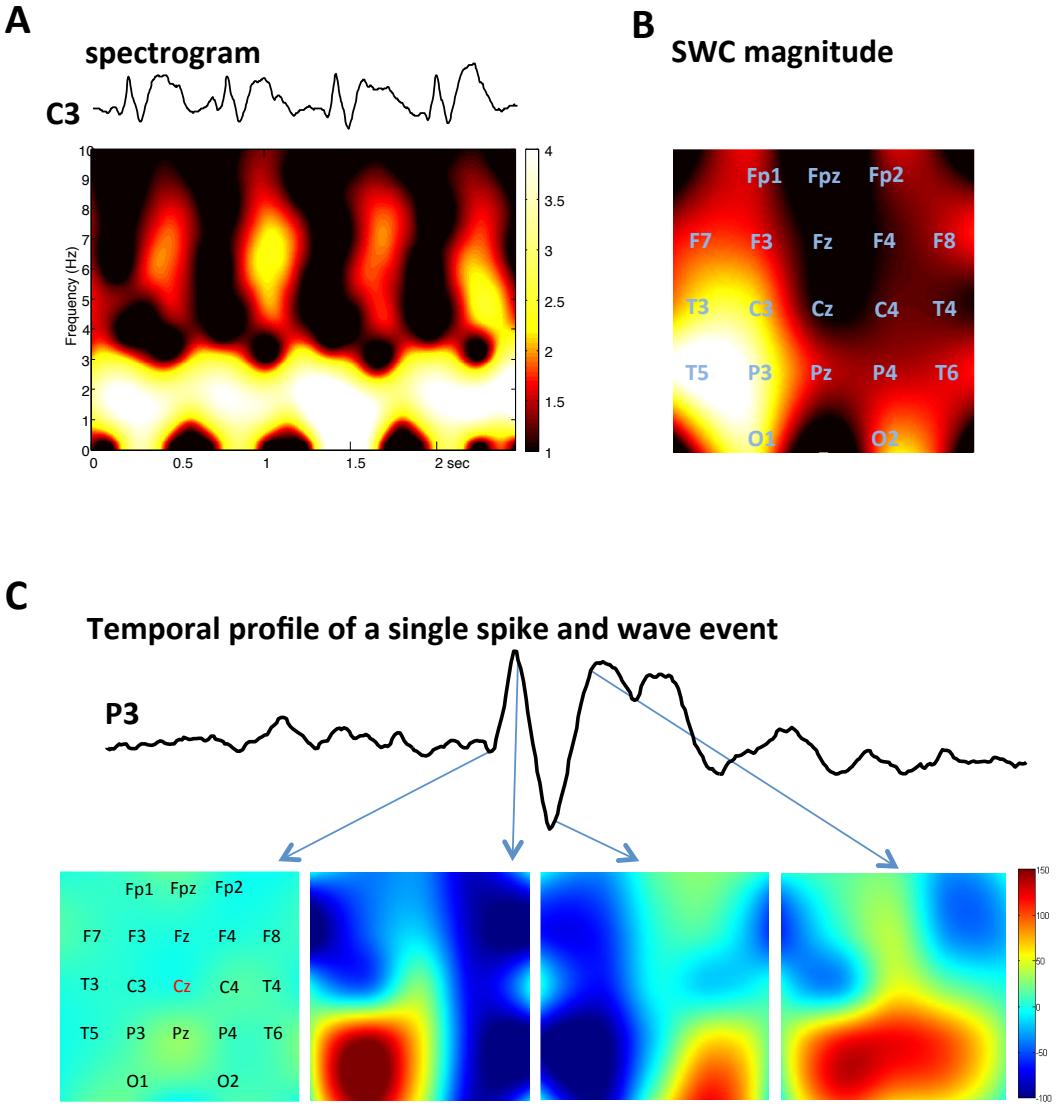

Figure 3.2: **Characterisation of clinical spike and wave discharges. A.** Example 2.5s epoch of data taken from electrode C3. Below is the spectrogram illustrating the ongoing delta activity interspersed with 4-9Hz (theta frequency range) spectral signature of each spike. Colourmap scale is in mV^2. **B.** Magnitude of spike and wave complexes (SWC) over 10s of activity (see 3.2), plotted over the electrode grid. Note the clear localisation of maximal activity in the right temporo-parietal axis in this patient. **C.** Spatial maps of raw electrode voltage during a single SWC. Note the 'flip-flop' of peak positive potential (red in the colourmap) during the spike component of the SWC.

base a model aims at uncovering general principles.

3. The spike component and the wave component should be clearly distinct entities. Spatial separation across EEG electrodes was clear in the patient data presented in this chapter. With this resolution, it is not clear whether this represents a large anatomical difference in the presence of underlying mechanisms, or a 'field orientation' issue where both components come from different cortical laminae. This will be addressed in chapter 6.

4. The association with the onset of sleep should be present in *in vitro* models through the relationship to known neuromodulator state differences between sleep and wakefulness. This point will be dealt with in more detail in the next chapter.

Chapter 4

Generation of epileptiform pathology from delta frequency activity

4.1 Introduction

4.1.1 Animal models of spike and wave discharges and their association with sleep

Two models of spike and wave related epilepsy dominate the literature: The Genetic absence epilepsy rat from Strasbourg (GAERS), and the Wistar albino Glaxo rat from Rijswilk (WAG/Rij). Both are inbred strains that spontaneously develop non-epileptic spike and wave seizures during development that persist robustly throughout adulthood [Marescaux et al., 1992]. In the case of GAERS rats, their seizure-like activity shares any features with human absence epilepsies indulging occasional generalised seizures interspersed with many bilateral spike and wave complexes (SWC), particularly along the frontoparietal attention axis [Danober et al., 1998]. The morphology and spatial localisation of the spike and wave complexes suggests a good model for sleep associated syndromes showing CSWS. However, in the GAERS rats abnormal activity is most prominent during relaxed wakefulness, with only sporadic occurrences during sleep. This casts doubt on the commonality of an underlying mechanism but some core features may be shared enough to warrant consideration here.

The second genetic inbred model, the WAG/Rij strain shows more complex seizure-like activity. At least two distinct types of spike and wave discharge are seen, one having obvious behavioural correlates seen during sleep and one without behavioural correlates seen during waking [Van Luijtelaar and Coenen, 1988]. The circadian pattern of these SWCs suggests a good relationship between the sleep-associated discharges and those associated with CSWS in humans [Van Luijtelaar and Coenen, 1988]. Given this, it is interesting to note that, like human sleep-associated seizures, WAG/Rij type one discharges were correlated with enhanced and slowed delta power in the cortex [van Luijtelaar et al., 2011]. Several other researchers have also noted a relationship between SWCs and sleep associated rhythms in these animal models [Pinault et al., 2001]. A common feature of these studies is the evidence for involvement of thalamus, in particular strong thalamocortical projections [Lüttjohann et al., 2013, Avoli, 1983]. However, these latter authors demonstrated that increases in spectral power, particularly in the lower frequency (delta) range, preceded SWCs more overtly in the somatosensory cortex. This region of the brain is analogous in part to human parietal regions also shown to demonstrate the strongest delta power and SWCs (see above).

As well as the two inbred strain models described above, SWCs are also seen in animal models of stroke. It is well recognised clinically that seizure-incidence increases after

central ischemic episodes [Beghi et al., 2011] and this can be modelled in rats with varying degrees of middle and anterior cerebral artery occlusion [Srejic et al., 2013]. These authors noted a rapid (within 1 hour) increase in the incidence of theta and gamma rhythm generation in the affected cortical areas leading to classic SWCs in about half of all the rats tested. The higher frequency rhythms (up to 120Hz) were also seen to occur transiently at the transition from wave to spike in the SWC, providing another marker which an *in vitro* model should include.

Given these models, and their caveats, what can we learn about putative primary mechanisms for spike and wave complex related seizure genesis?

4.1.2 Putative mechanisms of spike and wave complexes in animal models

Pharmacological manipulation is far more easily, and ethically, performed in animal models and therefore it is perhaps not surprising that the experimental platforms described in the previous section have yielded a substantial amount of data pointing to the mechanisms underlying SWCs and related seizure-like events.

In terms of synaptic inhibition, the clinical data paints a rather confused picture (see section 3.1). Antiepileptic drugs targeting $GABA_A$ receptors have mixed effects on sleep-associated epilepsies. In contrast, both clinical and animal studies have suggested that $GABA_A$ receptors play a role [Ostojić et al., 2013]. This form of synaptic inhibition is metabolism-sensitive and it known to participate in the type of slow wave rhythms that can transform into SWCs (e.g see [Craig et al., 2013]) so it is not clear whether this form of inhibition is deranged in sleep epilepsies or whether it simply needs to be present to trigger the seizures indirectly.

There is evidence that synaptic excitation may also play a role. NMDA receptors which control the excitability of deep layer (layer V and VI) cortical neurons appears to be hyperactive in some forms of absence epilepsy associated with SWCs [D'Antuono et al., 2006]. It is unclear from this study whether this reflects an increase in intrinsic excitability of deep layer neurons, being strongly interconnected by NMDA receptor-containing synapses, or whether the increase seen is directly responsible for the hyper-excitability. The situation is further complicated by the observation that dizoclipine (MK-801, a non-competitive NMDA receptor antagonist) when administered to rats produces SWCs *de novo* [Feinberg et al., 1995]. The large pyramidal cells in the deep layers of the cortex express a large, low voltage-activated calcium conductance (T-conductance) which pro-

motes intense but brief burst discharges in dendrites. It has been proposed that excessive excitation of this conductance may underlie many of the slow wave abnormalities and perhaps also SWCs in some epilepsies [Cheong and Shin, 2013]. The T-conductance is reduced by ethosuximide, which may provide a mechanism for the efficacy of this drug in spike and wave epilepsies clinically (see chapter 3.1).

Further evidence for a mechanistic role for glutamatergic excitatory synaptic transmission comes from studies looking at metabotropic glutamate receptors in seizure-prone inbred strains. Interestingly, increasing the activity via metabotropic glutamate receptors that enhance the postsynaptic excitation (Group 1, mGluR1 & 5) can actually decrease SWCs in WAG/Rij rats [D'Amore et al., 2013]. In line with this, increasing activity of metabotropic receptors that in turn decrease glutamate release presynaptically (therefore reducing postsynaptic excitation) have the opposite effect. Group 3 mGluRs enhance SWCs [Ngomba et al., 2008]. These receptors are known to inhibit the cyclic AMP cascade, hence they may potentiate seizures by altering adenosine phosphate-sensitive potassium channels [Cunningham et al., 2006] (see section 3.1).

Seizures that manifest, particularly during sleep should be sensitive to neuromodulatory cues that also change during the sleep/wake cycle. Noradrenaline, dopamine, serotonin and acetylcholine levels all change markedly during wakefulness and different stages of sleep, as previously described in section 1.2.1. It is perhaps not surprising then, that the incidence of SWCs has been shown to be related to the level of these chemicals in the brain [Bercovici et al., 2009]. The relationship between dopamine receptor function and SWCs is particularly interesting. Two distinct types of SWC associate differentially with wake and sleep states (see section 3.1). Dopaminergic agents also control these two different types of SWC by different means, such that events seen during sleep were increased by lower dopamine receptor function (as seen during deep sleep) while those seen during wakefulness (when dopamine levels are high), were attenuated [Midzianovskaia et al., 2001]. Using the same rat model, an experimental study by Sitnikova *et al* (2005) reported that lowering postsynaptic noradrenergic activity, which is normally seen during deep sleep, also increases the number of SWCs seen.

The relationship between SWCs and the cholinergic system is particularly intriguing. A range of drugs that boost cholinergic transmission in general (e.g. physostigmine) reduced the incidence of SWCs in a dose dependent manner *in vivo* [Danober et al., 1993]. Similarly, these authors showed that selective muscarinic receptor agonists also reduced SWCs. However, the role of muscarinic receptors in spike and wave generation is not straightforward. Application of the muscarinic receptor antagonist, scopolamine had

mixed effects. At low concentrations, SWCs were increased, but at high concentrations they were suppressed. Danober *et al* (1993), also showed that the acute application of the broad spectrum muscarinic receptor agonist, pilocarpine suppressed SWCs. However, following the administration of pilocarpine, a chronic epileptic syndrome develops over many months which is characterised by intense SWCs which are particularly associated with the sleep state [Ferreira et al., 1999].

The role of nicotinic receptors in seizure generation is similarly complex. In the inbred strain models of SWCs nicotine itself suppresses epileptiform activity [Danober et al., 1993]. However, these authors also demonstrated that the nicotinic receptor antagonist, mecamylamine had no effect. This may be due to the subunit selectivity of this drug at nicotinic receptors and this will be considered in detail in chapter 5.

Autosomal dominant nocturnal frontal lobe epilepsy (ADNFLE) is associated with high penetrance to several nAChR mutations, particularly α_4 and β_2 subunits. An "n of one" clinical study by Willoughby *et al* (2003) where the single female patient with pharmaco-resistant ADNFLE participated in an open and double blind trial of nicotine patch application, reported a significant decrease in the number of seizures in the presence of the nicotine patch when compared to the control. The average number of seizures a day decreased from 1.65 ± 2.36 to 0.01 ± 0.00 ($P < 0.0001$) when the nicotine patch was applied. A later clinical trial by Brodtkorb and Picard (2006) in which the epilepsy characteristics and nicotine habits of two families with two different α_4 mutations (776ins3 (insertion mutation) and S248F (missense mutation)), also reported a significant decrease in seizure occurrence when nicotine was administered ($P = 0.024$). *In vitro* studies have shown that these mutant nAChRs have increased sensitivity to acetylcholine, resulting in a gain of function [Moulard et al., 2001]. Nicotine is known to desensitize nAChRs, therefore it was hypothesised that this increased sensitivity could be combated by the administration of nicotine [Brodtkorb and Picard, 2006]. A molecular pharmacology study by Son *et al* (2009) reported that ADNFLE is related to the stoichiometry of the $\alpha_4\beta_2$ nAChRs, where $(\alpha_4)_3(\beta_2)_2$ has higher sensitivity than $(\alpha_4)_2(\beta_2)_3$. The authors results corroborated the previously mentioned theory with evidence that nicotine can revert the subunit stoichiometry to similar ratios measured in wild type mice i.e. seizure/epilepsy free state. Hence supporting the hypothesis that nicotine may decrease seizure frequency in ADNFLE patients. Very little literature is available relating other idiopathic epilepsies to nicotine. This may be due to the typical patients with nocturnal idiopathic epilepsies being children and generally not being old enough to smoke, however in 2011 it was estimated that 5% of children aged 11-15 years smoked at least one cigarette a week [Gill et al., 2012].

Nicotine however, is also known to induce seizures at higher doses. The mechanism underlying the convulsive effects of nicotine are relatively unknown, however several studies conducted on inbred strains of mice have indicated that several nAChRs may be involved [Bastlund et al., 2005, Franceschini et al., 2002, Salas et al., 2004, Stitzel et al., 2000, Broide et al., 2002]. Franceschini *et al* (2002) have reported that the α_7 nAChR is thought not to be necessary for the mechanisms underlying nicotine-induced seizures, as the dose dependant curve was similar across different strains of α_7 knockout mice. Whereas work by Salas *et al* (2004) has shown that β_4 and α_3 nAChR subunits are mediators of nicotine-induced seizures and hypolocomotion, as both aAChR subunit knockout mouse models displayed decreased sensitivity to acute nicotine. In addition, Stitzel *et al* (2000) have shown that by studying restriction fragment length polymorphisms in inbred lines, both the α_4 and α_6 nAChR subunits are linked with nicotine-induced seizure sensitivity.

4.1.3 Aims and Objectives

From the arguments above it was hypothesised that disruption of cholinergic neuromodulation should be necessary and sufficient to generate epileptiform activity from delta rhythms similar to that seen in patients during deep sleep. However, in the absence of an intact thalamocortical system in the slice, the aim was to see whether the local circuitry in neocortex alone was sufficient to support such pathology.

4.2 Methods

Adult male Wistar rats were utilised in the following *in vitro* experiments. 450μM slices were prepared and maintained as outlined in the methods chapter 2.2- 2.4. Analysis and statistical techniques used are detailed in chapters 2.8 and 2.9. All experiments recorded in this chapter utilised extracellular field recordings using glass electrodes. Oscillatory activity in the delta frequency range was initially induced by application of carbachol [4μM] and SCH23390 [7μM], a D1-like receptor antagonist.

The area power of oscillations were used as the primary indication of the strength of oscillatory activity, with the peak amplitude of the power spectra used as a secondary method of intensity. The area power of delta oscillations was taken between 0.5 and 5Hz. The frequency of activity was measured from the peak of the power spectra and hence represents the modal frequency of oscillatory activity over a 60 second epoch. As detailed in section 2.8.1, for an epileptiform event to be classified as a wave discharge (WD), it

must have a peak-to-peak amplitude of >200μV, be a smooth trace with no spikes interrupting the wave and easily distinguishable from the general LFP activity. Whereas for an epileptiform event to be classified as a spike wave complex, the wave portion must also have a peak-to-peak amplitude of >200μV, a positive spike which briefly interrupts the 'flow' of the wave before returning to complete the wave and be easily distinguishable from the general LFP activity.

4.3 Results

4.3.1 Laminar profile of induced delta rhythms in the rodent somatosensory cortex

In view of the work conducted by Carracedo (2010), carbachol [4μM] and SCH23390 [7μM] were bath applied to induce delta frequency oscillations. To confirm that the optimum oscillatory response in the somatosensory region was within layer V, as suggested by Carracedo (2010), laminar profiles were recorded from the six layers of the cortical column, as depicted in figure 4.1B. Oscillatory activity was observed within all layers, although principally between layers IV and VI. A significant variation in delta band power with reference to cortical layer was observed ($P<0.001$, n=7, One Way Repeated Measures ANOVA). This variation in mean power was greatest between layers I and IV ($P=0.02$, n=7, paired t-test) where the mean delta band power in layer I was $0.11\pm0.02\mu V^2$ in comparison to $0.36\pm0.06\mu V^2$, the delta power in layer IV. The variation in delta power between layer I and layer V was not considered to be statistically significant however this is likely to be due to the variation within the layer V dataset. The frequency of the delta oscillations within the cortical column did not significantly fluctuate, with the mean peak frequency of the delta oscillations in layer V of the somatosensory cortex being 1.5±0.18Hz ($P>0.05$, n=7, One Way Repeated Measures ANOVA, Figure 4.1Ci). In view of these results, along with Carracedo's (2010) findings, for the purpose of longitudinal profiles, and the pharmacological manipulations described in later chapters, extracellular field electrodes were positioned in Layer IV/V for all delta frequency manipulations.

4.3.2 Acute bath application of non-selective nicotinic acetylcholine receptor antagonist, d-tubocurarine causes a dose dependent increase in delta frequency activity in the somatosensory cortex

Delta frequency oscillations were induced in somatosensory cortex containing coronal rat slices by bath application of carbachol [4μM] and SCH23390 [7μM], as used in the

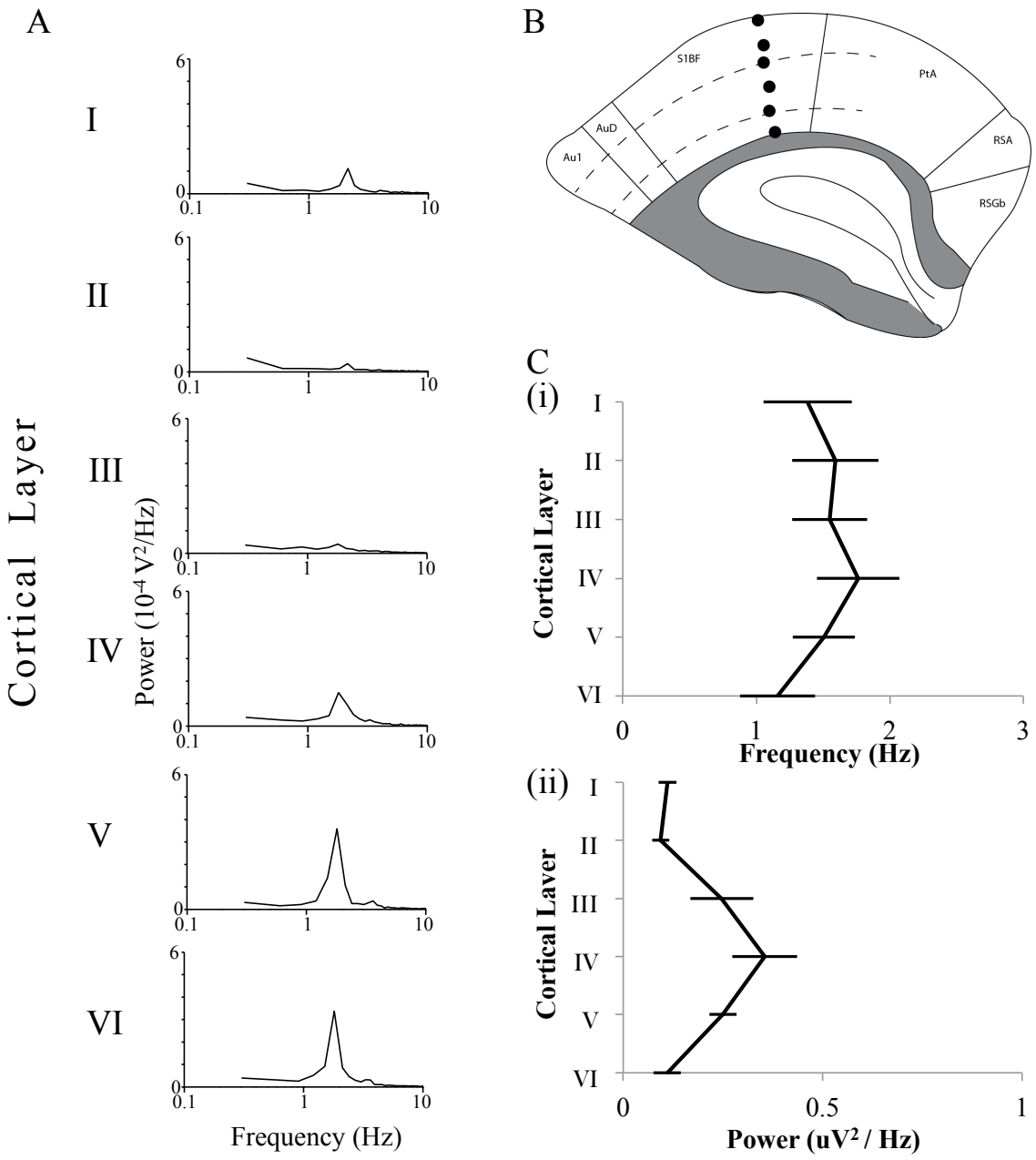

Figure 4.1: **Laminar profiles of delta activity in a coronal section of somatosensory cortex A.** A laminar profile of power spectra from 60s epochs of extracellular activity from Carbachol and SCH23390 induced delta oscillations in the Somatosensory region.**B.** A diagram of a coronal slice of the somatosensory region used in experiments and location of recording electrodes. **C.** Mean data comparing (i) the frequency and (ii) power of Carbachol and SCH23390 induced oscillations (n=7).

previous laminar study. In a previous study by Carracedo (2010), the application of d-tubocurarine (DTC) [10μM], a competitive, broad spectrum nAChR antagonist was associated with the induction of epileptiform activity in the slices, as it built upon the effect carbachol had on both the muscarinic and nicotinic receptor subtype, due to it's non-selective cholinergic agonistic properties. This epileptiform activity is very similar to the EEG and examples detailed in chapter 3. To ascertain the level of inducement needed for epileptiform activity to occur, DTC concentration response experiments [2 - 10μM] were undertaken.

During *in vitro* experimental conditions, the bath application of DTC resulted in no statistically significant change in mean delta frequency band power ($P>0.05$, n=17, One Way Repeated Measures ANOVA, figure 4.2Di). After 40 minutes of DTC [10μM] application, the mean power was $3.67\pm1.35\mu V^2$ compared to the mean power during the control state, $1.28\pm0.38\mu V^2$. Figure 4.2Dii displays a steady increase in mean delta band power however, due to the size of the error bars, it can be assumed that this result was not statistically significant due to the variation in the dataset. Figures 4.2A and B, display an example of how the delta band power is known to increase with DTC concentration.

The frequency of the delta rhythm saw a significant effect of DTC concentration ($P<0.001$, n=17, One Way Repeated Measures ANOVA, figure 4.2Dii). The ANOVA reported that all concentrations of DTC saw a significant effect when compared to the control state, however there was little change between the mean peak frequency of [5μM] and [10μM] concentrations, as can be seen in figure 4.2Di. Within 40 minutes of DTC [5μM] application, the mean peak frequency of the delta band was reduced from 1.74 ± 0.13Hz during the control condition to 1.0 ± 0.09Hz ($P<0.001$, n=17, paired t-test).

Autocorrelation analysis was conducted in order to assess the effects of the drug on the rhythmicity of the activity in the slice. Prior to DTC application, auto-correlation analysis of delta oscillations resulted in a graph that was sinusoidal in form indicating that the activity was intrinsically rhythmic. The autocorrelation data was normalised, thus the height of the central peak was always 1 with reference to the y-axis. Auto-correlation analysis revealed that no statistically significant effect of concentration was observed for the rhythmicity of the delta frequency oscillations ($P>0.05$, n=17, One Way Repeated Measures ANOVA, Figure 4.2Diii). The mean ratio of the first peak to the central peak during the control condition was 0.38 ± 0.05 whilst the mean ratio during the final concentration [10μM] was 0.35 ± 0.07. Therefore, it can be surmised that although DTC [10μM] concentration saw an increase in SWCs, the recorded data between these complexes saw little change in delta rhythm.

Laminar profile of delta frequency induced oscillations with acute application of non-selective nicotinic acetylcholine receptor antagonist, d-tubocurarine.

In Section 4.1, it was determined that Somatosensory cortex Layers IV and V were the most robust for delta frequency oscillations when using the delta inducing drugs, carbachol [4μM] and SCH23390 [7μM]. To understand the effect of DTC across the laminae on delta frequency oscillations, a further laminar profile experiment was conducted, in which the effect of DTC [5μM] application was compared with the laminar profile of the control state. As previously used, 60 second epochs of data were recorded for each of the six layers of a cortical column, as depicted in figure 4.3B. Statistical analysis reported that there was a significant effect of drug on mean power of the delta band (P=0.0003, n=7, Two Way Repeated Measures ANOVA), as was expected from the results of the previous subsection 4.3.2. The least square mean values as a comparison of drug only were 0.21$\pm$0.13μV^2 and 1.02$\pm$0.12μV^2 respectively. The difference in the mean delta power values for the different cortical layers is greater than would be expected by chance after allowing for effect of differences in drug (P=0.004, n=7, Two Way Repeated Measures ANOVA). The difference of the least square mean values for the effect of drug and cortical layer were particularly different for layers IV and V (as expected) which went from 0.36$\pm$0.21μV^2 and 0.25$\pm$0.21μV^2 respectively during the control state, to 1.91$\pm$0.21μV^2 and 1.37$\pm$0.21μV^2 following [5μM] DTC application. When compared to layer II, a significant difference was seen between these Layers (P=0.001, n=7, Holm-Sidak Pairwise Comparison). During the control state the mean delta band power in layer II was 0.09$\pm$0.21μV^2 and 0.52$\pm$0.21μV^2 after DTC application. Figure 4.3A portrays this effect of drug and cortical layer very nicely. There is, however, no significant interaction between drug and cortical layer relating to mean delta band power(P>0.05, n=7, Two Way Repeated Measures ANOVA).

The frequency of the delta rhythm saw a significant effect of drug (P=0.001, n=7, Two Way Repeated Measures ANOVA), as was expected from the results of the previous subsection 4.3.2. With no account for layer, the least square mean peak frequency during the control state was 1.46$\pm$0.05Hz in comparison to 0.94$\pm$0.05Hz following DTC [5μM] application. Unlike the result for mean delta band power, there was a significant interaction between drug and cortical layer i.e. the magnitude of the effect the drug had on the frequency depended on which cortical layer the electrode was recording from at that point (P=0.03, n=7, Two Way Repeated Measures ANOVA). Pairwise Multiple Comparison statistical methods reported that there was no significant effect of layer within drug, i.e. There was little variation in frequency between layers during a single drug concentration

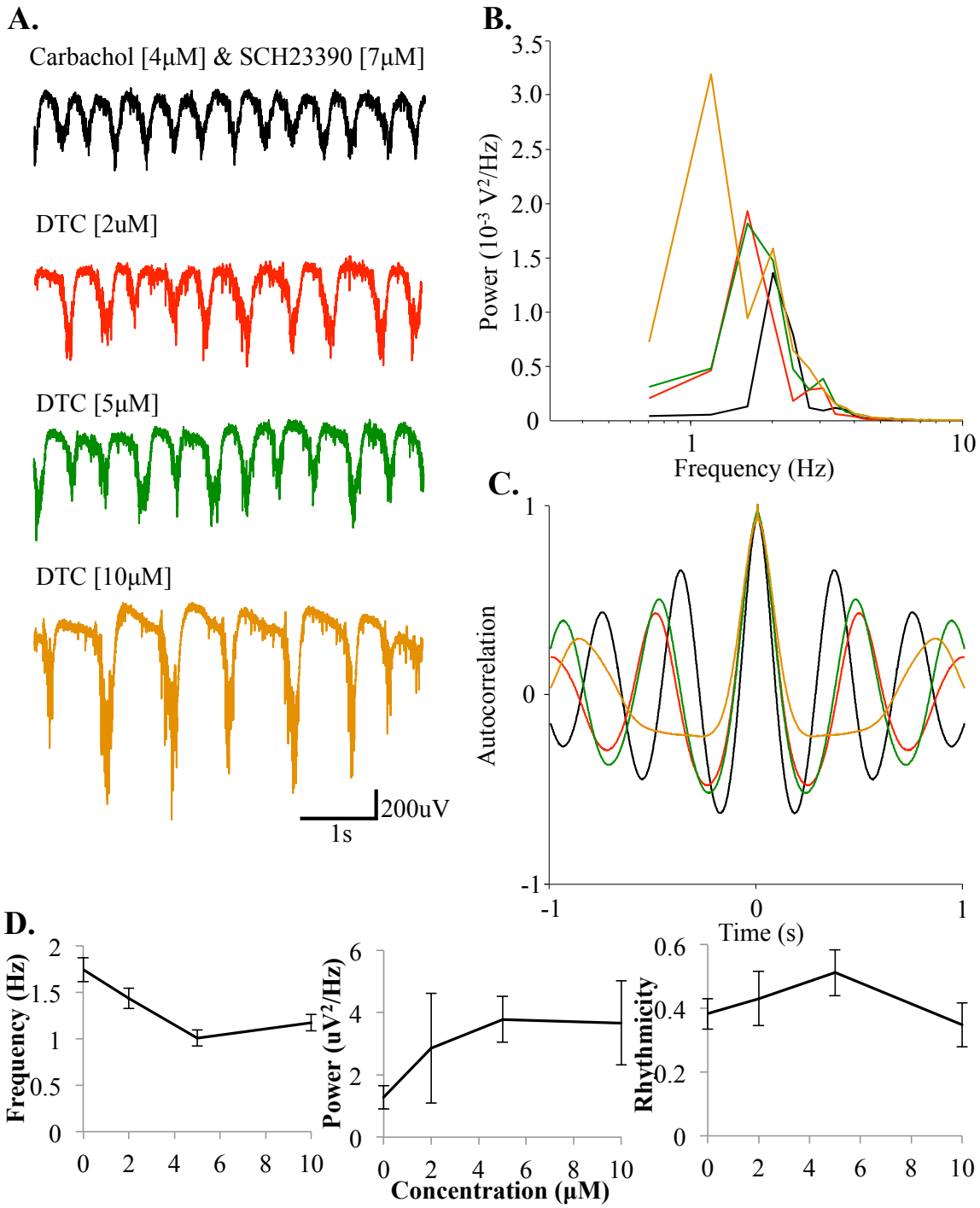

Figure 4.2: **A.** 5 second epoch of extracellular activity from layer V of the somatosensory cortex after application of delta inducing drugs and increasing d-tubocurarine concentration. **B.** Power spectra produced from 8 second epochs of data in the absence of epileptiform activity. **C.** Autocorrelation from an 8 second epoch of activity in the absence of epileptiform activity. **D.** Concentration response curves of mean frequency, mean power and mean rhythmicity ratio of activity (n=17) during DTC applications.

(P>0.05, n=7, Holm-Sidak Pairwise Comparison). However, within layers II to V individually, there was a significant effect of drug on mean delta frequency (P<0.02, n=7, Holm-Sidak Pairwise Comparison, figure 4.3Ci)). For example, in Layer V during the control condition the mean peak frequency was 1.51±0.18Hz compared to 0.77±0.09Hz after 40 minutes of DTC [5μM] bath application (P=0.002, n=7, paired t-test).

Cross-correlation analysis of delta frequency induced oscillations with acute application of non-selective nicotinic acetylcholine receptor antagonist, d-tubocurarine.

Cross-correlation analysis was used to determine the degree of phase lag and synchrony of the delta rhythm across the laminae of the cortical column. For this purpose, 60 second epochs of extracellular data were obtained simultaneously from two different locations for a comparison. A reference electrode was placed in deep layer V whilst a second roaming electrode was used to record from each of the other layers in turn, as depicted in figure 4.4B. From this analysis, it was discernible that the delta activity in each of the layers during the control state led that of Layer V, with the exception of Layer I, in which the activity seemed to lag behind it, as can be seen from the black line in Figure 4.4C. Layer I is also the only layer in which the delta rhythm appears to be 180 degrees out of phase with the reference electrode in Layer V, unlike the other layers, as shown in Figure 4.4A. The bath application of DTC [5μM] caused the deeper layers to slightly lag behind the reference electrode in Layer V (red line in figure 4.4C), however this is not easily discernible for figure 4.4A. However, Layer I remained approximately 180 degrees out of phase with the reference electrode in Layer V.

4.3.3 Epileptiform activity

In the previous subsections of this chapter, the main focus has solely been the delta rhythm and how DTC affects it. However, this is not the only activity that has been seen during these experiments. The other kind of activity that has been observed is epileptiform activity, which is detailed in depth in Section 1.7.1.

Of the twenty-eight experiments conducted, Wave Discharges (WDs) were present during 12 experiments resulting in a WD incidence rate of 0.43 per experiment. During these twelve experiments, the number of WDs detected during a 60 second epoch ranged from 2 to 8 following DTC [5μM] application and ranged from 1 to 3 WDs per 60 second epoch following DTC [10μM] application. In total, 45 WDs were detected during the recorded 60 sec on epochs from the twenty-eight experiments with the majority being

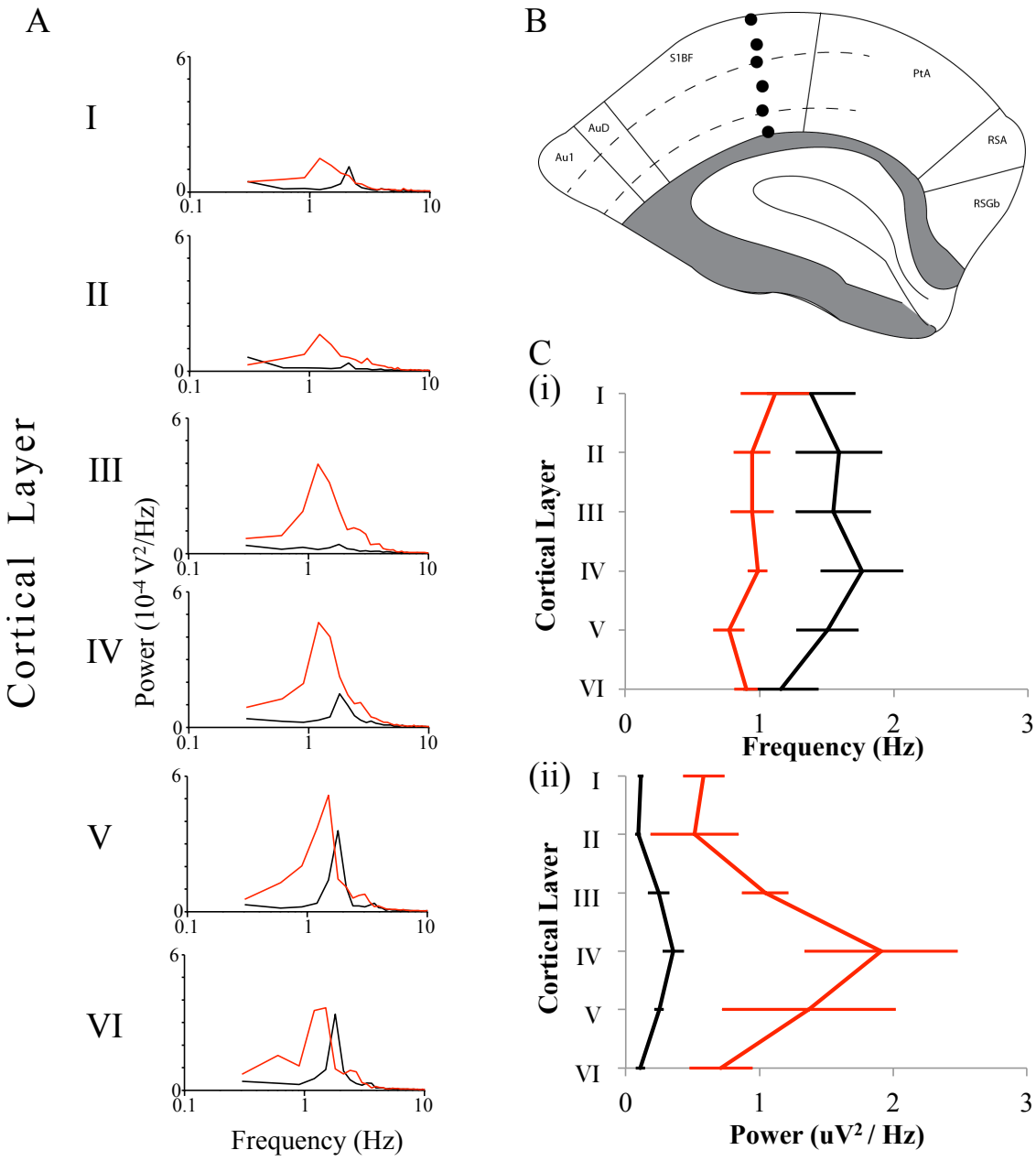

Figure 4.3: **D-tubocurarine increases the mean area power of delta activity whilst decreasing modal frequency A.** A laminar profile of power spectra from 60s epochs of extracellular activity from Carbachol and SCH23390 induced delta oscillations (black trace) and DTC [5μM] induced delta oscillations (red trace) in the Somatosensory region. **B.** A diagram of a coronal slice of the somatosensory region used in experiments and location of recording electrodes. **C.** Mean data comparing (i) the frequency and (ii) power of control state oscillations (black trace) and DTC induced oscillations (red trace) (n=4).

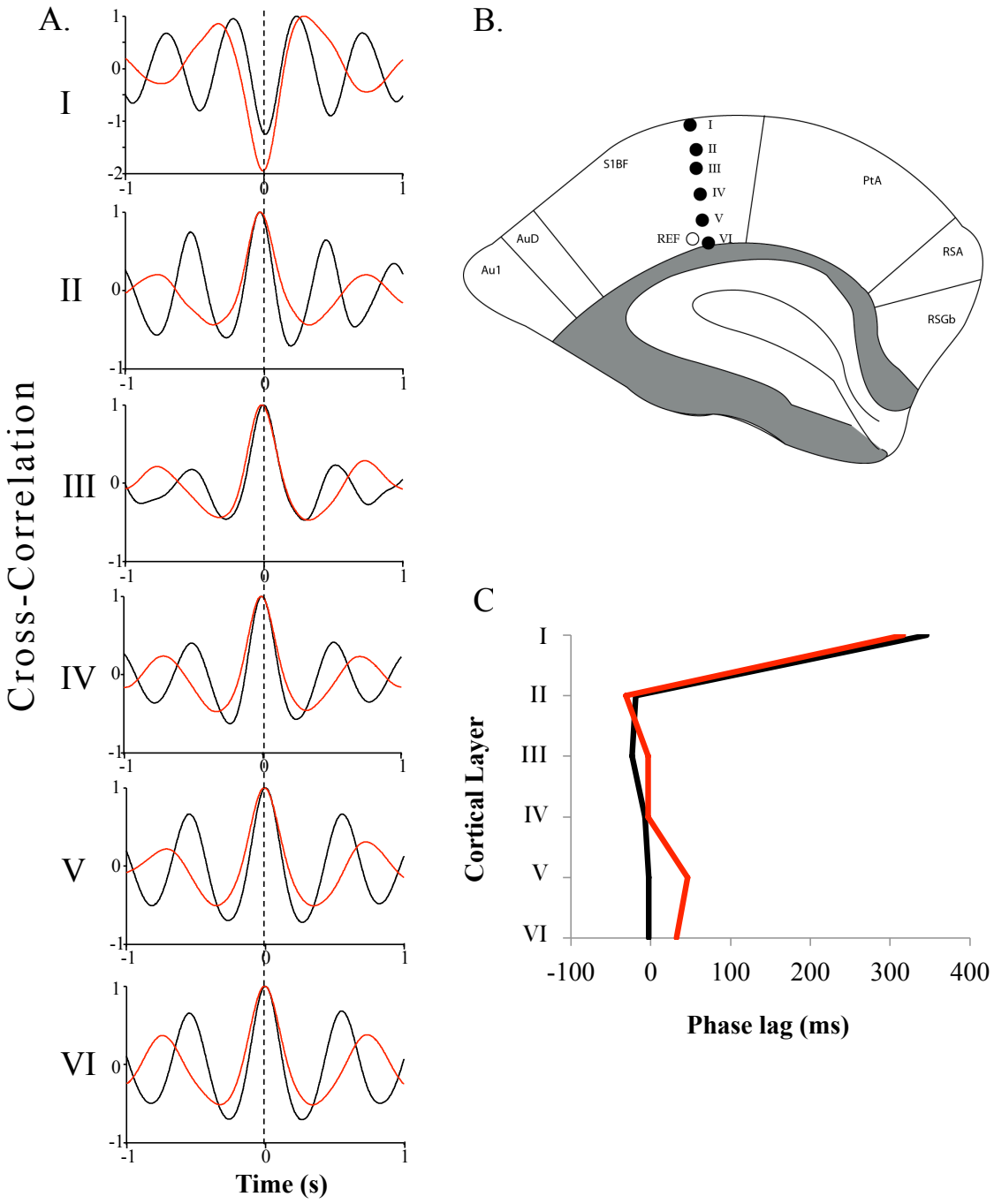

Figure 4.4: **Correlation analysis of delta activity throughout the laminae of a single cortical column in the somatosensory cortex A.** Cross-Correlations from a 60 second epoch of extracellular activity induced by Carbachol [4μM] and SCH23390 [7μM] (black trace) and d-tubocurarine (red trace) from different layers within a cortical column of somatosensory cortex (n=4). The reference electrode was positioned in layer VI, with a roaming electrode recording from layers I, II, III, IV, V and VI. **B.** A diagram of a coronal slice of the somatosensory region indicating positions of extracellular electrodes during the laminar profiles. **C.** A graph showing the mean phase angle of Carbachol and SCH23390 induced oscillations (black trace) and d-tubocurarine induced oscillations (red trace) in each layer of the somatosensory cortex (n=4).

detected during [5μM] application. Figure 4.5.1 shows a 1 second example of a WD during [5μM] DTC, extracted from a 60 second epoch. Below is the corresponding spectrogram (figure 4.5.1c). The number of WDs tends to peak during [5μM] concentration as can be seen from figure 4.5.3, however this effect is not considered to be statistically significant (P>0.05, n=20, One Way Repeated Measures ANOVA). The morphology of the wave discharge is generally very similar to a typical delta wave however the trough is much deeper, i.e. the majority of the WDs detected had an amplitude of greater than 250μV and interjected the typically delta rhythm. The WDs also generally lasted more than 500ms before the trace returned to it's initial position. The example WD shown in figure 4.5.1a, is embedded with frequencies less than 20Hz (delta, theta, alpha frequencies, figure 4.5.1b) for it's majority (figure 4.5.1c). However, the bottom of the trough co-insides with a short burst of gamma activity.

Spike Wave Complexes (SWCs) were present during nine of the twenty-eight experiments, resulting in an incidence rate of 0.32 SWCs per experiment. In total, 92 SWCs were detected during the recorded 60 second epochs from the nine successful experiments with the majority being detected during [10μM] application. Figure 4.5.2 shows a 1 second example of a SWC during [10μM] DTC extracted from a 60 second epoch. Below is the corresponding spectrogram (figure 4.5.2). The number of SWCs saw a significant effect of concentration (P=0.03, n=20, One Way Repeated Measures ANOVA, Figure 4.5.3). The median occurrence of SWCs during the control state was zero compared to 0 ($0 \rightarrow 5$) SWCs per 60 second epoch after 40 minutes of DTC [10μM] application (P=0.004, n=28, paired t-test). The morphology of the SWC is very different to the WD, however it is fairly similar to the spike and wave events detailed in Chapter 3. As with the WD, there are several different frequencies embedded in the SWC, however during and just following the spike there is a burst of activity in all frequency ranges below 100Hz. Also following the spike, the less than 20Hz frequencies are much more intense than during the WD as shown in figure 4.5.2c.

During a single experiment, electrodes were placed in both superficial (Layer I or II) and deep (Layer V) regions of a cortical column in the somatosensory region. The premise behind this experiment was to understand the corresponding effect seen in the superficial layers during the previously described epileptiform activity observed in the deep layers during DTC application. Figure 4.6 shows 5 second epochs of paired data during the control state and the different DTC concentrations used (10μM and 20μM). Throughout the different concentrations, the epileptiforms in the deep layers are very similar to those seen previously, as can be expected. During the control state, the superficial epoch is approximately 180 degrees out of phase with the deep epoch, which was also expected

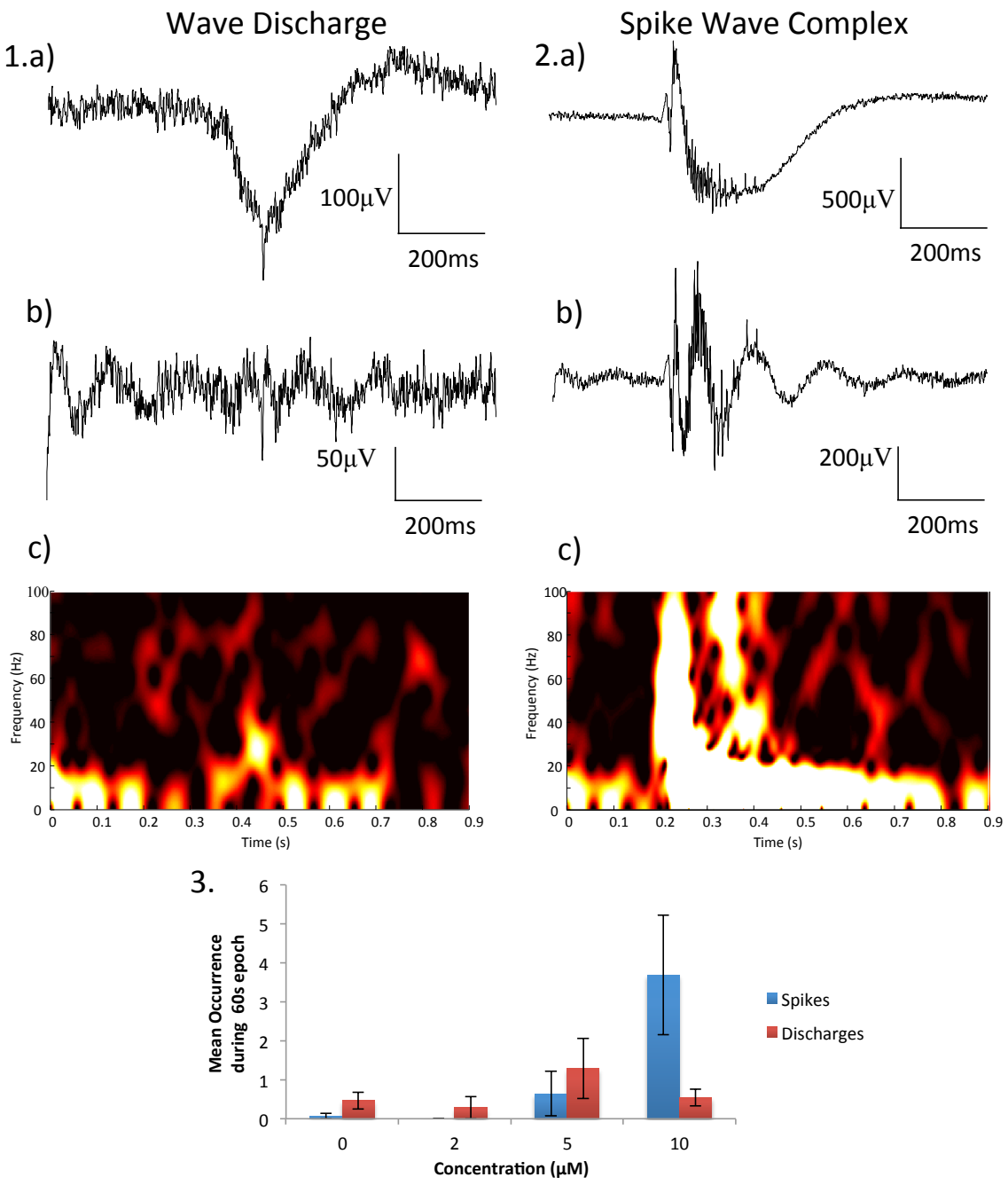

Figure 4.5: **Characteristics of epileptiform activity during d-tubocurarine application. 1a).** 1 second trace of a typical wave discharge extracted from 60 second epoch after 5μM application. **b).** Embedded frequencies extracted via the application of a high pass filter. **c).** Spectrogram corresponding to the trace shown above in a). **2a).** 1 second trace of typical spike wave complex extracted from 60 second epoch after 10μM application. **b).** Embedded frequencies extracted via the application of a high pass filter. **c).** Spectrogram corresponding to the trace shown above in a). **3.** Bar chart showing the mean occurrence of WDs and SWCs during a 60 second epoch with increasing concentration.

having seen the same phenomenon during the laminar profiles in Section 4.1. However, the delta rhythm seen in the superficial layers has a more sawtoothed appearance compared to the delta rhythm in the deep layers.

In figure 4.6, the corresponding spectrograms are adjacent to the recorded epochs. The spectrograms for all the superficial layers across all concentrations, visually, have a greater amount of sub-20Hz activity in comparison to the deep layers. The superficial layers also tend to retain their delta frequency oscillations more so than their deep layer counterparts, particularly following the bath application of [10μM] DTC. During [10μM] DTC application, the traces are still 180 degrees out of phase with each other however the magnitude of the epileptiform in the deep layer does not seem to be fully reflected in the superficial layer. Nevertheless, high frequency activity is detected in both regions simultaneously, as shown in the corresponding spectrogram. The magnitude of the deep layer epileptiform is matched following the bath application of [20μM] DTC, as seen in figure 4.6. The spike wave seen in the superficial layers is very similar to the EEG recordings detailed in Chapter 3, figure 3.1. The corresponding spectrograms show high frequency activity during the epileptiform activity, particularly in the deep layer. In contrast, very little low frequency activity is detected in the deep layers, unlike the superficial layers which seems to retain in low frequency activity however not to the extent seen during the previous concentrations.

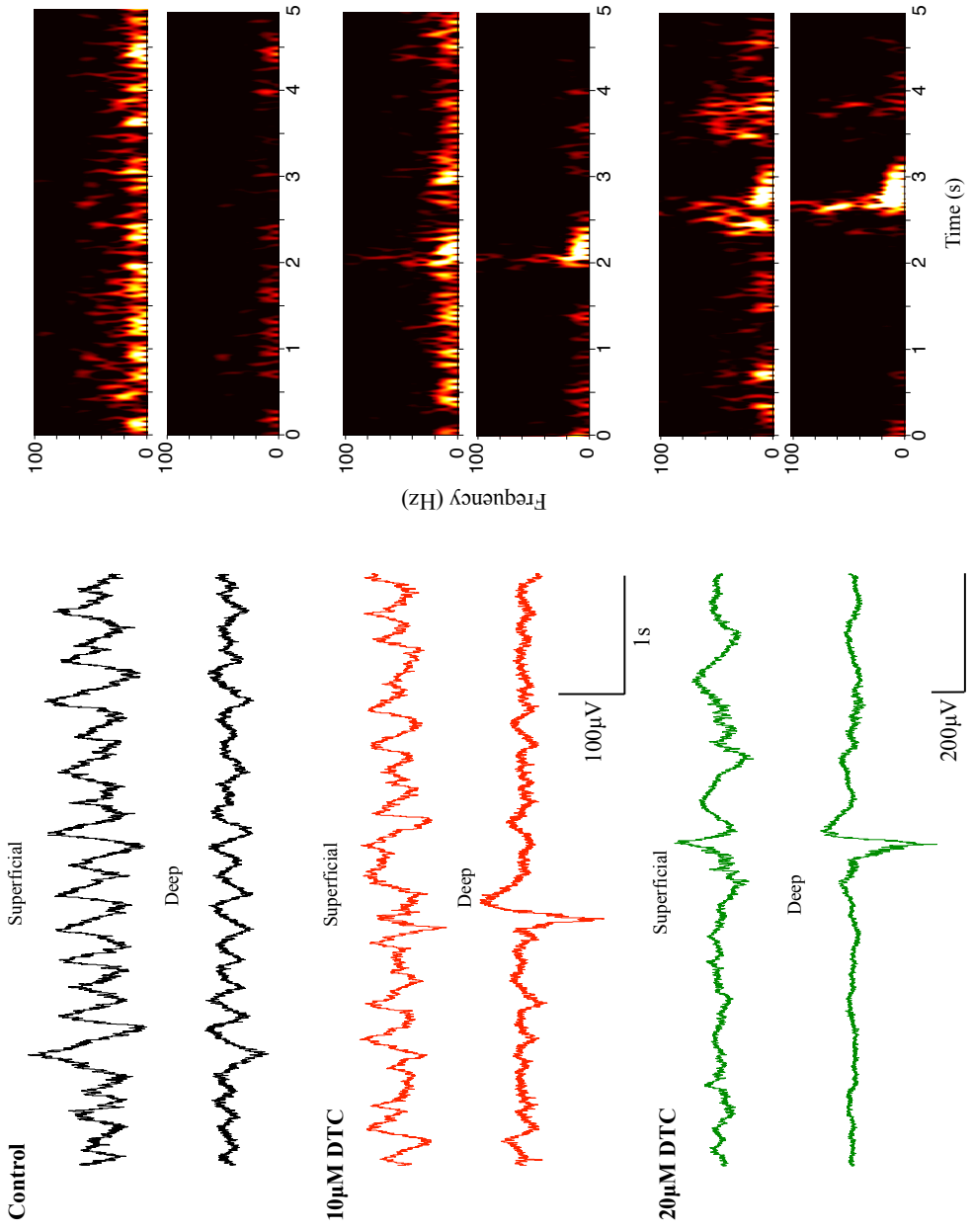

Figure 4.6: **Epileptiform activity seen in both superficial and deep layers following high concentrations of DTC.** 5 second epochs containing epileptiform activity were extracted from 60 second epochs during the control state and following the bath application of [10μM] and [20μM] DTC. The corresponding spectrograms for each trace can be found adjacent to the traces.

4.4 Discussion

The results reported in this chapter provide evidence that shows that epileptiform behaviour characteristic of that seen in EEG recordings during slow wave sleep in children with nocturnal epilepsies can be generated in the isolated brain slice preparation.

From the laminar profile analysis, delta rhythm activity was prominent throughout the cortical column although the power of the oscillation varied with location. As was expected, the power of the oscillations in deep layers, particularly layer V were greater than that in the superficial layers which corresponds to the results presented by Carracedo (2010). Also previously reported by Carracedo (2010), was the lag of layer V delta activity behind the activity in the other cortical layers (bar layer I) inferring layer V was the origin of the rhythm. Layer I is known to contain the apical dendrites of neurones in layer V, which may explain the inverse phase relationship between the two layers. The application of DTC resulted in the lag in layer V becoming more pronounced.

4.4.1 Paroxysm activity in the isolated cortex

Results from this chapter support work by L*ü*ttjohann *et al* (2013) and Avoli (1983) showing that SWCs can be observed in the somatosensory region of rat brain. Although no statistically significant increase in delta rhythm spectral power was observed preceding SWCs, visually there was a general increase in power spectra with concentration before SWCs occurred which has also been observed in the somatosensory cortex of WAG/Rij rats by the authors. This is of particular interest as the common feature between the studies by these authors is the involvement of the thalamus, which the isolated section of neocortex used within this thesis is independent of as well as other brain regions associated with sleep. A review by Blumenfeld (2005) presented many studies that demonstrated the need for the thalamus and cortex to be present for SWCs to occur. Conversely, he also presented several studies that argued that the thalamus does not need to be present to induce SWCs. The author further goes on to state, 'demonstrating that some forms of SWCs can arise from isolated cortex does not mean that all spike-wave discharges arise from cortex independently of the thalamus' [Blumenfeld, 2005]. Unlike the studies detailed in the authors review, the SWCs seen in this chapter are not continuous. On average, 1 SWC occurred every 15 seconds after the application of DTC [10μM], with the SWC lasting approximately 500ms in total. Is the reason behind these non-continuous SWCs due to the lack of true thalamo-cortical projections and the pharmacological delta frequency oscillation model being inadequate to permit continuous SWCs as seen in *in vivo* models? Work by Vergnes *et al* (1987) and Pelligrini *et al* (1979) describes the neocortex alone is less capable of sustaining paroxysm activity, therefore

suggesting that this may be the case. For the purpose of this research, the mere presence of SWCs is sufficient, however to understand if the findings are true, a future *in vivo* comparison study would be of interest.

4.4.2 Possible relationship between Wave Discharges and Spike-Wave Complexes

In section 2.8.1 in the main Methods chapters, wave discharges (WDs) are defined as a clearly distinguishable waveform from that of the general LFP activity, with an amplitude >200μV peak-to-peak and no spike interrupting the smooth wave. As stated, the only difference between a WD and a spike-wave complex (SWC) is the presence of a spike within the wave, the position of said spike within the wave is inconsequential to this research. The majority of the literature related to epileptiform activity only discusses SWCs, is this because SWCs are easily distinguishable to the ambient rhythm in comparison to the WD? The WD generally looks like an enhanced period of delta rhythm activity, although these are individual events and do not seem to effect the rhythmicity of the delta rhythm, instead they seem to interject it at random intervals. Therefore suggesting that these events are separate from the delta rhythm. With reference to this provisional research, the understanding is that the wave discharge is observed before the occurrence of SWCs. Whether the WD is a precursor to the SWC is unknown at present, however as the occurrence of SWCs increases, the number of WDs decreases therefore implying that this may indeed be the case. It may be possible that WDs are the beginning of SWCs before an unknown capacity is reached where the WDs morph into complete SWCs.

4.4.3 High frequency components of paroxysmal activity

Higher frequency activity, mainly gamma frequency oscillations were observed to coincide with the spike in the SWCs which were detected using spectrograms. This high frequency activity was followed by a high intensity of low frequency activity (<20Hz). This characteristic is typical of spike wave paroxysmal activity [Blumenfeld, 2005] and is also very similar to that seen in animal models of stroke. In cortex, gamma oscillations are thought to be related to the emergence of localised activity in a small region [Steriade and Amzica, 1996]. Recent studies have reported that low band gamma (30-60Hz) is localised to the deep layers, predominantly layer V, whereas the high band gamma (80-200Hz) is localised more superficially to layer II and generated by synaptic excitation and inhibition in layer III [Srejic et al., 2013]. Both of these gamma bands are thought to be mediated by GABA receptors, however there is some evidence that the high gamma oscillations are mediated by gap junctions instead [Whittington et al., 2000]. DTC is a

known $GABA_A$ antagonist and the disruption of GABA transmission is thought to induce seizures [Treiman, 2001]. In the feline generalised penicillin epilepsy model, a large dose of penicillin, a weak $GABA_A$ antagonist, induces 3-4Hz generalised SWCs and episodes of unresponsiveness which resemble human absence seizures [Avoli and Gloor, 1982]. This may mean that DTC is acting on the $GABA_A$ receptors instead of the nAChRs or the $5HT_3$ receptors, however at this point it is unclear. Future research is needed to understand the receptor subunits responsible for SWC inducement.

4.4.4 Low frequency components of paroxysmal activity

Intensity of alpha and beta frequencies oscillations present in all superficial recordings is greater than the deep layers across all concentrations states, except during an SWC where the intensities match. As stated in Section 1.5.2, alpha activity can be superimposed on delta rhythms during SWS and tends to be present when a person complains of non-restorative sleep and is generally observed in those with sleeping disorders [Jaimchariyatam et al., 2011]. This therefore could imply that as the alpha and beta frequency activity is present before the application of DTC, that the delta model used is itself a precursor to epileptiform activity in the superficial layers.

4.4.5 Relationship to nicotinic mechanisms of seizure reduction

Nicotine is thought to help decrease seizure frequency in ADNFLE patients as described in section 4.1. The SWC model derived in this chapter antagonises several different families of receptors to induce seizure-like activity, which clinically, nicotine would agonise to reduce the prevalence of seizures. Nicotine is known to effect specific subunits (α_4 and β_2) whereas DTC is a broad spectrum antagonist which blocks all nAChRs as well as the aforementioned 5-HT_3 and $GABA_A$ receptors. Therefore it is currently unknown if the nicotinic mechanisms involved in reducing seizures are related to those in this research which induce the epileptiform activity, or if other subunits play a role. As previously stated, further research is needed to understand the role the separate receptor subunits play in paroxysm evocation.

4.4.6 Current mediated paroxysm activity

The hyperpolarization-activated cation current, I_h, is known to play an important role in delta frequency activity, as the blockade of the current can result in the cessation of the delta rhythm [Hughes et al., 1998]. The delta rhythm model used in this thesis is known to respond in a similar way [Carracedo, 2010]. Studies by Schwindt *et al* (1988) and Spain *et al* (1987) have demonstrated that I_h cortical currents contribute

to spike repolarisation, spike frequency adaptation and afterhyperpolarisation magnitude and duration. Whilst alterations in I_h current are associated with SWCs in HCN2 knockout mice and *stargazer* mice [Di Pasquale et al., 1997], where reduced I_h is thought to enhance cortical excitability by increasing dendritic impedance. The I_h current can be modulated by 5-HT resulting in the inducement of a positive shift of up to 10mV in its half-maximal activation, which is of interest due to the antagonistic nature of DTC on 5-HT_3 receptors. The application of serotonin is known to increase the amplitude of I_h current, therefore it is possible that DTC would decrease the amplitude. During the DTC [10μM] application, the delta rhythm was shown to still be present in-between the SWCs (figure 4.2), however as shown in figure 4.6, although the delta rhythm is much less prominent, it has not ceased. These observations imply that with an increase in DTC, I_h may be decreased, however not sufficiently enough to result in the cessation of the delta rhythm. This possible decrease in I_h may also be involved in the inducement of SWCs through the enhancement of cortical excitability.

Ethosuximide, an anti convulsant drug, is known to block SWC firing in GAERS rats in the somatosensory cortex [Manning et al., 2004]. Interestingly, it is also used to reduce persistent sodium current in thalamic and cortical neurons [Leresche et al., 1998]. An increase in sodium current may therefore be associated with neuronal bursting, hyper excitability and subsequently, the generation of SWCs. This may be the molecular basis of SWCs in WAG/Rij rats, which are reported to have increased expression of voltage-gated sodium channels $Na_V1.1$ and $Na_V1.6$ compared with non-epileptic controls [Klein et al., 2004]. However, DTC antagonises ligand gated ion channels, therefore stopping the inflow of sodium ions. Hence, it can be concluded that although sodium currents are thought to be responsible for SWCs in some animal models of epilepsy, it may not be the molecular basis of the SWCs detailed in this thesis.

4.4.7 Summary

This chapter has described the processes involved in the optimisation of an *in vitro* spike wave complex in slow wave sleep model in the rat somatosensory cortex. With its conclusion, a reasonably reliable model of the epileptiform activity prevalent in childhood nocturnal epilepsies has been established. To reiterate, the conditions that were found to be most favourable for the production of epileptiform activity consist of the initial application carbachol [4μM] and SCH23390 [7μM] to induce the delta rhythm in 450μm sections of the somatosensory cortex cut in the coronal plane. Upon delta rhythm stabilisation, the application of DTC [10μM] would induce epileptiform activity similar to that seen in clinical EEG studies.

The development of this *in vitro* epileptiform activity model provides an introduction to a relatively novel area of study, hence providing significant opportunities for further investigation. The experiments in the subsequent chapters of this thesis will provide an in depth study of the rhythm, the mechanisms underlying its generation and it's spatial distribution through the cortical layers of the somatosensory cortex. Chapter 5 will explore the basic pharmacological properties of the epileptiform activity with the aim of identifying the key receptor subunits responsible for the generation of the SWCs and WDs.

Chapter 5

Pharmacological generation of epileptiform activity during cortical delta rhythm

5.1 Introduction

The previous chapter of this thesis described the discovery, optimisation and basic characterisation of the impact of the non-specific competitive nicotinic acetylcholine receptor antagonist, d-tubocurarine on a cortical delta model in the somatosensory cortex of the rat *in vitro*. This was elicited by mimicking the neuromodulatory processes associated with non-REM sleep. The basic electrophysiological properties of the delta rhythm and epileptiform activity were used to describe the effect of d-tubocurarine (DTC). The results of these experiments have strongly indicated that nAChRs are involved in the epileptiform activity relating to childhood nocturnal epilepsies. However, there are many nAChR subunits which DTC may be blocking, hence inducing the epileptiform activity. DTC is also known to be a potent 5-HT receptor antagonist [Gerschenfeld and Paupardin-Tritsch, 1974, Wonnacott and Barik, 2007], acting on the 5-HT_3 receptor subunit predominantly [Peters et al., 1990] particularly at concentrations between 1 and 10μM. Higher concentrations of DTC also block $GABA_A$ receptor mediated currents [Wotring and Yoon, 1995]. Therefore, it is currently unclear, the antagonism of which particular neuromodulator/s elicits the spike and wave epileptiform activity. The following sections briefly introduce what is currently known about the neuromodulator subunits DTC effects and how they are currently thought to link to childhood nocturnal epilepsies.

5.1.1 Nicotinic Acetylcholine Receptor Subunits

Acetylcholine (ACh) and it's receptor subtypes have previously been discussed in depth in section 1.2.1, however their response to d-tubocurarine has not, which will be remedied in this introduction.

Previous studies have reported that at low concentrations DTC has been shown to be a competitive antagonist, meaning that it can bind to any nAChR but will not activate the receptor. The antagonist will compete for binding sites with agonists, such as nicotine and acetylcholine, and at sufficient concentrations will displace the agonist [Pedersen and Cohen, 1990]. With a competitive antagonist, higher concentrations of the endogenous agonist, in this case acetycholine, can displace DTC and restore receptor function. However, at higher concentrations (like the ones used in the previous chapter) DTC is considered to be non-competitive. Therefore, the concentration of the agonist can be disregarded as, no matter the agonist concentrations, the antagonist cannot be removed from the receptor and therefore cannot restore function [Colquhoun et al., 1979]. DTC cannot normally cross the blood brain barrier. It is generally considered a neuromuscular relaxant with regards to nAChRs. However, it is also known to antagonise neuronal nAChRs in *in vitro* studies in chicks, specifically α_4 and non-α_7 subunits [Bertrand et al.,

1990]. Due to it's non-specific competitive nature, DTC is thought to block most AChR subunits, therefore understanding what role each subunit plays in the evocation of epileptiform activity seen in the present studies is necessary.

In 1959, a paper written by Nisbet reported the treatment of status epileptics with D-tubocurarine, in this case however, DTC was administered as a muscle relaxant during seizures. Several studies have explored intraventricular injections of DTC which have been monitored using EEG to understand their effect on hippocampal activity (e.g. [Carmichael et al., 1964, Feldberg and Fleischhauer, 1963]). In contrast to the results from the Nisbet (1959) study, results demonstrated that high doses of DTC elicited epileptic spike and wave complexes which were linked to the theta rhythm [Dajas et al., 1983]. As stated previously DTC cannot easily pass through the blood brain barrier, therefore in the body it acts as an anti-epileptic agent, whilst when directly introduced to the brain, it has an epileptogenic effect.

Several nAChRs have been linked to childhood idiopathic epilepsies. The α_7 subunit is linked to BECTS [Neubauer et al., 1998], mutations in γ_3 subunits have been linked to CAE [Everett et al., 2007] and α_{3-5}, α_7, β_2 and β_4 subunits have all been linked to rare genetic mutations in ADNFLE [Marini and Guerrini, 2007, Siddiqui et al., 2007, De-Fusco et al., 2000], of which all three conditions display epileptiform abnormalities during slow-wave sleep. As previously detailed in Chapter 1.7.2, patients with these idiopathic epilepsies have difficulty with executive tasks, i.e maintaining attention, visuo-spatial skills and working memory. The nAChR subunit antagonists used within this chapter have been chosen to selectively block these receptors, to help understand the mechanisms responsible for paroxysmal event generation.

The nAChR subunit antagonistic agents that will be utilised within this research have been chosen to allow for a greater understanding of which receptor subunits, if any, are responsible for the generation of epileptiform activity. Pancuronium dibromide was chosen due to its skeletal muscle relaxant properties which would relate to the Nisbet study mentioned previously. DHβE has been shown to disrupt cognitive performance when injected directly into the rodent brain [Felix and Levin, 1997]. This study also reported a similar result when MLA, a potent α_7 antagonist was similarly administered. Due to the agents ability to interact with both $\alpha_4\beta_2$ and $\alpha_6\beta_2$ receptors at concentrations >40nM, a more selective agent (MG624) was used in this study. As stated above, α_{3-5} and β_4 subunits have also been linked to idiopathic epilepsies, therefore agents that specifically act upon these subunits were required for this study (α-conotoxins PnlA ($\alpha_3\beta_2$) and AuIB ($\alpha_3\beta_2$)).

5.1.2 Serotonin

5-hydroxytryptamine (5-HT) or serotonin and it's subtypes have been discussed in depth in section 1.2.1 however, similarly to nAChRs above, their response to DTC has not which will be remedied in this introduction.

Over the past 15 years it has become well established that DTC is a potent antagonist of the 5-HT_3 receptor [Yan et al., 1998, Yan and White, 2002, Hope et al., 1999, Peters et al., 1990, Eisele et al., 1993] as well as a potent antagonist of nAChRs (as previously discussed). As stated in section 1.2.1, when the 5-HT_3 subtype receptor is antagonised, an increase in slow wave sleep (SWS) and/or rapid eye movement (REM) sleep is observed [Ponzoni et al., 1995]. DTC has similarly been documented to induce amplification of SWS EEG recordings and to desynchronise activity during REM sleep [Haranth and Venkatakrishna-Bhatt, 1977]. This would imply that the mechanisms behind the increased delta rhythms observed during slow wave sleep due to the antagonism of the $5HT_3$ receptor subunit are similar to those during DTC administration. It can therefore be hypothesised that a selective $5HT_3$ antagonist, such as MDL 7777 will elicit a similar response to that seen in the previous chapter, following the administration of DTC.

Through studies in both animal and human models of epilepsy, serotonin is generally known to play a role in epileptic mechanisms. In 1989, Dailey *et al* reported a decrease in the concentration of serotonin in the cortex of the genetically epilepsy-prone rat (GEPR) model of generalised epilepsy. While in 1996, Statnick *et al* further reported a decrease in V_{max} for [^{3}H] serotonin, a synaptosomal 5-HT uptake and tryptophan hydroxylase activity. Pharmacological studies on these animals as well as the maximal electroshock model and several others have shown that the administration of drugs that improve 5-HT transmission inhibit seizures [Statnick et al., 1996]. Whilst, susceptibility to seizures is increased with a reduction in neural 5-HT concentration both in animal models and humans [Lazarova et al., 1983, Wenger et al., 1973]. The antagonism of the 5-HT_3 subtype receptor has specifically been shown to lower the clonic seizure threshold of pentylenetetrazole induced seizures in mice [Gholipour et al., 2007]. Therefore, it is possible that the application of 5-HT_3 antagonist MDL 7777 will increase the possibility of epileptiform activity *in vitro*.

5.1.3 GABA

γ-aminobutyric acid (GABA) is considered to be the major inhibitory neurotransmitter in the central nervous system. There are three classes of GABA receptors: $GABA_A$, $GABA_B$ and $GABA_C$. $GABA_A$ receptors are ligand-gated chloride ionotropic receptors

which are the principal receptors in GABAergic synaptic transmission [Li and Xu, 2008]. $GABA_B$ receptors are G protein coupled receptors and are less prevalent in the CNS than $GABA_A$ receptors. $GABA_C$ receptors are also ligand-gated chloride ionotropic receptors, however unlike $GABA_A$ receptors, they only exist in the visual pathway [Li and Xu, 2008]. Research undertaken during this thesis is only interested in $GABA_A$ receptors due to the antagonistic effect DTC has on $GABA_A$ receptors [Wotring and Yoon, 1995]. Whole-cell patch-clamp experiments by Siebler *et al* (1988) demonstrated the decrease in GABA currents following micro molar concentrations of curare (also known as d-tubocurarine). As stated previously DTC, is known to be a non-selective competitive nAChR antagonist, however due to the similarities between the nACh and $GABA_A$ receptors, both members of a pentameric ligand gated family of channels, it would suggest they share common features and react similarly to DTC [Wotring and Yoon, 1995]. In some regions, the homology between nAChRs and $GABA_A$ receptors is 60%, both receptors contain a β subunit extracellular loop and a similar α helical protrusion into the pore which may act as a gate [Schofield et al., 1987]. Several articles have suggested that the $GABA_A$ receptor in the brain most likely consists of α_1, β_2 and γ_2 subunits [Laurie et al., 1992, Benke et al., 1994, Rabow et al., 1995, McKernan and Whiting, 1996]. Wotring *et al* (1995) believed that a single DTC molecule was able to block both GABA binding sites.

Kafka *et al* (1986) observed that GABA transmission increases during sleep when compared to the level observed during wakefulness. GABA transmission, which is mediated by the $GABA_A$ receptor subtype due to the abundance in the CNS, has been implicated in learning and memory processes. Interference of GABA mediated transmission has been shown to have a negative effect on learning and memory. As GABAergic activity is increased during sleep, this disruption may have a negative effect on sleep dependant memory processes. In 2010, Shen *et al* conducted a study into the role of $\alpha_4\beta\delta$ $GABA_A$ in shaping learning deficits during puberty in female mice. They found that, in female wild type mice, inhibition mediated by the $GABA_A$ receptor subtype resulted in deficits in learning during puberty and a decrease in ability to perform long term potentiation (LTP) - dependant memory tasks, whereas these deficits were not observed in prepubertal and pubertal δ-/- KO mice. This effect was thought to be as a result of a decrease in *N*-methyl-D-aspartate (NMDA) receptor activation and subsequently a decrease of LTP.

In a review of GABAergic mechanisms in Epilepsy, Treiman (2001) describes epileptic seizures as paroxysmal hyper synchronous transient events that are the result of either too much excitation or too little inhibition in the particular region of the brain where the abnormal activity is initiated. As previously stated, GABA is recognised as the principal inhibitory neurotransmitter hence it is likely that the antagonism of GABA induces

seizures whilst the agonism of GABA suppresses them [Treiman, 2001].

5.1.4 Aims and Objectives

The previous section provides a brief introduction to to earlier work and knowledge accumulated in which DTC has been shown to antagonise three specific types of receptors: nicotinic Acetylcholine, 5-HT_3 and $GABA_A$. The aims of this chapter are to:

- To understand which specific receptor subunits respond similarly to DTC application through pharmacological manipulation via receptor specific antagonists.
- To mimic oscillatory activity induced by DTC using pharmacological agents to investigate the mechanisms underlying DTC-induced epileptiform activity.
- To understand the variation in epileptiform activity and how it differs during the antagonism of different receptor subunits.

5.2 Methods

Methods were the same as those detailed in chapter 4. Delta activity was induced through the co-application of carbachol [4μM] and SCH23390 [7μM] and was allowed to develop and stabilise over a 2 hour period. All pharmacological compounds were bath applied to slices and allowed to act for 40 minutes, in order to allow for any effects to stabilise. Data from pharmacology experiments detailed within this chapter were obtained through extracellular field recordings. The power of the activity in the delta frequency band (0.5-5Hz) was compared before and after pharmacological manipulation and was taken as the primary indicator of the strength of the oscillation. All statistics will be written to two decimal places unless the number is less than 0.005 where it will be written as three decimal places.

During data analysis, if spike and wave complexes (SWCs) were present in the 60 second epochs, three separate epochs of either 8 or 3 seconds durations, dependent upon the frequency of the SWCs, per concentration were used during the frequency and power analysis to ascertain the pharmacological effect of the drug, solely upon the delta rhythm. The mean values were calculated for each 60 second epoch of data, which were then used to calculate the overall mean, standard deviation and standard error of the mean (SEM) values per concentration as shown in the concentration response graphs of each drug. Rhythmicity was also measured using the same 8 or 3 second epochs. Once the data had been extracted from the autocorrelation graphs, the same method was used to calculate the overall mean, standard deviation and SEM values as frequency and power. Single 8

or 3 second epochs were used to produce the frequency spectrums and autocorrelations seen in each figure in this chapter. To better understand the high frequency activity embedded within the delta oscillations, 1 second epochs were extracted from 60 second recordings during which epileptiform activity was present.

5.3 Results

5.3.1 The effect of the bath application of nicotinic acetylcholine α_7 subunit selective antagonist MG624 to delta frequency oscillations

Delta frequency oscillations were induced in somatosensory cortex containing coronal rat slices by the bath application of carbachol [4μM] and SCH23390 [7μM], as used in Chapter 4. To discover if disrupted signalling through nicotinic receptors containing the nAChR α_7 subunit was a component of the mechanism behind spike and wave complexes (SWCs) induced by general nicotinic antagonist (Chapter 4), MG624 concentration response experiments [1 - 10μM] were undertaken. Due to the results from Chapter 4, recordings were only taken from layer V of the somatosensory cortex as this layer was found to have both the most stable, large amplitude control delta oscillation and the largest observable effect of d-tubocurarine (DTC).

During *in vitro* experimental conditions, the bath application of the neuronal α_7 subunit containing nAChR subtype selective antagonist MG624 resulted in a significant decrease in power of the delta band from a median value of 0.30μV^2 (0.08μV^2 $\rightarrow$ 0.58μV^2) to 0.04μV^2 (0.03μV^2 $\rightarrow$ 0.05μV^2) after 40 minutes of MG624 [10μM] application (P=0.004, n=4, Friedman Repeated Measures Analysis of Variance on Ranks). This significant effect can be observed in figure 5.1D. There is an obvious decrease shown in figure 5.1D during the bath application of MG624 [2 and 5μM], however due to the variation in the dataset, the effect observed during these concentrations was not statistically significant (P>0.05, n=12, One Way Repeated Measures ANOVA).

The delta rhythm proved to be insensitive to a blockade of α_7 subunit containing nAChRs and the mean peak frequency remained fairly constant throughout the experiment (1.36 $\pm$ 0.1Hz during control versus 1.14$\pm$0.15Hz after MG624 [10μM], P>0.05, n=12, One Way Repeated Measures ANOVA).

Autocorrelation analysis was conducted in order to assess the effects of the drug on the rhythmicity of the activity in the slice. Prior to MG624 application auto-correlation

analysis of delta oscillations resulted in a graph that was sinusoidal in form indicating that the activity was intrinsically rhythmic. The autocorrelation data was normalised, thus the height of the central peak was always 1 with reference to the y-axis. Autocorrelation analysis revealed that no statistically significant effect of concentration was observed for rhythmicity ($P>0.05$, n=6, One Way Repeated Measures ANOVA). As shown in figure 5.1D, the variation in the dataset may be the cause of the lack of statistical significance. The mean ratio of the first peak to the central peak during the control condition was 0.48 ± 0.08 whilst the mean ratio during the final concentration [10μM] was 0.28 ± 0.01.

Of the eleven experiments conducted, wave discharges (WDs) were present during 5 experiments resulting in a WD incidence rate of 0.45 per experiment. Figure 5.2a shows a 1 second example WD following [2μM] MG624 bath application, extracted from a 60 second epoch recording. Below it, is it's corresponding spectrogram (figure 5.1c). In total, 39 WDs were detected during the increasing MG624 concentrations, the majority of which were detected during [2μM] application (figure 5.2e). The number of WDs tends to peak at 2μM however it is not considered to be statistically significant. Although statistical analysis did reveal that there was a significant effect of concentration on the number of WDs during a 60 second epoch ($P=0.04$, n=6, One Way Repeated Measures ANOVA). The mean occurrence of WDs during the control state was 0.64 ± 0.28 WDs per 60 second epoch compared to 2.33 ± 0.84 WDs per 60 second epoch after 40 minutes of MG624 [2μM] application. As with the WDs detailed in Chapter 4, during the trough there is an increased intensity of activity however in this case it is limited to frequencies below 20Hz. There is also very little low frequency activity preceding and following the trough, unlike during the DTC WDs.

Spike waves complexes (SWCs) were present during 2 of the five experiments, resulting in an SWC incidence rate of 0.18 per experiment. In total, 29 SWCs were detected during the 60 second epochs over the varying concentrations, 5 of these were spontaneous. The incidence rate of SWCs increased with concentration, however this was not found to be a statistically significant effect ($P>0.05$, n=6, One Way Repeated Measures ANOVA). The mean occurrence of SWCs during the control state was 0.46 ± 0.46 SWCs per 60 second epoch in comparison to 3 ± 3 SWCs per 60 second epoch following 40 minutes of MG624 [10μM] bath application. An example of a SWC following MG624 [10μM] application can be seen in figure 5.2b with it's corresponding spectrogram beneath (figure 5.2d). The morphology of the SWC looks very different to that seen during DTC application (refer to figure 4.5.2b), instead of the spike being at the beginning of the trough, it is just after the base of the trough. There is some high frequency activity

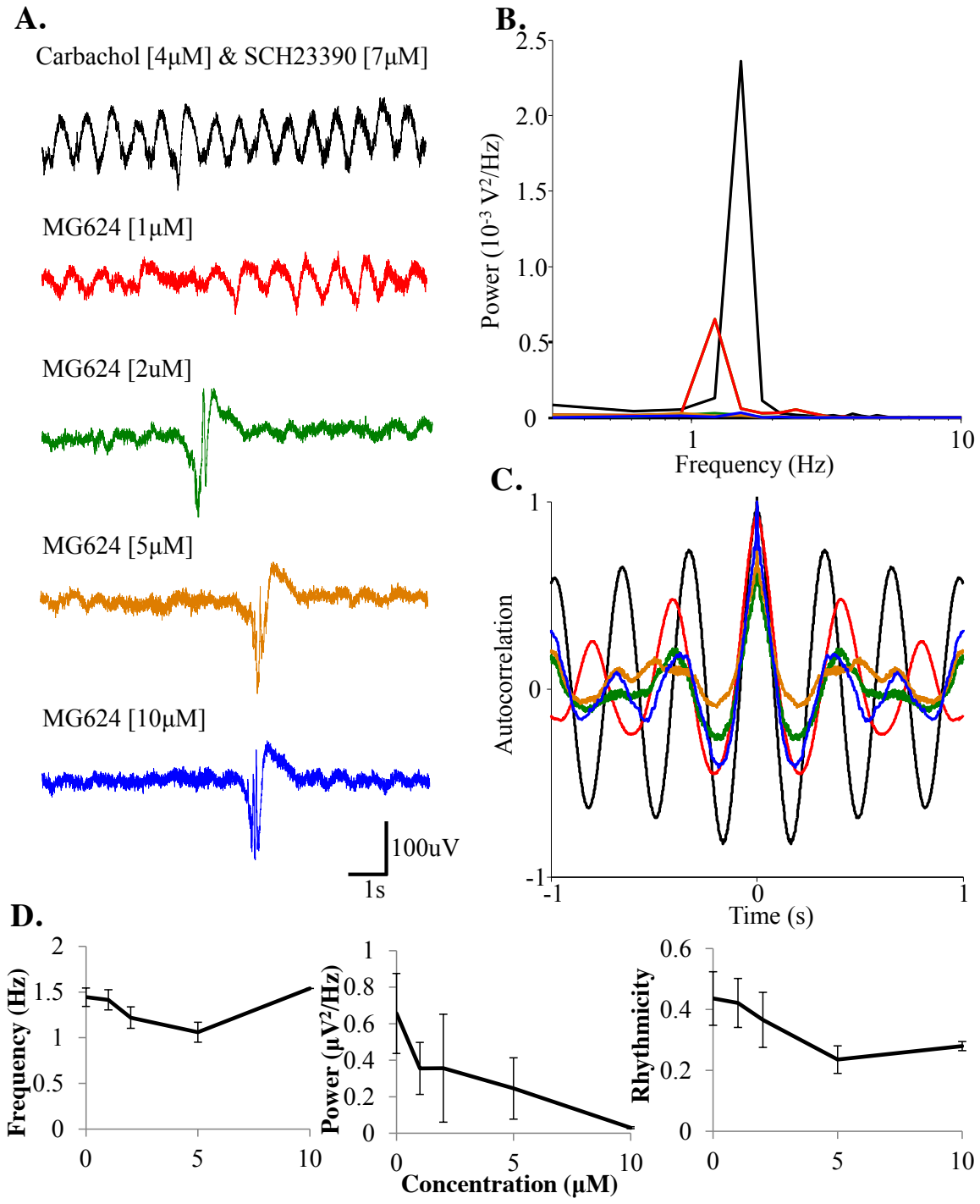

Figure 5.1: **Antagonism of nAChR subunit α_7 using MG624. A.** 10 second sample recording of extracellular activity from layer V of the somatosensory cortex after application of Carbachol[4μM] and SCH23390 [7μM], followed by the application of increasing concentrations of MG624. **B.** Power spectra produced from 8 second epochs of data in the absence of epileptiform activity. **C.** Autocorrelation from an 8 second epoch of activity in the absence of epileptiform activity, showing decreasing rhythmicity with concentration. **D.** Concentration response curves of mean frequency, mean power and mean rhythmicity ratio of activity (all n=6) during MG624 applications.

during the SWC, however the intensity is much lower than that seen during DTC, albeit during the SWC the intensity of the sub 20Hz frequencies increases. No pattern has been detected with regards to epileptiform activity during a 60 second epoch i.e. occurring at a regular frequency, however this may be due to the length of the epochs used.

5.3.2 The effect of the systematic application of nicotinic acetylcholine $\alpha_7^\star$ subunit selective antagonist, Pancuronium, on delta frequency oscillations.

The bath application of the neuronal $\alpha_7^\star$ subunit containing nAChR subtype selective antagonist, Pancuronium resulted in no statistically significant change in mean power in the delta band as can be seen in figure 5.3D. The mean delta band power during the control state was $0.83\pm0.12\mu V^2$ compared with the mean power after 40 minutes of the application of the final concentration [10μM], $1.34\pm0.27\mu V^2$ (P>0.05, n=34, One Way Repeated Measures ANOVA).

The frequency of the delta rhythm saw a significant effect of Pancuronium concentration (P=0.004, n=34, One Way Repeated Measures ANOVA). Within 40 minutes of Pancuronium [10μM] application the mean peak frequency of the delta band was reduced from 1.49 ± 0.09Hz during the control state to 1.19 ± 0.07Hz (P=0.002, n=34, paired t-test). This significant decrease is not easily observable in the concentration response graph in figure 5.3D, however this is likely due to the variance of the dataset and the small range the frequency varied over.

Autocorrelation analysis reported a near significant decrease in rhythmicity with concentration (P=0.07, n=17, One Way Repeated Measures ANOVA)(figure 5.3D. The mean height ratio of the first peak to the central peak with reference to the y-axis was 0.32 ± 0.05 during the control state, however as can be seen in figure 5.3C, this control signal was not always sinusoidal in appearance. Whilst the application of pancuronium may have improved the rhythmicity with regards to its sinusoidal appearance, as stated previously no significant change in rhythmicity was detected. After 40 minutes of Pancuronium [10μM] application, the mean height ratio of the first peak to the central peak was 0.2 ± 0.04.

Of the fifteen experiments conducted, WDs were present during six experiments resulting in an incidence rate of 0.35 per experiment. In total, 76 WDs were detected during the increasing Pancuronium concentration, the majority of which occurred following the application of [2μM] Pancuronium (see figure 5.4e. As can be seen from figure 5.4e, there

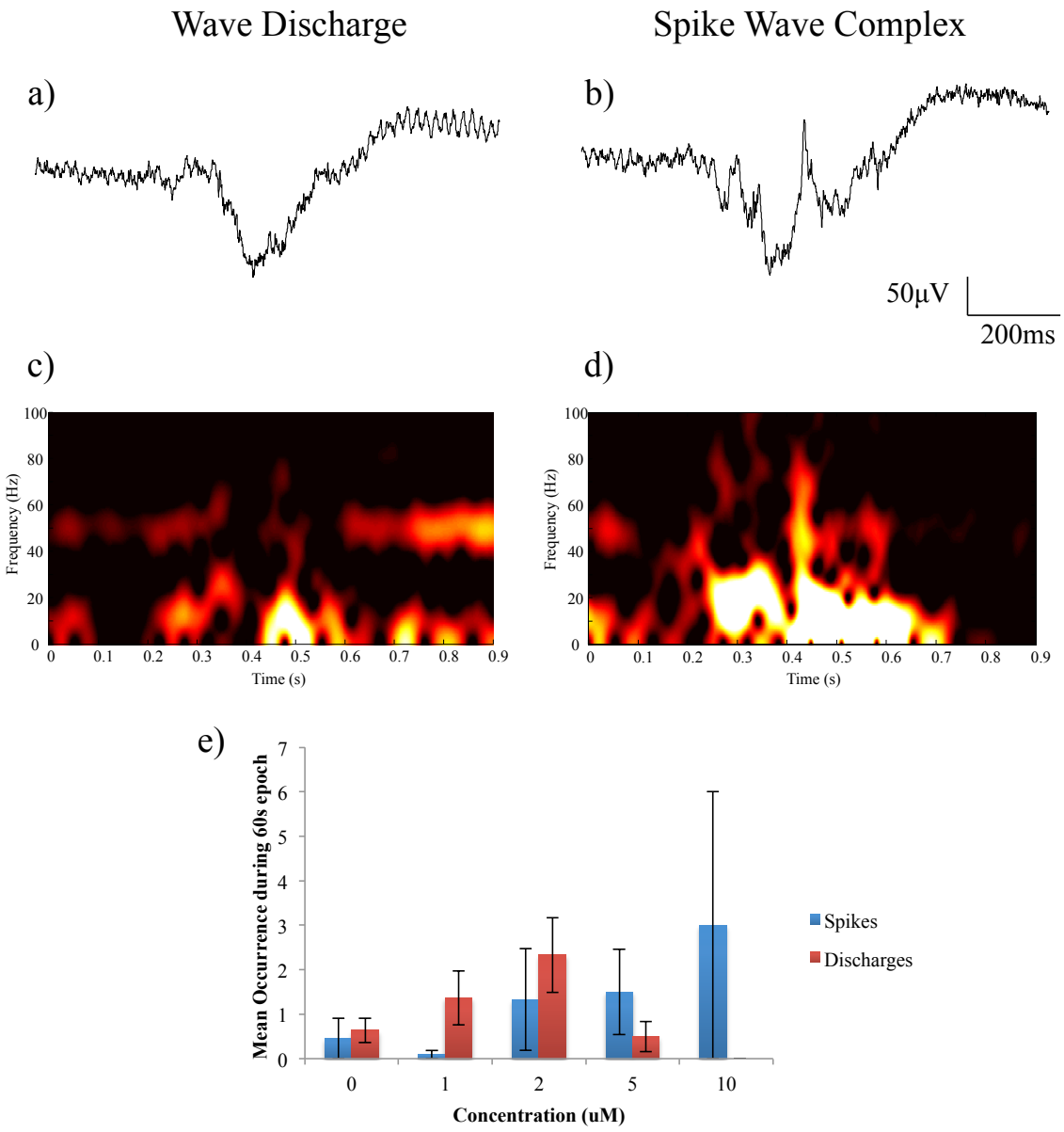

Figure 5.2: **Characteristics of epileptiform activity during MG624 application. a.** 1 second trace of wave discharge extracted from 60 second epoch after 10μM application. **b.** 1 second trace of spike wave complex extracted from 60 second epoch after 10μM application. **c.** Spectrogram corresponding to the trace shown above in a). **d.** Spectrogram corresponding to the trace shown above in b). **e.** Bar chart showing the mean occurrence of WDs and SWCs during a 60 second epoch with increasing concentration.

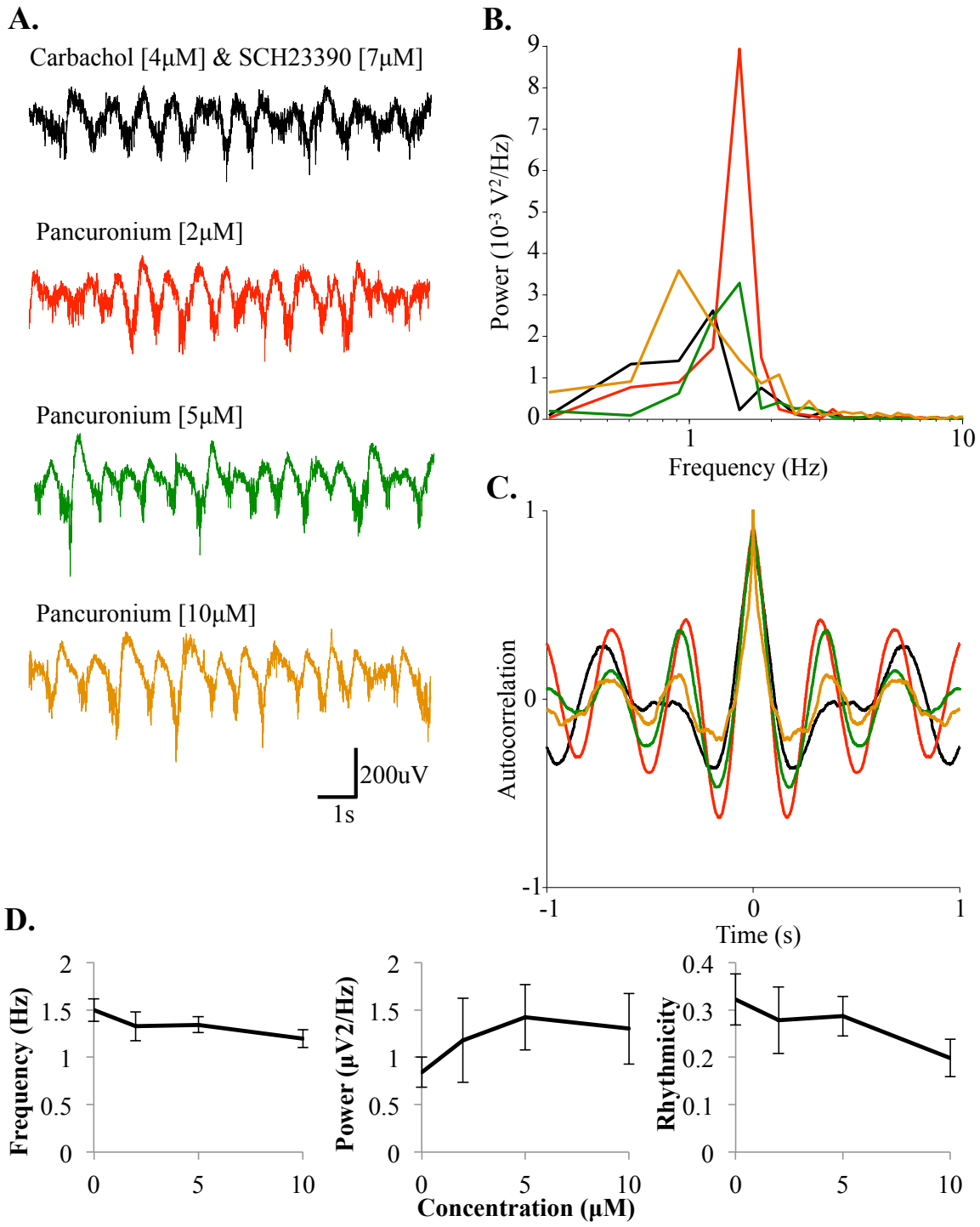

Figure 5.3: **Antagonism of nAChRs subunits $\alpha_7^\star$ using Pancuronium bromide.** **A.** 10 second sample recording of extracellular activity from layer V of the somatosensory cortex after application of Carbachol[4μM] and SCH23390 [7μM], followed by the application of increasing concentrations of Pancuronium bromide. **B.** Power spectra produced from 8 second epochs of data in the absence of epileptiform activity. **C.** Autocorrelation from an 8 second epoch of activity in the absence of epileptiform activity. **D.** Concentration response curves of mean frequency, mean power and mean rhythmicity ratio of activity (all n=8) during Pancuronium applications.

is no obvious trend when referring to the WD incident rate and statistical analysis has reported no significant effect of concentration (P>0.05, n=8, One Way Repeated Measures ANOVA). The mean occurrence of WDs during the control state was 0.35±0.35 WDs per 60 second epoch in comparison to 2±1.66 following 40 minutes of Pancuronium [10μM] application. The spectrogram for the example wave discharge, see figures 5.4a and 5.4c, contained a substantial amount of high frequency activity with the trough. Whereas after the trough, there was a high intensity of sub 20Hz activity embedded in the WD.

Spike wave complexes (SWCs) were only present during 3 experiments resulting in an incidence rate of 0.17 per experiment. In total, 14 SWCs were detected during the three experiments, 7 of which were spontaneous, i.e. occurring during the control state. The number of SWCs varied between experiments however no significant effect of drug concentration was observed (P>0.05, n=8, One Way Repeated Measures ANOVA, figure 5.4e. The mean occurrence of SWCs during the control state was 0.41±0.41 SWCs per 60 second epoch in comparison to 0.13±0.13 following the bath application of [10μM] Pancuronium. The morphology of the SWC was different from the DTC SWC, however the spectrogram contains similar features. For example, the high frequency activity occurring during the spike as well as the increased intensity of sub 30Hz frequency activity after the spike. However, the location of the spike in the SWC and the amplitude of the complete SWC differ greatly from that seen during DTC application (refer to figure 4.5.2).

5.3.3 The effect of the bath application of nicotinic acetylcholine α_4 subunit selective antagonist, DHβE on delta frequency

The bath application of the α_4 subunit containing nAChR subtype selective antagonist, Dihydro-β-erythroidine hydrobromide (DHβE) resulted in a statistically significant change in mean power in the delta band with increasing drug concentration from the control state to 20μM can be seen in figure 5.5D (P< 0.001, n=32, One Way Repeated Measures ANOVA). The mean delta band power during the control state was 0.22μV^2 (0.07$\mu V^2 \rightarrow$ 0.42μV^2) compared with the mean power after 40 minutes of the [10μM] application, 0.22μV^2 (0.16$\mu V^2 \rightarrow$ 0.83μV^2) (P=0.001, n=32, paired t-test). Although the ANOVA stated that all three concentration states were significant, the number of data points for the final concentration [20μM] (n=4) were not enough to confirm statistical significance when a paired t-test was performed (P> 0.05, n=4, paired t-test).

The frequency of the delta rhythm saw a near significant effect of DHβE concentration (P=0.052, n=32, One Way Repeated Measures ANOVA). This lack of significance

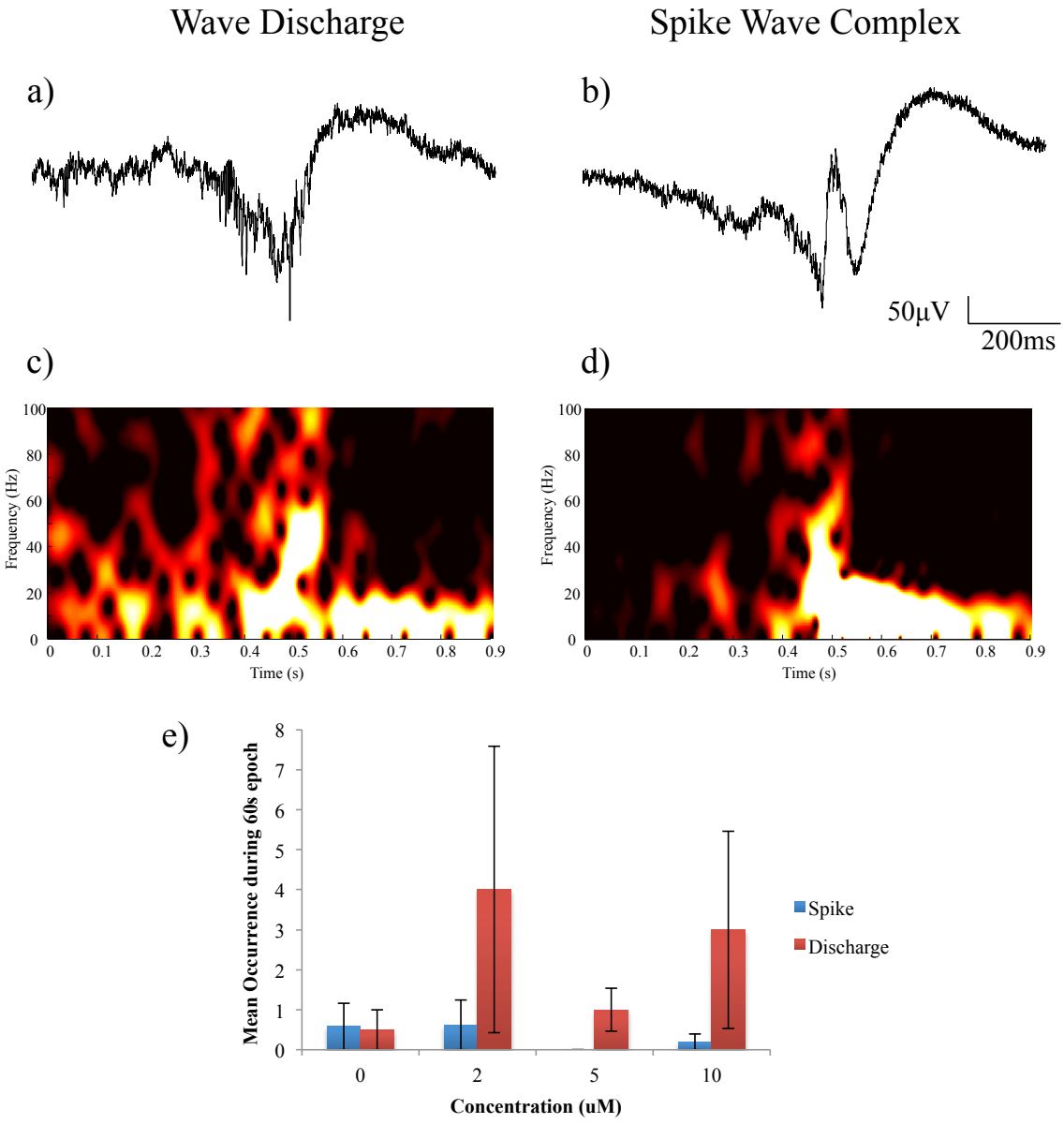

Figure 5.4: **Characteristics of epileptiform activity during Pancuronium application a.** 1 second trace of wave discharge extracted from 60 second epoch after 10μM application. **b.** 1 second trace of spike wave complex extracted from 60 second epoch after 10μM application. **c.** Spectrogram corresponding to the trace shown above in a). **d.** Spectrogram corresponding to the trace shown above in b). **e.** Bar chart showing the mean occurrence of WDs and SWCs during a 60 second epoch with increasing concentration.

may be due to the size of and variation in the final concentration dataset (n=4) in comparison to the control and first concentration datasets (n=32). As shown in figure 5.5D, a decrease in delta band frequency was observed from 1.33±0.08Hz during the control state to 0.83±0.08Hz during the final concentration [20μM].

Autocorrelation analysis reported a statistically significant difference in rhythmicity with concentration (P=0.023, n=17, One Way Repeated Measures ANOVA) (figure 5.5D). The ANOVA reported a non significant different between the control state and the first concentration, whilst the other two comparisons were considered significant. The mean height ratio of the first peak to the central peak with reference to the y-axis was 0.28±0.05 during the control state. Following the application of [10μM] DHβE, the height ratio was 0.34±0.04 after 40 minutes. As can be seen from figure 5.5C and D, the [10μM] concentration generally improves the rhythmicity of the signal, however not significantly so (P>0.05, n=17, Pairwise Comparison (Holm-Sidak)). After 40 minutes of [20μM] DHβE, the height ratio was 0.13±0.01. As was observed previously with mean delta band power and frequency, the size of the 20μM dataset (n=3) is not large enough to exclude to possibility that the difference between itself and the control state is due to chance (P>0.05, n=3, paired t-test).

Of the fourteen experiments conducted, WDs were present during 5 experiments resulting in a WD incidence rate of 0.29 per experiment. During these five experiments, the number of WDs detected during a 60 second epoch ranged from 1 to 10 once DHβE had been applied, with a total of 26 being detected overall. Figure 5.6c implies that there is an effect of concentration, however due to the size of the [20μM] dataset, there is not enough data to determine if there is a statistically significant effect of concentration or not. The mean occurrence of WDs during the control state was zero compared to 4.67± 2.41 following DHβE [20μM] application. The morphology of the WD in figure 5.6 is again different from the previous WDs seen in this and the previous chapter. It is much slower and the trough takes up a greater proportion of the 1 second epoch. There is also very little high frequency activity occurring during the very base of the trough, however there is the sub 20Hz activity present, as seen previously. Spike wave complexes (SWCs) were not detected during any of the epochs recorded during the fourteen experiments, hence an incidence rate of zero. No pattern has been detected with regards to the WD activity i.e. occurring at a regular frequency, however this may be due to the length of the epochs used or due to the low number of DHβE [20μM] experiments.

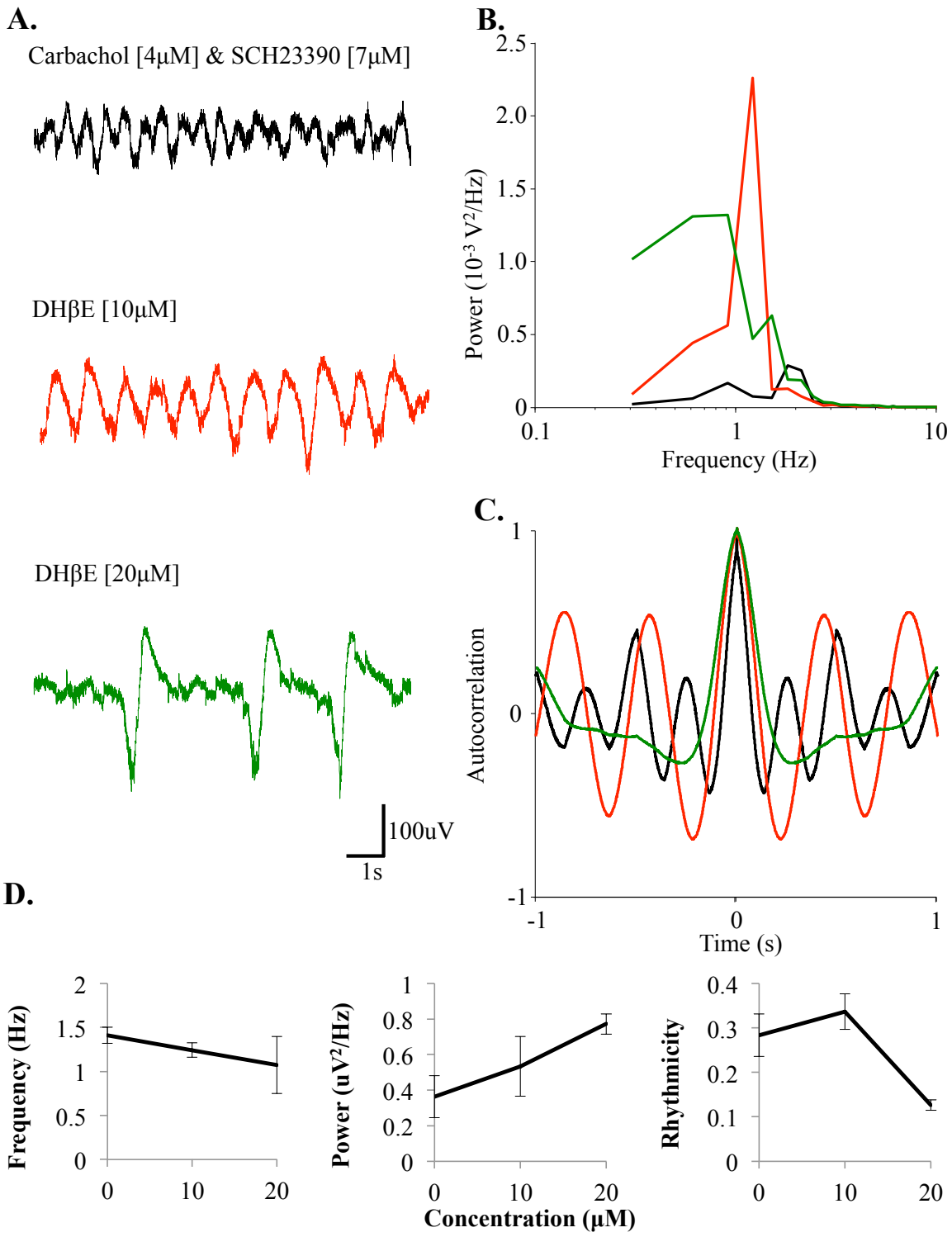

Figure 5.5: **Antagonism of nAChR subunit α_4 β_2 using DHβE. A.** 10 second sample recording of extracellular activity from layer V of the somatosensory cortex after application of Carbachol[4μM] and SCH23390 [7μM], followed by the application of increasing concentrations of DHβE. **B.** Power spectra produced from 8 second epochs of data in the absence of epileptiform activity. **C.** Autocorrelation from an 8 second epoch of activity in the absence of epileptiform activity. **D.** Concentration response curves of mean frequency, mean power and mean rhythmicity ratio of activity (control and 10μM n=17, 20μM n=3) during DhβE applications.

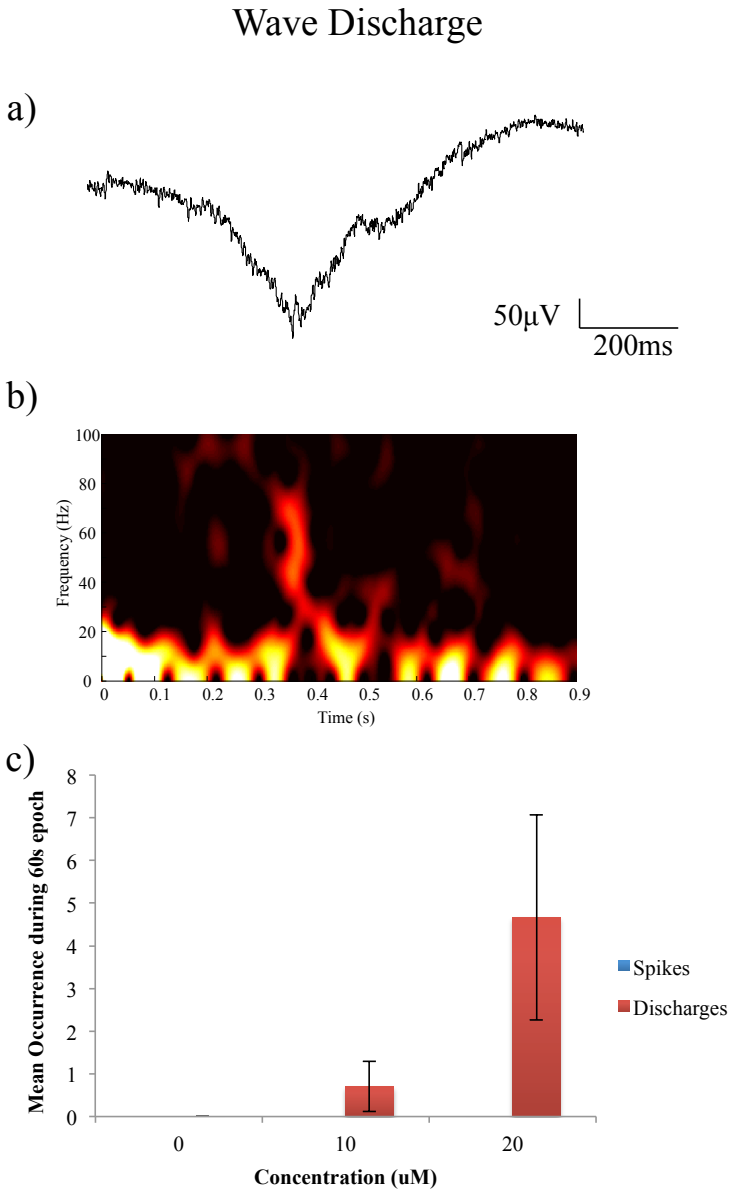

Figure 5.6: **Characteristics of epileptiform activity during DHβE application a.** 1 second trace of wave discharge extracted from 60 second epoch after 20μM application. **b.** Spectrogram corresponding to the trace shown above in a). **c.** Bar chart showing the mean occurrence of WDs and SWCs during a 60 second epoch with increasing concentration.

5.3.4 The effect of the systematic application of nicotinic acetylcholine α_3 subunit selective antagonists, α-conotoxins PnlA and AuIB on delta frequency oscillations.

The contribution of the nAChR α_3 subunit to the generation of the delta rhythm and SWDs was investigated using specific α_3 subunit antagonists. These antagonists also had the benefit of aiding the understanding of the specific roles of the nAChR β_2 and β_4 subunits.

α_3 β_2 subunit results

During *in vitro* experimental conditions, the bath application of the neuronal α_3 β_2 subunit containing nAChRs subtype selective antagonist α-contoxin PnlA (hereafter referred to as PnlA), resulted in a statistically significant decrease in the mean power of the delta band from 2.48±0.67μV^2 to 0.7±0.25μV^2 after 40 minutes of PnlA [10μM] application (P<0.001, n=11, One Way Repeated Measures ANOVA). As can be seen in figure 5.7D, there is a significant decrease from the control state of 2.48±0.67μV^2 to the second concentration level [2μM] PnlA of 0.94±0.36μV^2(P=0.002, n=11, paired t-test). However, after the [2μM] concentration application, the power in the delta band measured during [5μM] and [10μM] PnlA concentrations remained stable as there is no significant change between these three concentrations (P>0.05, n=11, Holm-Sidak Pairwise Multiple Comparison).

The delta rhythm proved to be insensitive to a blockade of α_3 β_2 subunit containing nAChRs and the mean peak frequency remained fairly constant throughout the experiments (1.02±0.12Hz during the control state versus 1.08±0.08Hz after PnlA [10μM], P>0.05, n=11, One Way Repeated Measures ANOVA). These data are displayed in figure 5.7D.

Autocorrelation analysis revealed that no statistically significant effect of concentration was observed for rhythmicity (P>0.05, n=8, One Way Repeated Measures ANOVA). As can be seen from both Figure 5.7C and D respectively, the sinusoidal form remains present throughout the concentrations indicating no decrease in rhythmicity, and little variation in the mean height ratio of the central peak to the first peak with respect to PnlA concentration. During the control state, the mean height ratio was 0.32±0.08 in comparison to 0.27±0.07 40 minutes after PnlA [10μM] application.

Of the eight experiments conducted, Wave Discharges (WDs) were present at varying concentrations in all experiments, resulting in a WD incidence rate of 1. Figure 5.8a

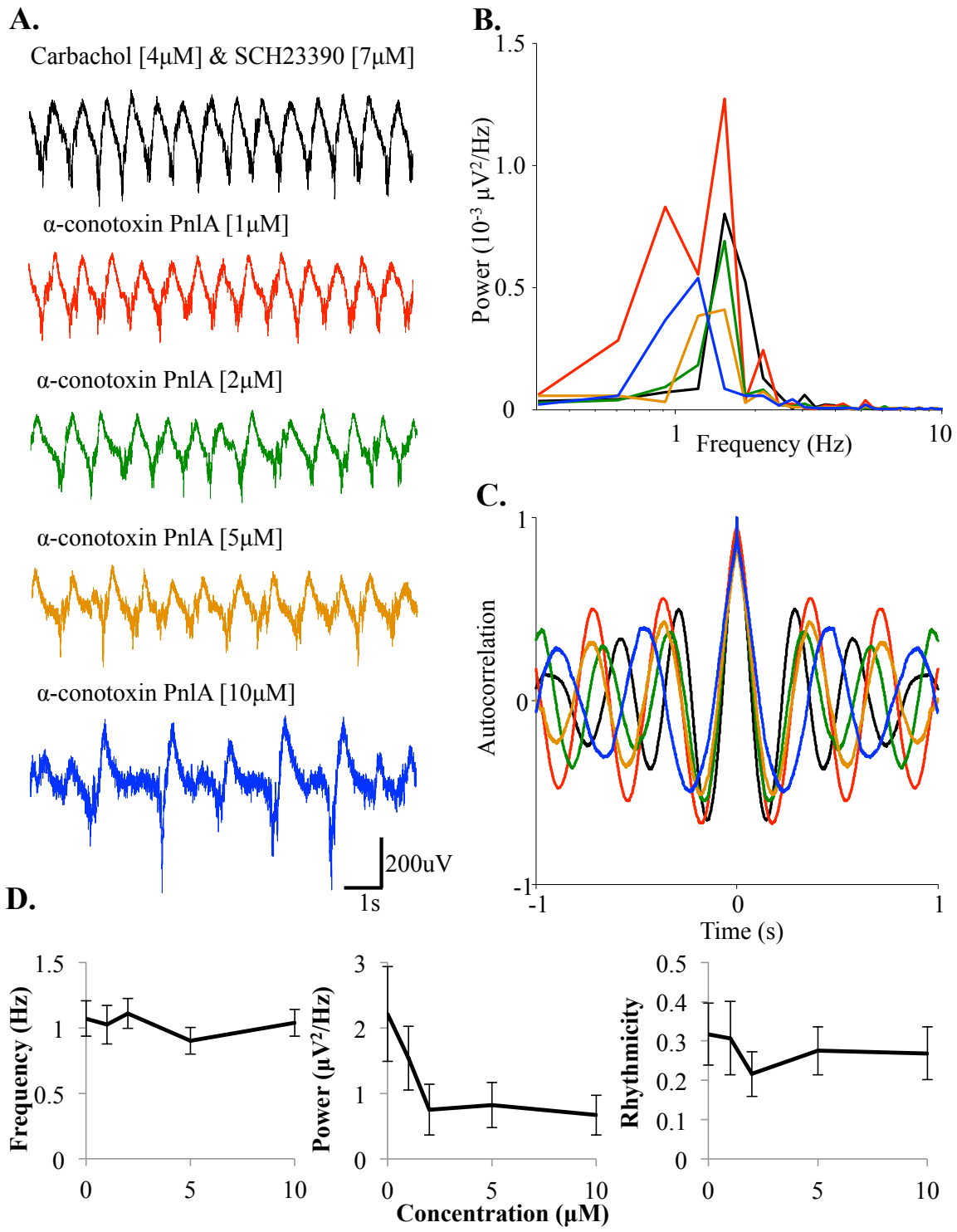

Figure 5.7: **Antagonism of nAChRs subunits α3 β2 using α-conotoxin PnlA. A.** 10 second sample recording of extracellular activity from layer V of the somatosensory cortex after application of Carbachol[4μM] and SCH23390 [7μM], followed by the application of increasing concentrations of α-conotoxin PnlA. **B.** Power spectra produced from 8 second epochs of data in the absence of epileptiform activity. **C.** Autocorrelation from an 8 second epoch of activity in the absence of epileptiform activity. **D.** Concentration response curves of mean frequency, mean power and mean rhythmicity ratio of activity (n=8) during α-conotoxin PnlA applications.

shows a 1 second example of a WD during a [10μM] PnlA extracted from a 60 second epoch. Below is it's corresponding spectrogram (figure 5.8c). In total, 151 WDs were detected during the recorded 60 second epochs. The number of WDs tends to decrease with concentration following an initial significant abundance of WDs following the initial bath application of PnlA [1μM](P=0.02, n=8, One Way Repeated Measures ANOVA, Figure 5.8e). The mean occurrence of WDs during the control state was 0.63±0.5 wave discharges per 60 second epoch compared to the 6.13±2.19 WDs per 60 second epoch after 40 minutes of PnlA [1μM] application (P=0.04, n=8, paired t-test). The morphology of the WDs is quite similar to that seen during DHβE application, particularly when looking at the width of the trough. Likewise there is very little high frequency activity embedded in the WD. Although there does seem to be a higher concentration of low frequency activity preceding the trough than after it.

Spike Wave Complexes were also detected at varying concentrations during four of the eight experiments, hence resulting in a SWC incidence rate of 0.5. Figure 5.8b shows a 1 second example of a SWC during a [10μM] PnlA extracted from a 60 second epoch. Below is it's corresponding spectrogram (figure 5.8d). In total, 38 SWCs were detected during the increasing concentrations of PnIA. The number of SWCs was seen to significantly increase with concentration (P=0.05, n=8, One Way Repeated Measures ANOVA)(Figure 5.8e). The ANOVA indicated that there may be a significant different between the number of SWCs detected during the control state (0.13±0.13 SWCs per 60s epoch) and the final concentration of PnlA [10μM] (2.33±1.31 SWCs per 60s epoch) (unadjusted P=0.003, n=8, Holm-Sidak Pairwise Multiple Comparison), however the paired t-test proved this not to be significant (P$>$ 0.05, n=8, paired t-test). With the data presented previously and the aid of figure 5.8e, it is reasonable to hypothesise that as the number of WDs decrease, the number of SWCs increase. The morphology of the PnIA SWC has some similar characteristics to those seen during DTC application. The amplitude of the spike overshoots the amplitude of the following wave and the intensity of the high frequency activity that coincides with the spike and it's following low frequency activity. However, unlike during DTC application, there is some high frequency activity before the spike, which with DTC, occurs after the spike.

α_3 β_4 subunit

The bath application of the neuronal α_3 β_4 subunit containing nAChRs subtype selective antagonist α-conotoxin AuIB (hereafter referred to as AuIB), resulted in no statistically significant change in the mean power of the delta frequency band as can be seen in figure 5.9D. The mean delta band power during the control state was 0.85μV^2 (0.2μV^2 $\rightarrow$

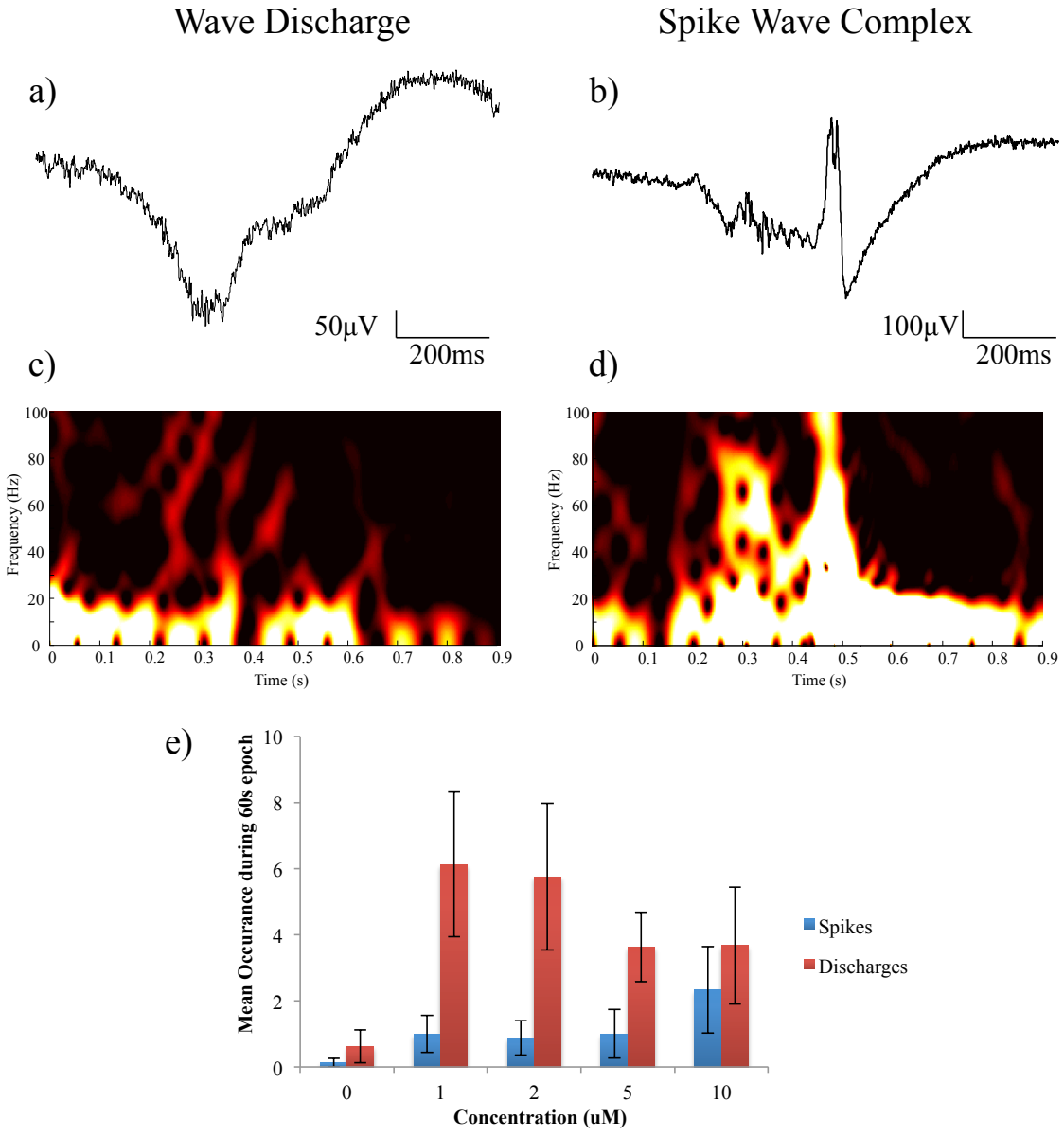

Figure 5.8: **Characteristics of epileptiform activity during α-conotoxin PnlA application a.** 1 second trace of wave discharge extracted from 60 second epoch after 10μM application. **b.** 1 second trace of spike wave complex extracted from 60 second epoch after 10μM application. **c.** Spectrogram corresponding to the trace shown above in a). **d.** Spectrogram corresponding to the trace shown above in b). **e.** Bar chart showing the mean occurrence of WDs and SWCs during a 60 second epoch with increasing concentration.

$1.22\mu V^2$) compared with the mean power after 40 minutes of the final AuIB concentration [1μM], $0.56\mu V^2$ ($0.16\mu V^2 \rightarrow 0.96\mu V^2$).

The peak frequency of the delta rhythm saw a significant effect of AuIB concentration as can be seen in figures 5.9B and D (P=0.01, n=8, Kruskal-Wallis One Way ANOVA on Ranks). After 40 minutes of AuIB [1μM] application, the mean peak frequency of the delta band was reduced from 1.83Hz (1.54Hz $\rightarrow$ 1.84Hz) during the control state to 0.91Hz (0.6Hz $\rightarrow$ 1.22Hz). Although the ANOVA indicated that the relationship between these two concentrations was significant, this was disproved by a paired t-test (P>0.05, n=8, paired t-test).

Autocorrelation analysis was conducted in order to assess the effects of the drug on the rhythmicity of the activity of the slice. Prior to AuIB application, autocorrelation analysis of delta oscillations resulted in a graph that was sinusoidal in form indicating that the activity was intrinsically rhythmic (black trace in figure 5.9C). The analysis revealed that no statistically significant effect of AuIB concentration was observed for rhythmicity (P>0.05, n=8, One Way Repeated Measures ANOVA). The mean height ratio during the control condition was 0.53±0.09 in comparison to the mean height ratio during the final AuIB concentration [1μM], 0.35±0.09. As can be seen in figure 5.9C, an example of the autocorrelation analysis result produced, the sinusoidal form remained intact and very closely followed the control state (black trace). Figure 5.9D also shows a slight loss of rhythm which correlates with the example traces in figure 5.9A.

Of the eight experiments, WDs were present during two experiments resulting in an incidence rate of 0.25 per experiment. However, this value is misleading as out of all the eight experiments, only 4 WDs were detected (in comparison to the 151 WDs detected during the eight PnlA experiments). An example 1 second trace of a WD extracted from a 60 second epoch recording can be seen in figure 5.10a as can it's respective spectrogram below it (figure 5.10c). The morphology of the wave discharge is very similar to those seen during MG624 application, with respect to amplitude, trough width and embedded frequency intensity.

Whilst, SWCs were present during only 1 experiment resulting in an incidence rate of 0.125 per experiment. As with the number of WDs, only 1 SWC (pictured in figure 5.10b) was detected during the eight experiments. As with the WDs, the SWC was very similar in morphology to MG624, however there is a lack of high frequency activity which has previously been seen during all SWCs (figure 5.10d). Epileptiform activity after application of AuIB is barely present (figure 5.10e) in comparison to the other drugs used in

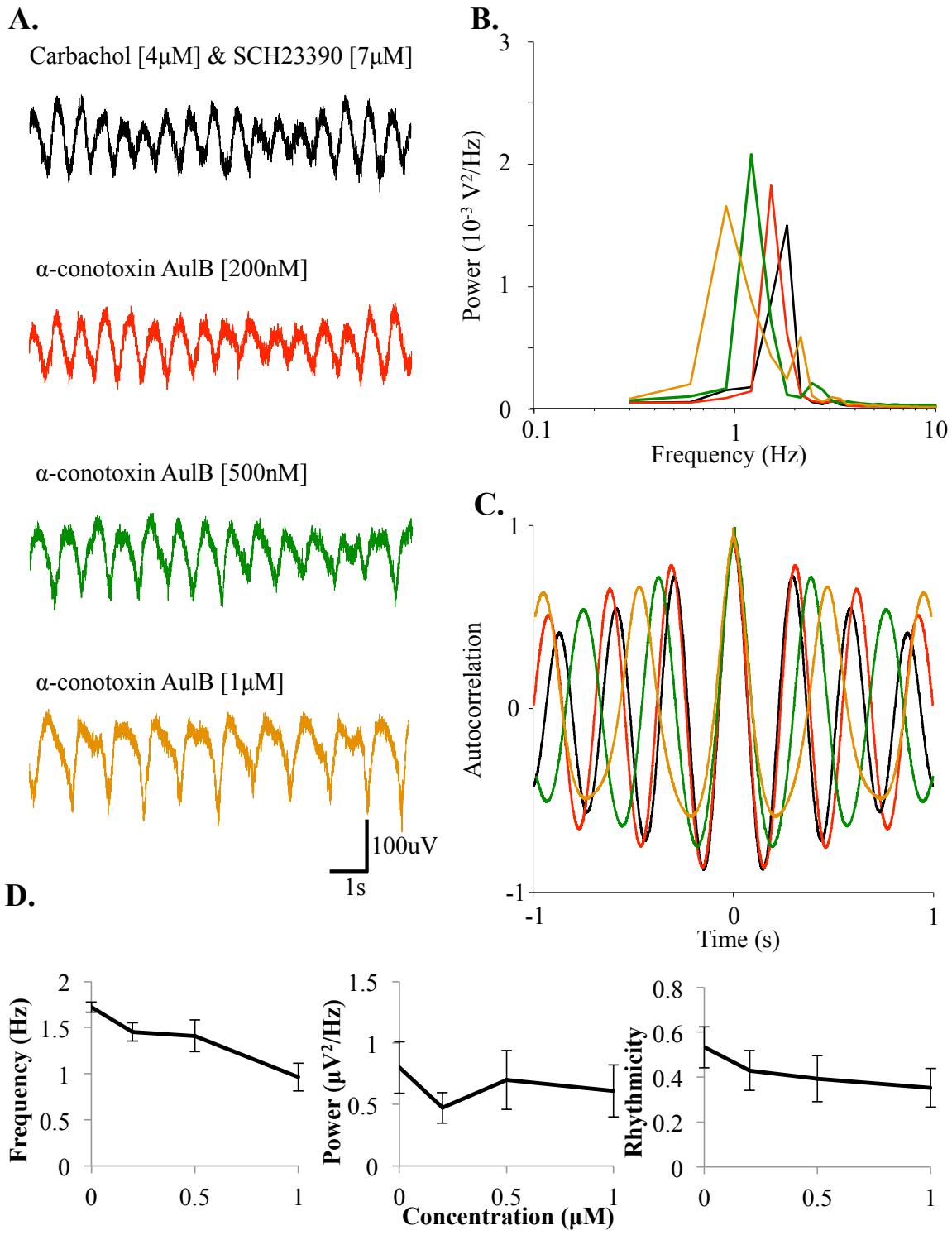

Figure 5.9: **Antagonism of nAChRs subunits α_3 β_4 using α-conotoxin AuIB. A.** 10 second sample recording of extracellular activity from layer V of the somatosensory cortex after application of Carbachol[4μM] and SCH23390 [7μM], followed by the application of increasing concentrations of α-conotoxin AuIB. **B.** Power spectra produced from 8 second epochs of data in the absence of epileptiform activity. **C.** Autocorrelation from an 8 second epoch of activity in the absence of epileptiform activity. **D.** Concentration response curves of mean frequency, mean power and mean rhythmicity ratio of activity (n=8) during α-conotoxin AuIB applications.

this chapter.

5.3.5 The effect of the systematic application of nicotinic acetylcholine $\alpha_9\alpha_{10}$ subunit selective antagonist, ACV1 on delta frequency oscillations.

The bath application of the neuronal $\alpha_9\alpha_{10}$ subunit containing nAChR subtype selective antagonist, ACV1 resulted in a statistically insignificant change in delta band mean power (P>0.05, n=15, One Way Repeated Measures ANOVA). As can be seen from figure 5.11D, the mean power remained fairly constant with increasing ACV1 concentration, although the large error bars portray a large variation in the dataset. This variation can also be seen in figure 5.11B, which displays large delta band power during the control state in comparison to the power during the ACV1 concentration states, which is small by comparison. The mean power of the delta band during the control state was $0.97\pm0.30\mu V^2$ in comparison to $0.80\pm0.36\mu V^2$ during the final ACV1 concentration [1μM].

The mean peak frequency of the delta rhythm saw little effect of increasing ACV1 concentration (P>0.05, n=15, One Way Repeated Measures ANOVA). The peak frequency remained moderately stable with increasing concentration, as displayed in figure 5.11D. The mean peak frequency during the control state was 1.48±0.09Hz compared to 1.16±0.13Hz during the final ACV1 concentration [1μM] application.

Autocorrelation analysis reported no statistically significant change in rhythmicity with ACV1 concentration (P>0.05, n=8, One Way Repeated Measures ANOVA) (figure 5.11D). The mean height ratio of the first peak to the central peak with reference to the y-axis was 0.36±0.67 during the control state. Following the application of [1μM] ACV1, the height ratio was 0.29±0.07 after 40 minutes.

Of the eight experiments conducted, WDs were present during six experiments, resulting in a WD incidence rate of 0.75. In total, 78 WDs were detected during the 60 second epochs over the varying concentrations. The number of WDs tends to decrease with concentration following an initial increase following the initial bath application of ACV1 [200nM], however it is not considered to be a statistically significant trend (P>0.05, n=8, One Way Repeated Measure ANOVA). The mean occurrence of WDs during the control state was 2.75±1.13 WDs per 60 second epoch compared to the 4.25±1.53 WDs per 60 second epoch after 40 minutes of ACV1 [200nM] application. The morphology of the wave discharge following [1μM] ACV1 seems to have a greater amplitude than those seen

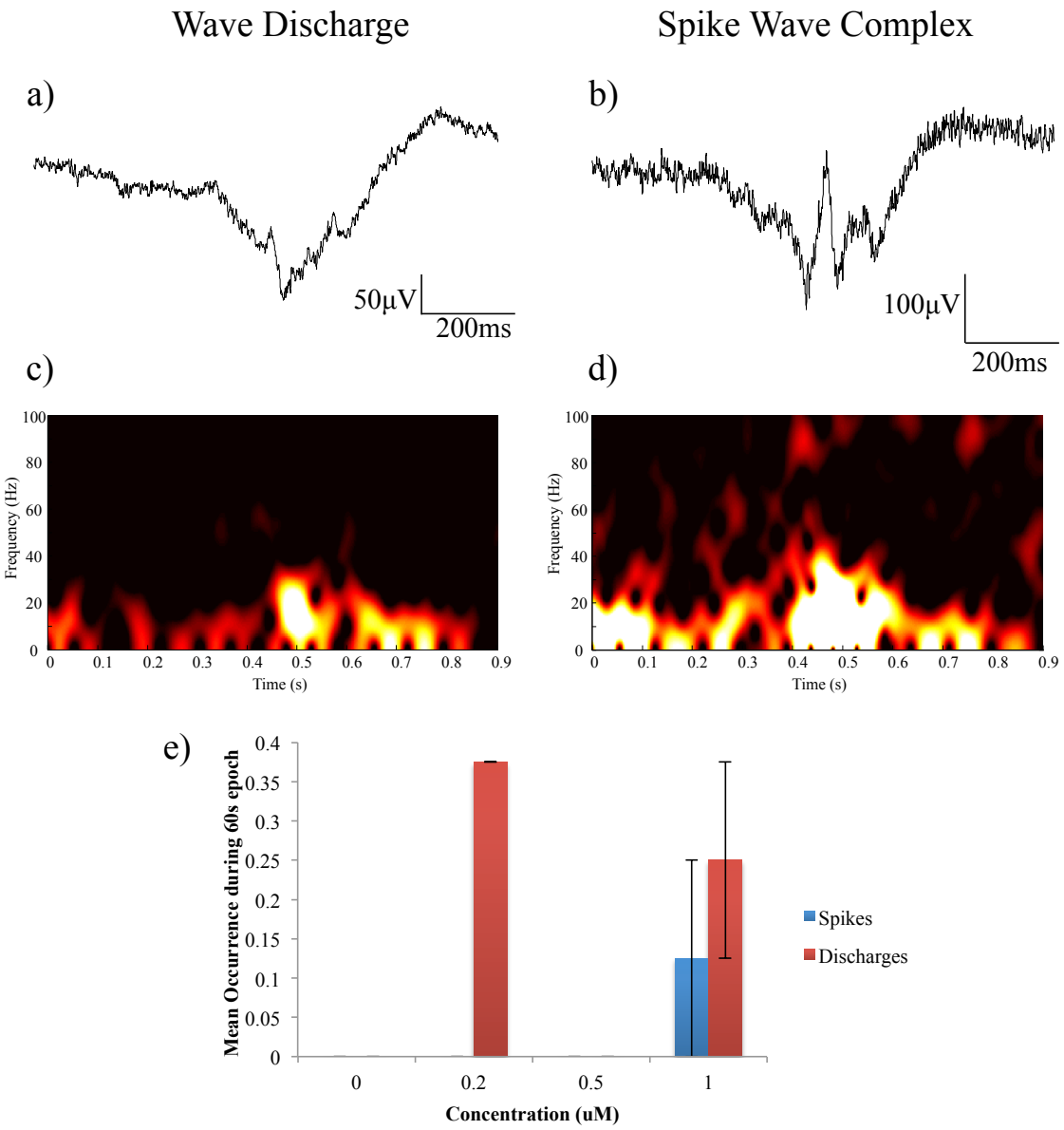

Figure 5.10: **Characteristics of epileptiform activity during α-conotoxin AuIB application a.** 1 second trace of wave discharge extracted from 60 second epoch after 1μM application. **b.** 1 second trace of spike wave complex extracted from 60 second epoch after 1μM application. **c.** Spectrogram corresponding to the trace shown above in a). **d.** Spectrogram corresponding to the trace shown above in b). **e.** Bar chart showing the mean occurrence of WDs and SWCs during a 60 second epoch with increasing concentration.

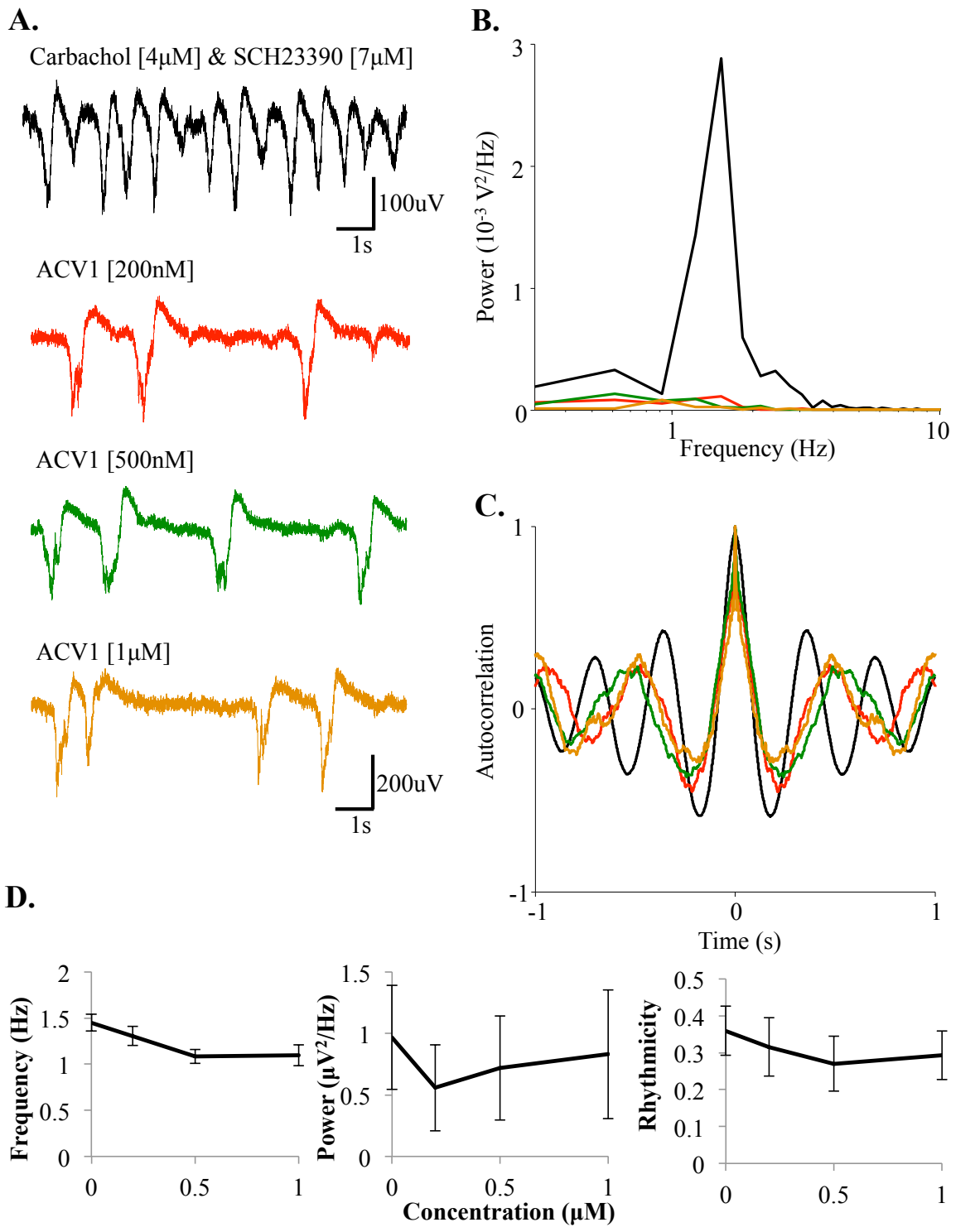

Figure 5.11: **Antagonism of nAChR subunits α_9 and α_{10} using ACV1. A.** 10 second sample recording of extracellular activity from layer V of the somatosensory cortex after application of Carbachol[4μM] and SCH23390 [7μM], followed by the application of increasing concentrations of ACV1. **B.** Power spectra produced from 8 second epochs of data in the absence of epileptiform activity. **C.** Autocorrelation from an 8 second epoch of activity in the absence of epileptiform activity. **D.** Concentration response curves of mean frequency, mean power and mean rhythmicity ratio of activity (n=8) during ACV1 applications.

during previous drug applications. It also seems to have more activity embedded within itself. This can also be seen from the spectrogram beneath, particularly the activity that coincides with the trough of the WD, as well a the 'normal' sub 20Hz activity, there is also some lower gamma activity present (25-40Hz).

Spike Wave Complexes were present during 5 of the eight experiments, resulting in a SWC incidence rate of 0.625 per experiments. In total, 70 SWCs were detected during the 60 second epochs over the varying concentrations, 10 of these were spontaneous. There was no significant pattern detected with regards to the number of SWCs detected with increasing concentration. The morphology of the SWC seen during ACV1 application is quite similar to that seen during DTC experimentation, both in overall amplitude and the general appearance of the spectrogram. However, the ACV1 spectrogram only shows activity directly related to the occurrence of the SWC, in particular the high frequency activity that consider with the spikes which peters off to lower frequencies as the trace returns to normal.

5.3.6 The effect of the systematic application of $5HT_3$ selective receptor antagonist, MDL 72222 on delta frequency oscillations.

The bath application of the $5HT_3$ subunit selective antagonist, MDL 72222 resulted in no statistically significant change in the mean power of the delta frequency band as can be seen in figure 5.13D ($P > 0.05$, n=40, One Way Repeated Measures ANOVA). The mean delta band power during the control state was $0.85 \pm 0.1 \mu V^2$ compared with the mean power after 40 minutes of the final MDL 72222 [10μM], $1.03 \pm 0.12 \mu V^2$.

The mean peak frequency of the delta rhythm saw a statistically significant effect with increasing MDL 72222 concentration ($P < 0.001$, n=40, One Way Repeated Measures ANOVA). The ANOVA reported that a significant change in mean peak frequency occurred between the control state and both [5μM] and [10μM], however there was no significant change between the two concentration states, hence the most significant change compared to the control occurred at [5μM]. The median peak frequency during the control state was 1.54Hz (1.21Hz $\rightarrow$ 1.83Hz) in comparison to 1.21Hz (0.9Hz $\rightarrow$ 1.54Hz) during 40 minutes of MDL 72222 [5μM] application ($P < 0.001$, n=40, paired t-test).

Autocorrelation analysis reported no significant change in rhythmicity with MDL 72222 increasing concentration [1 - 10μM] ($P > 0.05$, n=40, One Way Repeated Measures ANOVA). As can be seen in figure 5.13D, the rhythmicity stays fairly stable with the exception of

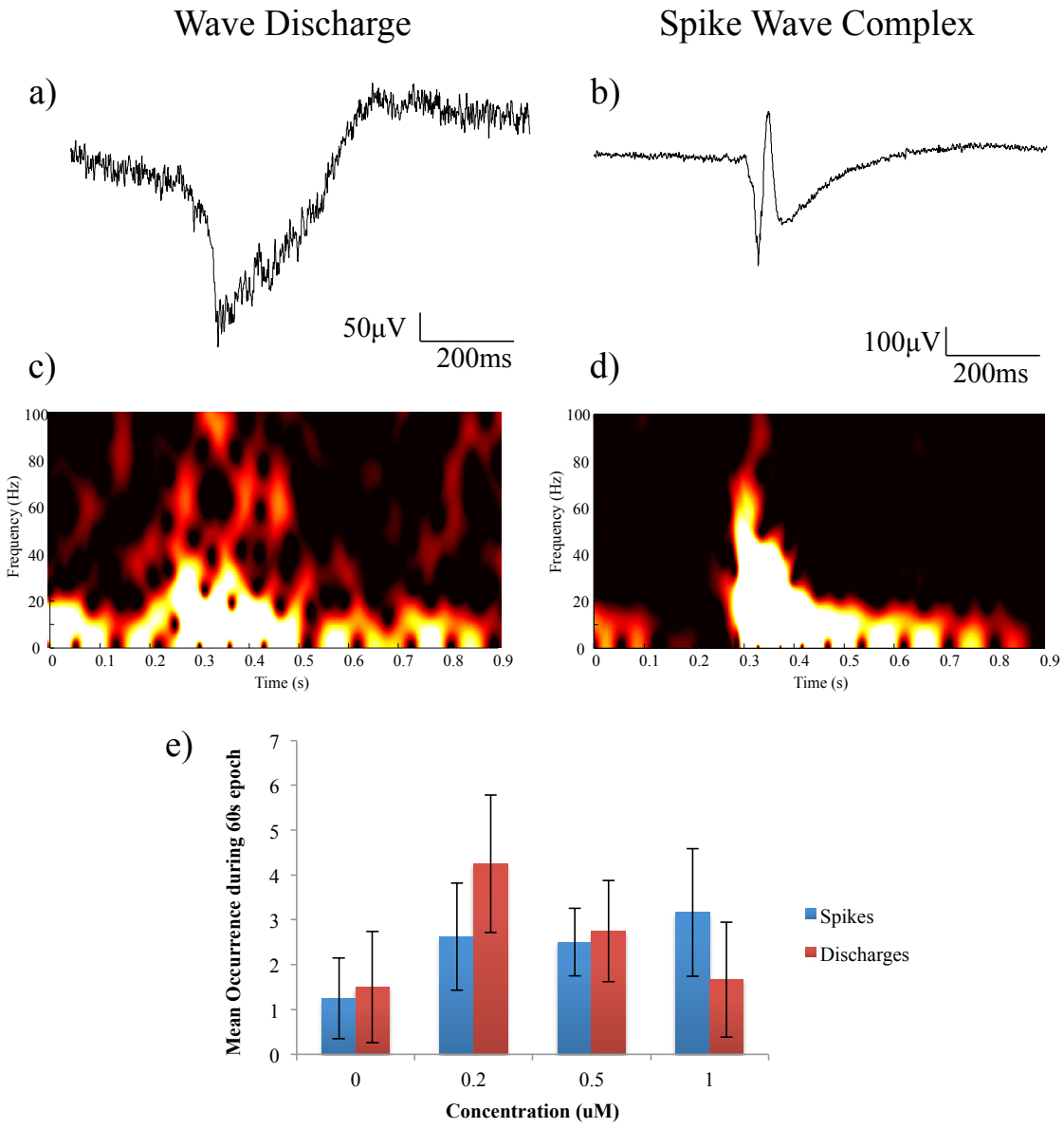

Figure 5.12: **Characteristics of epileptiform activity during ACV1 application** **a.** 1 second trace of wave discharge extracted from 60 second epoch after 1μM application. **b.** 1 second trace of spike wave complex extracted from 60 second epoch after 1μM application. **c.** Spectrogram corresponding to the trace shown above in a). **d.** Spectrogram corresponding to the trace shown above in b). **e.** Bar chart showing the mean occurrence of WDs and SWCs during a 60 second epoch with increasing concentration.

the anomalies during [2μM] concentration detrimentally lowering the mean value. During the control state, the mean height ratio was 0.41±0.04 in comparison to 0.4±0.04, 40 minutes after MDL 72222 [10μM] application.

Of the twenty experiments conducted, Wave Discharges (WDs) were present during nine experiments, resulting in an incidence rate of 0.45 WDs per experiment. In total, 125 WDs were detected during the recorded 60 second epochs from the twenty experiments at varying concentrations. The bar chart in figure 5.14 indicates that WDs are more likely to occur during [2μM] application, in fact this is not the case. The data was skewed by 21 WDs detected in one 60 second epoch and the small dataset for [1μM] and [2μM] concentrations (n=4). The number of WDs was not significantly changed with concentration (P>0.05, n=40, Friedman Repeated Measures ANOVA on ranks). An example 1 second trace of a WD extracted from a 60 second epoch recording can be seen in figure 5.14a. as can it's respective spectrogram in figure 5.14c. The morphology of the WD is very similar to the previous WDs seen in this chapter. As with during MG624 and α-conotoxin AuIB, there is very little, if any, high frequency activity embedded in the WD. Unlike some of the previous WDs, the majority of the embedded activity occurs before the trough instead of after.

Spike Wave Complexes (SWCs) were present during four of the experiments, resulting in an incidence rate of 0.2 SWCs per experiment. In total, 8 SWCs were detected during the recorded 60 second epochs from the twenty experiments, the majority being detected during [10μM] application. The number of SWCs was not significantly changed with concentration (P=0.09, n=40, One Way Repeated Measures ANOVA). An example 1 second trace of a SWC extracted from a 60 second epoch recording can be seen in figure 5.14b. with it's corresponding spectrogram in d. The morphology of the SWC is similar to those seen during α-conotoxin PnIA application with respect to the location of the spike within the SWC, the embedded activity preceding the spike and the amplitude of the spike in comparison to the subsequent wave. Although there is some high frequency activity, it does not have the intensity of some of the previously seen SWCs, in particular PnIA and MDL 72222.

5.3.7 The effect of the systematic application of $GABA_A$ selective receptor antagonist, Gabazine on delta frequency oscillations.

During *in vitro* experimental conditions, the bath application of the $GABA_A$ selective receptor antagonist Gabazine result in no significant change in mean power of the delta

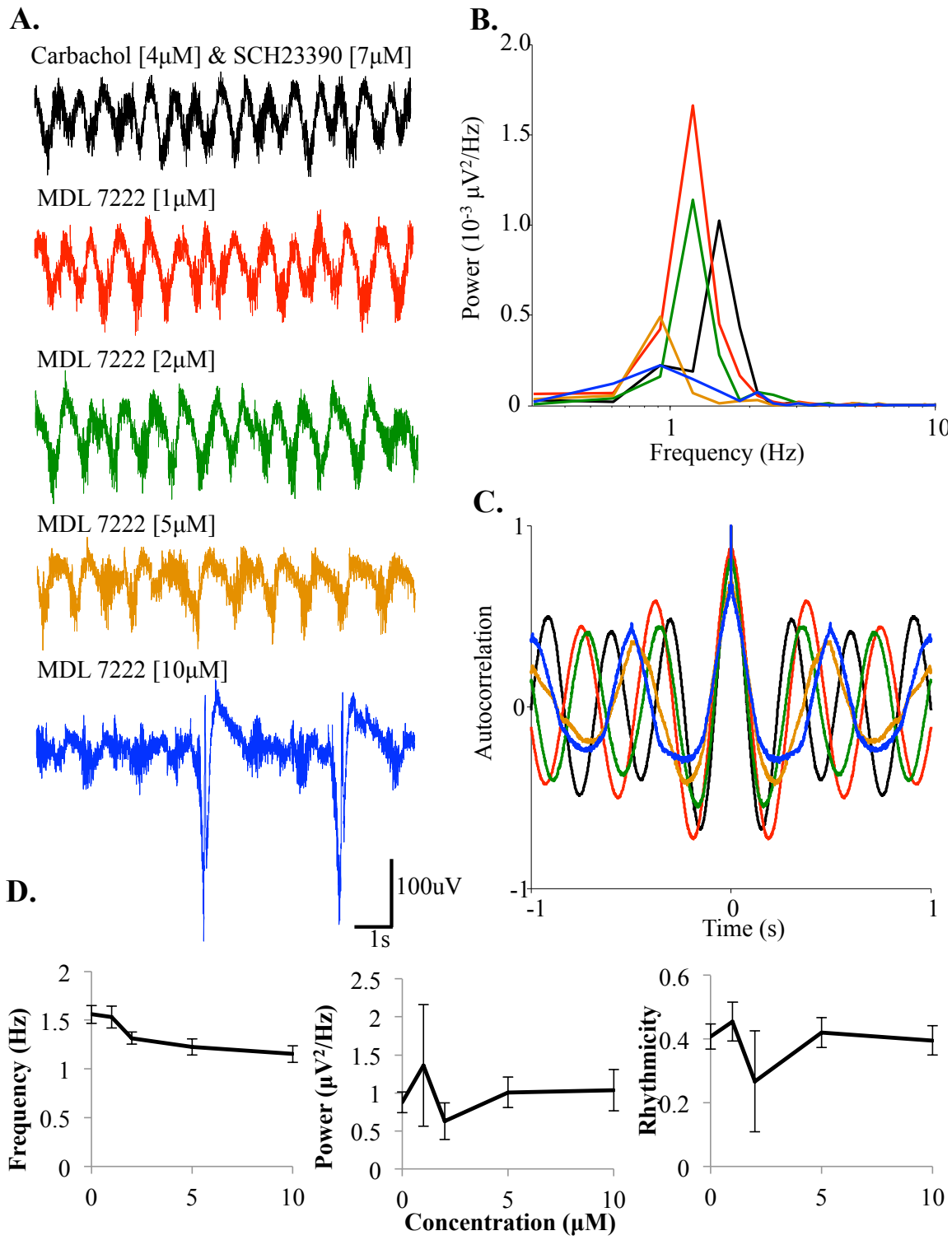

Figure 5.13: **Antagonism of $5HT_3$ selective receptors using MDL 72222. A.** 10 second sample recording of extracellular activity from layer V of the somatosensory cortex after application of Carbachol[4μM] and SCH23390 [7μM], followed by increasing concentrations of MDL 72222. **B.** Power spectra produced from 8 second epochs of data in the absence of epileptiform activity. **C.** Autocorrelation from an 8 second epoch of activity in the absence of epileptiform activity. **D.** Concentration response curves of mean frequency, mean power and mean rhythmicity ratio of activity (control, 10μM and 20μM n=20, 1μM and 2μM n=4) during MDL 72222 applications.

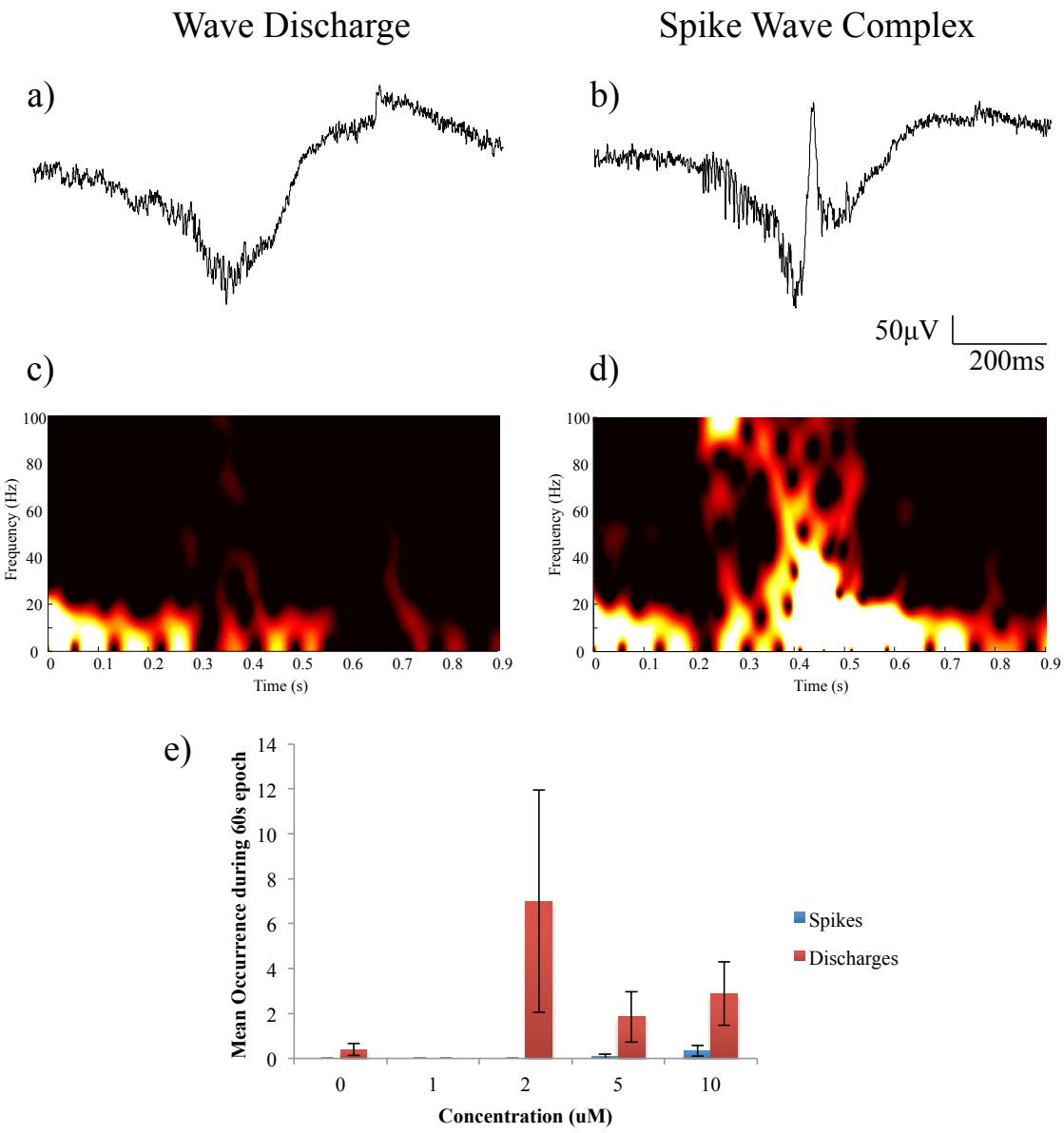

Figure 5.14: **Characteristics of epileptiform activity during MDL 7222 application a.** 1 second trace of wave discharge extracted from 60 second epoch after 10μM application. **b.** 1 second trace of spike wave complex extracted from 60 second epoch after 10μM application. **c.** Spectrogram corresponding to the trace shown above in a). **d.** Spectrogram corresponding to the trace shown above in b). **e.** Bar chart showing the mean occurrence of WDs and SWCs during a 60 second epoch with increasing concentration.

band. The mean delta band power during the control state was $0.44\pm0.13\mu V^2$ compared to $0.37\pm0.16\mu V^2$ after 40 minutes of Gabazine [1μM] application (P>0.05, n=20, One Way Repeated Measures ANOVA).

The delta rhythm proved to be insensitive to a blockade of $GABA_A$ subunit containing receptors (P>0.05, n=20, One Way Repeated Measures ANOVA). The mean peak frequency remained fairly constant through the experiments, 1.5±0.13Hz during the control state versus 1.36±0.14Hz after Gabazine [1μM] application, as depicted in figure 5.15D.

Autocorrelation analysis revealed a statistically significant change in rhythmicity with Gabazine concentration (P=0.014, n=10, One Way Repeated Measures ANOVA, Figure 5.15D). As can be seen from the example, figure 5.15C, the sinusoidal appearance was diminished with increasing Gabazine concentration. The mean height ratio of the first peak to the central peak of the autocorrelation analysis was 0.32±0.06 during the control state in comparison to 0.09±0.04 after Gabazine [1μM] was applied (P=0.016, n=10, paired t-test).

Of the ten experiments conducted using Gabazine, WDs were present during all concentration resulting in an incidence rate of 1. An example of the type of WD seen during the Gabazine experiments is depicted in figure 5.16a. In total, 56 WDs were detected during the varying Gabazine concentrations. The number of WDs was not significantly changed with concentration, however figure 5.16e would indicate a positive trend. (P>0.05, n=10, One Way Repeated Measures ANOVA). The type of WD seen during Gabazine application is different from those seen during the previous drug experiments in this chapter for the following reasons: the amplitude of the WD is approximately four times greater; the morphology of the WD, particularly the initiation of the discharge; and although, according to the spectrogram, the frequency of the activity embedded on the WD is similar to the previous drug experiments, the intensity is much greater.
Spike Wave Complexes (SWCs) were present during six of the eight experiments, resulting in an incidence rate 0.75 SWCs per experiment. In total, 40 SWCs were detected during the increasing Gabazine concentrations, the majority were detected during [1μM] application. The number of SWCs present during the 60 second epochs was significantly changed with concentration (P=0.05, n=10, One Way Repeated Measures ANOVA). The median occurrence of SWCS during the control state was zero compared to 2 ($0 \rightarrow 3$) SWCs per 60 second epoch after 40 minutes of Gabazine [1μM] application (P=0.03, n=10, Wilcoxon Signed Rank Test). The same differences that applied to Gabazine WDs also apply to Gabazine SWCs: the amplitude is at least 4 times greater; the morphology is different to the SWC examples seen previously; the location of the spike itself within

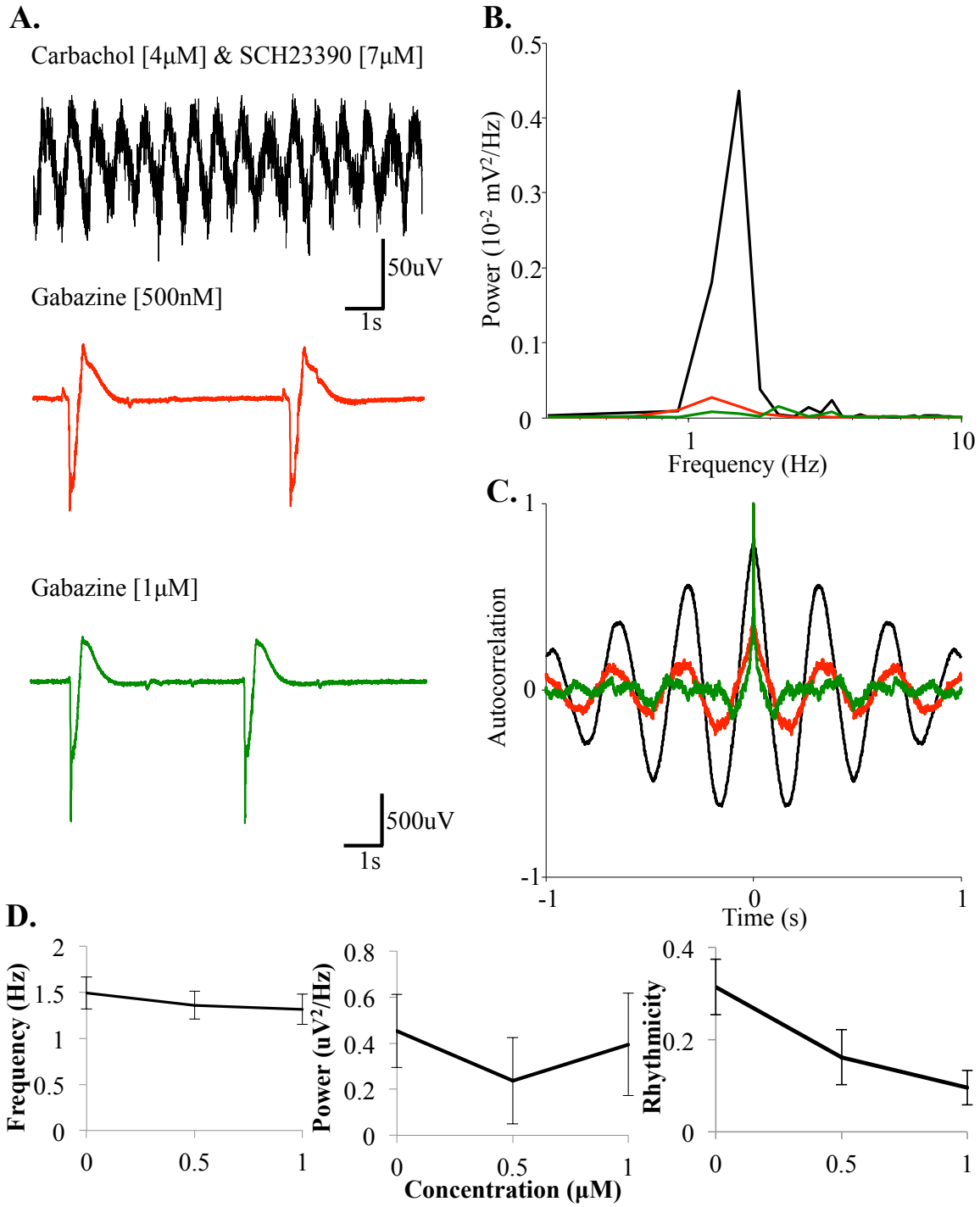

Figure 5.15: **Antagonism of $GABA_A$ selective receptors using Gabazine. A.** 10 second recording of extracellular activity from layer V of the somatosensory cortex after application of Carbachol[4μM] and SCH23390 [7μM], followed by increasing concentrations of Gabazine. **B.** Power spectra produced from 3 second epochs of data in the absence of epileptiform activity. **C.** Autocorrelation from a 3 second epoch of activity in the absence of epileptiform activity. **D.** Concentration response curves of mean frequency, mean power and mean rhythmicity ratio of activity (n=10) during Gabazine applications.

the SWC, and although the spectrogram shows that the activity embedded on the SWC is similar to the WD and previous SWCs, the intensity is much greater and reaches much higher frequencies (refer to figure 5.16d).

5.3.8 The affect of the application of AMPA receptor modulator on carbachol and SCH23390 induced delta frequency oscillations and Spike-Wave Discharges.

The systematic bath application of the positive allosteric AMPA receptor modulator, Cyclothiazide (CTZ) resulted in a near significant change in mean delta band power with concentration(P=0.057, n=20, One Way Repeated Measures ANOVA). The mean power during the control condition was 3.14±0.58μV^2, this increased to 4.34±0.97μV^2 during [10μM] application, only to decrease to 1.74±0.3μV^2 during CTZ [20μM] application. This is more easily portrayed in figure 5.17D.

The mean peak frequency of the delta rhythm proved to be insensitive to the modulation of AMPA receptors (P=0.05, n=20, One Way Repeated Measures ANOVA). The mean peak frequency during the control state was 1.77±0.13Hz, which remained fairly constant throughout the experiment and concluded with a mean peak frequency of 1.61±0.19Hz after CTZ [20μM].

Autocorrelation analysis reported that no statistically significant effect of concentration was observed for rhythmicity (P>0.05, n=10, One Way Repeated Measures ANOVA). The mean height ratio during the control state was 0.24±0.05 compared to 0.24±0.06 after CTZ [20μM] application.

Of the ten experiments, WDs were present during six experiments, resulting in an incidence rate of 0.6 WDs per experiment. In total, 33 WDs were detected during the 60 second epochs over the varying concentrations. Unlike many of the other drug experiments detailed in this chapter, WDs occurred spontaneously during the control condition in five of the ten experiments. When no epileptiform activity occurred spontaneously, only once did they occur during CTZ concentrations. Figure 5.18a shows a 1 second example of a WD extracted from a 60 second epoch during CTZ [20μM]. The corresponding spectrogram is shown in figure 5.18c. CTZ concentration had no significant effect on the mean occurrence of WDs (P>0.05, n=10, One Way Repeated Measures ANOVA).

Of the ten experiments conducted, SWCs were detected during five experiments, resulting in an incidence rate of 0.5 SWCs per experiment. As with the CTZ WDs, spontaneous

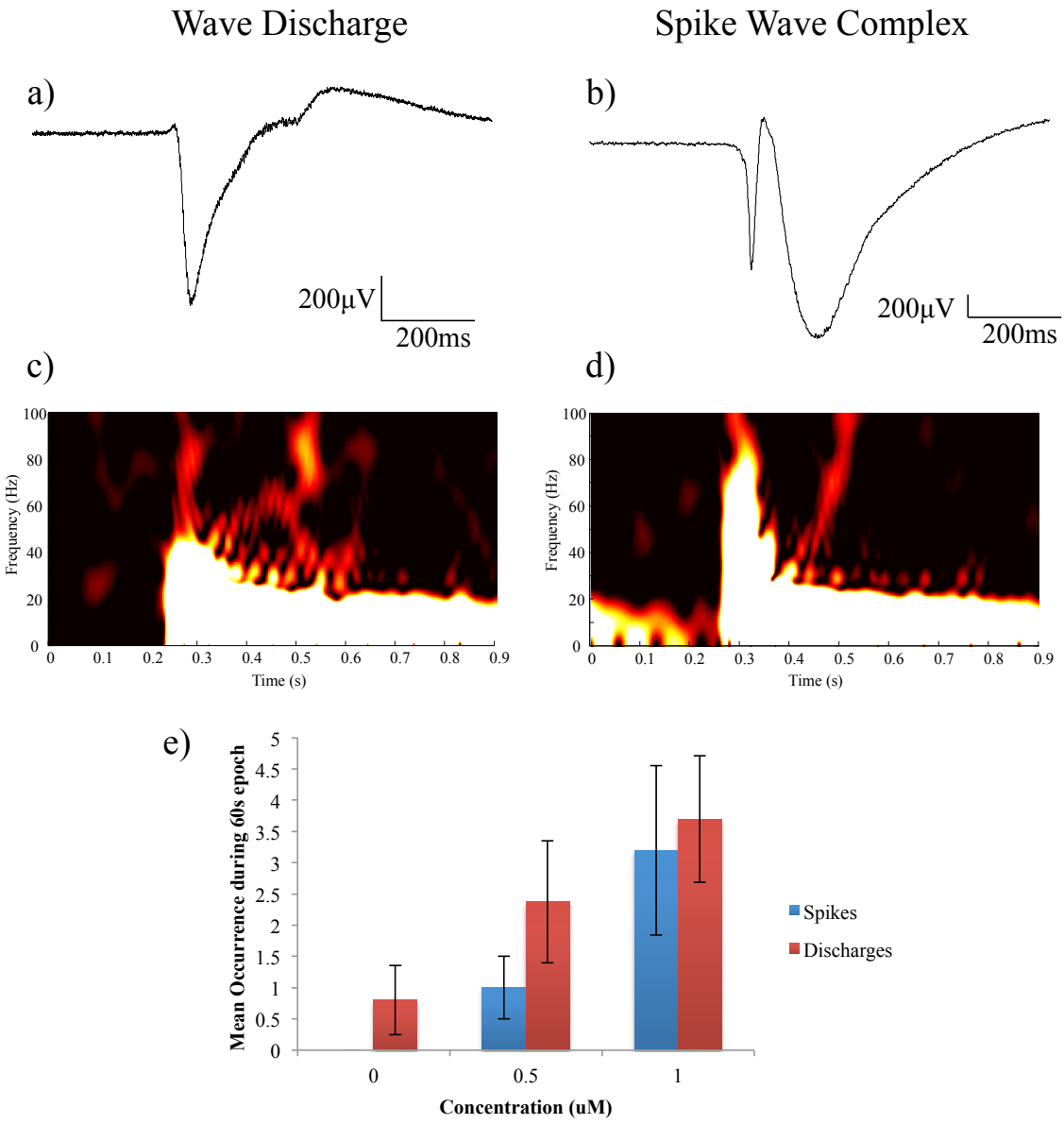

Figure 5.16: **Characteristics of epileptiform activity during Gabazine application a.** 1 second trace of wave discharge extracted from 60 second epoch after 1μM application. **b.** 1 second trace of spike wave complex extracted from 60 second epoch after 1μM application. **c.** Spectrogram corresponding to the trace shown above in a). **d.** Spectrogram corresponding to the trace shown above in b). **e.** Bar chart showing the mean occurrence of WDs and SWCs during a 60 second epoch with increasing concentration.

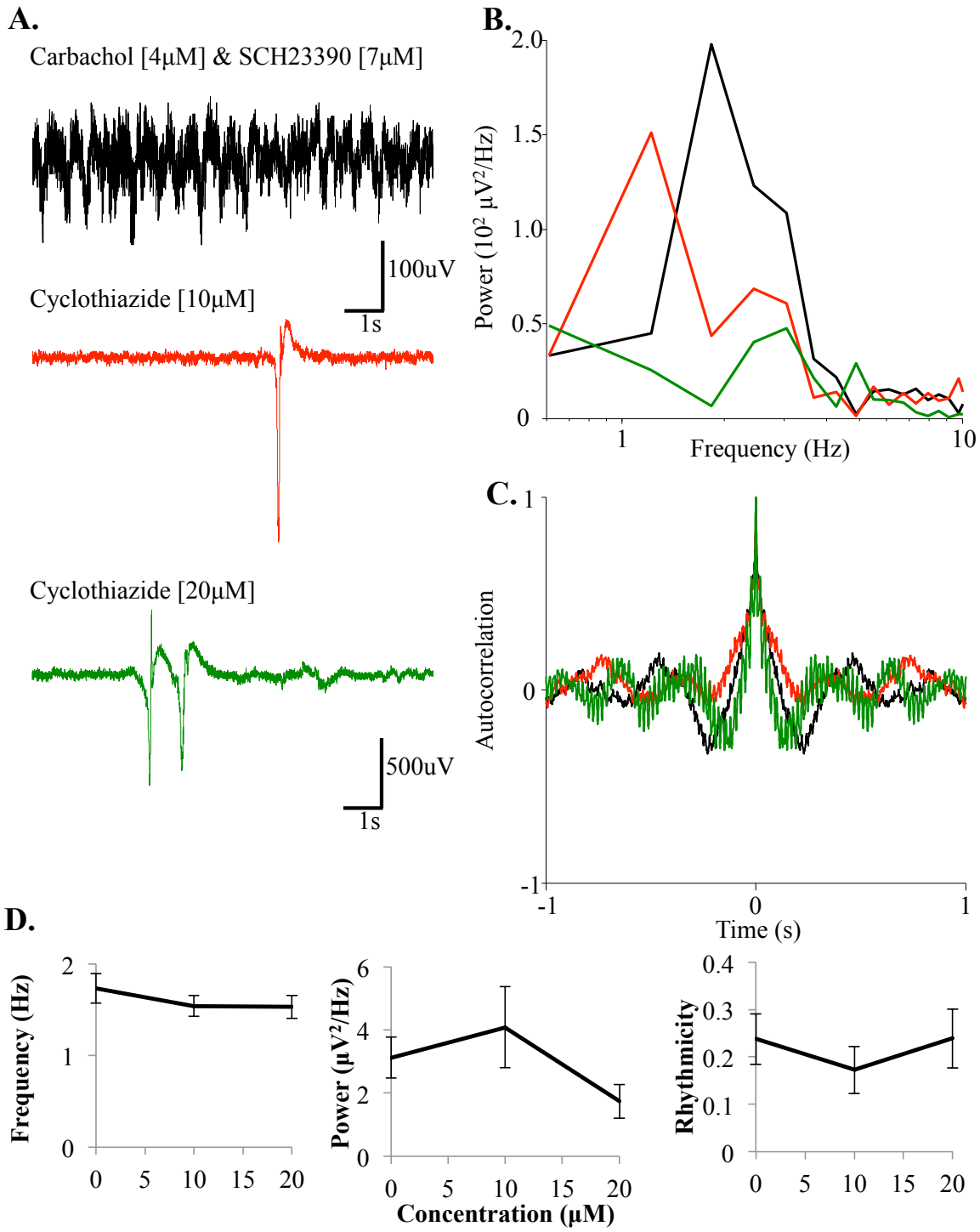

Figure 5.17: **Inhibition of AMPA receptor desensitization using Cyclothiazide.** **A.** 10 second recording of extracellular activity from layer V of the somatosensory cortex after application of Carbachol[4μM] and SCH23390 [7μM], followed by increasing concentrations of cyclothiazide. **B.** Power spectra produced from 4 second epochs of data in the absence of epileptiform activity. **C.** Autocorrelation from a 4 second epoch of activity in the absence of epileptiform activity. **D.** Concentration response curves of mean frequency, mean power and mean rhythmicity ratio of activity (n=7) during Gabazine applications.

SWCs were also present during the control condition. In total, 39 SWCs were detected during the 60 second epochs over the varying concentrations. CTZ is the only drug in this chapter to have a greater number of SWCs in comparison to WDs. The number of SWCs was significantly increased with concentration (P=0.05, n=10, One Way Repeated Measures ANOVA, Figure 5.18e. The mean occurrence of SWCs during the control condition was 0.5±0.34 compared to 2.71±1.21 after CTZ [20μM] (P>0.05, n=10, paired t-test). The morphology of the CTZ SWCs is different from those of the previously detailed drugs: the discharge part of the SWC is approximately 5 times larger in amplitude, the spike is very late in the duration of the SWC and barely crests the wave, as shown in figure 5.18b. The corresponding spectrogram (Figure 5.18d.) displays a high intensity of broad spectrum frequency activity embedded in the SWC, much unlike the majority of responses seen in this chapter.

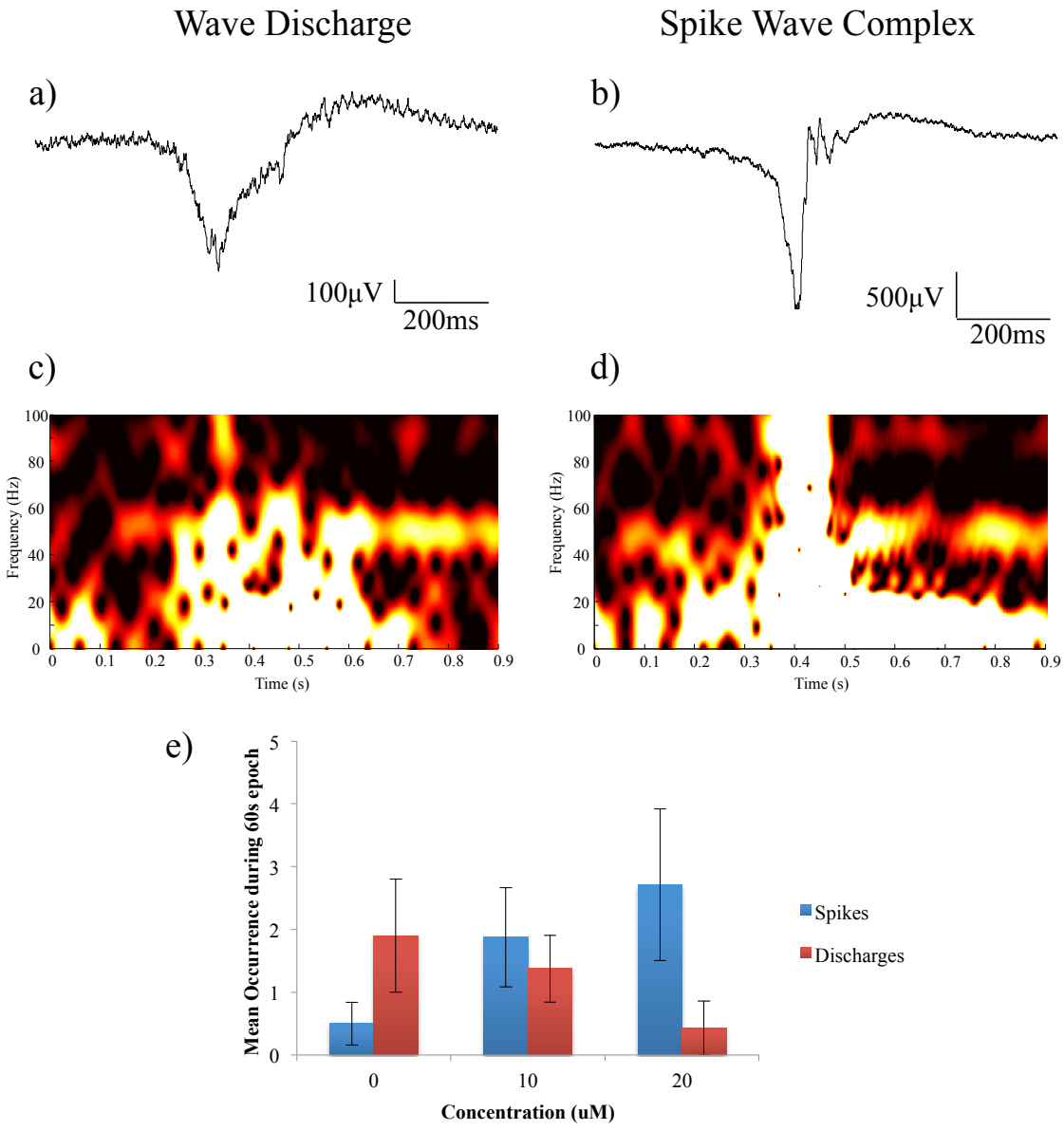

Figure 5.18: **Characteristics of epileptiform activity during Cyclothiozide application a.** 1 second trace of wave discharge extracted from 60 second epoch after 20μM application. **b.** 1 second trace of spike wave complex extracted from 60 second epoch after 20μM application. **c.** Spectrogram corresponding to the trace shown above in a). **d.** Spectrogram corresponding to the trace shown above in b). **e.** Bar chart showing the mean occurrence of WDs and SWCs during a 60 second epoch with increasing concentration.

Drug	Receptor Subunit	Concentration (μM)	Somatosensory Cortex		WD		SWC	
			Frequency	Power	Inc. rate	Trend	Inc. rate	Trend
DTC	nAChRs	2	$\Downarrow$	-	0.23		0	
	$5HT_3$	5	$\Downarrow$	$\uparrow$	1.29	$\sim$	0.64	$\uparrow$
	$GABA_A$	10	$\Downarrow$	$\uparrow$	0.55		3.68	
MG624	α_7	1	-	$\downarrow$	1.36		0.05	
		2	$\downarrow$	$\downarrow$	2.33	$\downarrow$	1.33	$\uparrow$
		5	$\downarrow$	$\downarrow$	0.5		1.5	
		10	$\uparrow$	$\Downarrow$	0		3.0	
Pancuronium	$\alpha_7{}^\star$	2	-	$\uparrow$	4.0		0.63	
		5	-	$\uparrow$	1.0	$\sim$	0	$\sim$
		10	$\Downarrow$	-	3.0		0.2	
DHβE	α_4	10	$\downarrow$	$\Uparrow$	0.71	$\uparrow$	0	-
	β_2	20	$\downarrow$	$\uparrow$	4.67		0	
α-conotoxin	α_3	1	-	$\downarrow$	6.13		1.0	
PnlA	β_2	2	-	$\Downarrow$	5.75	$\downarrow$	0.88	$\uparrow$
		5	-	-	3.63		1.0	
		10	-	-	3.67		2.33	
α-conotoxin	α_3	0.2	$\downarrow$	-	0.38		0	
AuIB	β_4	0.5	-	-	0	$\sim$	0	$\sim$
		1	$\Downarrow$	-	0.25		0.13	
ACV1	α_9	0.2	-	-	4.25		2.63	
	α_{10}	0.5	$\downarrow$	-	2.75	$\downarrow$	2.5	$\uparrow$
		1	-	-	1.67		3.17	
MDL7222	$5HT_3$	1	-	-	0		0	
		2	-	-	7.0	$\uparrow$	0	$\sim$
		5	$\Downarrow$	-	1.85		0.05	
		10	-	-	2.89		0.33	
Gabazine	$GABA_A$	0.5	-	-	2.38	$\uparrow$	1.0	$\uparrow$
		1	-	-	3.7		3.2	
Cyclothiazide	AMPA	10	-	$\uparrow$	1.38	$\downarrow$	1.88	$\uparrow$
	$GABA_A$	20	-	$\Downarrow$	0.43		2.71	

Table 5.1: **A summary of the pharmacological manipulation of the induced delta rhythm in the rodent somatosensory cortex.** $\Downarrow$ = A significant decrease observed ($P \leq 0.05$), $\Uparrow$ = A significant increase observed ($P \leq 0.05$), $\downarrow$ = A decrease observed ($0.1 < P < 0.05$), $\uparrow$ = An increase observed ($0.1 < P < 0.05$), - = No significant change.

5.4 Discussion

5.4.1 Pharmacological manipulation of the Delta rhythm

In the previous chapter, DTC was shown to significantly decrease the frequency of the delta rhythm with increasing concentration, whilst also increasing the mean power of the delta rhythm, although not significantly. With regards to mirroring this response in this chapter, very few of the agents used responded in a similar way (refer to Table 5.1). All of the agents used, bar PnIA, Gabazine and CTZ, saw a decrease in frequency in the delta rhythm, however only after Pancuronium, AulB and MDL 72222 application was this statistically significant. Of particular interest is the difference in responses between MG624 and Pancuronium (both α_7 nAChRs sunbunit antagonists), and between DHβE, PnIA and AulB (each of which has selectivity for α_3, β_2 and/or β_4).

Firstly, the classification of neuronal and muscular nAChR subunits is not definitive, as neuronal nAChRs have been found in non-neuronal cells [Flora et al., 2000, Grando et al., 1995] whilst muscle subunits have been found in neuronal cells [Pugh et al., 1995]. Pancuronium dibromide is a nicotine neuromuscular antagonist with selectivity for α_7 subunit containing (α_7*) nAChRs [Tsuneki et al., 2003]. When the results from the application of pancuronium bromide are compared to those from the application of MG624, it can be assumed that MG624 is antagonising a key component of the delta rhythm that helps maintain the rhythmicity as it's presence results in the a decrease in delta rhythm power as well as a decrease in frequency. In comparison, Pancuronium generated a mean increase in power, although not significantly so. This would suggest that the neuromuscular variant of the α_7 nAChR does not mediate the cortical delta rhythm.

DHβE, AulB and PnIA all share common nAChR subunit specificity. DHβE blocks type II currents, which are attributed to $\alpha_4\beta_2$* at concentrations below 100nM, whereas type I currents which are mediated by α_7 nAChRs are insensitive to DHβE concentrations of less than 10μM [Alkondon and Albuquerque, 1993]. Therefore DHβE is generally regarded as a non-α_7 nAChR antagonist with a preference for β_2 subtypes. α-Conotoxin AuIB is currently the only toxin to have selectivity for $\alpha_3\beta_4$* nAChRs. It is known that 1-10μM concentrations are required for complete blockade of $\alpha_3\beta_4$ nAChR subtypes [Wonnacott and Barik, 2007]. α-Conotoxin PnIA preferentially blocks $\alpha_3\beta_2$ nAChRs but also α_7 nAChRs in the rat cortex with less affinity. Both DHβE and AulB see a decrease in delta rhythm frequency. This may be linked to the partial inhibition of nicotine-evoked [^{3}H]-noradrenaline and [^{3}H]-ACh release thought to be related to the blockade of $\alpha_3\beta_4$* nAChRs by AulB, which is consistent with weak sensitivity to DHβE (DHβE weakly blocks $\alpha_3\beta_4$ [Harvey et al., 1996]). Noradrenaline and ACh are both related to wake-

fulness, therefore the blockade of these and the decrease of delta frequency seen upon application of these two agents would infer the further progression into deep slow-wave sleep.

PnIA in comparison sees no change in the frequency of the delta rhythm, however the delta frequency power is significantly decreased with increasing concentration. $\alpha_3\beta_2$ containing nAChRs are thought to mediate dopamine release [Luo et al., 1998]. DHβE and PnIA share specificity for the β_2 subunit however, their LFP responses are opposite, this would suggest that the α_4 and β_4 subunits have a greater effect on the delta rhythm. α_3 may only have a slight effect on the delta rhythm as AulB only increases the frequency, it doesn't effect the power of the delta rhythm.

With reference to table 5.1, the results of this chapter would suggest that nAChRs have more influence on the delta rhythm than the 5HT and GABA receptors targeted, however can the same be said for the epileptiform activity seen?

5.4.2 Pharmacological evocation of paroxysm activity

Of the nine agents which were used to directly antagonise specific nAChR, 5-HT and GABA subunits, all resulted in the evocation of some form of epileptiform activity, either wave discharges (WDs) or spike-wave complexes (SWCs). Table 5.1 in columns titled WD and SWC, summarises the trend in epileptiform activity with increasing drug concentration. As the results in the previous chapter demonstrated, the application of DTC to a delta rhythm in the somatosensory cortex resulted in a concentration dependent response of SWCs, where the higher the concentration applied the greater the number of SWCs recorded during each 60 second epoch. With reference to table 5.1, a similar trend is seen for MG624 (α_7 nAChR antagonist), α-conotoxin PnIA (α_3, β_2 nAChR antagonist), ACV1 (α_9, $\alpha_1$0 nAChR antagonist), Gabazine ($GABA_A$ receptor antagonist) and CTZ (AMPA PAM and $GABA_A$ receptor antagonist). This therefore implies that each of these receptor subunits is important in mediating epileptiform activity, however the questions: why these subunits? and how do they mediate this activity? still need to be answered.

As stated in section 1.7.2, several childhood nocturnal epilepsies have been related to mutations in the α_{3-5}, α_7, γ_3, β_2 and β_4 nAChR subunits. The blockade of the $\alpha_4\beta_2$ nAChR subunits produced very little epileptiform activity in comparison to the antagonistic affects of the other agents used. A similar lack of paroxysm response is seen during the blockade of the $\alpha_3\beta_4$ nAChR subunits. The AuIB results from this chapter would

imply that the α_3 subunit does not mediate SWD generation whereas, the PnlA ($\alpha_3\beta_2$ subunit antagonist) results indicate that it may when it is partnered with the β_2 subunit. This may be due to the enhancement of α_3 nAChR currents when the β_2 subunit is also present [Nai et al., 2003]. Mutations in these sets of subunits have been implicated in ADNFLE, however gene mutations are rare in ADNFLE. Therefore these results suggest that mutations in the $\alpha_4\beta_2$ and $\alpha_3\beta_4$ nAChR subunit pairs may not be solely responsible for the epileptiform abnormalities observed in this idiopathic epilepsy, whilst the $\alpha_3\beta_2$ nAChR subunit pair may have a greater role to play.

The α_7 nAChR subunit has been linked to BECTS [Neubauer et al., 1998]. This would coincide with the results from this chapter, as antagonism of this receptor has been shown to evoke a significant amount of epileptiform activity at high concentration of the specific agent. However, the chromosome location of the α_7 gene is the same location of a cation-chloride cotransporter gene [Mount et al., 1999] which play a major role in $GABA_A$ and glutamatergic signalling [Blaesse et al., 2009]. Modulation of the metabotropic glutamate receptor 5 subunit and the $GABA_A$ receptor subunit have both been implicated in paroxysm generation [Bianchi et al., 2009], which is synonymous with the results in this chapter as the application of an AMPA PAM and $GABA_A$ antagonising agents have evoked huge paroxysm events. The possible role of glutamatergic signalling is discussed further in detail in section 5.4.4.

The $\alpha_9\alpha_{10}$ antagonist ACV1 is generally considered a pain analgesic however it's selectivity for these two nAChR subunits made it attractive to this study. The α_9 nAChR is linked to cochlear hair cell development, chronic pain and breast and lung cancers [Azam and McIntosh, 2012], hence the evocation of epileptiform activity upon application of ACV1 was unexpected. All nAChRs belong to the family of ionotropic receptors, therefore it is possible to assume that the epileptiform activity upon blockade of these receptors is linked to this status.

As stated in the previous chapter, manipulation of Na^{2+} currents are thought to be responsible for SWCs in some animals models of epilepsy [Klein et al., 2004], however due to the antagonising effects of ACV1, the epileptiform activity is not thought to be mediated by these currents in this model. The mechanistic basis of this response to ACV1 is currently unclear and would benefit from further investigation in the future.

5.4.3 Possible role of Calcium Currents in childhood epilepsies

The spatiotemporal distribution of Ca^{2+} ions is known to play an important role in neuronal behaviour and survival, as well as affecting the release of other neurotransmitters. Many physiological and therapeutic neuronal functions are Ca^{2+} dependent, hence balance needs to be maintained or cellular death may occur. The flow of Ca^{2+} ions is partially controlled by the activation of ligand and voltage gated Ca^{2+} ion channels. α_7 is known to play a fundamental role in Ca^{2+}-dependent activation of signalling pathways that can modulate intracellular events involved in learning and memory. This is due to its permeability to Ca^{2+} and it's ability to substantially increase intracellular calcium levels upon activation [Gubbins et al., 2010]. *In vitro* studies have shown that the activation of presynaptic α_7 nAChRs induces LTP, hence disruption of this pathway via the antagonism of these receptors may contribute to cognitive decline [Shen and Yakel, 2009], like that seen in LGS, CAE and ADNFLE.

5.4.4 Possible role of Glutamate in epileptiform activity

Glutamate is an excitatory neurotransmitter found in abundance in the CNS. It is known to play an important role in synaptic plasticity, hence it is involved in cognitive functions like learning and memory processes [McEntee and Crook, 1993]. Over the last several decades, glutamate has been shown to play a role in epilepsy through NMDA, AMPA and kainate metabotropic glutamate receptor mediated mechanisms [Chapman, 2000]. Nicotine activates α_7 and β_2 containing nAChRs within the mouse cortex, which has been shown to decrease glutamate-mediated Ca^{2+} influx via a Ca^{2+}-dependent signal transduction cascade that involves the depression of L-type voltage-gated Ca^{2+} channels [Stevens et al., 2003]. Therefore it is possible that the blockade of α_7 and/or β_2 containing nAChRs may increase glutamate concentration. Within the experiments in this chapter, the application of α_7 selective antagonists (MG624 and PnIA) has resulted in an increase in epileptiform activity, in particular, evoking SWCs like those seen previously in our epileptiform activity model in chapter 4 and also seen in EEGs of children with nocturnal epilepsies. This would suggest that there was an increase in glutamate within these brain slices.

An increase in glutamate via microinjection into neurons results in spontaneous depolarisations approximately one second apart, which is similar to the paroxysmal depolarising shift seen during epileptic seizures [Bawari, 2010]. This change in resting membrane potential at seizure foci could result in the spontaneous opening of voltage-activated calcium channels. Which in turn would increase glutamate concentration, producing further depolarisation. This depolarisation is analogous to a huge excitatory synaptic potential.

Chapman (2010) states that it's earliest component is due to activation of AMPA receptors and its later component to activation of NMDA receptors. Cyclothiazide (CTZ), a positive allosteric modulator (PAM) of the AMPA receptor, utilised within this thesis, is known to be capable of reducing or eliminating rapid desensitisation of the receptor and increasing glutamate currents [Bertolino et al., 1993]. Within this chapter, the application of CTZ was shown to evoke SWCs with increasing concentration, however these SWCs were much greater in amplitude when compared to the SWCs evoked by nAChR antagonism. This would suggest that AMPA receptors have a more direct effect on epileptiform activity than nAChRs alone. Muldrum (1994) reported that, glutamate antagonists selective for NMDA and non-NMDA receptors are potent anticonvulsants when given systemically in a wide variety of animal models of epilepsy [Meldrum, 1994], therefore adding to the argument that epileptiform activity is mediated by glutamate currents.

CTZ is also a $GABA_A$ negative allosteric modulator (NAM) which potently inhibits $GABA_A$ mediated currents [Deng and Chen, 2003]. Due to the inhibitory nature of GABA, the blockade of this receptor would increase excitatory responses similar to that seen during increased glutamate mediated currents. From the results in this chapter, it is shown that the blanket blockade of inhibition with gabazine generated far more severe discharges than any of the nAChR or 5-HT agents tested. This would suggest that only partial disinhibition is required to generate WD and SWC activity. So which interneurons are selectively targeted? Both 5-HT and nAChRs are found on dendrite targeting interneurons preferentially (rather than perisomatic targeting neurons). Specifically, $5\text{-}HT_{3A}$ receptor expressing interneurons in the somatosensory cortex make up approximately 30% of cortical interneurons and are found predominantly in superficial layers [Lee et al., 2010a]. These $5\text{-}HT_{3A}$R-expressing interneurons uniformly respond to serotonergic and cholinergic modulation [Lee et al., 2010a]. Therefore it is possible that the 5-HT and nAChR agents used within this chapter are acting directly on these interneurons. Coupled with the effects of CTZ, this suggests a failure to control dendritic AMPA-receptor mediated inputs onto pyramidal cells, particularly in superficial layers.

5.4.5 Summary

The work described in this chapter has outlined the basic pharmacological properties of epileptiform activity during slow-wave sleep. These findings suggest that epileptiform generation is mediated by dendrite targeting interneurons through the blockade $5\text{-}HT_3$ and nAChR subunits. The data in this chapter also suggests that the differences in WDs and SWCs may simply be the degree of recruitment of superficial layers in addition to paroxysmal events in the delta-generating layer V pyramidal cells. It is therefore

important to observe the activity of individual neurons during paroxysmal events within both layer V and superficial layers to investigate the interplay between the neurones located in these regions. The next chapter will therefore explore this, through the use of intracellular and multichannel unit recordings. When combined with results from this and the previous chapter, these studies should provide a more definitive picture of the network activity underlying these events.

Chapter 6

Mechanisms underlying the generation of the epileptiform activity in the cortical delta rhythm: Cellular Recording Studies

6.1 Introduction

The results of the previous chapter outlined the complex pharmacological properties of epileptiform activity resembling that seen in children with nocturnal epilepsies. The results from chapters 4 and 5 have demonstrated that as a network, the neurons in the deep layers of the cortex, layer V in particular, result in epileptiform behaviour following the application of d-tubocurarine (DTC) or selective antagonists that mimic DTC. However, the effect on individual neurons as well as the spatial effect across the cortical layers is currently unknown. By using intracellular methods, it aids the formation of a more definitive picture of the mechanisms proposed in the pharmacology chapter by elucidating the input/output activity of individual neuronal cell types during delta oscillations. Whereas the use of a multi channel electrode array allows for a greater understanding of the distribution and spatial extent of the two individual induced paroxysmal events in terms of their laminar distribution in the cortical column and longitudinal distribution through the region of interest.

6.1.1 Mechanisms underlying epileptiform discharges

Local field potential and EEG recordings are readily able to distinguish between normal brain activity and epileptiform activity in the majority of cases. However, the nature of the recordings (i.e. gross population averages, distal electrode location and indirect measurement of neuronal activity) often excludes the possibility of determining what neuronal processes underlie the pathology. In contrast, intracellular studies are able to

provide direct observations of individual neuronal subtype inputs and outputs, and the relationship between them. This form of data is crucial for understanding the processes underlying the pathological activity patterns associated with seizures.

It is thought that the first intracellularly identified correlate of seizure-like activity was the so-called paroxysmal depolarising shift: A grossly exaggerated excitatory response to synaptic input [Johnston and Brown, 1981]. Studies have suggested a range of causal mechanisms for this; from general imbalance of synaptic excitation and inhibition, alteration in the expression of glutamate receptor subunits in favour of NMDA receptor-mediated postsynaptic events, potentiation of extracellular potassium ion concentration and enhanced intrinsic calcium conductance activation [Johnston and Brown, 1984, Traub, 1979, Korn et al., 1987, Whittington et al., 1995]. All of these studies were performed on crude *in vitro* models of epileptiform activity and their relevance to human epilepsy is still questionable. Direct studies on human epileptic tissue, like those by Sloviter (1991) do support - at least partially - an imbalance in inhibition due to failure to activate local circuit interneurons. However, a study by Roopun *et al* (2010) reported that in human tissue, a causal role of non-chemical synaptic transmission appeared dominant.

A comparison of human and animal model studies does not necessarily negate the findings of the latter. There is a remarkable diversity in the type of epileptiform discharge observed, even within identified subgroups of epilepsy, clinically. It is therefore likely that a broad range of mechanisms lead to a disruption of neuronal excitability, which themselves may differentially contribute to the generation of seizures in different epilepsy syndromes. It is therefore important to focus on the type of epileptiform activity being studied and the specific modifications made to the system to experimentally generate it.

6.1.2 Relevance to nicotinic receptor function

Acetylcholine has been associated with both cognitively relevant brain function and seizures [Gähwiler and Dreifuss, 1982, Mansvelder et al., 2006]. The former will be detailed in the following section. While the latter demonstrates the complexity of the effects of this neuromodulatory system. In the study by Gähwiler and Dreifuss (1982), both excitatory and inhibitory effects of ACh on neurons were observed, with the excitatory effects predominantly mediated by the muscarinic subtype of ACh receptors (which have been blocked by atropine). Muscarinic receptors increase neuronal excitability by partially blocking a particular type of potassium conductance [Brown and Adams, 1980]. Thus, 'K+ current' is critically important for limiting the output of neurons, in terms of

numbers of action potentials, for a given excitatory input. It is present in most neuronal compartments but its ability to promote burst activity, which is often seen during epileptiform discharges, correlates best with its presence in axonal membranes [Shah et al., 2011].

Severe, chronic epilepsy can be pharmacologically induced experimentally by selectively targeting muscarinic receptors in rodents through the administration of pilocarpine [Turski et al., 1983]. The epileptiform events seen during seizures have a major components of spike and wave discharges in this model. However, it is still not known exactly how a muscarinic agonist generates seizures. For example, in animal models of absence seizures (which are also associated with spike and wave discharges), the addition of pilocarpine to the epileptic animal actually decreased these events [Danober et al., 1993]. Interestingly in this study, agonism of nicotinic receptors also reduced spike and wave discharges. Again, the story is complex though. For about 50 years, it has been known that nicotine central administration generates seizures [Orcutt et al., 1963]. However, a recent study by Zerem *et al* (2013) has reported the potent anti-epileptic properties of small doses of nicotine when administered transdermally to patients with epileptic encephalitis.

The previously mentioned study is of particular relevance to the model of spike and wave discharges studied in this thesis. Other work has also shown that disrupting nicotinic receptor function is associated with seizures: A number of studies have shown a genetic link between disrupted nicotinic receptors and seizures (refer to Chapter 1.7.2), and animal models clearly show a seizuregenic action of nicotinic antagonists (see Chapter 4.1). A solution to this confusing collection of findings may come from the work of Dobelis *et al* (2003). These researchers noted that both agonists and antagonists of nicotinic receptors generated epileptiform activity. But when relating these findings to GABA release (as a measure of inhibitory neurone function) they found that both agonist and antagonists disinhibited the cortex - the former effect being related to receptor desensitisation. In other words, too much nicotinic cholinergic tone was just as detrimental as having too little owing to rapid adaptation of nicotinic receptor postsynaptic responses.

6.1.3 Relevance to physiological correlates of learning and memory

As mentioned above, nicotinic receptor agonism has strong cognitive effects. Disruption of nicotinic receptor/ionophore assembly in rare genetic disorders is strongly associated with learning disabilities [Chung et al., 2012]. In particular, the endogenous nicotinic receptor agonist modulator LYPD6 has been shown to disrupt nicotinic receptor calcium

conductance [Darvas et al., 2009] - a property which is closely related to the potentiation of synaptic plasticity as a physiological substrate of learning and memory by nicotine [Jia et al., 2010]. However, whether this has a direct effect on synaptic plasticity during sleep, or whether plasticity is disrupted by the change in cortical dynamics associated with spike and wave discharges remains to be elucidated and will be considered in this chapter.

6.1.4 Aims and objectives

This aims of this chapter are to:

- Utilize current intracellular recording methods to create a more definitive picture of the mechanisms proposed in the previous chapter by clarifying the input/output activity of individual neuronal cell types during delta oscillations.
- Investigate and interpret the distribution and spatial extent of the wave discharge and spike-wave complex events in terms of laminar distribution in the cortical column and the longitudinal distribution through the rodent somatosensory cortex spatiotemporal activity, through the use of a multi channel electrode array.

6.2 Methods

6.2.1 Slice preparation and maintenance

Rodent brain slices from the somatosensory region were prepared as previously described in chapter 2.3 and maintained according to the methods detailed in chapter 2.4. The acquisition of intracellular data and it's subsequent analysis can be found in chapter 2, sections 2.6, 2.7 and 2.8.2. Delta rhythm oscillations were induced in the slice through the bath application of carbachol [4μM] and SCH23390 [7μM] into the circulating oxygenated ACSF medium. Before either intracellular or multichannel recordings were performed, the presence of delta frequency activity in layer V was first confirmed using an extracellular field electrode. During intracellular experiments, this extracellular electrode remained in the slice in it's set position with the intracellular electrode being placed either adjacent to it, which would allow for a direct comparison in the activity of the individual neurons, or in the same cortical column but in layer II/III, which would allow for a better understanding of the neuronal connections between layers II/III and V. During multichannel experiments, this extracellular electrode was removed after confirming the presence of delta frequency activity in the slice/s.

6.2.2 Intracellular methods

Intracellular recordings were obtained using sharp borosilicate glass electrodes containing potassium acetate solution [2M], an electrolytic medium similar to that of the internal composition of neurons as previously described in section 2.6. Characterisation of individual neurons was achieved using a 0.2nA depolarising or 0.3nA hyperpolarising current injection step with a duration of approximately 200ms. Further detail on these intracellular methods can be found in chapter 2.8.2.

6.2.3 Multichannel unit recording techniques

Following the confirmation of delta activity using an extracellular electrode, a utah multichannel electrode array was positioned onto the slice ready for multichannel recordings as described in section 2.7. The orientation of the electrode grid was noted and mapped onto a sketch of each slice used to allow for a more accurate definition of superficial and deep cells. The number of the utah array was also noted to allow for the correct mapping on the array and the correct impedances of each electrode.

6.3 Results

6.3.1 Laminar distribution of field potential SWC components

The wave discharges (WD) described in the previous chapter were reminiscent of paroxysmal depolarising shifts seen in many models of epilepsy (see section 6.1.1). However, spike and wave complexes (SWCs) appeared to be far more complex phenomena. In order to understand more about them to guide intracellular recordings, a more laminar analysis (see figure 4.6) with field electrodes was first performed.

As WD and SWC incidence was variable, only slices with a high SWC incidence rate were used for this part of the study. In 5/12 slices deemed suitable, occasional runs of SWCs were seems where epileptiform events of the SWC type occurred with a frequency of 3.1 $\pm$0.s, with 5 - 24 events per run (mean 12$\pm$4 events, figure 6.1A). These events has the same spectral characteristics as the human EEG spike and wave recordings (Figures 3.1 and 3.2) and the SWCs quantified in the previous chapter (e.g. see figure 5.8): Events occurred off a delta frequency baseline with a transient increase in delta power corresponding to the 'wave' of the SWC and a broadband of higher frequencies corresponding to the 'spike' components (Figure 6.1B).

Moving the extracellular recording electrode into different laminae between runs of SWCs

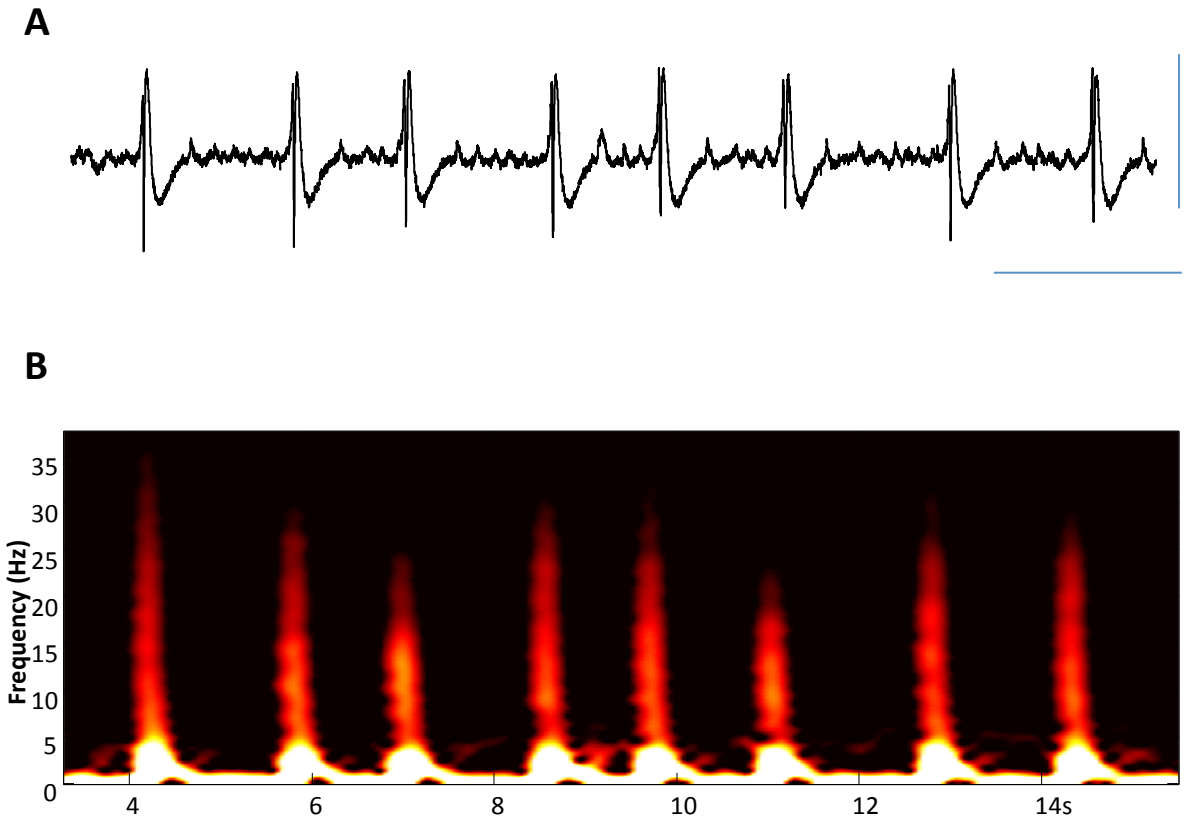

Figure 6.1: **Repetitive, spontaneous spike and wave discharges arising from a delta rhythm. A.** Example trace from layer 1 of association cortex showing low amplitude delta rhythm interspersed with spike and wave discharges occurring approximately every 2s. Delta was induced as described in chapter 4 and discharges generated on top of this by bath application of 10μM DTC. Scale bar 2sec, 0.2mV. **B.** Spectrogram of the data in A showing continuous $\sim$1Hz delta and spike wave discharges consisting of broadband power with modal peaks in the low theta range and 10-20Hz corresponding to the spike component of the spike and wave discharge (refer to figure 3.1A).

allowed a crude estimate of layer origin of the wave and spike components of the SWC. Classic, and inverted SWC shapes were seen with the electrode at the very edge of each slice (Layer I / pail surface recording) and within Layer V (Figure **??**).

These data strongly suggested that the spike and the wave components of the SWC were generated by different mechanisms / neurons located in supra- and infragranular layers respectively. Intracellular recordings were therefore aimed at principal neurons in these two areas.

6.3.2 DTC effects in Layer V

DTC, and some more specific agents, effects on the delta rhythm were associated with decreases in rhythmicity and frequency. As the principal neuron responsible for delta rhythms has been shown to be the layer V intrinsically bursting (IB) neuron [Carracedo et al., 2013], recordings from this cell type in the presence of DTC were studied in detail. In general, a trend towards longer, more intense (in terms if spikes generated during the depolarisation) burst discharges was seen as DTC concentration increased (Figure 6.3). Quantification of depolarisation time, spike number per burst and interburst spike frequency all revealed increasing mean values with 5 and 10μM DTC (Figure 6.4). However, as DTC concentration increased so did the variance in these measures (taken from 60s epochs of data from n=5 IB neurons). For example, DTC caused a change in depolarisation time from 200±20ms to 605±395ms. As the standard error increased from ∼10% of the mean to ∼65% of the mean, no significant difference was seen despite the near 3-fold increase in mean burst duration ($P>0.05$, Figure 6.4A). Similarly, spike numbers per burst changed from 5±3 in control conditions to 14±8 in the presence of 10μM DTC ($P>0.05$, Figure 6.4B). Although, for the intermediate concentration of DTC, a significant increase in spike numbers per burst was seen with the data available (5±3 vs. 13±3, n=5, $P<0.05$). Despite, this significant effect, no changes in spike frequency were seen at either of the concentrations used.

As two types of principal cell are found in Layer V, readily identified by their responses to depolarising current injection (see Figure **??**), the effects of DTC were also examined on regular spiking (RS) neurons. During control delta rhythms RS cells do not generate a delta frequency output. Instead, they show a range of spike profiles over a narrow range of membrane potentials (Figure 6.5). At membrane potentials between -65mV and -70mV RS cells generate either a single spike or none at all (mean spike incidence 0.6±0.3, n=5 cells from 5 slices, total 300 delta periods). Between -65mV and -60mV these cells generated brief packets of 2 or 3 spikes phase locked to each delta period.

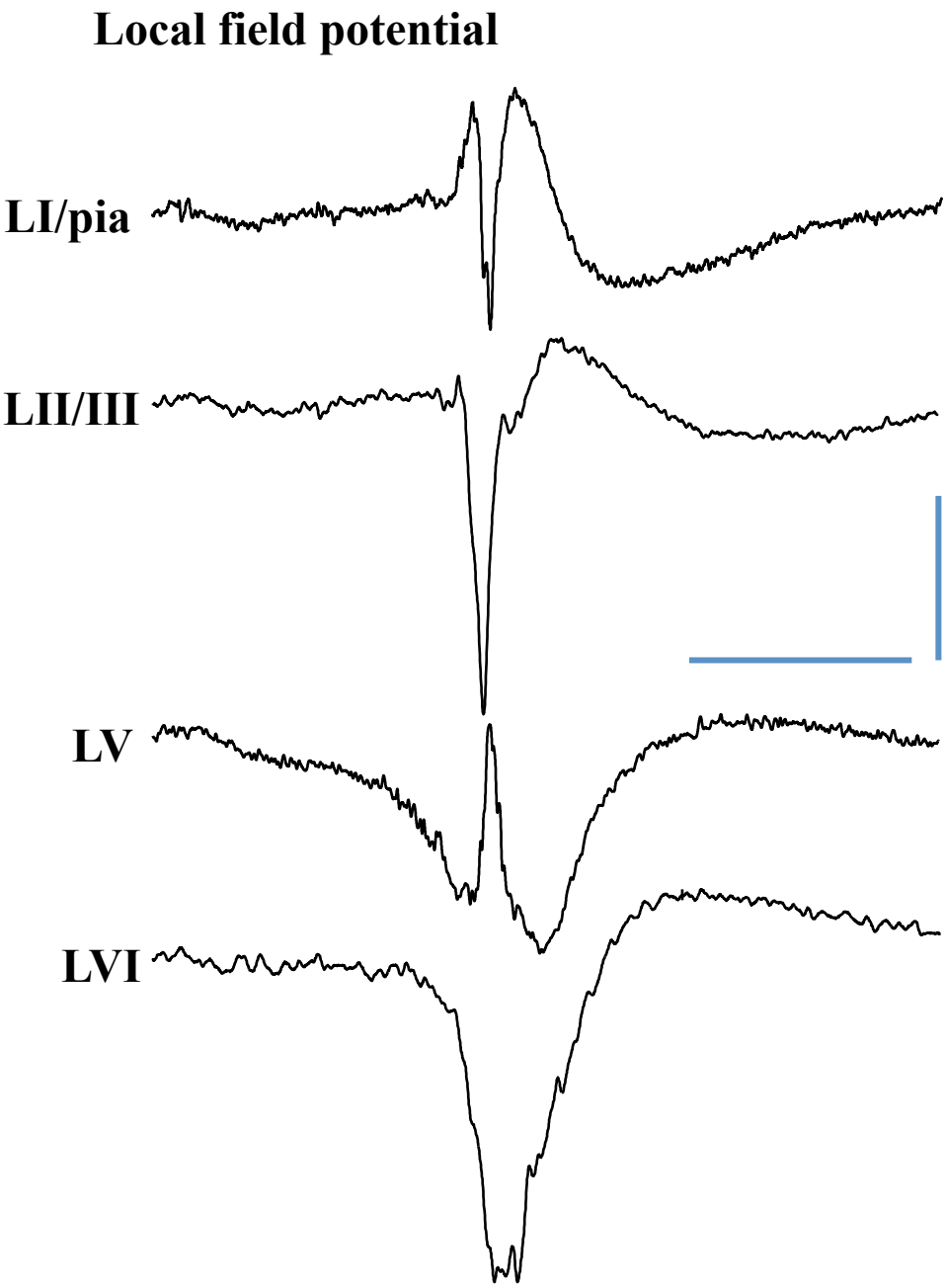

Figure 6.2: **Detailed laminar profile of spike and wave discharges shows separation of the spike and the wave component in superficial and deep layers respectively.** Example traces for each layer were taken from the same slice under conditions described in chapter 4. Note the wave component of the wave and wave discharge is maximal in deep layers, as with pure wave discharges (WD, without the spike component, refer to figure 4.6). Also note the wave discharge reverse in superficial layers - a property shared with control delta rhythms, and the spike component reveres dramatically between LII/III and LV. Scale bars 400ms, 0.2mV.

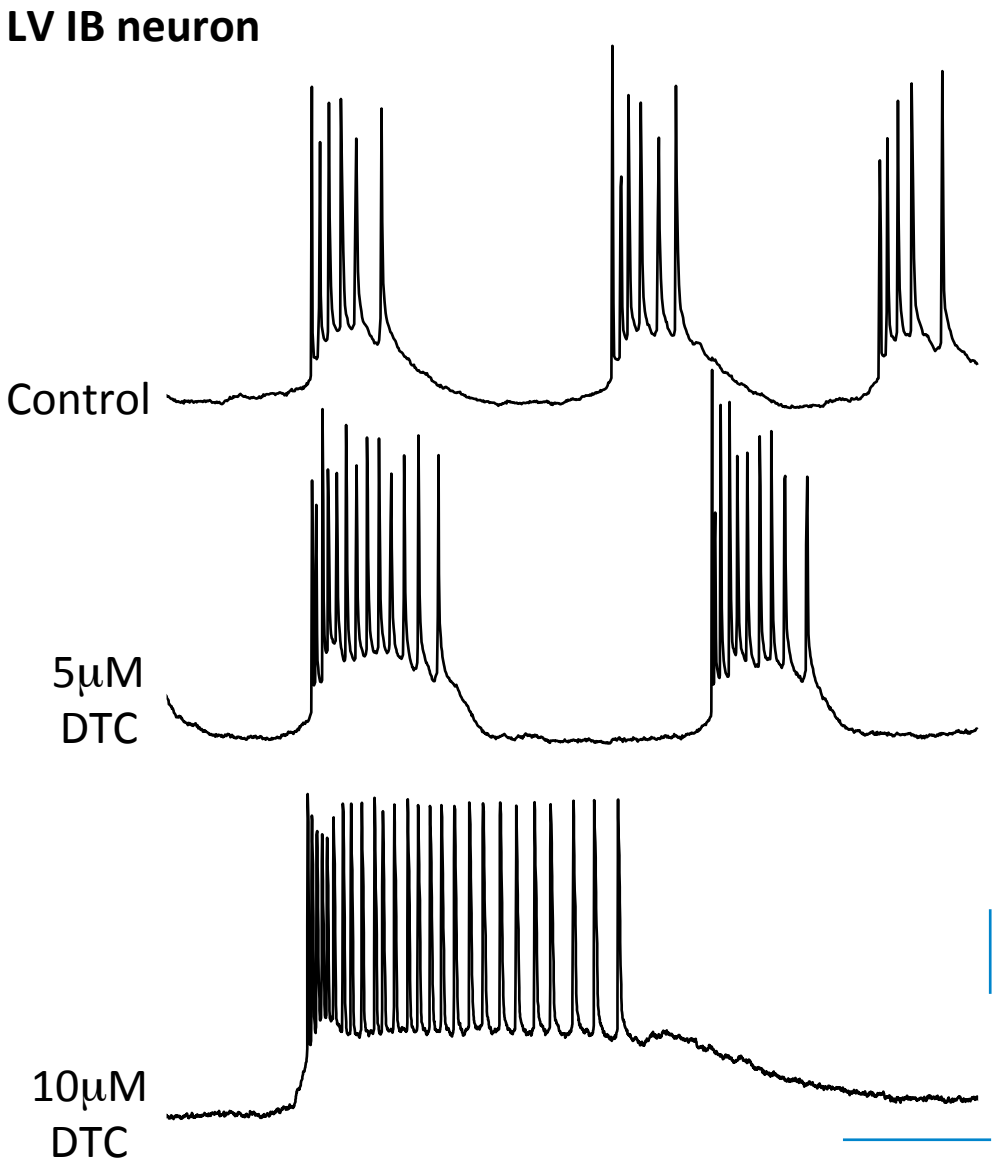

Figure 6.3: **Example of change in layer V intrinsically bursting (IB) neuron behaviour with increasing concentrations of DTC.** In all conditions IB neurons were seen to generate near-plateau potentials corresponding to the negative-going part of each field potential in layer V. The duration and output intensity (frequency and number of action potentials) increased with increasing concentrations of DTC. All traces illustrated were from sharp electrode, intracellular recording of a single neurone held throughout the cumulative DTC concentrations changes. Scale bars 200ms, 15mV.

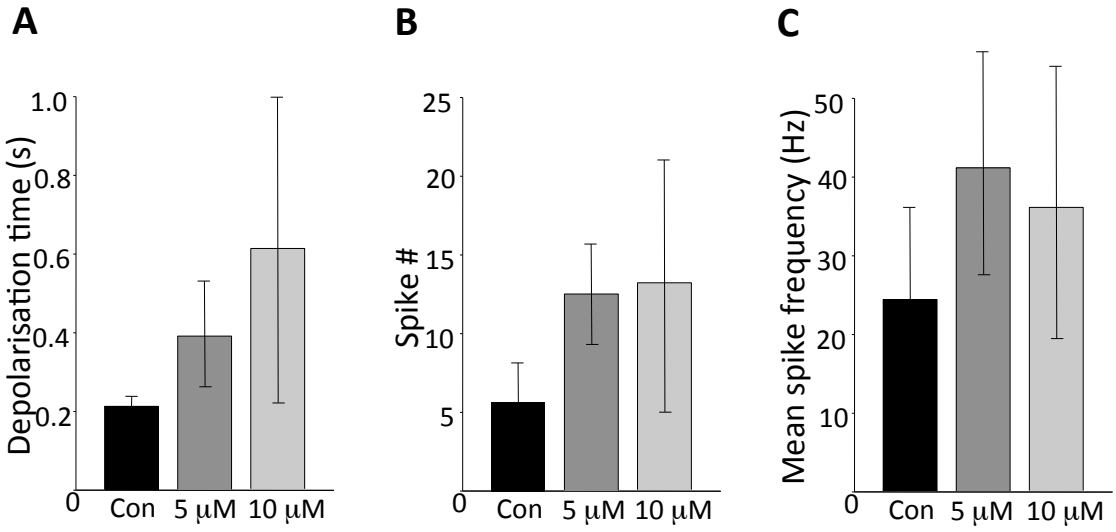

Figure 6.4: **Quantification of changes in IB neuron discharge with increasing concentrations of DTC. A.** Mean ± SEM of the duration of IB cell depolarisation (taken at half maximal deflection - excluding action potentials) plotted against DTC concentration. **B.** Mean ± SEM of the number of spikes per IB cell discharge plotted against DTC concentration. **C.** Mean ± SEM of the spike frequency during IB cell discharge plotted against DTC concentration. Note that as DTC concentration increases, the variance in these datasets markedly increases also.

Mean interspike interval (during a spike packet) was 150±12ms, corresponding to theta rhythm frequency [Carracedo et al., 2013]. At membrane potentials of -60mV or more depolarised these cells spiked continuously at this theta frequency irrespective of the on-going delta rhythm.

This continuous pattern of spiking was preserved in the depolarised state in the presence of DTC (5μM, no 10μM concentration was attempted during recordings from these cells). However, the theta frequency was significantly slowed, with interspike intervals increasing from 150±12ms (control) to 223±10ms ($P<0.05$, n=300 events from n=5 cells). Interestingly, at membrane potentials more hyperpolarised than this, single or double events were seen phase locked to the delta rhythm. Howvere, instead of single spikes, DTC transformed spike outputs into brief intense hurts consisting of 2-5 spikes (Figure 6.5). These burst discharges were associated with the appearance of significantly larger, longer excitatory postsynaptic potentials (EPSPs) occurring at the on-going delta frequency (control 2.1±0.4mV, DTC 3.5±0.5mV, $P< 0.05$).

The changes outlined above in both cell types were seen on every delta period in the presence of DTC. The only significant difference associated with SWC occurrence was an increase in Layer V IB cell burst duration. In 'normal' delta rhythms in the presence of

DTC burst duration was 605±395ms (see above). IB cell burst duration during a SWC was 720±58ms, a considerably less variable measure which was highly significant different from control delta values (200±20ms, $P<0.001$). In contrast, behaviour of Layer II/III regular spiking (RS) cells changed starkly between delta and SWC events.

6.3.3 DTC effects in Layer II/III

During normal delta rhythms, Layer II/III RS cells fired very infrequently: Mean spike rate per delta period was 0.2±0.1. The cells received weak, compound EPSPs on every delta period which often displayed dual peaks (Figure 6.6A). This infrequent spiking was not altered by the presence of DTC, even at the highest concentration used (10μM). Mean spike rate with DTC present was identical to control ($P>0.5$, n=300 events, n=5 cells). This was seen despite a significant increase in EPSP amplitude and a qualitative collapse in the dual peaked nature of many EPSPs seen during the control state (control 3.1±0.4mV, DTC 4.3±0.3mV, $P<0.05$, Figure 6.6A). In striking contrast, on every SWC observed, Layer II/III RS cells generated intense, brief bursts seen immediately prior to each spike in the SWC field recording (Figure 6.6B). Spike rates per burst were more variable in Layer II/III RS cells compared to those in Layer V RS cells, with 1-7 bursts seen. In addition, the nature of the spike in the SWC was mirrored by the burst pattern in Layer II/III RS cells. Bursts were seen either early in the wave component of the SWC, 100-150ms later in the SWC or both early and late. Om each case a field spike was seen corresponding to the intracellularly recorded output of these cells. This behaviour is illustrated in figure 6.6B which shows 3 types of behaviour, where field potentials from Layer V and RS cell potentials from Layer II/III were recorded from simultaneously.

A further correlation was observed between burst behaviour in superficial RS cells and the field spike component of the SWC (Figure 6.7A, B). Plotting the amplitude of the field spike component of the SWC against the amplitude of the superficial RS cell EPSP, which was held at -80mV to prevent burst generation, showed a strong correlation. Linear regression analysis gave a line with slope=17.46 ($r^2=0.87$). Similarly, at resting membrane potential, a comparison of SWC field spike component amplitude and number of action potential spikes generated per burst gave a linear regression line of slope=6.25 ($r^2=0.82$).

These data strongly suggest that excessive synaptic excitation onto Layer II/III RS cells was, at least in part, responsible for the spike component of the SWC. However, some data was collected that suggested that other factors may also play a role. One RS neuron was recorded in which clear spikelets were seen, as shown in figure 6.8. These increased

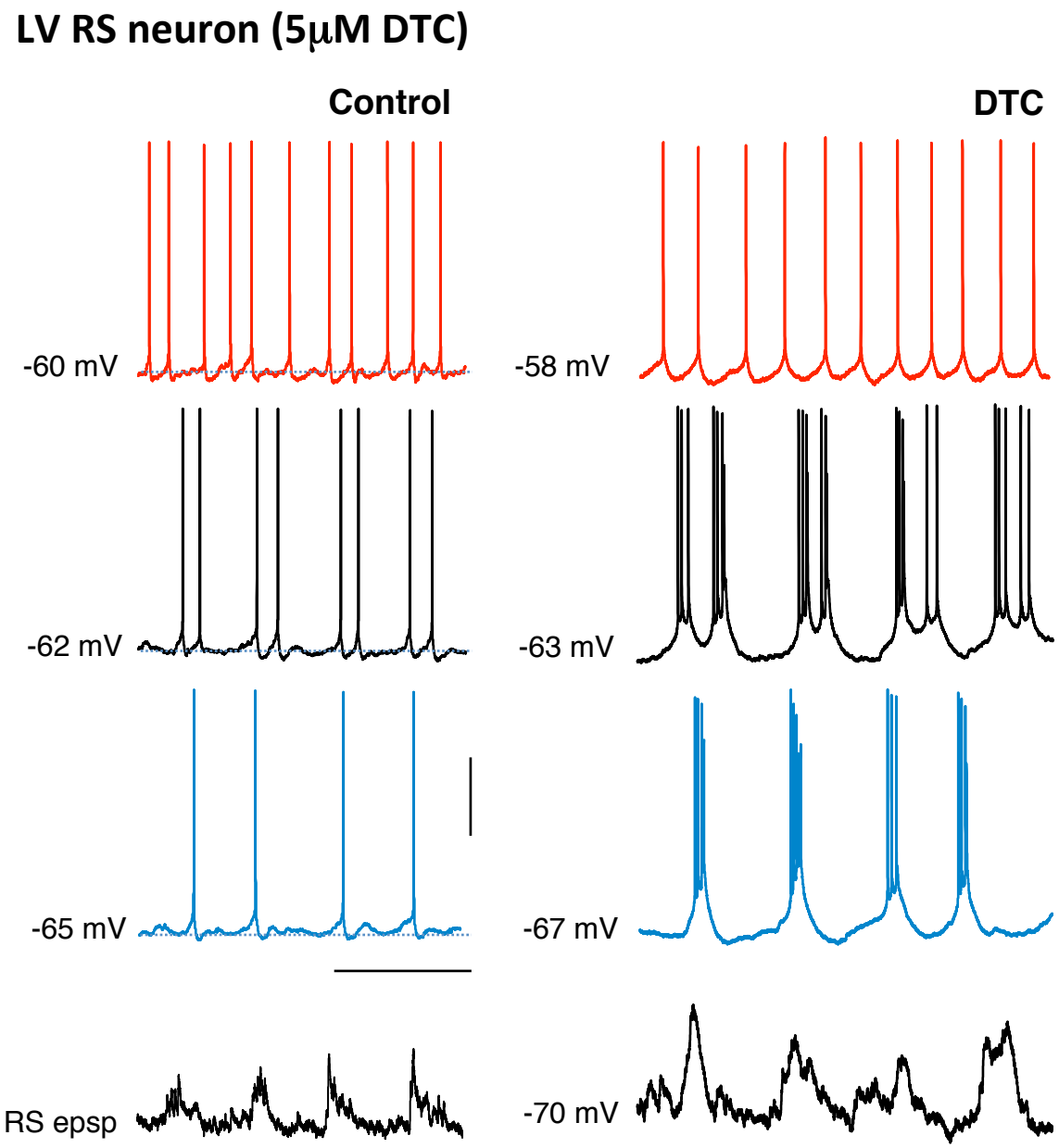

Figure 6.5: **DTC caused an increase in burst spiking in layer V regular spiking neurons.** Left panel shows data from a single layer V regular spiking neuron (RS) during control delta activity (4 consecutive periods illustrated). Spike behaviour is shown at 3 different membrane potentials generated by tonic injection of current through the recording electrode. EPSP recordings were taken with negative current injection to hold the membrane potential at -70mV. Right panel shows the behaviour of the same cell 30 minutes after bath application of 5μM DTC. Cell is illustrated at approximately the same 3 membrane potentials as in control conditions. Note the transformation of single spikes to bursts at the more hyperpolarised membrane potentials and the large increase in EPSP amplitudes. Scale bars 1s, 20mV.

in frequency immediately before an RS burst in Layer II/III during an SWC. In addition, on one occasion, the recording electrode appeared to have impaled a dendrite in the superficial layers (see section 6.4). This recording was held during an entire experiment allowing comparison of dendritic electrogenesis in control, delta rhythms and with increasing concentrations of DTC (5 and 10μM, Figure 6.8B). During the control state, delta rhythm EPSP amplitude appeared to be larger than that recorded from the soma in layer II/III RS cells (6.2±0.5mV, n=120 events, n=1 cell). However, no signs of local electrogenesis were seen on any delta period. In contrast, in the presence of 5μM DTC, single or double bursts of small, sharp dendritic spikes were seen riding on the EPSPs. The spike amplitude saw very little variation in amplitude with a mean of 10±0.5mV. With further increase in DTC concentration to 10μM, these bursts became prolonged and more amalgamated which also containing larger, broader dendritic spikes.

6.3.4 Preliminary evidence for synaptic plastic changes associated with SWC

Given the extreme changes in output of Layer II/III RS cells, from infrequent single spikes to bursts, evidence for plastic changes in Layer II/III RS cell inputs was gathered. Spike and wave discharges during sleep have been associated with cognitive deficits in patients with a range of primary pathologies (refer to Chapter 1), so the identification of the mechanisms responsible for the relationship between physiological correlates of memory (synaptic plasticity) and the pathophysiology of SWCs would be potentially valuable. Intracellular recording were taken from 5 superficial RS cells before, during and after runs of SWC activity (see above) consisting of between 8 and 24 spike and wave discharges (Figure 6.9). Cells were held at -70mV to minimise the contribution of inhibitory postsynaptic potentials (IPSPs) to the data gathered. Layer V field potentials were obtained simultaneously. Prior to an SWC run, the mean RS cell EPSP amplitude was 4.2±0.5mV. During the SWC run, EPSP amplitude (per delta rhythm, excluding those associated with each SWC) was dramatically reduced, with many delta periods no associated with any recordable superficial RS cell EPSPs at all (asterisks, Figure 6.9). Mean EPSP amplitude was 1.1±0.6mV ($P<0.05$, n=124 events from n=5 cells). Interestingly, on termination of each SWC run, EPSP amplitude recovered rapidly. Amplitudes were not significantly different from pre-run measures within 8-15s of the last SWC in the run. However, within 30s of the termination of the SWC run, EPSPs settled at significantly higher amplitudes that those that occurred pre-run (6.4±0.6mV, $P<0.05$, 10 events from each of n=5 cells starting 30s post SWC run).

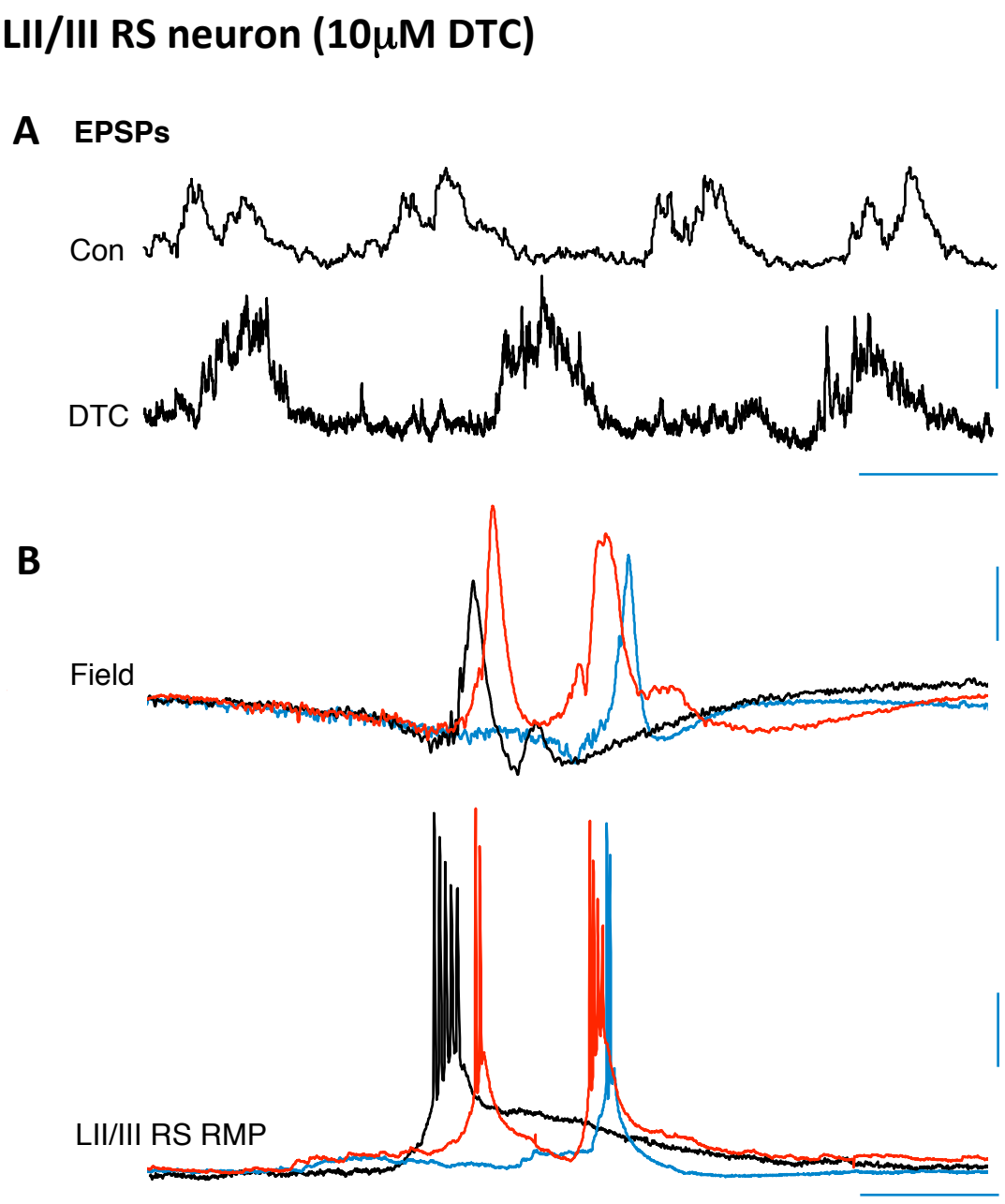

Figure 6.6: **Spike and wave discharges were associated with burst discharges in superficial (LII/III) regular spiking (RS) neurons. Burst timing corresponded to bursts seen in layer V RS neurons. A.** Example traces illustrating the pattern of EPSPs onto layer II/III RS cells in control conditions (delta only) and with bath application of 10μM DTC. Note the larger, more erratic events in the presence of DTC. No spike and aves complexes occurred during the time epochs shown. Scale bars 400ms, 3mV. **B.** Illustration of the variable pattern in timing of spikes within an SWC concurrently in layer V field potential (upper traces) and LII/III RS cell intracellular recordings (lower traces). Note that spikes can occur 'early' in the SWC (black), late (blue) or both (red). In each case the field spike corresponded to a burst in the cell (refer to figure 6.5 right panel -63mV recording from layer V RS cell). Scale bars 100ms, 0.2mV (field), 15mV (intracellular).

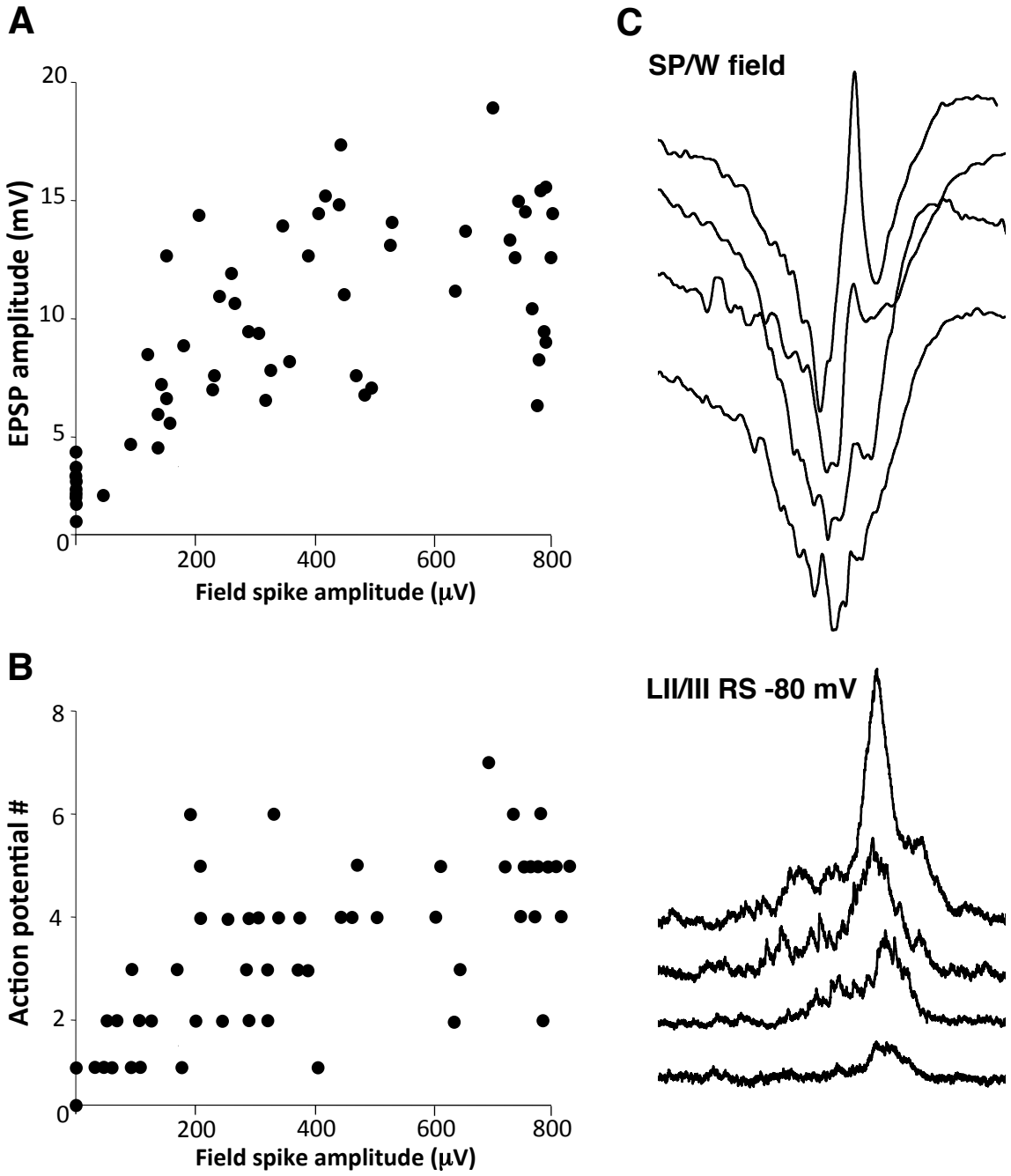

Figure 6.7: **The spike amplitude in a spike and wave discharge correlated with layer II/III RS action potential burst intensity and excitatory postsynaptic potential (EPSP) amplitude. A.** Pooled data showing 60 paired recordings of SWC events in layer V field potential and layer II/III RS intracellular recordings. Spike amplitude was derived from low-pass filtered field data (panel **C** upper traces). EPSP amplitude was taken from -80mV (panel **C** lower traces). Note the EPSP amplitude correlated well with field spike amplitude up to 0.4mV before plateau. **B.** Pooled data showing 74 paired recordings of SWC events in layer V field potentials and action potential numbers per SWC from concurrent layer II/III RS intracellular recordings from resting membrane potential. Note the similar relationship to **A.**

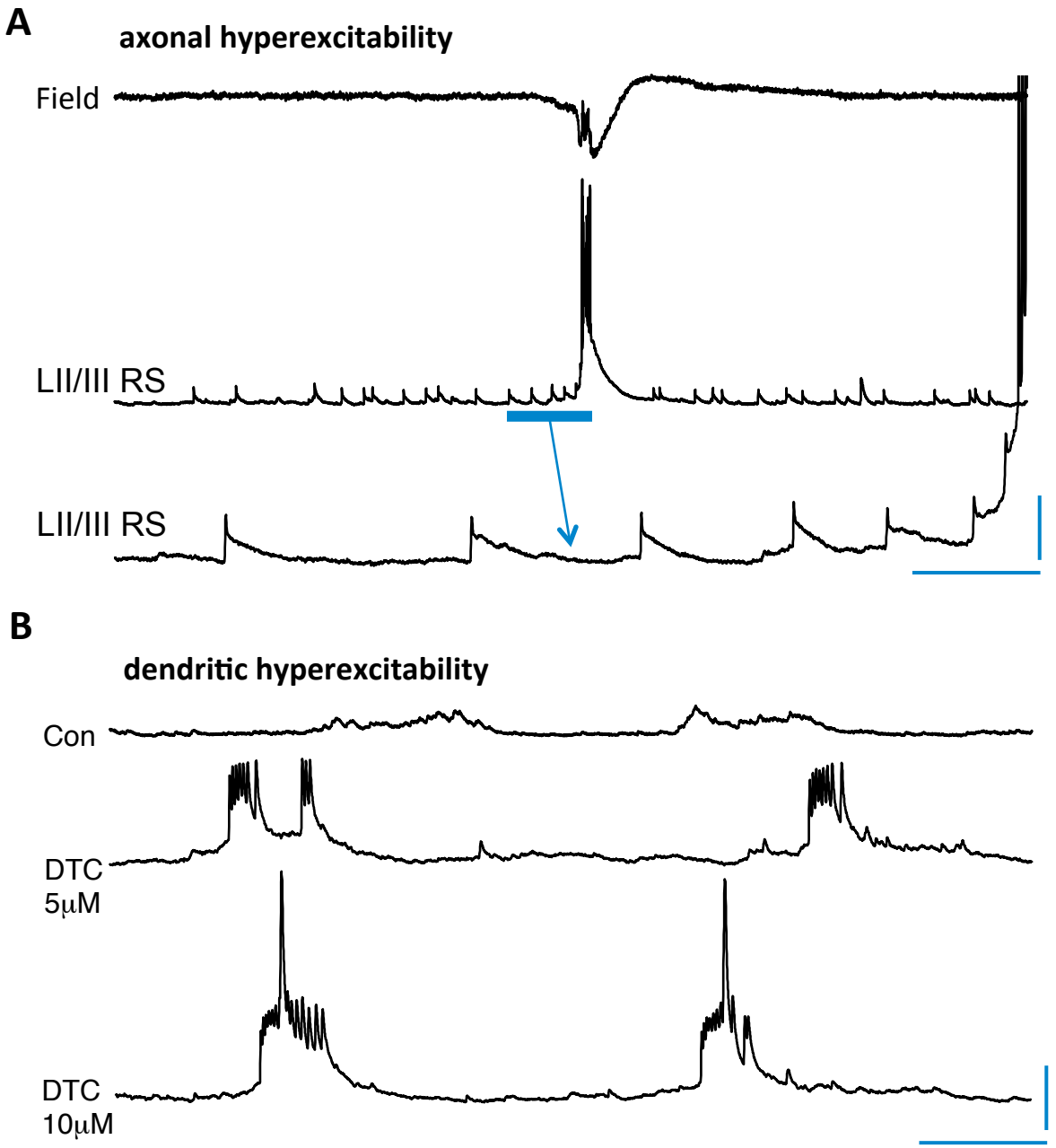

Figure 6.8: **Evidence for non synaptic excitability changes in layer II/III RS neurons associated with spike generation in spike and wave discharges. A.** Example of a single spike and wave complex recorded as layer V field potential concurrently with intracellular recording from a layer II/III RS neuron at resting membrane potential. Note the occurrence of spikelets which increase in frequency prior to the EPSP/action potential burst associated with the field spike (expanded section in the lower trace). Scale bars 1s (upper trace), 50ms (expanded, lower trace), 0.5mV (field), 15mV (intracellular trace), 5mV (expanded trace). **B.** Recording from a putative apical dendrite in upper layer II. Example traces are shown during the control state (delta only, two consecutive periods shown) and with increasing concentrations of DTC. Note that only compound EPSPs are seen in control conditions, but these transform into simple and then complex spike bursts. Scale bars 200ms, 10mV.

Figure 6.9: **Evidence for disrupted plastic changes in excitatory inputs to layer II/III RS cells.** Concurrently recorded layer V field potential and layer II/III RS neuron intracellular data are illustrated before, during and after a spontaneous transition from delta activity to spike and wave complexes in the presence of 5μM DTC. Blue bar represents 60s of data during the spike and wave complex behaviour. Note the absent layer II/III cell EPSPs following SWC discharges despite the continued presence of delta in layer V (asterisks). Also note the slow increase in EPSP amplitude following termination of the SWC epoch. Scale bars 3sec, 0.5mV (field), 15mV (intracellular).

6.3.5 Further Evidence for selective superficial layer recruitment during SWC from electrode arrays

A small number (n=5) of slices were placed under Utah micro electrode arrays to determine a more detailed map of layer specificity with SWC and WD. Unfortunately the majority of these slices failed to yield delta rhythms to allow fro baseline comparison (perhaps owing to the severity of so many concurrent electrode placements). However, recordings showing WDs and those showing SWCs could be spatially reconstructed from local field potential and unit activity recorded.

Figure 6.10 shows a typical wave discharge in the presence of 5μM DTC. Of 14 channels showing spontaneous activity, 13 of these demonstrated an overt, transient increase in spike rate corresponding to the WD. Increased spike rates were seen across all layers in the cortex simultaneously with maxima in layer II and layer IV-VI. The profile of the spike rate changes with time appeared to wax and wane in all active layers simultaneously (Figure 6.10a-e). In contrast, during an SWC in neocortex, spike rates increased first in deep layers, then peak activity switched to superficial layers (Figure 6.11a-e). In addition, overall spike rates were much higher with SWC than with WD, though insufficient replicates were taken to quantify this.

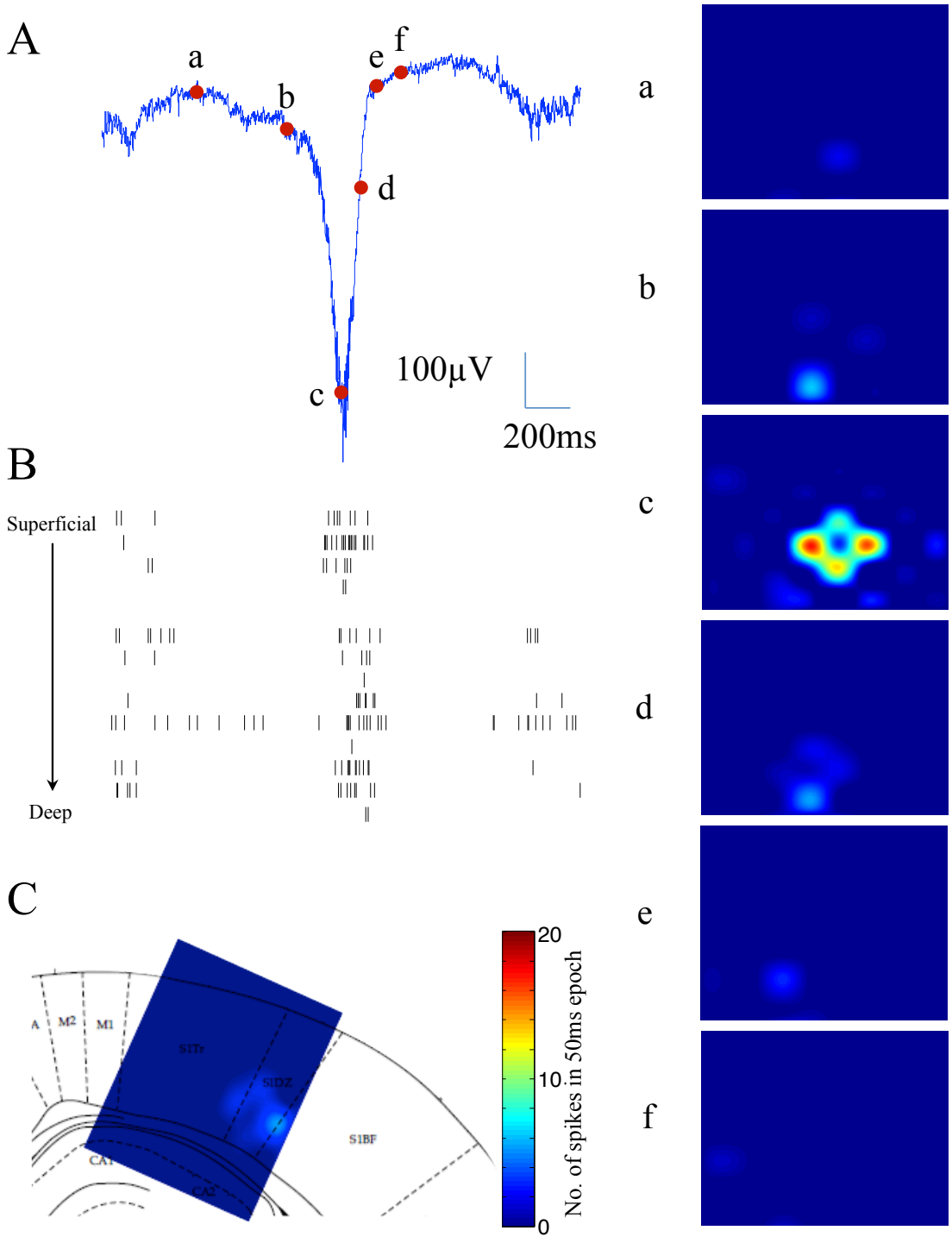

Figure 6.10: **The spatiotemporal progression of unit activity during a DTC induced wave discharge. A.** A 2 second epoch of a typical wave discharge following the application of DTC [5μM] in the somatosensory cortex. The spatiotemporal maps labeled a - e correspond with the points marked on the WD. Each spatiotemporal map displays the spike intensity during a 50ms window of activity. **B.** Spike timing of units which correspond to the WD in A. **C.** Displays the approximate location of the 96 channel electrode array in the somatosensory cortex, shows activity map 'd' displaying activity in the deep layers of the cortex.

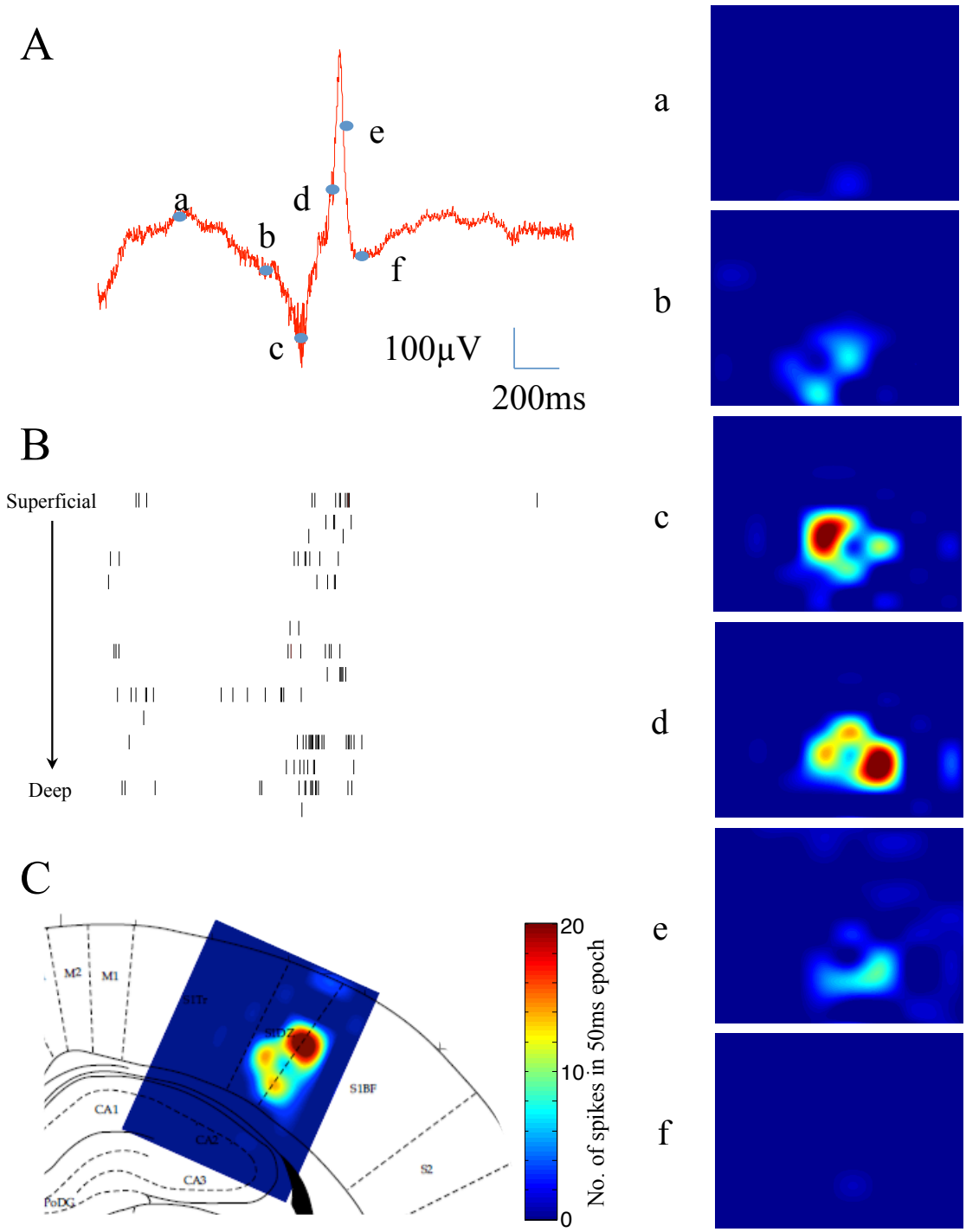

Figure 6.11: **The spatiotemporal progression of unit activity during a DTC induced spike-wave complex. A.** A 2 second epoch of a typical spike-wave complex following the application of DTC [10μM] in the somatosensory cortex. The spatiotemporal maps labeled a - e correspond with the points marked on the SWC. Each spatiotemporal map displays the spike intensity during a 50ms window of activity. **B.** Spike timing of units which correspond to the SWC in A. **C.** Displays the approximate location of the 96 channel electrode array in the somatosensory cortex, shows activity map 'd' displaying activity in the deep layers of the cortex.

6.4 Discussion

The data presented in this chapter tentatively suggests that spike and wave discharges represent the interplay between excessive deep layer cortical excitability (the 'wave' component of the SWC) and excessive excitation in superficial layers (the 'spike' component of the SWC). Interplay between these deep and superficial layers has been proposed to represent a substrate for unsupervised learning in neocortex during sleep [Carracedo et al., 2013]. DTC appears to 'hijack' the subtle interplay between delta and theta rhythms shown in this work, transforming infrequent single spiking in superficial layers into overt burst discharges. The difference between WDs and SWCs quantified in previous chapters in this thesis may therefore represent the ability of the model to increase excitation in either deep, or in both deep and superficial layers respectively.

Transforming infrequent single spikes into burst discharges would be expected to have profound effects on synaptic plasticity. The interplay between single spike and spike-burst discharges has been shown to be critical for network homeostasis [Buzsáki et al., 2002]. Transition from single spiking to burst discharges changes the entire landscape of spike timing dependent synaptic plasticity, with timing dependant generation of both potentiation and depression largely disrupted (e.g. [Queiroz and Mello, 2007, Harvey-Girard et al., 2010]). Both of these reported effects would be expected to disrupt the 'synaptic rescaling' associated with memory consolidation during sleep. The preliminary data presented in this chapter suggest both processes may be occurring: A short term decrease in EPSPs onto Layer II/III pyramidal cells was directly associated with SWC generation, and a longer term potentiation of these inputs followed by runs of SWCs. It is therefore not surprising that the delicate balance of network function required for synaptic rescaling may be disrupted in patients with deep sleep-associated spike and wave discharges, with a consequent disruption in cognitive performance.

What is not clear, however, from the work presented here is what the locus of the changes in inputs to superficial layer neurons may be. Nor is it clear, as of yet, which synaptic pathways are important for sleep-associated rescaling. For example, is the interlaminar pathway more important? Or is it equally as important as the intralaminar pathway in superficial layers? Further work is required to resolve this issue but sufficient data were gathered here to at least attempt to suggest a mechanism for the enhanced excitation to pyramidal cells leading to SWC generation.

The timing of the enlarged EPSPs observed in superficial pyramidal cell somata suggested that they were, at least in part, generated by enhanced outputs of deep layer RS

cells. The timing of burst generation in these deep layer neurons would predict enhanced inputs in superficial layer neurons early and/or late in the wave discharge, but not in the middle. This was the pattern observed (Figure 6.6). However, changes in intrinsic excitability may also have a role to play. Tentative evidence for an increase in axonal excitability, leading to partially back propagated action potential (spikelets) was seen in superficial pyramidal cells in the presence of DTC but not during the delta rhythms seen during the control state. Nicotinic receptors are present on axons and may directly affect axonal excitability [Lin et al., 2010]. Similarly, the intrinsic excitability of dendrites of these cells may contribute to the excessive response to excitatory input. Dendrites receiving large excitatory synaptic inputs can generate a range of electrogenic phenomena, often called 'compound spikes' [Andreasen and Lambert, 1995]. While there is little data of relevance collected here that does not allow for a separation of intrinsic and synaptic processes on dendrites, it is interesting to suggest that enhanced dendritic electrogenesis may play a role in the hyperexcitability leading to the spike component of the SWC. But how might this occur?

In terms of direct excitatory effects on dendrites, nicotinic receptor activation has been shown to enhance calcium spikes and electrogenesis in dendrites [Szabo et al., 2008]. These findings would suggest that reduced nicotinic receptor tone (as expected in the presence of DTC) would reduce dendritic excitability. But the opposite was seen in the present work. However, presynaptic nicotinic receptors, and nicotinic terminals adjacent to dendritic inhibitory terminals also have a profound effect on phasic and tonic GABA release. Phasic GABA release is potentiated by presynaptic nicotinic receptor activation via T-type calcium channels [Tang et al., 2011]. Similarly, tonic GABA release is facilitated by nicotinic terminals on Layer V pyramidal cells [Aracri et al., 2010]. This latter observation may be directly relevant to the enhanced excitability of deep layer neurons leading wave discharges seen with DTC. In addition, the dominant (in terms of number) inhibitory neuronal population in superficial cortical layers are neuropeptide Y-expressing, dendrite targeting cells arising from the central ganglionic eminence [Lee et al., 2010b]. These interneurons express both 5-HT_3 and nACh receptors and both are strongly excitatory. As DTC blocks both these receptors, it is interesting to suggest that, at least, the superficial layer hyperexcitability associated with SWCs may be primarily mediated by a lack of appropriate excitatory tone in this inhibitory interneuron subtype. This, in turn leading to disinhibition, spike generation and disruption of the interplay between deep and superficial layers which has been suggested to be important for sleep-associated synaptic plastic changes.

To investigate the spatiotemporal properties of cortical networks during sleep and its

pathologies, the use of arrays of extracellular electrodes proved reasonably useful in the work presented in this chapter. However, as mentioned in section 6.1, this approach is limited by uncertainty about what mechanisms underlie the dynamics and any changes in them. If it were possible to combine the advantages of multichannel, simultaneous recording with the detail afforded by intracellular recording, a much richer, more informative picture would emerge. The following chapter of the thesis details attempts to provide a device to address this need.

Chapter 7

Fabrication and Design of Intracellular Electrode Array

7.1 Introduction

The research detailed in the preceding chapters has highlighted limitations in understanding the local communications between neurons within a particular region of a tissue slice. As has been shown, monitoring cells and networks can be achieved with a variety of methods. The main methods being: extracellular recordings of local field potentials and unit activity; intracellular recordings of single cells; and patch clamping of ion channels of single cells, all of which, bar the latter, have been utilised in the compilation of this thesis. However, it is not currently possible to record from multiple single cells simultaneously without using many single glass pipette electrodes, which can become cumbersome and manipulation of multiple pipette electrodes is time consuming and doesn't produce a high yield for the time dedicated to the task. Detailed below is a brief introduction to the theory of cellular recordings, as well as some of the current methods used within electrophysiology, which have been utilised during this research.

7.1.1 Principles of Cellular Recording

Several types of electrodes are used for electrophysiological recording, but before being able to discuss the types of electrodes used, it is firstly necessary to explain what is being recorded and why. Communication between neurons is at the core of how the brain operates and understanding the signalling is vital to understanding the complexities of how the brain functions. Therefore to be able to understand cellular recording, a basic knowledge of the electrical properties of cells and their connections is necessary.

Neurons are electrically excitable cells that process and transmit information via elec-

trical and chemical signalling. They consist of a cell body, nucleus, dendrites and an axon which are all surrounded by a thin fatty lipid layer forming the cell membrane (figure 7.1). Inputs from other neurons are delivered from the axon via chemicals known as neurotransmitters diffusing across the synapse from one or more presynaptic neurons as is shown in the inset in Figure 7.1. There are many different neurotransmitters, many of which have been detailed in Section 1.2.1, which can either instigate or modify an electrical response within that particular system.

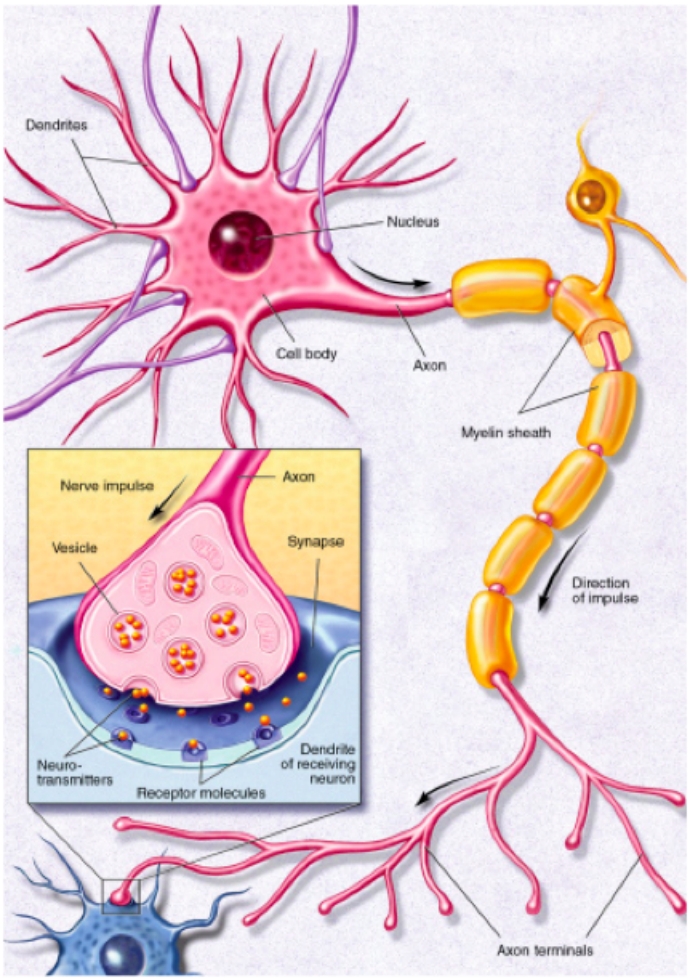

Figure 7.1: The neuron is comprised of a cell body, nucleus, dendrites and an axon. The dendrites and the cell body receive input signals across synapses and the cell's response then propagates down the axon on to other neurons synapses at the terminal. The inset shows a more detailed diagram of how the neurotransmitters are released into the synapse and how they are received by the next neuron in the signal flow. *Taken from [Carey and McCoy, 2006]*

The arrival of the electrical impulse causes a dramatic reversal of the membrane potential at one point on the cell's membrane resulting in an action potential. The action potential

causes a depolarisation in the membrane potential as it passes down the membrane, causing voltage gated sodium channels to open allowing Na^+ ions to flow into the cell. The sodium channels close while potassium channels open and K^+ ions flow out of the cell into the extracellular fluid causing the cell to hyperpolarise. The cell is then stabilised by the Na^+/K^+ pump which allows the cell to return to resting potential. The action potential travels along the membrane and down the axon where the electrical impulse causes the release of more neurotransmitters to diffuse across another synapse to the next neuron. Axons vary in length from a tiny fraction of a inch to more than three feet long in some cases [Carey and McCoy, 2006], allowing signals to be sent to different regions of the brain and CNS. These axons are covered in an insulated myelin sheath made up of oligodendrocytes (in the brain) or Schwann cells (in the Peripheral Nervous System (PNS)), which speeds up the transmission of the signals, sometimes reaching up hundred metres per second [Carey and McCoy, 2006].

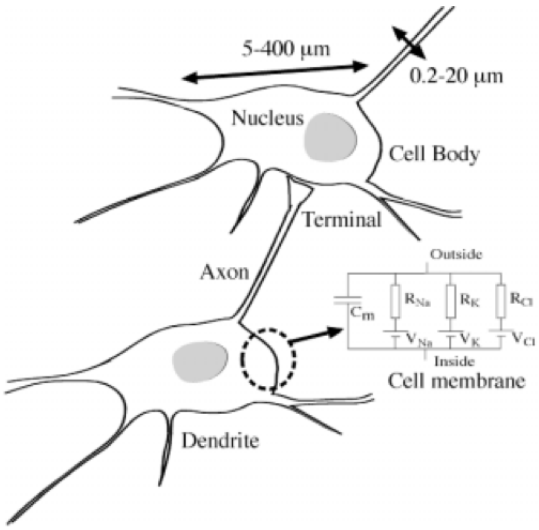

Figure 7.2: The cell membrane is a thin fatty layer that electrically separates the interior and exterior walls of the cell body. Hence, it can be modelled as a capacitor with additional voltage sources and resistors representing the many ion channels in the membrane. The equivalent circuit of the membrane based on the Hodgkin-Huxley approach can be seen above. *Taken from [Hanein et al., 2002].*

7.1.2 Cellular recording methods

Electrodes are used by neuroscientists to observe, measure and record how neurons work individually and as a network. Two methods are used: the intracellular method can be used to record postsynaptic potentials, both inhibitory and excitatory, and action potentials; and the extracellular method can be used to record local field potentials from

the extracellular fluid. As previously stated, the current methods utilised in electrophysiology are detailed below, the majority of which were employed in the research for this thesis.

Patch Clamp Electrodes

Neher and Sakmann developed the patch-clamp method during the late 1970s as an advancement of the voltage clamp technique. This resulted in an increase in the knowledge of fundamental cell processes, resulting in Neher and Sakmann receiving the Nobel Prize in Physiology or Medicine in 1991.

Patch-clamp uses a pulled pipette with a finely polished end with a diameter of approximately 1μm, which is large enough to encompass a region of the cell membrane containing several ion channels. The electrode can be gently attached to the cell membrane, and by applying negative pressure through the electrode, a piece of the membrane is sucked into the electrode as shown in figure 7.3. This is also known as the 'Patch'. This results in the section of the cell being electrically and mechanically isolated from the extracellular fluid due to the high resistance of the seal (in excess of a giga Ohm). By applying a short low pressure pulse through the electrode, the 'patch' can be punctured resulting in a direct connection between the electrolytic fluid in electrode and the inside of the cell [Buzsaki, 2006]. Current waveforms can be applied to the electrode to allow some of the intracellular fluid to flow up into the electrode which allows for information to be learnt about the cell.

There are several variations of Patch Clamp recordings: Whole cell recordings, where the electrode remains sealed to the whole cell during the recording process; Outside-out patch, where the electrode is slowly pulled away from the membrane allowing a bulb of membrane to bleb out of from the cell. When detached from the membrane, the bleb reforms inside out so that the original outside of the membrane is now facing the electrode. This method is useful when the experimenter wished to manipulate the extracellular surface of the isolated ion channels; Inside-out patch, is similar to the outside-out patch, but where the original outer of the membrane is facing the electrode, instead it is the inner membrane facing the electrode. This method is useful when the experimenter wishes to manipulate the environment at the intracellular surface of the ion channels.

One problem with whole cell recordings, the electrolytric fluid in the electrode will slowly diffuse into the intracellular fluid causing the cell to become 'dialyzed'. Thus changing the internal environment of the cellular structure. Therefore, recording should only be taken during the first 10 minutes to achieve successful recordings before the cell is dia-

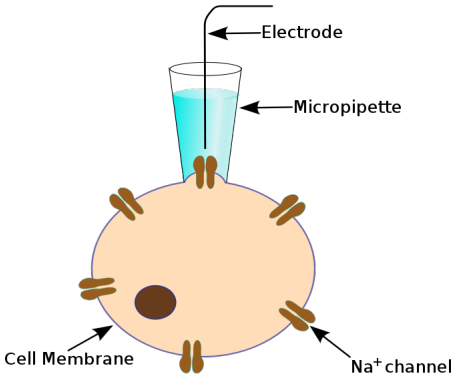

Figure 7.3: Patch-Clamp electrode attached to the cell membrane to enable recording from the inside of the cell.

lyzed. This method of cellular recording was not used during the research for this thesis as the facilities were not available and to allow for a comparison between previous work by Carracedo (2010) and others, this method was deemed redundant.

Extracellular Electrodes

Despite the fact that recordings had been made from many locations in the brain since 1875 by Richard Caton [Finger, 1994], extracellular microelectrodes were only readily available from the 1950s. At this time, Vernon Mountcastle and his colleagues were developing techniques for recording from the cerebral cortex at the cellular level [Kandel et al., 2000]. Extracellular electrodes can record two types of responses: Unit recordings; and Local Field Potentials. When electrodes are placed near cells it is possible to record action potentials - single unit recordings - at the millisecond temporal resolution that they occur [Montgomery, 2002]. Although this method can be informative of how a neuron responds to stimulation either electrically or pharmocologically, it is not able to show the synaptic activity of the cell, excitatory post-synaptic potentials (EPSPs) or inhibitory post-synaptic potentials (IPSPs) except under specific conditions. Whereas, if the electrode is placed in the extracellular space, the electrode can record the summation of all the dendritic synaptic responses in the local field, hence a local field potential recording. This type of recording, as seen in chapters 4 and 5, offers the ability to understand the combined synaptic inputs into the cell population [Montgomery, 2002]. Importantly for this research, the summation of dendritic responses leads to an oscillating signal which can be monitored and manipulated through the application of specific chemicals depending upon the frequency of the oscillation.

Extracellular electrodes are typically constructed from one of three types of electrodes: Metal electrodes, glass micropipette electrodes, and solid-state microprobes as shown in figure 7.4.

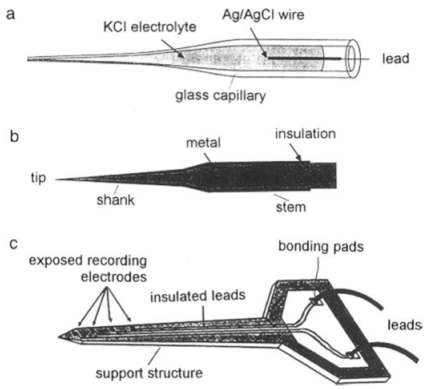

Figure 7.4: Biopotential electrodes: a) glass micropipette electrode; b) insulated metal electrode; and c) solid-state multisite recording microprobe. *Taken from [Enderle et al., 2000]*

Metal Electrodes

Metal electrodes are one of the simplest methods of recording from the cortex is the use of insulated wires with small tip diameters that have been stripped of the insulator, as shown in figure 7.4b). This is also one of the oldest techniques used for recording from many cells. Strumwasser (1958) implanted several 80μm tipped stainless-steel microwire electrodes into the brain of a live ground squirrel and successfully recorded firing neurons . Microwires are frequently used in *in vivo* studies due to it's flexibility compared with both glass electrodes and solid-state electrodes. Microwire electrodes are also easily arranged into arrays to allow for multiple recordings from one localized site. These microwires are usually produced from either tungsten or platinum, and have an insulative layer of polyimide.

Glass micropipette electrodes

Glass micropipette electrodes are typically made from borosilicate glass capillary tubes that have been heated to near melting point at the middle within a small filament and pulled sharply by a Flaming/Brown micropipette puller. This process creates two similar capillary electrodes with an open tip that has diameter of 1-10μm, which typically have a resistance of 2-5MΩ. The larger end of the electrode is then filled with an electrolyte, which is biologically compatible with the tissue sample, usually artificial cerebrospinal fluid (ACSF)(see chapter 2. Bare Ag/AgCl wire is inserted through the larger end of the electrode to provide an electrical connection with the electrolytic solution. One limiting factor of extracellular electrodes is the reproducibility, as the exact dimensions of the tapered end of the electrode cannot be strictly controlled, although variations can be made to the 'pulling' program to modify the tip dimensions. Glass capillary electrodes are also very fragile, hence they can only be used once and this also impacts reproducibility.

Extracellular Solid State Electrodes

Michigan Array

Since 1970, when Wise *et al* first designed the silicon multi-electrode array, numerous studies have been undertaken to improve upon and modify the original design. These planar multi-electrode arrays are more commonly known as Michigan Arrays. These arrays are composed of planar probes with multiple recording sites located along the shank of each structure. Hence these probes provide a greater recording density whilst minimising tissue damage compared to microwire arrays.

A typical design consists of one to four probes with four recording sites with the thickness of the probes aiming to be 25μm but is dependent on SOI wafer specification. The length of the probe is typically 3mm with the distance between the probes being 200μm [Chen et al., 2009]. The process for michigan array fabrication is shown in detail in figure 7.5 below.

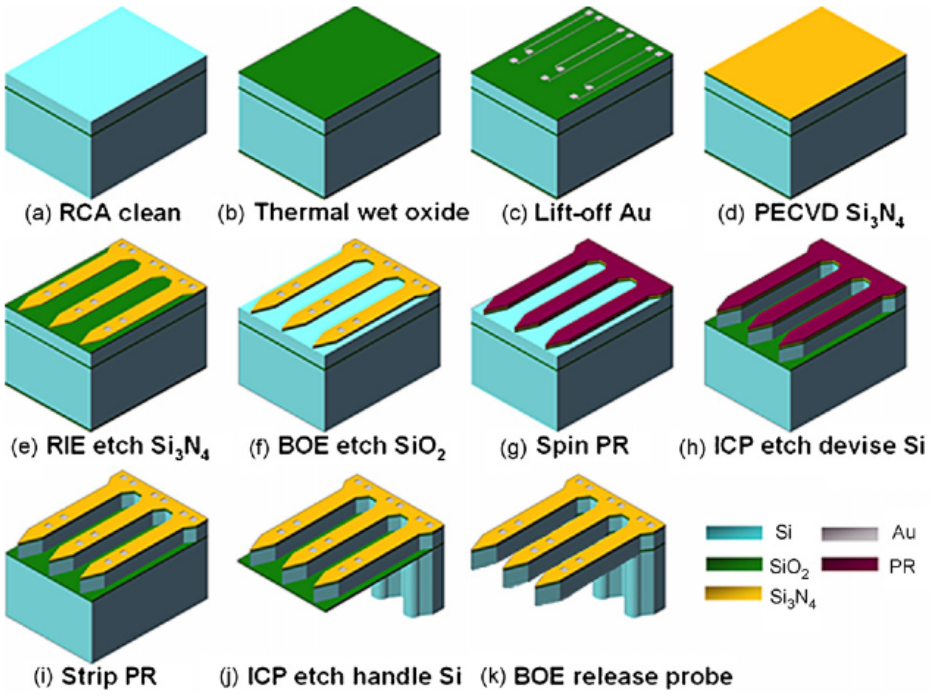

Figure 7.5: Fabrication process for michigan array probes. *Taken from [Chen et al., 2009]*

Michigan Arrays are usually used as an *in vivo* recording device [Kipke et al., 2003, Chen et al., 2009, Csicsvari et al., 2003, Bai et al., 2000, Cheung et al., 2007, Anderson, 2008] as they are able to easily penetrate tissue without doing excessive residual damage and

also their ability to record from multiple sites in the same plane, enabling the tracking of neural signals. Michigan Arrays are not typically used for *in vitro* recordings due to the size of the probes compared to the size and thickness of the brain slice ($\sim$450μm). Brain slices would also not to able to 'sit' on the probes as when the brain is cut into slices, many neuronal connections are severed. This results in the first 100μm of tissue not being a viable recording site.

sim

The Utah Electrode Array

The Utah Electrode Array (UEA), which was briefly described in chapter 6. is a three-dimensional electrode array consisting of 100 needle-like conductive electrodes approximately 1.5mm in length, where each electrode is electrically isolated from it's neighbours. The sharpened tip of each electrode is coated in platinum to facilitate charge transfer [Campbell et al., 1991] and then coated with polyimide for electrical isolation, excluding the tip. These arrays are fabricated from a thick n-type silicon wafer, through which highly conductive p^+ trails are created via thermomigration resulting in electrical isolation by opposing pn junctions. The wafers are then micro-machined to expose the pillars of p^+ trails, followed by a spun acid etch to produce the needle-like tips (Figure 7.6). The electrical contacts to the electrodes are made from the reverse side using gold wire bonded to aluminium contact pads.
These arrays have had many uses over the last decade, since they were first fabricated and published by Campbell *et al* in 1990 [Campbell et al., 1990]. They have been used *in vivo* in the cat somatosensory cortex [Rousche and Normann, 1998], visual cortex [Normann et al., 1999], the dorsal root ganglion [Aoyagi et al., 2002] and electrophysiological *in vitro* studies in the neocortex, including those detailed in this thesis.

As described in Chapter 6, when utilised during experiments, the UEA was able to record a magnitude of data, including both local field potentials and unit recordings from the same electrodes which allows for correlation and spatial analysis. These are of particular interest when investigating the relationship between cellular layers, as was the aim of Chapter 6.

Intracellular Electrodes

Microelectrodes have been used greatly over the last 60 years or so in the field of electrophysiology to aid in the understanding of many electrochemical biological processes. For example, in 1951 Brock, Coombs and Eccles succeeded in the first intracellular recordings from nerve cells in the CNS with the use of microelectrodes [Eccles, 1953]. These were

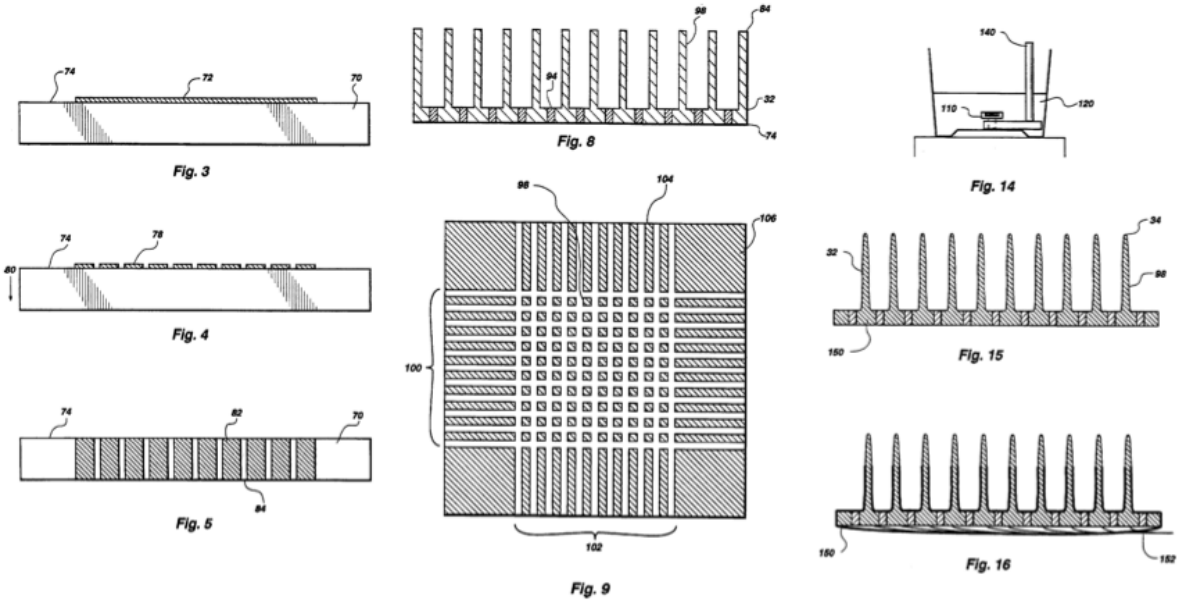

Figure 7.6: A simplified process flow for the fabrication of a UEA.
(left) Aluminium pads are created on one side of an n-type silicon wafer. During the process a temperature gradient is applied to the silicon wafer which drives Si-Al eutectic droplets through the wafer. After the process, highly doped p^+ silicon trails result from the eutectic droplet passage through the n-type substrate [Campbell et al., 1991].
(centre) A dicing saw is used to micro-machine the high-aspect ratio columns from the p^+ trails in the n-type silicon by creating deep orthogonal cuts.
(right) Array is then slowly spun in acid etchant to smooth and sharpen the columns. The needle-like tips are then pushed through a metal foil layer and sputtered with a thin layer of Pt/Au. (Figures taken from US Patent 5,215,088 [Normann et al., 1993]).

able to record the electrical responses seen during excitatory and inhibitory postsynaptic potentials.

Today in electrophysiological studies, the most common method of recording intracellular potentials is via a sharp glass capillary electrode filled with Potassium Acetate (CH_3CO_2K). Potassium acetate is the electrolytic fluid used as potassium is the chief cation of intracellular fluid, therefore allowing effective signal propagation. This signal is then detected by the Ag/AgCl wire immersed in the electrode where the signal crosses the electrolyte/metal interface. The signal is then fed into data acquisition and analysis software where it is recorded.

Intracellular recording methods are rather limited as only one or two electrodes can be recorded from simultaneously when using capillary electrodes, as previously stated. Therefore a way to record from multiple cells simultaneously would be to employ a similar device as the UEA, albeit on a much smaller scale. This would not be possible using capillary electrodes, although it may be possible using solid state electrodes.

Intracellular Solid State Electrodes

In the past, it would have been difficult to fabricate large solid structures with features of less than 1μm. In 2001, Hanein *et al* designed and fabricated one of the first individual intracellular solid state electrodes. The method was based on the UEA fabrication method, pillars were diced into a silicon wafer, and sharpened with SF_6 via RIE fabricating needle-like electrodes approximately 250μm in height and with sub-micron tips. A sea slug brain was used to test the viability of the electrode due to the large size of the brain cells ($\sim$400μm in diameter) and the comparative size of the electrode tip. The electrodes were successful in recording action potentials, albeit small signals (10mV instead of $\sim$100mV) from *Tritonia diomedea*.
Hanein *et al* have since improved the fabrication method [Hanein et al., 2003]. This other method used sacrificial satellite pillars to improve protection of the central pillar from unwanted SF_6 etching during the self-sharpening process. This method resulted in needle-like electrodes, 230μm in height and with a 200nm tip diameter. The efficacy of this method with regards to intracellular measured voltage potentials is unknown as no electrophysiological results were published.

7.1.3 Aims and Objectives

Thus, the aim of this chapter is to investigate the possible methods for producing an array of electrically active, isolated, solid state intracellular electrodes. This will begin with the design and fabrication of a single electrode to understand what is required to achieve the necessary dimensions and to understand the mechanical properties required. This preliminary research will also influence the design of the subsequent, electrically active single electrode or array of electrodes.

7.2 Efficacy of Mechanical Properties

7.2.1 Design Specifications

Before a design can be drawn or a process flow be discerned, the required dimensions of the desired intracellular solid state electrode first need to be understood.

Tip dimensions

Pyramidal cells are prevalent in the cortex and are the largest neuron in both the human and rodent brain, with the soma averaging approximately 20μm in diameter. The cell membrane is typically less than 10nm in thickness, hence the thickness of the membrane does not affect the electrode tip design, however the lipid structure of the membrane does (i.e. the elasticity, see figure 7.7). The glass capillary electrodes which have been traditionally used for intracellular recordings have a tip diameter ranging from 0.06-0.7μm (60-700nm). Based on this information, the diameter of the electrode tip would have to be less than 200nm, ideally less than 100nm. This would be to ensure that when the cell membrane was pierced, it would close around the tip as would happen during a successful impalement by a glass capillary electrode.

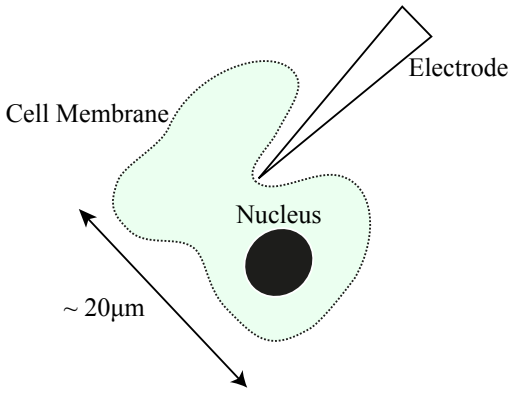

Figure 7.7: Schematic diagram depicting the bending of the cell membrane during penetration of a sharp electrode. The electrode cannot penetrate the lipid layer that forms the cell membrane if the tip of the electrode is too dull, or too short to compensate for the bending of the membrane. Adapted from [Hanein et al., 2001].

Electrode shaft dimensions

When preparing the rodent brain slices as detailed in chapter 2, the first 50μm of the top and bottom surfaces of the slice are abundant with broken connections between neurons. This needed to be taken into account when considering the required electrode length as to make sure the electrode tip would have the range to penetrate through this layer. The dimensions of the electrically active tip would also have to be considered, as to ensure that the electrode would only be recording from inside the cell and not from the extracellular fluid simultaneously.

The typical slice thickness used in the electrophysiology labs is 140μm. Therefore to be able to penetrate the majority of the slice (ignoring the bottom 50μm), the electrode shaft length had to be greater than 90μm in height. To allow for ease of manipulation (i.e. to be detectable by the human eye), the electrode shaft length would ideally need to be greater than 500μm. Several limitations meant that this shaft length would not be achievable with the facilities or materials available, therefore a modest target of 300μm was the desired length of the electrode shaft during these trials.

As described previously, the desired tip dimensions are known, however the base diameter of the shaft required to achieve this tip dimension is not. The diameter of the base would have to be larger enough that it would withstand the etching process and also retain it's structural integrity when inserted into the brain slice, particularly if this was not conducted perpendicular to the slice surface. Therefore the electrode base diameter would have to be investigated to understand the optimal dimension for the desired tip and shaft dimensions.

Substrate Biocompatibility

A further initial consideration was, which substrate the array would be fabricated from? Due to the nature of the end application, the substrate would need to be biocompatible. When developing a cell based biosensor, the biocompatibility of the materials used is fundamental to the project. Biocompatibility is a fairly ambiguous term as it reflects the ongoing development and insights into how materials interact with the human body and therefore determines whether a medical device will be a clinical success [Mahmoodi and Ghazanfari, 2011]. In the case of this project, during the mechanical efficacy phase, the level of biocompatibility of the material was not considered to be of high importance, provided that biocompatibility was enough that the substrate could be in contact with living tissue for several hours without causing adverse damage. Several semi-conductor substrates were considered including: Silicon, Silicon Carbide and Diamond.

Diamond, although having immense biocompatibility characteristics [Freitas Jr, 1999], the dimensions needed to create a successful electrode would not be achievable through the application of etch chemistry via the use of a reaction ion etching (RIE) machine. Previous studies have shown that using a mixture of CF_4 and O_2 plasmas can produced a perpendicular etch rate of 50nm/min [Leech et al., 2001]. For the purpose of understanding the efficacy of the mechanical properties of a needle-like intracellular electrode, the use of the substrate would be costly, in terms of time, money and resources.

Silicon Carbide (SiC) is a wide-band gap semiconductor which has many applications, including use in high frequency, high power, high voltage and high temperature devices [Wright and Horsfall, 2007]. It is also known to be biocompatible in it's single-crystal cubic form and as a coating deposited by chemical vapour deposition (CVD) [Kotzar et al., 2002, Frewin et al., 2011]. With the utilisation of microelectromechanical systems (MEMS) machining methods, large aspect ratios have been achieved with SiC. Tanaka *et al* (2001) reported an etch depth of approximately 120μm with 5 hours of etch time, however this was achieved by ICP and not RIE alone, which is one of the limiting factors for this project. Therefore it was decided that SiC would also be too time intensive due to the lack of an inductively coupled plasma (ICP) machine being available.

Silicon has been employed by many research groups over the past several years in the biomedical field due to the extensive knowledge of fabrication methods available. Of particular interest to this work, silicon has the ability to be mass produced to produce neural electrodes with high accuracy and reproducibility [Ji et al., 1989, Olsson III et al., 2005, Muthuswamy et al., 2005]. This therefore shows that the efficacy and biocompatibility of this substrate as a sensor for biomedical purposes has already been proved. Not all silicon has the same properties. The level of electrical conductance a substrate has depends on the 'doping' level. For example the substrate used in this mechanical efficacy study has a doping level of $N_D = 10^{14}\text{cm}^{-3}$. Reading off Figure 7.8, the resistivity of this N type substrate is 40Ωcm. Using Equation 7.1, the conductance of the silicon substrate is 25mS.

$$\sigma = \frac{1}{\rho} = q(\mu_n n + \mu_p p) \tag{7.1}$$

Where σ is the conductivity, ρ the materials resistivity, μ_n and μ_p the minority carrier mobilities and n and p the carrier concentrations.

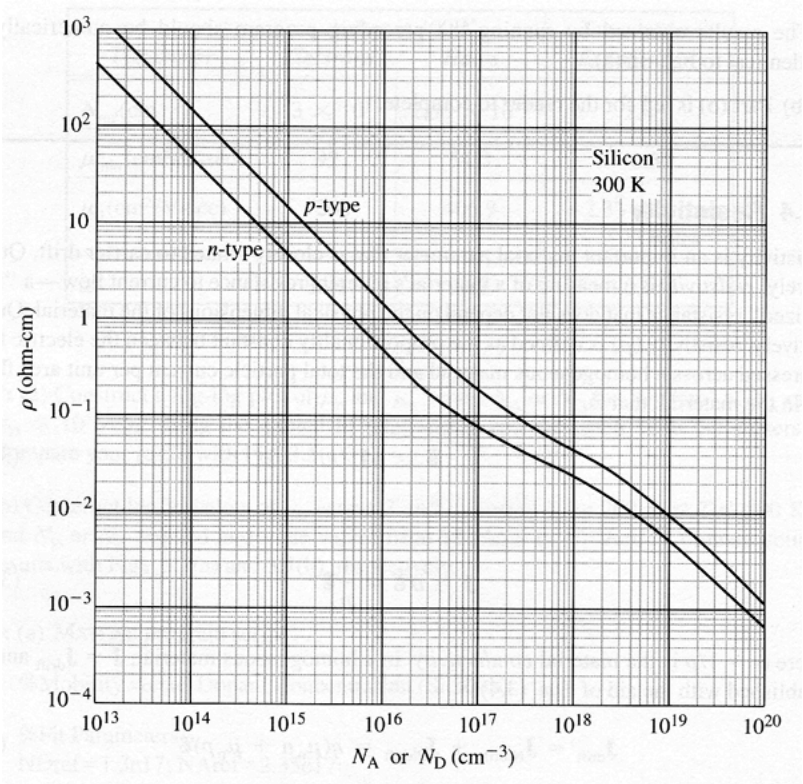

Figure 7.8: Resistivity versus carrier concentration for silicon at 300K [Beadle et al., 1985]. Increasing the carrier concentration would result in a more conductive substrate.

For the purpose of a mechanical study, an electrically conductive substrate is not necessary as it would increase both resource and machining costs. Hence a lowly doped silicon substrate will be used.

Manipulation

To be able to appropriately test the electrodes produced during the mechanical study, the backplate would need to be attached to an object which would allow for greater control and manipulation of an electrode of less than 500μm in height. The experimental results achieved using an utah electrode array detailed in chapter 6, were possible partly due to the manipulation setup. The array was attached to a rod (8mm in diameter and 150mm in length) using either araldite or epoxy, hence allowing greater ease during array placement. A similar method of manipulation would be ideal for the electrodes produced within this research, although due to the size of the backplate, a rod with a smaller diameter would be needed.

7.2.2 Process Design

It is known that during a deep reactive ion etching (DRIE) process, the sidewall angle depends on the mask geometry and loading effects. Single free stranding pillars tend to develop a more negative profile, hence the use of the sacrificial satellite pillars surrounding the central pillar, as used by [Hanein et al., 2003]. However, due to the equipment and materials available, the configuration, dimensions and process flow needed to differ significantly from this previous work. Figure 7.9 shows a schematic of the layout of the sacrificial pillars with reference to the central pillar.

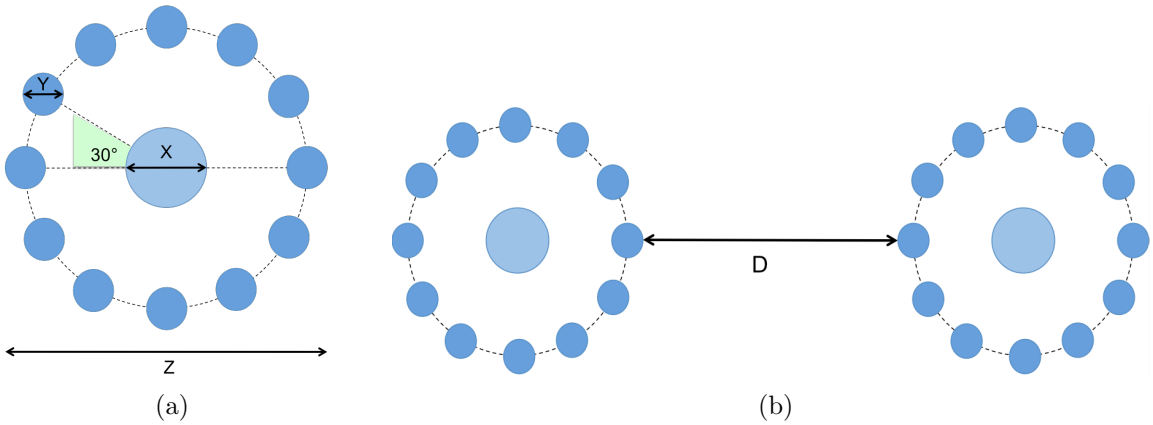

Figure 7.9: **Schematic of pillar configuration.** a) The central pillar measures 'x' in diameter, the satellite pillar measures 'y' in diameter and the outer diameter of the ring of satellite pillars is measure as 'z'. b) The spacing distance between 2 pillar arrangements measures as 'd'.

A photolithography mask was designed to investigate the optimal dimensions and spacing needed to create a mechanically viable electrode suitable for impaling a pyramidal cell. The mask design measurements Hanein *et al* (2003) used to fabricate their pillars (pre-sharpened electrodes) with respect to figure 7.9, were x=70μm, y=30μm, z=250μm and the diagonal distance between the central pillars was 400μm due to the hexagonal nature of the mask layout [Hanein et al., 2003]. The mask design related to this thesis contained a 3x3 repeating matrix, each individual cell consisted of a 6x6 array of central pillars with 12 sacrificial satellite pillars surround them (subcells). Each of the 9 cells had varying: central pillar dimeters (x, varying between 50 - 100μm), satellite pillar dimensions (y, varying between 20-50μm), outer diameter of the ring of sacrificial pillars (z, varying between 200-300μm). However, all 9 cells had the same distance between subcells (d, 300μm).

7.2.3 Fabrication

To fabricate spike electrodes, that were mechanically suitable for intracellular recording, <100> oriented lightly doped N-type (Phosphorus doped, $10^{14}cm^{-3}$) 6inch silicon wafers, approximately 650μm thick were used. The wafers were patterned using an SiO_2 mask, as photoresist was not been able to withstand the etching process (see figure 7.10a). The wafer was then placed in a DRIE to etch pillar approximately 350μm tall, the result is shown in figure 7.10b. The pillar fabrication was undertaken at the Scottish Microelectronics Centre (SMC), University of Edinburgh.

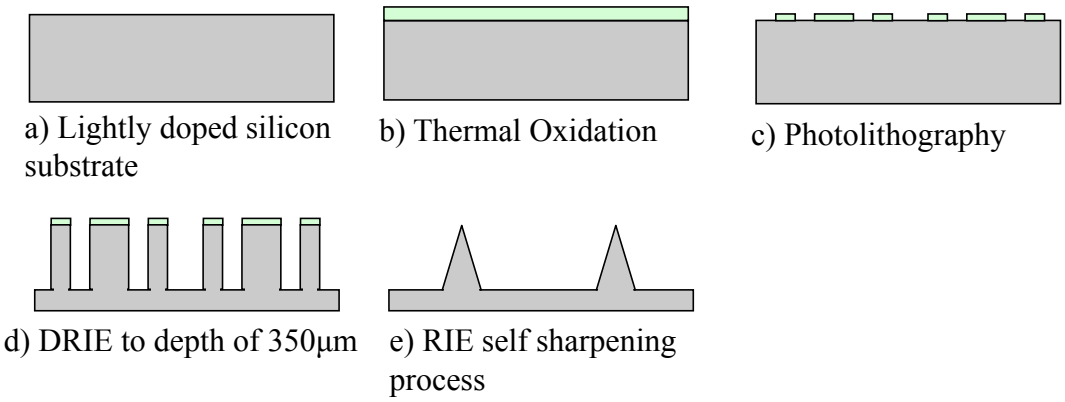

(a)

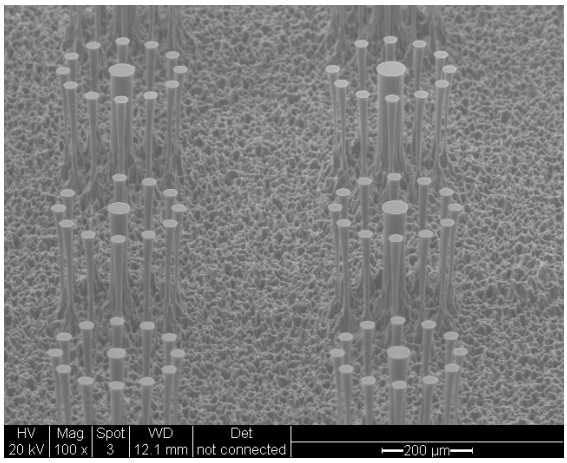

(b)

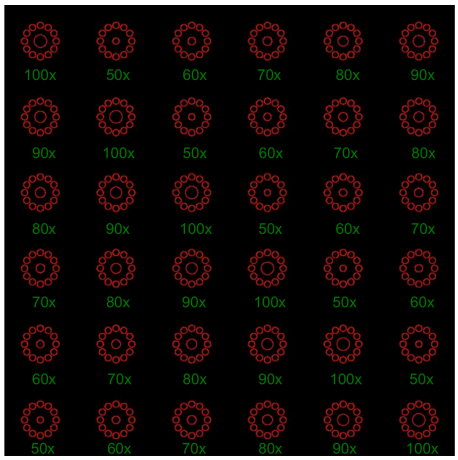

(c)

Figure 7.10: **Pillar Design** a) Process flow used to fabricate spike electrodes from a silicon substrate wafer b) SEM of DRIE etched central and sacrificial pillars. Tilt = 60°, Magnification = x100. c) Variation of x in μm in every cell. The other parameters of this particular schematic are a follows: y = 50μm and z = 300μm.

After the DRIE process, the wafers were cleaved and an array of 6x6 pillars, of varying dimensions, as shown in Figure 7.10c (random sized samples followed by ~5mm x 5mm samples), were placed in the reactive ion etcher (RIE) chamber (PlasmaTherm 790).

Using an optimised self-sharpening etch process using 80% sulphur hexafluoride (SF_6) and 20% oxygen (O_2), the samples were etched for varying degrees to time, between 1 and 2 hours, to achieve optimal spike electrode dimensions. Table 7.1 details the 2 hour etch program used by the PlasmaTherm790, as an example.

No.	Process	Pressure (mTorr)	RF Power (W)	SF_6 (sccm)	O_2 (sccm)	Time (mm:ss)	Σ Time (h:mm:ss)
1	Initial Set Up	0.1	0			00:10	0:00:10
2	Purging	50	0	72	18	20:00	0:20:10
3	Evacuation	0.1	0			15:00	0:35:10
4	Set Pressure	50	0	20	5	00:10	0:35:20
5	Set Flow	50	0	72	18	00:10	0:35:30
6	Etch 0.5	50	150	72	18	30:00	1:05:30
7	Evacuation	0.1	0	0	0	20:00	1:25:30
8	Set	50	0	72	18	00:10	1:25:40
9	Etch 1	50	150	72	18	30:00	1:55:40
10	Evacuation	0.1	0	0	0	20:00	2:15:40
11	Set	50	0	72	18	00:10	2:15:50
12	Etch 1.5	50	150	72	18	30:00	2:45:50
13	Evacuation	0.1	0	0	0	20:00	3:05:50
14	Set	50	0	72	18	00:10	3:06:00
15	Etch 2	50	150	72	18	30:00	3:36:00
16	Evacuation - end 1	10	0	0	0	00:10	3:56:10
17	Purge - end 1	100	0	0	0	00:10	3:56:20
18	Evacuation - end 2	10	0	0	0	00:10	3:56:30
19	Purge - end 2	100	0	0	0	00:10	3:56:40
20	End	0.1	0	0	0	00:10	3:56:50

Table 7.1: Step by step recipe for a 2 hour etch of silicon pillars using the PlasmaTherm790 RIE machine.

7.2.4 Results

The initial etch optimisation experiments used set etch times of a) 1 hour, b) 1 hour 30 minutes and c) 2 hours. The outcome of experiment a) can be seen in figure 7.11a. As the SEM image shows, the sacrificial pillars have been etched away whilst only the top of the central pillar has begun to etch isotropically (etching the side walls) and the bottom of the pillars retains the original profile. This therefore justifies the original reasoning to include the sacrificial pillars to protect against creating a negative profile. Although a greater etch time was needed to achieve the desired electrode dimensions. The results of experiment b) can be seen in figure 7.11b. The etch time of 1hour and 30 minutes saw further sidewall etching of the central pillars. Although two of the central pillars in figure 7.11b have a spike-like form, the base diameter was determined to be too small and the pillar could easily be broken by applying a very small force. Hence, only the central

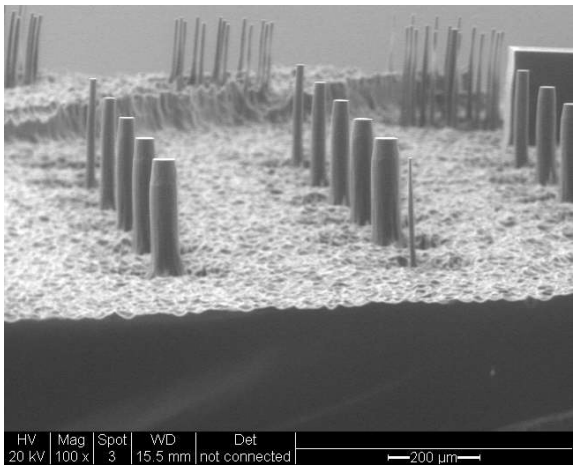

a) 1hour etch

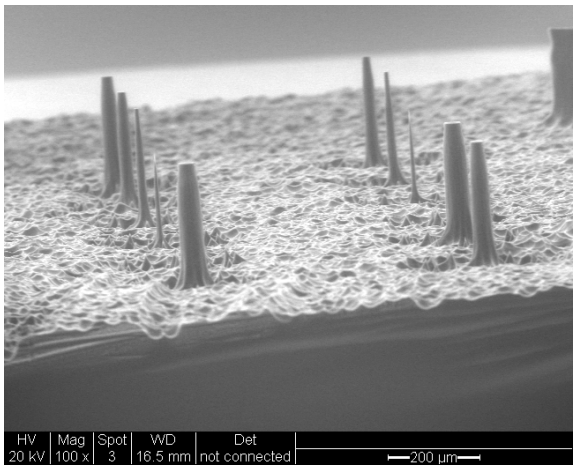

b) 1hour 30minute etch

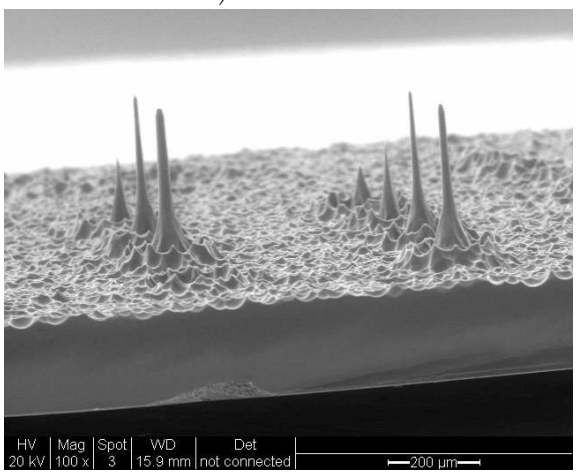

c) 2hour etch

Figure 7.11: **Outcome of initial etch experiments - SEM images.** All images with 85° tilt and x100 magnification.

pillar with a diameter of 80-100μm would be considered during the following etches. Experiment c) produced promising results with regards to the 90 and 100μm pillars as shown in figure 7.11c. However, after considering the size of the sample used in the previous experiments, it was decided that two cells on separate pieces of silicon would be etched simultaneously in the RIE in place of the random sizes used during experiments a - c. Due to this change in methodology, it was assumed that the etch times taken from these three experiments would be incorrect due to the amount of silicon that would be etched. This was shown to be true after a second 2 hour etch using the newly proposed sample sizes, as all pillars had been etched away completed (no SEM image available). To further control the reproducibility of the etching process, two specific cells were chosen to be used for all subsequent experiments. The two cells chosen were:

- 30y 300d (cell 6)
- 50y 300d (cell 9)

These cells were chosen to allow for an effect of satellite pillar diameter (y) on the central pillar. An iterative approach was utilised to achieve the optimum etch time. Figure 7.12 portrays the outcome of the iterative approach. As etch time increased the shaft length (right hand side axis), the shaft length decreased, however a rapid exponential decrease was observed after an etch time of 1hour 52minutes and 30 seconds. A similar response was observed for the tip diameter, however this was seen to be decreasing before 1hour 50 minutes. Where the lines cross could be considered the optimal etch time, however as stated in section 7.2.1, the tip diameter needs to be <200nm and the shaft needs to be as long as possible, therefore an etch time of 1hour 54 minutes and 30 seconds would be considered to be the optimum etch time.

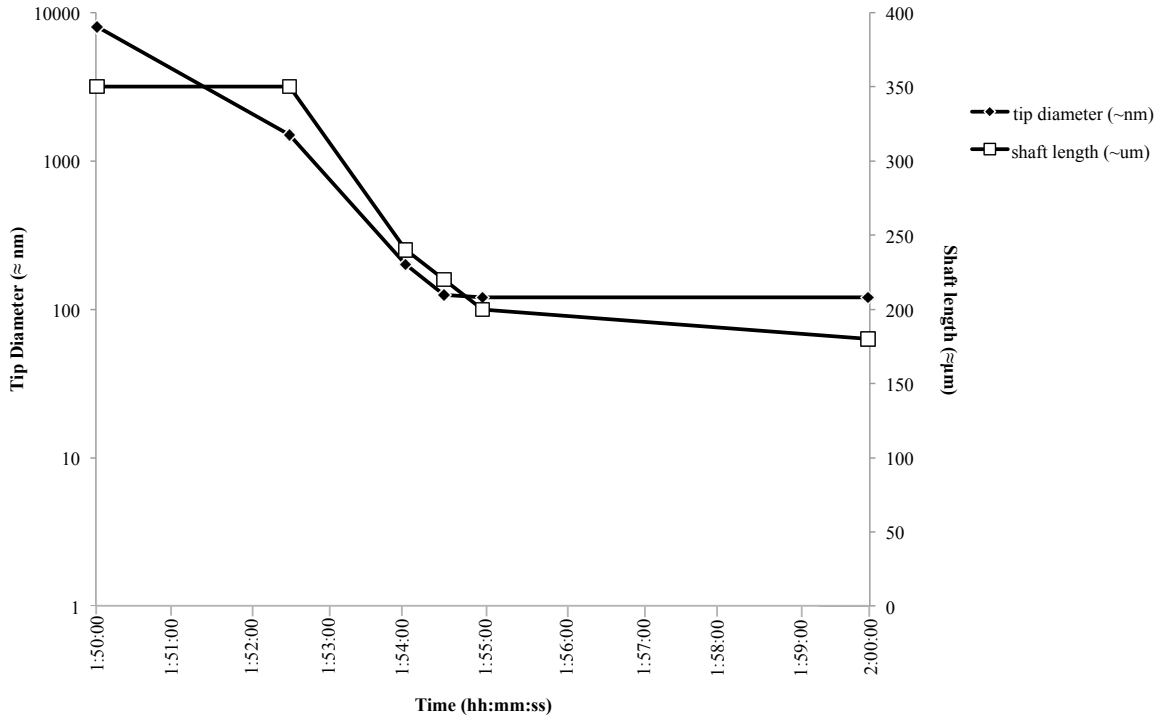

Figure 7.12: **Outcome of Iterative approach to optimal etch time.**

To test the mechanical properties of these spike electrodes, all electrodes bar the electrodes with an original base diameter of 100μm were removed from the substrate. The baseplate was then fixed to a plastic rod with a diameter of 4mm using araldite. This was allowed to cure overnight to ensure a strong bond was formed. The rod was clamped to a micro-manipulator, with the spike electrode being perpendicular to a petty dish containing agar (depth ∼15mm), a solid gelatinous substance used in electrophysiology to stabilise tissue during slicing which has a similar surface rigidity to brain tissue. The rod was lowered down until the base plate was nearly touching the agar, therefore resulting in the spike electrode being inserted into the medium. The spike was examined using

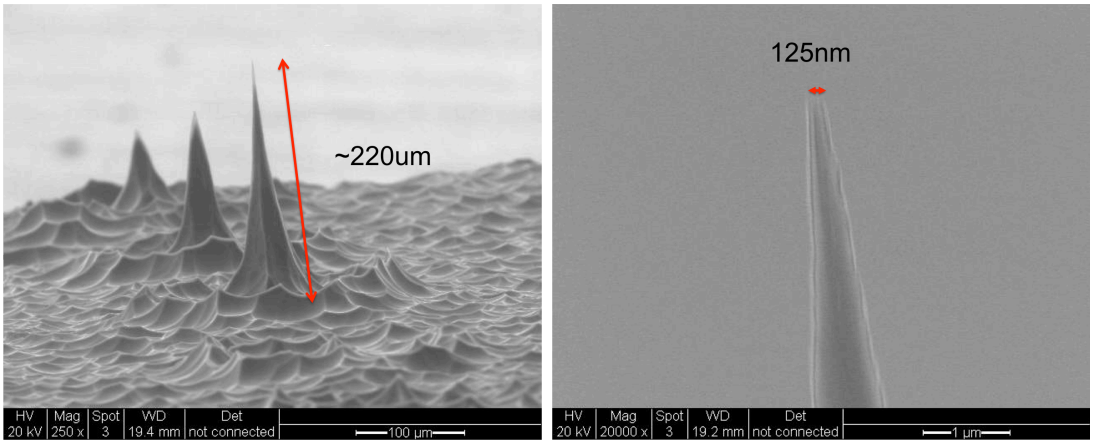

(a) (b)

Figure 7.13: **Optimum etch time for Mechanical purposes** - 1hour 54 minutes and 30 seconds. a)100μm diameter spike measuring approximately 220μm in height. b) tip diameter of spike shown in a) measuring approximately 125nm.

SEM and no damage was found to be present (no image available).

7.2.5 Summary of the mechanical testing

The silicon wafer used for the initial spikes was not sufficiently doped for the spikes to be electrically conductive. However it did possess the mechanical properties required to fabricate an electrode with a base diameter of approximately 100μm, a shaft length of approximately 220μm and a tip diameter of approximately 125nm. It was also able to sustain insertion into a tissue-like medium without damage. To successfully record intracellularly, the active region of the electrode requires an impedance of less than 100MΩ at 1kHz. The typical impedance of a typical glass capillary intracellular electrode capable of successfully recording from a cell is $\sim$70MΩ. To ensure that the electrode is recording exclusively from inside the cell, the shaft of the electrode needs to be electrically isolated from the tip. The current electrode design does not allow for the electrodes to be individually isolated, hence any signal detected by one electrode will be seen across all electrodes which will impede in the understanding of the cellular network. Therefore, every electrode needs to be electrically isolated whilst also having a back contact to allow for ease of connectivity and addressability in arrays. The electrical and isolation properties required of a solid state silicon electrode will be discussed in section 7.3.

7.3 Efficacy of Electrical Properties

7.3.1 Design

Addressability

Previous studies have utilised thermomigration to create electrically isolated electrodes. For example, Campbell *et al* (1991) used thermomigration to define p-doped columns in an n-doped substrate. Due to the nature of P-N junction isolation, no electrical current will pass from the 'p' region to the 'n' region, hence resulting in an electrically active and isolated column.

The height of the pillars that were required for this test dictated that thermomigration would not be suffice. To achieve the height required for the pillars, it was decided a thick, highly doped n-type wafer and a thin, lowly doped p-type wafer would be bonded together to create a type of SOI (Silicon on Insulator) wafer. The layer between the two wafers would be SiO_2, therefore as well as separating the two wafers, it would act as a stop etch when etching the pillars from the highly doped wafer. Hence each electrode would be electrically isolated.

To be able to record from each individual electrode, the addressability had to be considered. A via would be wet etched through the thin wafer, using KOH, to correspond to the location of each central pillar. Once the wafers were bonded together, the vias would undergo metal deposition. This would then be patterned to create a back contact large enough to bond to. The addition of interconnects would allow for a manipulating device to be attached to the back of the array without sitting directly on the back contacts in the middle of the array.

Insulation Medium

The conductive nature of the material used to allow for a biological signal to pass through the electrode tip has previous been discussed, however to record from only the tip, it is necessary for the majority of the electrode shank to be coated in an insulating medium. Thin film chemistry can be used to create both conductive and insulative surfaces, although for the purpose of this research only insulative films will be detailed. For an insulative material to be viable, it needs to be biocompatible. As previously stated to be considered biocompatible, a material needs to have a non-toxic or injurious effect on biological systems. Another important consideration needs to be whether the insulative material used is etch-able. Due to the nature of the electrode, the tip would need to be bare of insulative material to allow an electrical signal to be sent to the recording

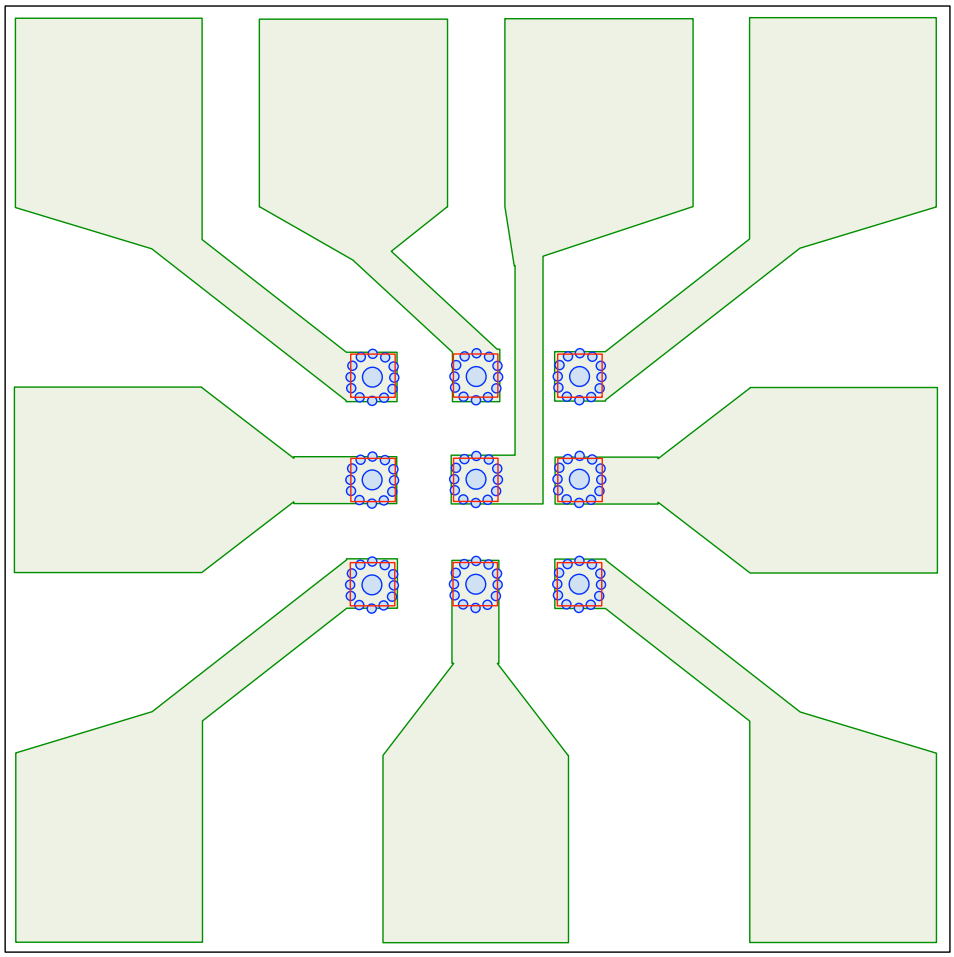

Figure 7.14: **Addressable array mask design.** This basic mask design shows a 3 x 3 array of central pillars surrounded by sacrificial pillars (Blue), the pattern for the via to be used during the wet etch (Red) and the interconnects from the centre of the 5mm square substrate to the outer edges to allow for easy access and addressability (Green).

software. Both wet and dry etch methods may be viable, however due to the microsmall area of the tip, a controllable process such as dry etching may be more viable. Several criteria need to be investigated before the insulative material is chosen:

- Biocompatibility
- Dielectric Properties
- Tensile Strength
- Adherability
- Etchability

Polyimide

Aromatic polyimide (PI) has been at the forefront of microelectronics encapsulation for many years due to its resistance to solvents, strong adhesion to metal oxides and dielectric properties. Photolithography and dry etching methods can be utilised to pattern PIs, which allows them to be very versatile. PIs exhibit high electrical resistivity, thermal stability, chemical inertness and good adhesion to common substrates [Beebe and Denton, 1994]. PI has been shown to have a lower dielectric constant than Si_3N_4 and SiO_2 (refer to table 7.3) however PI is an organic polymer and hence it is not as durable [Borkholder, 1998]. Repeated use may result in the degradation of the thin film layer and hence the deterioration of the biological signal. Until recently, PIs would have been the obvious choice for isolating sterilizable medical devices due to its biocompatibility [Richardson et al., 1993] and dielectric properties. PI has a Young's modulus of 2.8GPa which would allow the thin film to provide support to a structure whilst also allowing for a degree of flexibility before fracturing. One disadvantage would be the etch rate of PI. It is well documented that PI can be etched in a fluorinated oxygen plasma, however the etch rates are $>1\mu$m per minute [Turban and Rapeaux, 1983, Bagolini et al., 2002]. To be able to control the etch rate of the insulative material covering the tip, a much lower etch rate is needed. Another disadvantage of PIs is their tendency towards moisture uptake.Consequently, the use of alternative biocompatible thin film materials with improved moisture absorption and dielectric properties, such as Parylene or Benzocyclobutene.

Silicon Dioxide

Silicon Dioxide (SiO_2) has been used for many years in the microelectronics industry as a thin film insulator. It is considered an almost perfect insulator with a resistivity in excess of $10^{16}\Omega$cm. SiO_2 can be thermally grown or deposited via chemical vapour deposition. These films are smooth and coherent, with no pin holes, ranging in thickness down to a single atomic layer, although it is known that to be insulative, SiO_2 needs to be at

least five atoms thick [Schulz, 1999]. Unlike PI, SiO_2 does not have a tendency towards moisture uptake therefore making it suitable for biomedical applications. However, it is not at durable as several of the following materials detailed, hence it is not the primary choice. It is however, easily and controllably etched via both wet (e.g. Potassium hydroxide ∼8nm/minute) and dry (RIE, SF_6 + O_2 ∼25nm/minute) etching methods [Williams et al., 2003].

Silicon Nitride

A convenient way to achieve insulation is by using sputtered silicon nitride (Si_3N_4). It is often used as an insulator and a chemical barrier in manufacturing. Owing to superior durability, Si_3N_4 is better suited for thin film dielectric coatings than SiO_2 or PI. SI_3N_4 deposited via CVD experiences strong tensile stress which can result in cracks in films thicker than 200nm. However, it does have a superior resistivity and dielectric strength when compared to other insulators commonly used in the micro-fabrication industry. A study by Neumann *et al* (2004) confirmed that Si_3N_4 adhered to a variety of surfaces and acted as a physiochemical barrier allowing cell cultures to survive on non-biocompatible mediums. The biocompatibility of Si_3N_4 was greater on polished surfaces [Neumann et al., 2004]. However, due to fabrication method employed to produce the needle-like electrodes in this thesis, the exterior surface of the electrodes are unlikely to be smooth or uniform hence the use of Si_3N_4 as the insulative medium may not be suitable.

Parylene

Parylene is a type of CVD unique polymer which is used widely as a moisture barrier and an electrical isolator. There are currently three types of parylene films: Parylene N (poly-para-xylylene) is the base member first reported in 1947 [Tracton, 2007], which can sustain high temperatures (>220°C) vacuum environments; Parylene C is produced from the same monomer but replaces an aromatic hydrogen atom with a chlorine atom. It is the most widely used polymer due to it low permeability to moisture and gases while also retaining exceptional electrical properties; Parylene D, which is very similar to Paylene C in characteristics but can withstand higher temperatures, albeit not the the same magnitude as Parylene N.

One of the benefits of using parylenes is that they can be used to form very thin layers. Table 7.2 demonstrates the excellent dielectric properties of Parylene for coatings with a depth of less than 1μm. It is well documented that both Parylene C and N can be etched in an oxygen-based plasma [Callahan et al., 2003, Callahan et al., 2001].

Properties (1)		**Parylene N**	**Parylene C**	**Epoxy**	**Silicone**	**Polyurethane**
Dielectric Strength, V/mil		7,000	5,600	2,200	2,000	3,500
Dielectric Constant						
60Hz		2.65	3.15	3.3 - 4.6	3.1 - 4.2	4.1
1KHz		2.65	3.10	-	-	-
1MHz		2.65	2.95	3.1 - 4.2	3.1 - 4.0	3.8 - 4.4
Dissipation Factor						
60Hz		0.0002	0.020	0.008 - 0.011	0.011 - 0.02	0.038 - 0.039
1KHz		0.0002	0.019	-	-	-
1MHz		0.0006	0.013	0.004 - 0.006	0.003 - 0.006	0.068 - 0.074
Surface Resistivity (Ω)		10^{13}	10^{14}	10^{13}	10^{13}	10^{14}
Volume Resistivity (Ω/cm)		$1.4x10^{17}$	$8.8x10^{16}$	10^{12} - 10^{17}	10^{15}	10^{11} - 10^{15}
Youngs Modulus (GPa)		2.41	2.75	2.41	0.0062	0.0068 - 0.068
Gas Permeability						
at 25°C	N_2	3.0	0.4	-	-	31.5
(cc.mm)/	O_2	15.4	2.8	-	19,685	78.7
(m^2.day.atm)	CO_2	84.3	3.0	-	118,110	1,181
	H_2	212.6	43.3	-	17,717	-

Table 7.2: Electrical Properties of Parylene. *Data taken from [SCS, b]*

To be considered biocompatible, a material needs to have superior chemical resistance, barrier properties and insolubility when placed in living tissue for a length of time. Parylene solubility in organic or other media is very low, less than 0.1% after 24 hours. Due to the method of deposition, Parylene produces pin-hole free films which provide an excellent barrier to both liquids and gases. Table 7.2 shows gas permeability values have been measured at thicknesses below 0.1μm. Parylene is also resistant to chemical at room temperature and is also insoluble in all organic solvents up to 150°C [SCS, a].

Although Parylene C has all the attributes required of a biocompatible insulation layer, it does not adhere to substrate metals sufficiently to withstand the necessary lifetime required for many implants [Stark, 1996]. With regards to the needle-like electrodes in this thesis, the lifetime of parylene is not paramount provided that it can withstand multiple uses. To improve parylene adhesion to the silicon substrate, A174, an adhesion promotor, can be initially applied to the inorganic silicon surface [Stark, 1996]. This presents an organic face to Parylene C monomers, allowing for satisfactory adhesion. A-174 is also biocompatible, hence as a consequence of these combined properties, Parylene C is

considered to be a viable candidate for the electrical insulation layer.

Benzocyclobutene

Benzocyclobutene (BCB) polymers have been used since the late 1980's in the microelectronics industry for packaging and interconnect applications. BCB is a material widely used in the electronics industry due to its low dielectric constant, low moisture absorption, excellent chemical resistance and low electrical current loss factor at high frequencies. It has also recently been used in preference to PI for medical devices due to its greater tensile strength [Lee et al., 2005]. Lee *et al* (2005) reported that BCB coated electrodes passed stringent biocompatibility tests when cells were cultured on the top surface of the planar electrodes, as no change of morphology was seen and hence were considered non-toxic. BCB can be etched through the use of plasma processes, however some fluorinated etch gas component must be present as BCB cannot be asked in pure oxygen [FIRST, 2001]. The gas mixture used to etch the silicon spikes would be suitable for etching BCB. However, trials would need to be performed to understand both the adherability to the spike electrode due to the small tip dimensions, in conjunction with etch rate trials to calculate the etch rate in the machines available; and whether using RIE will result in the BCB being removed from the sidewalls of the electrode. Due to the nature of the needle-like electrodes in this thesis, BCB is an insulative medium to consider due to the superior tensile strength, biocompatibility, ease of fabrication and low dielectric constant.

Properties	**Benzocyclobutene**	**Polyimide**
Dielectric Constant		
60Hz	-	-
1KHz	2.65	3.5
1MHz	2.65	3.5
Dissipation Factor		
60Hz	-	-
1KHz	0.0008	-
1MHz	0.0008	0.005
Breakdown Voltage (V/cm)	$3x10^6$	$3x10^6$
Volume Resistivity (Ω/cm)	$1x10^{19}$	$1x10^{16}$
Youngs Modulus (GPa)	3.1	2.8
Water Uptake (23°C and 84% relative humidity)	0.14%	4%

Table 7.3: Electrical Properties of BCB

Fabrication Process

All pre-sharpening fabrication was to be undertaken by SMC, Edinburgh. Figure 7.15 shows a schematic of the fabrication process to be used to create the conductive, addressable spike electrodes. To fabricate spikes suitable for intracellular recording, a thin lightly doped silicon (6inch, (100), p-type 10-20 Ω cm, 150μm thick) wafer was to be coated in a silicon nitride (Si_3N_4) film via low pressure chemical vapor deposition (LPCVD), as shown in Figure 7.15b. Photolithography was to be used to pattern the nitride film to create the back contact cavities. The dimensions of Mask 1 (see figure 7.15c) were chosen to allow for a Potassium Hydroxide (KOH) etch to create a cavity with a 20μm square base at the Si_3N_4 etch stop layer (see figure 7.15d). The base of the cavity was to be opened by striping the nitride from the thin p-type silicon (Figure 7.15e) that was to be replaced with a thermally grown silicon dioxide (SiO_2) layer. The thin wafer was then to be bonded to a highly conductive silicon (6 inch, (100), n-type, 0.0015 Ω cm, 500μm thick) wafer. Once bonded the vias and the edges of the cavity were to be deposited with aluminium (Al). The Al is patterned via photolithography to produce the back contacts for the pillars (see figure 7.15i). The top surface was then to be patterned to create the mask for the central (100μm diameter) and sacrificial (50μm diameter) pillars

to be etched using DRIE. The Bosch process was to be used to etch the pillars until the SiO_2 etch stop was reached; hence pillars would have been approximately 500μm tall (see figure 7.15j).

The process described below would have initially been used for producing an individual spike, then further developed to enable the production of addressable arrays.

As with the preliminary samples, the wafer would have been cleaved into 5mm x 5mm samples that would have been placed in the RIE chamber and etched to spikes (see figure 7.15k). Due to the doping level of the wafer used to produce the spike electrodes in the second batch, the etch time to produce the required tip dimensions would be different from that of the preliminary spike electrodes described in section 7.2. It is well known that the dry etch rate of lightly doped silicon is independent of dopant type and doping concentration, however the etch rate for heavily doped silicon is dependent on dopant type and doping concentration [Kojima et al., 1994]. The etch rate of heavily doped n-type silicon is increased with an increase in donor impurity concentration [Kojima et al., 1994] hence, the dry etch time of the secondary electrodes is likely to be greater than the etch time previously used in the preliminary fabrication. Therefore, several test runs would have to have been undertaken to determine the etch rate of the heavily doped n-type wafer.

Manipulation

As with the mechanical efficacy electrodes discussed in section 7.2.1, manipulation of the electrical efficacy electrodes must be considered. The aspects considered in this previous section can all be applied to the manipulation of the electrically conductive electrodes, however a robust method for attaching the rod is required due to the fragility of the electrode tips and the electrical contacts that would be on the reverse side of the substrate.

Two methods were considered. The first would involve bonding a gold wire to each contact on the reverse side of the substrate followed by a coating of epoxy to protect and strengthen the bond. The electrode would be carefully inserted, electrode side down, into a hollow jig approximately the same size as the electrode base, this would allow for the electrode base to be perpendicular to the rod. The rod would be attached to the reverse side with epoxy, ensuring it remained perpendicular to the base during curing. The wire would be wrapped loosely around the wire and fed into the electrical recording system.

The second method would utilise sprung gold contact pins and clips attached to the four corners of the electrode base plate. This method allows for a efficient transference

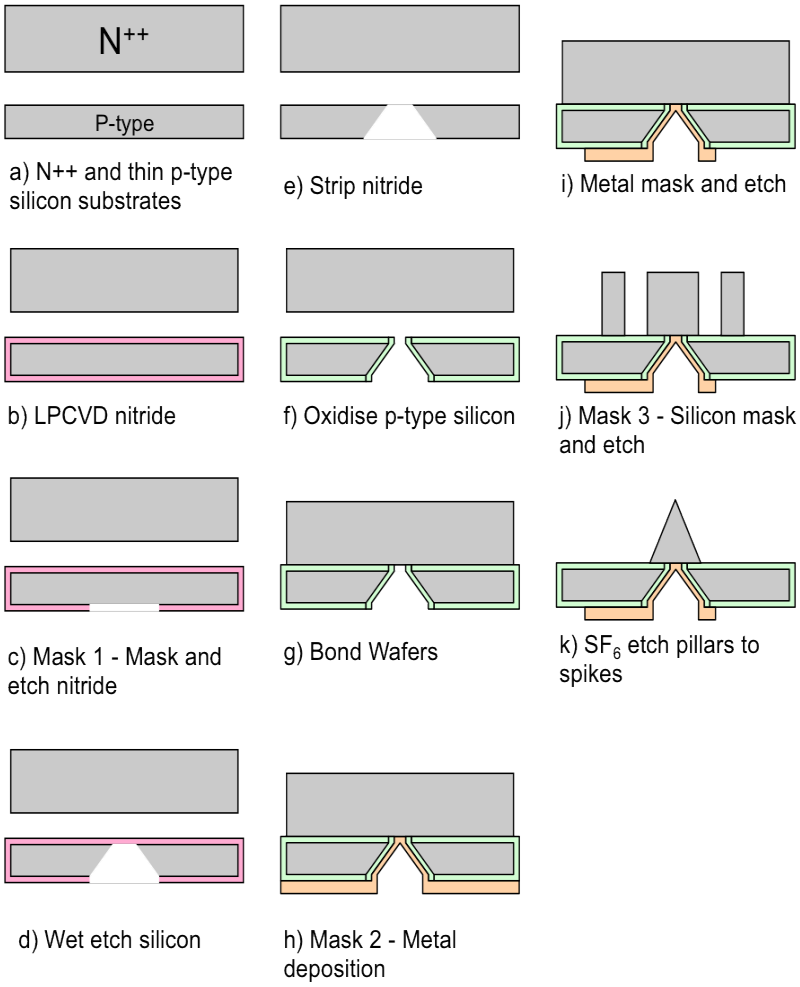

Figure 7.15: Schematic of process steps involved in fabrication of intracellular electrode array

from one electrode/array to another as the rod is not permanently attached to the base plate. The pins instead make the contact with the mapped location of the base contact pads of the electrodes. This method would be more appropriate when dealing with an array than a single electrode as it removes the possibility of cross talk between the electrodes due to wires touching.

7.3.2 Summary

The aim of the electrical testing was to produce a viable solid state intracellular electrode, whether it be a single electrode or an array of multiple addressable electrodes. Due to unforeseen fabrication difficulties by SMC, University of Edinburgh, this was not possible during the time available. However, the design of these electrode arrays may still be used in the future to fabricate electrically conductive arrays given time and resources.

7.4 Conclusions

The ability to record from multiple channels simultaneously has greatly improved the understanding of spatio-temporal effects of pharmacological agents in *in vitro* studies. It is also allowing for advances in medical systems linked to giving sight to blind people and giving quadriplegics control over the muscles in their hands and arms through the implementation of this technology *in vivo*. It was therefore realistic to presume that the fabrication of an intracellular electrode array would also be hugely beneficial to not only to those working in the field of electrophysiology but to those researching rehabilitation technologies. The mechanical efficacy test results detailed in this chapter have shown that it is possible to create solid state electrode from a silicon substrate with the dimensions necessary for penetrating a pyramidal cell in the neocortex. Although timing constraints and unforeseen difficulties removed the possibility of achieving a functional intracellular electrode array, the designs, research and materials used within this chapter would allow for future work to be conducted without delay.

Chapter 8

Conclusion

8.1 Overview

Sleep has been extensively studied through the use of EEG, *in vivo* and *in vitro* experimental methods, as has the pathophysiology of epilepsy and neurological disorders related to deep sleep. The mechanisms responsible for the EEG traits, particularly the spike-wave complex or otherwise known as the spike and wave discharge, were previously unknown. Hence, the aims of this thesis were to establish an *in vitro* model of the spike-wave complex (SWC) and to elucidate the pharmacological properties of the SWC. Following this, the aim was to establish the contribution of specific types of neurons to this phenomenon in order to determine the cellular basis of the pathology and the interactions between local neuronal populations in superficial and deep layers of the neocortex. The final aim of this work was to design a method for improving current *in vitro* intracellular recording methods to allow for improved understanding of the interactions between the individual neurons in a local population.

The general introduction to this thesis presented a detailed introduction and literature review of the knowledge and previous work relating to the neurobiology of sleep, concentrating particularly on the neuromodulators; acetylcholine, serotonin and dopamine. Also reviewed, due to it's importance in sleep research, was electroencephalography and the frequency ranges relating to the sleep-wake cycle typically seen when large populations of neurons are recorded simultaneously. Due to nocturnal idiopathic epilepsies in childhood being the basis of this theses, a number of the most prevalent types are also detailed in this chapter. Of particular interest was the paroxysmal events typically observed in EEGs from these individuals as well as the genetic mutations present.

Chapter 3 provided clinical data from an 11 year old female with a history of learn-

ing difficulties from the age of 4. The patient presented with sleep-associated generalised seizures which had gradually worsened over the previous year. Spectrographic analysis conducted demonstrated the relationship between delta frequency activity and spike-wave complexes. This analysis displayed the peak of the SWC activity to be located along the left temperoparietal axis. This provided a direct comparison with results from the experimental model detailed in the subsequent chapters. This analysis supported the parietal dominance of general epileptiform abnormalities observed in disorders such as benign childhood epilepsy with centrotemporal spikes (BECTS) and Continuous spike and wave during sleep (CSWS), which in turn defined the most suitable region of the cortex to conduct the research in - the somatosensory cortex.

Several genetic models of spike and wave related epilepsy have been establish. The two which dominate the literature are the Genetic absence epilepsy rat from Strasbourg (GAERS) and the wistar albino Glaxo rat from Rijswilk (WAG/Rij), both of which spontaneously develop non-epileptic spike and wave seizures which persist into adulthood. Many of the neuromodulatory systems have been linked to spike and wave seizures through the use of these models, of which the cholinergic system was of particular interest due to the complex role of nicotinic receptors in seizure generation. As a result of this, the aim of Chapter 4 was to investigate whether the disruption of the cholinergic system would be sufficient to generate epileptiform activity from delta rhythms similar to that seen in patients during deep sleep. Due to the *in vitro* nature of the experiments and in the absence of an intact thalamocortical system in the slice, the aim was to see whether the local circuitry in neocortex alone was sufficient to support such pathology.

D-tubocurarine (DTC), a competitive non-selective nAChR antagonist, was selected due to the agents ability to generate epileptiform activity [Carracedo, 2010]. Laminar profiles of the cortical column of the somatosensory cortex reported a typical reversal in phase angle when the local field potential was recorded from Layer I during both the control state and following the application of DTC. As expected from [Carracedo, 2010], Layers IV/V displayed the most robust delta rhythm, which also remained true upon application of DTC. Whilst DTC did not effect the delta frequency band power of the LFP, it did significantly reduce the frequency of the rhythm. As has previously been seen with tuber sclerosis [Nishida et al., 2008], the slowing of the delta rhythm coincided with the generation of epileptiform activity. The epileptiform activity was split into two different types due to morphology and embedded frequencies: wave discharges - an exaggerated delta wave with little embedded high frequency activity, and spike-wave complexes - as per the wave discharge but with a positively reaching spike situated within the wave with high frequency activity occurring at the time of the spike.

Where Chapter 4 had successfully demonstrated the abilities of the model to mimic epileptiform activity observed in nocturnal epilepsies and sleep related neurological disorders, the basic pharmacological properties of the epileptiform behaviour were not understood. Chapter 5 therefore characterised this behaviour. The results from Chapter 4 strongly indicated that nAChRs were involved in the generation of epileptiform activity however the particular subunits responsible for this was unknown. Therefore due to this, as well as the known antagonist nature of DTC on 5-HT_3 and $GABA_A$ receptors, specific subunit blocking agents were chosen to understand the impact these subunits had on the generation of the epileptiform activity. Hence the aims of this chapter were to understand which subunits responded similarly to DTC application, to understand the mechanisms underlying DTC-induced epileptiform activity and to understand the variation in epileptiform activity and how it varies depending upon the blockade of specific receptor subunits.

To understand whether a change in the rhythm of slow-wave sleep was seen with this epileptiform activity, the frequency and power of the delta rhythm was monitored separately from the epileptiform activity. 6 out of the 9 agents used resulted in a decrease in delta frequency, whilst only 2 of those 6 saw an increase in delta band power as was seen upon DTC application. Interestingly, these two agents (Pancuronium and DHβE) resulted in the generation of WDs but very few, if any SWCs. Four of the agents, with increasing concentration, were found to, after initially generating WDs, decrease the number of WDs whilst increase the number of SWCs per 60 second epoch.

The results from this chapter suggest that the disruption of the Ca^{2+}- dependent pathway via the blockade of presynaptic α_7 nAChRs may result in a decrease in long term potentiation [Shen and Yakel, 2009], contributing to cognitive deficits in disorders like CAE and ADNFLE, due to the the epileptogenic effect of the α_7 antagonist, MG624. This result paired with the blockade of $\alpha_3\beta_2$ nAChR subunits [Stevens et al., 2003] and the application of the AMPA receptor PAM [Bertolino et al., 1993], suggests that epileptiform activity is mediated by glutamate currents which is consistent with the use of glutamate antagonists as anticonvulsants [Meldrum, 1994]. The severe discharges generated upon $GABA_A$ antagonist and $GABA_A$ negative allosteric modulator application are thought to be due to the blanket blockade of inhibition, hence hugely increasing excitatory response. This suggest thats only a partial disinhibition is required to generate WDs and SWCs as both nAChRs and 5-HT_3 receptors are located on dendrite targeting interneurons. These results indicate a failure to control dendritic AMPA receptor mediated inputs onto pyramidal cells, particularly in superficial layers.

The results from Chapter 5 imply that the difference between the two types of epileptiform activity seen in this thesis may simply be due to the degree of recruitment of superficial layers in addition to paroxysm events in the delta-generating Layer V pyramidal cells. Hence the aim of Chapter 6 was to elucidate the input/output activity of individual neuronal cell types during delta oscillations and paroxysm events. As well as investigating the spatiotemporal distribution of the individual paroxysm events through the cortical column and somatosensory cortex.

The results from this chapter suggest that enhanced dendritic electrogenesis may result in the hyperexcitability responsible for the generation of the spike component of the SWC. As DTC blocks both 5-HT_3 and nACh receptors it may be possible that this hyperexcitability is mediated by a lack of excitatory tone in these receptor expressing inhibitory interneuron subtypes. This, in turn may lead to disinhibition, spike generation and disruption of the interplay between deep and superficial layers, all of which is thought to be associated with changes in synaptic plasticity.

The limiting factor in chapter 6 was the ability to obtain definitive insight of what mechanisms underlie the spatiotemporal dynamics of the cortical networks. The aim of Chapter 7 was to investigate the efficacy of fabricating an array of electrically active, addressable, solid state intracellular electrodes to aid in this insight. This involved an initial study to acknowledge if the necessary dimensions required to successfully penetrate the membrane of a pyramidal cell (typically $\sim$20μm in diameter) without rupturing the cell, were achievable through fabrication methods available. Single electrodes were fabricated from mildly conductive n-type silicon substrate. These electrodes were $\sim$220μm long, conical in appearance with a base diameter of $\sim$100μm and a tip diameter of $\sim$125nm. All of which were theoretically sufficient to penetrate the membrane of a pyramidal cell however due to the low conductivity of the substrate used these electrodes were not electrical conductive enough to record from a cell. A subsequent design process was derived to fabricate the desired array based upon the knowledge obtained during the preliminary study. Due to time constraints and unforeseen fabrication technicalities, these electrically active electrode were not completed.

8.2 Future Work

The future work which can build upon this thesis can be split into two clear stages. The first would be to complete the fabrication of the electrically active electrodes described in Chapter 7.3 using the process flow and the photolithography masks. These were designed based on what was learnt during the mechanical efficacy study of these electrode arrays

as well as extensive research into previous studies on this topic [Hanein et al., 2002]. The second stage would be to complete comparison studies between the fabricated single solid state electrodes and the current glass capillary electrodes utilised in current intracellular studies. This would allow for further improvement in the fabrication methods used to create a reliable and comparable electrode to the current techniques utilised in electrophysiology. A direct comparison between the current extracellular multichannel arrays and the fabricated intracellular arrays would also be of interest. If this work were to be carried out and completed, it could have a huge impact on electrophysiological research resulting in a greater understanding of the roles individual neurons play in the local neuronal population.

Bibliography

Parylene conformal coating specifications and properties. Collated by Nanobiotechnology center at Cornell University.

Adrien, J. (1992). Are other 5-ht receptors besides 5-ht1a and 5-ht2 involved in the regulation of sleep and wakefulness? *Journal of Sleep Research*, 1(3):176–7.

Aeschbach, D. (2009). Slow waves and learning: Beyond correlations. *Sleep*, 32(10):1253–4.

Aggrawal, A. (1995). *Narcotic Drugs*, chapter The story of opium. Number 2. National Book Trust, India.

Aghajanian, G. and Rasmussen, K. (1989). Intracellular studies in the facial nucleus illustrating a simple new method for obtaining viable motoneurons in adult rat brain slices. *Synapse*, 3:331–8.

Aldrich, M. S. (1999). *Sleep Medicine*. Number 53 in Contemporary Neurology series. Oxford University Press.

Alkondon, M. and Albuquerque, E. X. (1993). Diversity of nicotinic acetylcholine receptors in rat hippocampal neurons. i. pharmacological and functional evidence for distinct structural subtypes. *J Pharmacol Exp Ther*, 265(3):1455–73.

Alkondon, M., Pereira, E. F., Barbosa, C. T., and Albuquerque, E. X. (1997). Neuronal nicotinic acetylcholine receptor activation modulates gamma-aminobutyric acid release from ca1 neurons of rat hippocampal slices. *J Pharmacol Exp Ther*, 283(3):1396–411.

Aloe, F., Pinto de Azevedo, A., and Hasan, R. (2005). Sleep-wake cycle mechanisms. *Revista Brasileira de Psiquiatria*, 27(S1):33–9.

Amir, R. E., Van den Veyver, I. B., Wan, M., Tran, C. Q., Francke, U., and Zoghbi, H. Y. (1999). Rett syndrome is caused by mutations in x-linked mecp2, encoding methyl-cpg-binding protein 2. *Nature Genetics*, 23:185–188.

Amzica, F. and Steriade, M. (1997). The k-complex: Its slow (¡1-hz) rhythmicity and relation to delta waves. *Neurology*, 49(4):952–959.

Amzica, F. and Steriade, M. (1998). Electrophysiological correlates of sleep delta waves. *Electroencephalography and Clinical Neurophysiology*, 107:69–83.

Andersen, P., Gingrich, J., Bates, M., Dearry, A., Falardeau, P., Senogles, S., and Caron, M. G. (1990). Dopamine receptor subtypes: beyond the d1/d2 classification. *Trends in Pharmacological Sciences*, 11(6):231–6.

Anderson, D. (2008). Penetrating multichannel stimulation and recording electrodes in auditory prosthesis research. *Hearing research*, 242(1-2):31–41.

Andreasen, M. and Lambert, J. D. (1995). Regenerative properties of pyramidal cell dendrites in area ca1 of the rat hippocampus. *J Physiol*, 483 (Pt 2):421–41.

Aoyagi, Y., Stein, R. B., Weber, D. J., McDonnall, D., Branner, A., and Normann, R. A. (2002). Recording capabilities of a penetrating microelectrode array in dorsal root ganglia and its usefulness for coding of limb position. *Proceedings of the 6th Annual Conference, IFESS*, 1:109–11.

Aracri, P., Consonni, S., Morini, R., Perrella, M., Rodighiero, S., Amadeo, A., and Becchetti, A. (2010). Tonic modulation of gaba release by nicotinic acetylcholine receptors in layer v of the murine prefrontal cortex. *Cereb Cortex*, 20(7):1539–55.

Arts, W. F. M., Aarsen, F. K., Scheltens-de Boer, M., and Catsman-Berrevoets, C. E. (2009). Landau-kleffner syndrome and csws syndrome: treatment with intravenous immunoglobulins. *Epilepsia*, 50 Suppl 7:55–8.

Aston-Jones, G. S., Gonzalez, M., and Doran, S. (2007). *Brain Norepinephrine*, chapter 6 Role of the locus coeruleus-norepinephrine system in arousal and circadian regulation of the sleep–wake cycle, pages 157–195. Neurobiology and Therapeutics. Cambridge University Press.

Avoli, M. (1983). Participation of cortical and thalamic cells in the feline association system to thalamocortical recruiting responses. *Neurosci Lett*, 38(2):151–6.

Avoli, M. and Gloor, P. (1982). Role of the thalamus in generalized penicillin epilepsy: observations on decorticated cats. *Exp Neurol*, 77(2):386–402.

Azam, L. and McIntosh, J. M. (2012). Molecular basis for the differential sensitivity of rat and human 910 nachrs to -conotoxin rgia. *J Neurochem*, 122(6):1137–44.

Baars, B. J. (1998). Metaphors of consciousness and attention in the brain. *Trends Neurosci*, 21(2):58–62.

Bagolini, A., Pakula, L., Scholtes, T., Pham, H., French, P., and Sarro, P. (2002). Polyimide sacrificial layer and novel materials for post-processing surface micromachining. *Journal of Micromechanics and Microengineering*, 12(4):385.

Bagshaw, A. P., Jacobs, J., LeVan, P., Dubeau, F., and Gotman, J. (2009). Effect of sleep stage on interictal high-frequency oscillations recorded from depth macroelectrodes in patients with focal epilepsy. *Epilepsia*, 50(4):617–28.

Bai, Q., Wise, K., and Anderson, D. (2000). A high-yield microassembly structure for three-dimensional microelectrode arrays. *IEEE Transactions on Biomedical Engineering*, 47(3):281–289.

Baker, E. R., Zwart, R., Sher, E., and Millar, N. S. (2004). Pharmacological properties of alpha 9 alpha 10 nicotinic acetylcholine receptors revealed by heterologous expression of subunit chimeras. *Mol Pharmacol*, 65(2):453–60.

Bastlund, J. F., Berry, D., and Watson, W. P. (2005). Pharmacological and histological characterisation of nicotine-kindled seizures in mice. *Neuropharmacology*, 48:975–83.

Bawari, M. (2010). Glutamate as a selective neurotoxin - a review. *Assam University Journal of Science and Technology: Biological and Environmental Sciences*, 5(1):147–53.

Beadle, W., Tsai, J. C. C., and Plummer, R. (1985). *Quick reference manual for silicon integrated circuit technology*. Wiley, New York.

Bear, M. F., Connors, B. W., and Paradiso, M. A. (2006). *Neuroscience: Exploring the Brain*. Lippincott Williams and Wilkins, 3rd edition.

Beaulieu, J.-M. and Gainetdinov, R. R. (2011). The physiology, signaling and pharmacology of dopamine receptors. *Pharacological Reviews*, 63(1):182–217.

Beebe, D. J. and Denton, D. D. (1994). A flexible polyimide-based package for silicon sensors. *Sensors and Actuators A: Physical*, 44(1):57 – 64.

Beghi, E., D'Alessandro, R., Beretta, S., Consoli, D., Crespi, V., Delaj, L., Gandolfo, C., Greco, G., La Neve, A., Manfredi, M., Mattana, F., Musolino, R., Provinciali, L., Santangelo, M., Specchio, L. M., Zaccara, G., and Epistroke Group (2011). Incidence and predictors of acute symptomatic seizures after stroke. *Neurology*, 77(20):1785–93.

Benington, J. H. and Heller, H. C. (1995). Restoration of brain energy metabolism as the function of sleep. *Progress in Neurobiology*, 45:347–60.

Benke, D., Fritschy, J. M., Trzeciak, A., Bannwarth, W., and Mohler, H. (1994). Distribution, prevalence, and drug binding profile of gamma-aminobutyric acid type a receptor subtypes differing in the beta-subunit variant. *J Biol Chem*, 269(43):27100–7.

Bercovici, E., Cortez, M. A., Wang, X., and Snead, 3rd, O. C. (2009). Monoamine variability in the chronic model of atypical absence seizures. *Epilepsia*, 50(4):768–75.

Berroya, A. M., Bleasel, A. F., Stevermuer, T. L., Lawson, J., and Bye, A. M. E. (2005). Spike morphology, location, and frequency in benign epilepsy with centrotemporal spikes. *J Child Neurol*, 20(3):188–94.

Berry-Kravis, E. (2002). Epilepsy in fragle x syndrome. *Developmental Medicine and Child Neurology*, 44:724–28.

Bertolino, M., Baraldi, M., Parenti, C., Braghiroli, D., DiBella, M., Vicini, S., and Costa, E. (1993). Modulation of ampa/kainate receptors by analogues of diazoxide and cyclothiazide in thin slices of rat hippocampus. *Receptors Channels*, 1(4):267–78.

Bertrand, D., Ballivet, M., and Rungger, D. (1990). Activation and blocking of neuronal nicotinic acetylcholine receptor reconstituted in xenopus oocytes. *Proceedings of the National Academy of Sciences of the USA*, 87:1993–7.

Bianchi, R., Chuang, S., Zhao, W., Young, S., and Wong, R. (2009). Cellular plasticity for group i mglur-mediated epileptogenesis. *The journal of Neuroscience*, 29(11):3497–507.

Bjorvatn, B., Fagerland, S., Eid, T., and Ursin, R. (1997). Sleep/waking effects of a selective 5-ht1a receptor agoniss given systemically as well as perfused in dorsal raphe nucleus in rats. *Brain Research*, 770:81–8.

Blaesse, P., Airaksinen, M. S., Rivera, C., and Kaila, K. (2009). Cation-chloride cotransporters and neuronal function. *Neuron*, 61:820–838.

Blumenbach, F. (1828). *The Elements of Physiology*. Longman, London, England, 4th edition edition.

Blumenfeld, H. (2005). Cellular and network mechanisms of spike-wave seizures. *Epilepsia*, 46(S9):21–33.

Bölsterli, B. K., Schmitt, B., Bast, T., Critelli, H., Heinzle, J., Jenni, O. G., and Huber, R. (2011). Impaired slow wave sleep downscaling in encephalopathy with status epilepticus during sleep (eses). *Clin Neurophysiol*, 122(9):1779–87.

Borbely, A., Trachsel, L., and Tobler, I. (1988). Effect of ritanserin on sleep stages and sleep eeg in the rat. *European Journal of Pharmacology*, 156:275–8.

Borkholder, D. A. (1998). *Cell based biosensors using microelectrodes*. PhD thesis, Standford University.

Born, J., Rasch, B., and Gais, S. (2006). Sleep to remember. *Neuroscientist*, 12(5):410–24.

Boutrel, B., Franc, B., Hen, R., Hamon, M., and Adrien, J. (1999). Key role of 5-ht1b receptors in the regulation of paradoxical sleep as evidenced in 5-ht1b knockout mice. *Journal of Neuroscience*, 19:3204–12.

Bragin, A., Mody, I., Wilson, C. L., and Jr, J. E. (2002). Local generation of fast ripples in epileptic brain. *The Journal of Neuroscience*, 22(5):2012–21.

Brodtkorb, E. and Picard, F. (2006). Tobacco habits modulate autosomal dominant nocturnal frontal lobe epilepsy. *Epilepsy Behav*, 9(3):515–20.

Broicher, T., Seidenbecher, T., Meuth, P., Munsch, T., Meuth, S. G., Kanyshkova, T., Pape, H.-C., and Budde, T. (2007). T-current related effects of antiepileptic drugs and a ca2+ channel antagonist on thalamic relay and local circuit interneurons in a rat model of absence epilepsy. *Neuropharmacology*, 53(3):431 – 446.

Broide, R. S., Salas, R., Daoyun, J., Paylor, R., Patrick, J. W., Dani, J. A., and De Biasi, M. (2002). Increased sensitivity to nicotine-induced seizures in mice expressing the l250t 7 nicotinic acetylcholine receptor mutation. *Molecular Pharmacology*, 61(3):695–705.

Brown, D. A. and Adams, P. R. (1980). Muscarinic suppression of a novel voltage-sensitive k+ current in a vertebrate neurone. *Nature*, 283(5748):673–6.

Brown-Sequard, C. (1889). Le sommeil normal, comme le sommeil hypnotique, est le resultant d'une inhibition de l'activite intellectuelle. *Arch Physiol Norm Path*, 1:333–335.

Bureau, M. (1995). *Continuous Spikes and Waves During Slow Sleep, Electrical Status Epilepticus During Slow Sleep: Acquired Epileptic Aphasia and Related Conditions*, chapter Continuous spikes and waves during slow sleep (CSWS): definition of the syndrome, pages 17–26. John Libbey.

Buzsaki, G. (2006). *Rhythms of the Brain*. Oxford University Press Inc., 198 Madison Avenue, New York, New York 10016.

Buzsáki, G., Bickford, R. G., Armstrong, D. M., Ponomareff, G., Chen, K. S., Ruiz, R., Thal, L. J., and Gage, F. H. (1988). Electric activity in the neocortex of freely moving young and aged rats. *Neuroscience*, 26(3):735–44.

Buzsáki, G., Csicsvari, J., Dragoi, G., Harris, K., Henze, D., and Hirase, H. (2002). Homeostatic maintenance of neuronal excitability by burst discharges in vivo. *Cereb Cortex*, 12(9):893–9.

Buzsáki, G., Leung, L. W., and Vanderwolf, C. H. (1983). Cellular bases of hippocampal eeg in the behaving rat. *Brain Res*, 287(2):139–71.

Callahan, R. R., Pruden, K. G., Raupp, G. B., and Beaudoin, S. P. (2003). Downstream oxygen etching characteristics of polymers from the parylene family. *Journal of Vacuum Science and Technology B: Microelectronics and Nanometer Structures*, 21(4):1496–1500.

Callahan, R. R., Raupp, G. B., and Beaudoin, S. P. (2001). Effects of gas pressure and substrate temperature on the etching of parylene-n using a remote microwave oxygen plasma. *Journal of Vacuum Science and Technology B: Microelectronics and Nanometer Structures*, 19(3):725–731.

Campbell, P. K., Jones, K. E., Huber, R. J., Horch, K. W., and Normann, R. A. (1991). A silicon-based, three-dimensional neural interface: manufacturing processes for an intracortical electrode array. *IEEE Transactions on Biomedical Engineering*, 38(8):758–768.

Campbell, P. K., Jones, K. E., and Normann, R. A. (1990). A 100 electrode intracortical array: structural variability. *Biomedical sciences Instrumentation*, 26:161–5.

Cantero, J. L., Atienza, M., Stickgold, R., Kahana, M. J., Madsen, J. R., and Kocsis, B. (2003). Sleep-dependent theta oscillations in the human hippocampus and neocortex. *The Journal of Neurocience*, 23(34):10897–903.

Caplan, R., Siddarth, P., Stahl, L., Lanphier, E., Vona, P., Gurbani, S., Koh, S., Sankar, R., and Donald Shields, W. (2008). Chilldhood absence epilepsy: Bahvioural, cognitive and linguistic comorbidities. *Epilepsia*, 49(11):1838–46.

Caraballo, R., Cersosimo, R., and Fejerman, N. (2007). Panayiotopoulos syndrome: A prospective stufy of 192 patients. *Epilepsia*, 48(6):1054–61.

Caraballo, R. H., Cersósimo, R. O., and Fejerman, N. (2008). Childhood occipital epilepsy of gastaut: a study of 33 patients. *Epilepsia*, 49(2):288–97.

Carey, J. and McCoy, D., editors (2006). *Brain Facts*. Society of Neuroscience, fifth edition.

Carmichael, E. A., Feldberg, W., and Fleischauer, K. (1964). Effects of tubocurarine perfused through different parts of the cerebral ventricles. *J Physiol*, 175:303–19.

Carracedo, L., Kjeldsen, H., Cunnington, L., Jenkins, A., Schofield, I., Cunningham, M. O., Davies, C. H., Traub, R. D., and Whittington, M. A. (2013). A neocortical delta rhythm facilitates reciprocal interlaminar interactions via nested theta rhythms. *Journal of Neuroscience*, In Press.

Carracedo, L. M. (2010). *Properties and Mechanisms of the Cortical Delta Rhythm in vitro*. PhD thesis, Institute of Neuroscience, Newcastle University.

Cavazzuti, G. B., Cappella, L., and Nalin, A. (1980). Longitudinal study of epileptiform eeg patterns in normal children. *Epilepsia*, 21(1):43–55.

Cavitt, J. and Privitera, M. (2004). Levetiracetam induces a rapid and sustained reduction of generalized spike-wave and clinical absence. *Arch Neurol*, 61(10):1604–7.

Cerminara, C., Coniglio, A., El-Malhany, N., Casarelli, L., and Curatolo, P. (2012). Two epileptic syndromes, one brain: Childhood absence epilepsy and benign childhood epilepsy with centrotemporal spikes. *Seizure*, 21:70–74.

Chadwick, J. and Mann, W. (1978). *Hippocratic writings*. Penguin Books, London, England.

Chan, W. K., Wong, P. T.-H., and Sheu, F.-S. (2007). Frontal cortical a7 and a4b2 nicotinic acetylcholine receptors in working and reference memory. *Neuropharmacology*, 52(8):1641–9.

Chapman, A. G. (2000). Glutamate and epilepsy. *J Nutr*, 130(4S Suppl):1043S–5S.

Chen, C., Yao, D., Tseng, S., Lu, S., Chiao, C., and Yeh, S. (2009). Micro-multi-probe electrode array to measure neural signals. *Biosensors and Bioelectronics*, 24:1911–1917.

Cheong, E. and Shin, H. S. (2013). T-type ca(2+) channels in absence epilepsy. *Biochim Biophys Acta*.

Cheung, K., Renaud, P., Tanila, H., and Djupsund, K. (2007). Flexible polyimide microelectrode array for in vivo recordings and current source density analysis. *Biosensors and Bioelectronics*, 22(8):1783–1790.

Chung, B. H. Y., Mullegama, S., Marshall, C. R., Lionel, A. C., Weksberg, R., Dupuis, L., Brick, L., Li, C., Scherer, S. W., Aradhya, S., Stavropoulos, D. J., Elsea, S. H., and Mendoza-Londono, R. (2012). Severe intellectual disability and autistic features associated with microduplication 2q23.1. *Eur J Hum Genet*, 20(4):398–403.

Clark, M., McDevitt, R., and Neumaier, J. (2006). Quantitative mapping of tryptophan hydroxylase-2, 5-ht1a, 5-ht1b and serotonin transporter expression across the anteroposterior axis of the rat dorsal and median raphe nuclei. *Journal of Comparative Neurology*, 498:611–23.

Colquhoun, D., Dreyer, F., and Sheridan, R. E. (1979). The actions of tubocurarine at the frog neuromuscular junction. *J Physiol*, 293:247–84.

Compte, A., Reig, R., Descalzo, V., Harvey, M., Puccini, G., and Sanchez-Vives, M. (2008). Spontaneous high-frequency (10-80hz) oscillations during up states in the cerebral cortex in vitro. *Journal of Neuroscience*, 28(51):13828–44.

Craig, M. T., Mayne, E. W., Bettler, B., Paulsen, O., and McBain, C. J. (2013). Distinct roles of gabab1a- and gabab1b-containing gabab receptors in spontaneous and evoked termination of persistent cortical activity. *J Physiol*, 591(Pt 4):835–43.

Crunelli, V. and Hughes, S. W. (2010). The slow (¡1 hz) rhythm of non-rem sleep: a dialogue between three cardinal oscillators. *Nat Neurosci*, 13(1):9–17.

Csicsvari, J., Henze, D., and Jamieson, B. (2003). Massively parallel recording of unit and local field potentials with silicon-based electrodes. *Journal of Neurophysiology*, 90:1314–1323.

Culebras, A., editor (2005). *Sleep Disorders and Neurological Disease*. Marcel Dekker, New York, USA.

Cunningham, M. O., Pervouchine, D. D., Racca, C., Kopell, N. J., Davies, C. H., Jones, R. S. G., Traub, R. D., and Whittington, M. A. (2006). Neuronal metabolism governs cortical network response state. *Proc Natl Acad Sci U S A*, 103(14):5597–601.

Dailey, J., Reigel, C., Mishra, P., and Jobe, P. (1989). Neurobiology of seizure predisposition in the genetically epilepsy-prone rat. *Epilepsy Research*, 3:317–20.

Dajas, F., Gaztelu, J. M., Zavalla, C. R., Macadar, O., and García-Austt, E. (1983). Effects of intraventricular curarimimetics on hippocampal electrical activity. *Exp Neurol*, 79(1):160–7.

Dalla Bernadino, B., Sgro, V., and Fejerman, N. (2002). *Epileptic Syndromes in infancy, childhood and adolescence*, chapter Chapter 14: Epilepsy with centro-temporal spikes and related syndromes, pages 181–2002. John Libbey, third edition.

D'Amore, V., Santolini, I., van Rijn, C. M., Biagioni, F., Molinaro, G., Prete, A., Conn, P. J., Lindsley, C. W., Zhou, Y., Vinson, P. N., Rodriguez, A. L., Jones, C. K., Stauffer, S. R., Nicoletti, F., van Luijtelaar, G., and Ngomba, R. T. (2013). Potentiation of mglu5 receptors with the novel enhancer, vu0360172, reduces spontaneous absence seizures in wag/rij rats. *Neuropharmacology*, 66:330–8.

Danober, L., Depaulis, A., Marescaux, C., and Vergnes, M. (1993). Effects of cholinergic drugs on genetic absence seizures in rats. *Eur J Pharmacol*, 234(2-3):263–8.

Danober, L., Deransart, C., Depaulis, A., Vergnes, M., and Marescaux, C. (1998). Pathophysiological mechanisms of genetic absence epilepsy in the rat. *Prog Neurobiol*, 55(1):27–57.

D'Antuono, M., Inaba, Y., Biagini, G., D'Arcangelo, G., Tancredi, V., and Avoli, M. (2006). Synaptic hyperexcitability of deep layer neocortical cells in a genetic model of absence seizures. *Genes, Brain and Behavior*, 5(1):73–84.

Darvas, M., Morsch, M., Racz, I., Ahmadi, S., Swandulla, D., and Zimmer, A. (2009). Modulation of the ca2+ conductance of nicotinic acetylcholine receptors by lypd6. *Eur Neuropsychopharmacol*, 19(9):670–81.

De-Fusco, M., Becchetti, A., Patrignani, A., Annesi, G., Gambardella, A., and Quattrone, A. (2000). The nicotinic receptor beta 2 subunit is mutant in nocturnal frontal lobe epilepsy. *National Genetics*, 26(3):275–6.

Del Arco, A., Segovia, G., Canales, J., Garrido, P., de Blas, M., García-Verdugo, J., and Mora, F. (2007). Environmental enrichment reduces the function of d1 dopamine receptors in the prefrontal cortex of the rat. *Journal of Neural Transmission*, 114(1):43–8.

Delacour, J. (1997). Neurobiology of consciousness: an overview. *Behav Brain Res*, 85(2):127–41.

Deng, L. and Chen, G. (2003). Cyclothiazide potently inhibits gamma-aminobutyric acid type a receptors in addition to enhancing glutamate responses. *Proc Natl Acad Sci U S A*, 100(22):13025–9.

Derry, C. P., Heron, S. E., Phillips, F., Howell, S., MacMahon, J., Phillips, H. A., Duncan, J. S., John C. Mulley and, S. F. B., and Scheffer, I. E. (2008). Severe autosomal dominant nocturnal frontal lobe epilepsy associated with psychiatric disorders and intellectual disability. *Epilepsia*, 49(12):2125–29.

D'Hulst, C., Heulens, I., Brouwer, J., Willemsen, R., De Geest, N., Reeve, S., De Deyn, P., Hassan, B., and Kooy, R. (2009). Expressions of the gabaergic system in animal models fro fragile x syndrome and fragile x associated tremor/ataxia syndrome (fxtas). *Brain Research*, 1253:176–83.

Di Pasquale, E., Keegan, K. D., and Noebels, J. L. (1997). Increased excitability and inward rectification in layer v cortical pyramidal neurons in the epileptic mutant mouse stargazer. *J Neurophysiol*, 77(2):621–31.

DiCara, B., Panayi, F., Gobert, A., Dekeyne, A., Sicard, D., De Groote, L., and Millan, M. (2007). Activation of dopamine d1 receptors enhances cholinergic transmission and social cognition: a parallel dialysis and behavioural study in rats. *The International Journal of Neuropsychopharmacology*, 10(3):383–99.

Diekelmann, S. and Born, J. (2010). The memory function of sleep. *Nature Review Neuroscience*, 11(2):114–26.

Diels, H. and Kranz, W. (1952). *Die Fragmente der Vorsokratiker*. Number Chapter 24 in 1. Weidmann.

Dobelis, P., Hutton, S., Lu, Y., and Collins, A. C. (2003). Gabaergic systems modulate nicotinic receptor-mediated seizures in mice. *J Pharmacol Exp Ther*, 306(3):1159–66.

Du Bois, R. (1895). Autonarcose carbon-acetonemique or sommeil hivernal de la marmotte. Revue de l'hypnotisme.

Dudai, Y. (2004). The neurobiology of consolidations, or, how stable is the engram? *Annu Rev Psychol*, 55:51–86.

Dugovic, C. (1993). Functional activity of 5-ht2 receptors in the modulation of the sleep/wakefulness states. *Journal of Sleep Research*, 1:163–8.

Dugovic, C. and Wauquier, A. (1987). 5-ht2 receptors could be primarily involved in the regulation of slow wave sleep in rats. *European Journal of Pharmacology*, 137:145–6.

Dugovic, C., Wauquier, A., Leysen, J. E., Marrannes, R., and Janssen, P. A. J. (1989). Functional role of 5-ht2 receptors in the regulation of sleep and wakefulness in the rat. *Psychopharmocology*, 97(4):436–442.

Dzirasa, K., Ribeiro, S., Costa, R., Santos, L. M., Lin, S.-C., Grosmark, A., Sotnikova, T. D., Gainetdinov, R. R., Caron, M. G., and Nicolelis, M. A. L. (2006). Dopaminergic control of sleep-wake states. *The Journal of Neuroscience*, 26(41):10577–10589.

Eccles, J. (1953). *The neurophysiological basis of the mind: The principles of Neurophysiology*. Oxford University Press.

Eder, D., Zdravkovic, M., and Wildschiodtz, G. (2003). Selective alterations of the first nrem sleep cycle in humans by a dopamine d1 receptor antagonist (nnc-687). *Journal of Psychiatric Research*, 37:305–12.

Eisele, J.-L., Bertrand, S., Gaizi, J.-L., Devillers-Thiery, A., Changeus, J.-P., and Bertrand, D. (1993). Chimaeric nicotinic-serotonergic receptor combines distinct ligand binding and channel specificities. *Letters to Nature*, 366:479–83.

Encyclopedia-Britannica. Nicotinic acetylcholine receptor. http://www.britannica.com/EBchecked/media/138258/The-nicotinic-acetylcholine-receptor-is-an-example-of-a-ligand.

Enderle, J. D., Blanchard, S. M., and Bronzino, J. D., editors (2000). *Introduction to Biomedical Engineering*. Academic Press, 1st edition edition.

Eriksson, K., Stevens, D., and Haas, H. (2001). Serotonin excites tuberomammillary neurons by activation of na+/ca2+ exchange. *Neuropharmocology*, 40:345–351.

Everett, K., Chioza, B., Aicardi, J., Aschauer, H., Brouwer, O., Callenbach, P., Covanis, A., Dulca, O., Eeg-Olofsson, O., Feucht, M., Friis, M., Goutieres, F., Guerrini, R., Heils, A., Kjeldsen, M., Lehesjoki, A.-E., Makoff, A., Nabbout, R., Olsson, I., Sander, T., Siren, A., McKeigue, P., Robinson, R., Taske, N., Rees, M., and Gardiner, M. (2007). Linkage and association analysis of cacng3 in childhood absence epilepsy. *Eur J Hum Genet.*, 15(4):463–72.

Fehrenbach, M. J., Emmons, M., and Babbush, C. A., editors (2007). *Mosby's Dental Dictionary*. Elsevier Health Sciences, 2 edition.

Feinberg, I., Campbell, I. G., and Marrs, J. C. (1995). Intraperitoneal dizocilpine induces cortical spike-wave seizure discharges in rats. *Neurosci Lett*, 196(3):157–60.

Feldberg, W. and Fleischhauer, K. (1963). The hippocampus as the site of origin of the seizure discharge produced by tubocurarine acting from the cerebral ventricles. *J Physiol*, 168:435–42.

Felix, R. and Levin, E. D. (1997). Nicotinic antagonist administration into the ventral hippocampus and spatial working memory in rats. *Neuroscience*, 81(4):1009–17.

Fell, J., Elfadil, H., Roschke, J., Burr, W., Klaver, P., Elger, C., and Fernndez, G. (2002). Human scalp recorded sigma activity is modulated by slow eeg oscillations during deep sleep. *International Journal of Neuroscience*, 112(7):893–900.

Ferreira, B. L., Valle, A. C., Cavalheiro, E. A., and Timo-Iaria, C. (1999). Prevalence of epileptic seizures along the wakefulness-sleep cycle in adult rats submitted to status epilepticus in early life. *Dev Neurosci*, 21(3-5):339–44.

Finger, S. (1994). *Origins of Neuroscience: a history of explorations into brain function*. Oxford University Press Inc., New York, 1st edition edition.

FIRST (2001). Cyclotene advanced electronic resins. Technical report, Swiss Federal Institute of Technology Zurich.

Flora, A., Schulz, R., Benfante, R., Bettaglioli, E., Terzano, S., Clementi, F., and Fornasari, D. (2000). Transcriptional regulation of the human alpha5 nicotinic receptor subunit gene in neuronal and non-neuronal tissues. *European Journal of Pharmacology*, 393:85–95.

Fogel, S. and Smith, C. (2011). The function of the sleep spindle: A physiological index of intelligence and a mechanism for sleep-dependent memory consolidation. *Neuroscience and Biobehavioral Reviews*, 35(5):1154–65.

Foster, D. and Wilson, M. A. (2006). Reverse replay of behavioural sequences in hippocampal place cells during the awake state. *Nature*, 440:680–83.

Franceschini, D., Paylor, R., Broide, R., Salas, R., Bassetto, L., Gotti, C., and De Biasi, M. (2002). Absence of 7-containing neuronal nicotinic acetylcholine receptors does not prevent nicotine-induced seizures. *Molecular Brain Research*, 98(1-2):29–40.

Freitas Jr, R. A. (1999). Nanomedicine: Is diamond biocompatible with living cells? IMM Report 12, Institute for Molecular Manufacturing.

Frewin, C., Locke, C., Saddow, S., and Weeber, E. (2011). Single-crystal cubic silicon carbide: An in vivo biocompatible semiconductor for brain machine interface devices. In *Engineering in Medicine and Biology Society, EMBC, 2011 Annual International Conference of the IEEE*, pages 2957–2960. IEEE.

Fuxe, K., Ferre, S., Zoli, M., and Agnati, L. (1998). Integrated events in central dopamine transmission as analyzed at multiple levels. evidence for intramembrane adenosine a2a/dopamine d2 and adenosine a1/dopamine d1 receptor interactions in the basal ganglia. *Brain Research Reviews*, 26:258–73.

Gähwiler, B. H. and Dreifuss, J. J. (1982). Multiple actions of acetylcholine on hippocampal pyramidal cells in organotypic explant cultures. *Neuroscience*, 7(5):1243–56.

Gastaut, H. and Gastaut, J. (1976). Computerized transverse axial tomography in epilepsy. *Epilepsia*, 17:325–336.

Gennaro, L. D. and Ferrara, M. (2003). Sleep spindles:an overview. *Sleep Medicine Reviews*, 7(5):423–40.

Gennaro, L. D., Ferrara, M., and Bertini, M. (2000). The spontaneous k-complex during stage 2 sleep: is it the 'forerunner' of delta waves? *Neuroscience Letters*, 291(1):41–43.

Gerschenfeld, H. M. and Paupardin-Tritsch, D. (1974). On the transmitter function of 5-hydroxytryptamine at excitatory and inhibitory monosynaptic junctions. *Journal of Physiology*, 243(2):457–481.

Gholipour, T., Mojtahed, A., and Dehpour, A. (2007). The 5-ht3 receptor antagonist granisetron lowers clonic seizure threshold in pentylenetetrazole induced seizure in mice: The involvement of nitric oxide system. In *Neurology Asia*, volume 12, page 110.

Gill, V., Hawkins, V., Mandalia, D., Whalley, R., and Fuller, E. (2012). Smoking, drinking and drug use among young people in england in 2011. *Health and Social Care Information Centre*.

Gillard, M., Chatelain, P., and Fuks, B. (2006). Binding characteristics of levetiracetam to synaptic vesicle protein 2a (sv2a) in human brain and in cho cells expressing the human recombinant protein. *European Journal of Pharmacology*, 536(1-2):102 – 108.

Grando, S., HOrton, A., Pereira, E., Diethelm-Okita, B., George, P., Albuquerque, E., and Conti-Fine, B. (1995). A nicotinic acetylcholine receptor regulating cell adhesion and motility expressed in human keratinocytes. *Journal of Investigative Dermatology*, 105:774–81.

Granon, S., Poucet, B., Thinus-Blanc, C., Changeux, J., and Vidal, C. (1995). Nicotinic and muscarinic receptors in the rat prefrontal cortex: differential roles in working memory, response selection and effortful processing. *Psychopharmacology*, 119:139–44.

Grenier, F. and Steriade, M. (2001). Spontaneous field potentials influence the activity of neocortical neurons during seizures. *Society of Neuroscience Abstr*, 27:559.

Grenier, F., Timofeev, I., and Steriade, M. (2003). Neocortical very fast oscillations (ripples, 80-200 hz) during seizures: Intracellular correlates. *Journal of Neurophysiology*, 89(2):841–52.

Gubbins, E. J., Gopalakrishnan, M., and Li, J. (2010). Alpha7 nachr-mediated activation of map kinase pathways in pc12 cells. *Brain Res*, 1328:1–11.

Haas, H. and Panula, P. (2003). The role of histamine and the tuberomammillary nucleus in the nervous system. *Nature Review Neuroscience*, 4:121–130.

Haas, H., Sergeeva, O., and Selbach, O. (2008). Histamine in the nervous system. *Physiology Review*, 88:1183–1241.

Hagberg, B., Aicardi, J., Dias, K., and Ramos, O. (1983). A progressive syndrome of autism, dementia, ataxia and loss of pureposeful hand use in girls: Rett's syndrome: Report of 35 cases. *Annals of Neurology*, 14(4):471–79.

Hagerman, P. and Stafstrom, C. (2009). Origins of epilepsy in fragile x syndrome. *Epilepsy Currents*, 9(4):108–112.

Hanein, Y., Böhringer, K., Wyeth, R. C., and Willows, A. O. D. (2002). Towards mems probes for intracellular recording. *Sensors Update*, 10:47–75.

Hanein, Y., Lang, U., Theobald, J., Wyeth, R., Daniel, T., Willows, A., Denton, D., and Böhringer, K. (2001). Intracellular neuronal recording with high aspect ratio mems probes. *Proceedings of the 11th International Conference on Solid-State Sensors and Actuators*, -:386.

Hanein, Y., Schabmueller, C. G. J., Holman, G., Lucke, P., Denton, D. D., and Böhringer, K. F. (2003). High-aspect ratio submicrometer needles for intracellular applications. *Journal of Micromechanical Microengineering*, 13(4):S91–S95.

Haranth, P. and Venkatakrishna-Bhatt, H. (1977). Sleep induced by drugs injected into the inferior horn of the lateral cerebral ventricle in dogs. *British Journal of Pharmacology*, 59(2):231–6.

Harvey, S. C., Maddox, F. N., and Luetje, C. W. (1996). Multiple determinants of dihydro-β-erythroidine sensitivity on rat neuronal nicotinic receptor α subunits. *Journal of neurochemistry*, 67(5):1953–1959.

Harvey-Girard, E., Lewis, J., and Maler, L. (2010). Burst-induced anti-hebbian depression acts through short-term synaptic dynamics to cancel redundant sensory signals. *J Neurosci*, 30(17):6152–69.

Hedlund, P. B., Huitron-Resendiz, S., Henriksen, S. J., and Sutcliffe, J. G. (2005). 5-ht7 receptor inhibition and inactivation induce antidepressantlike behavior and sleep pattern. *Biological Psychiatry*, 58(10):831–837.

Heubel, E. (1876). Die abhängigkeit des wachen gehirnzhstandes von ausseren erregungen. *Pflugers Arch.*, XIV.

Hill, L. (1866). *The physiology and pathology of the cerebral circulation; an experimental research*. J. and A. Churchill, London, England.

Hobson, J. A. and Pace-Schott, E. F. (2002). The cognitive neuroscience of sleep: Neuronal systems, consciousness and learning. *Nature Reviews Neuroscience*, 3:679–93.

Holmes, G. L. and Lenck-Santini, P.-P. (2006). Role of interictal epileptiform abnormalities in cognitive impairment. *Epilepsy and Behaviour*, 8(3):504–15.

Holscher, C., Anwyl, R., and Rowan, M. (1997). Stimulation on the positive phase of hippocampal theta rhythm induces long-term potentiation that can be depotentiated by stimulation on the negative phase in area ca1 in vivo. *The Journal of Neurocience*, 17:6470–6477.

Hope, A., Belelli, D., Mair, I., Lambert, J., and Peters, J. (1999). Molecular determinants of (+)-tubocurarine binding at recombinant 5-hydroxytryptamine3a receptor subunits. *Molecular Pharmacology*, 55(6):1037–43.

Huber, R., Ghilardi, M. F., Massimini, M., and Tononi, G. (2004). Local sleep and learning. *Nature*, 430:78–81.

Huerta, P. and Lisman, J. (1996). Bidirectional synaptic plasticity induced by a single burst during cholinergic theta oscillation in ca1 in vitro. *Neuron*, 15:1053–63.

Hughes, J. R. (1994). *EEG in Clincial Practice*. Butterworth-Heinemann, 2nd edition.

Hughes, S. W., Cope, D. W., and Crunelli, V. (1998). Dynamic clamp study of ih modulation of burst firing and delta oscillations in thalamocortical neurons in vitro. *Neuroscience*, 87(3):541–50.

Idzikowski, C., Mills, F., and Glennard, R. (1986). 5-hydroxy-tryptamine-2 antagonist increase human slow waves sleep. *Brain Research*, 378:164–8.

Inoue, S., Honda, K., and Komoda, Y. (1995). Sleep as neuronal detoxification and restitution. *Behavioural Brain Research*, 69(1):91.

Ioannides, A. A., Kostopoulos, G. K., Liu, L., and Fenwick, P. B. C. (2009). Meg identifies dorsal medial brain activations during sleep. *Neuroimage*, 44(2):455–68.

Isomura, Y., Sirota, A., Ozen, S., Montgomery, S. M., Mizuseki, K., Henze, D., and Buzsaki, G. (2006). Integration and segregation of activity in entorhinal-hippocampal subregions by neocortical slow oscillations. *Neuron*, 52(5):871–82.

Jaimchariyatam, N., Rodriquez, C., and Budur, K. (2011). Prevalence and correlates of alpha-delta sleep in major depressive disorders. *Innovations in Clinical Neuroscience*, 8(7):35–49.

Ji, D. and Dani, J. A. (2000). Inhibition and disinhibition of pyramidal neurons by activation of nicotinic receptors on hippocampal interneurons. *J Neurophysiol*, 83(5):2682–90.

Ji, J., Najafi, K., and Wise, K. (1989). A scaled electronically-configurable multichannel recording array. *Sensors and Actuators A: Physical*, 22(1):589–591.

Jia, Y., Yamazaki, Y., Nakauchi, S., Ito, K.-I., and Sumikawa, K. (2010). Nicotine facilitates long-term potentiation induction in oriens-lacunosum moleculare cells via ca2+ entry through non-alpha7 nicotinic acetylcholine receptors. *Eur J Neurosci*, 31(3):463–76.

Johnson, P., Moratalla, R., Lightman, S., and Lowry, C. (2005). Are tuberomammillary histaminergic neurons involved in co2-mediated arousal? *Exp Neurology*, 193:228–233.

Johnston, D. and Brown, T. H. (1981). Giant synaptic potential hypothesis for epileptiform activity. *Science*, 211(4479):294–7.

Johnston, D. and Brown, T. H. (1984). The synaptic nature of the paroxysmal depolarizing shift in hippocampal neurons. *Ann Neurol*, 16 Suppl:S65–71.

Jones, E. (1998). *Neuroscience*, 85(331-45).

Jouvet, M. (1969). Biogenic amines and the states of sleep. *Science*, 163:32–41.

Jouvet, M. (1999). Sleep and serotonin: An unfinished story. *Neuropsychopharmocology*, 21(2S):24S–27S.

Kabuto, H., Yokoi, I., and Ogawa, N. (1998). Melatonin inhibits iron-induced epileptic discharges in rats by suppressing preoxidation. *Epilepsia*, 39(3):237–43.

Kafka, M. S., Benedito, M. A., Blendy, J. A., and Tokola, N. S. (1986). Circadian rhythms in neurotransmitter receptors in discrete rat brain regions. *Chronobiol Int*, 3(2):91–100.

Kaiser, M., Hilgetag, C. C., and Kotter, R. (2010). Hierarachy and dynamics of neural networks. *Frontiers in Neuroinformatics*, 4(112):1–3.

Kandel, E. R., Schwartz, J. H., and Jessell, T. M., editors (2000). *Principles of Neural Science*. McGraw-Hill Companies Inc., international edition edition.

Karlin, A. (2002). Emerging structure of the nicotinic acetylcholine receptors. *Nat Rev Neurosci*, 3(2):102–14.

Kipke, D. R., Vetter, R. J., Williams, J. C., and Hetke, J. F. (2003). Silicon-substrate intracortical microelectrode arrays for long-term recording of neuronal spike activity in cerebral cortex. *IEEE Transactions on Neural Systems and Rehabilitation Engineering*, 11(2):151–155.

Klein, J. P., Khera, D. S., Nersesyan, H., Kimchi, E. Y., Waxman, S. G., and Blumenfeld, H. (2004). Dysregulation of sodium channel expression in cortical neurons in a rodent model of absence epilepsy. *Brain research*, 1000(1):102–109.

Klink, R., de Kerchove d'Exaerde, A., Zoli, M., and Changeux, J. P. (2001). Molecular and physiological diversity of nicotinic acetylcholine receptors in the midbrain dopaminergic nuclei. *J Neurosci*, 21(5):1452–63.

Kojima, M., Kato, H., and Gatto, M. (1994). Model for the dry etching of heavily doped n-type silicon by atomic fluorine in the absence of ion bombardment. *Journal of applied physics*, 75(11):7507–7513.

Korn, S. J., Giacchino, J. L., Chamberlin, N. L., and Dingledine, R. (1987). Epileptiform burst activity induced by potassium in the hippocampus and its regulation by gaba-mediated inhibition. *J Neurophysiol*, 57(1):325–40.

Kotzar, G., Freas, M., Abel, P., Fleischman, A., Roy, S., Zorman, C., Moran, J. M., and Melzak, J. (2002). Evaluation of mems materials of construction for implantable medical devices. *Biomaterials*, 23(13):2737–2750.

Krahn, L. E., Silber, M. H., and Morgenthaler, T. I. (2009). *Atlas of Sleep and Sleep Medicine*. Taylor & Francis.

Kubota, F., Shibata, N., Shiihara, Y., Takahashi, S., and Ohsuka, T. (1997). Frontal lobe epilepsy with secondarily generalized 3 hz spike-waves: a case report. *Clin Electroencephalogr*, 28(3):166–71.

Kuenzi, F. M., Fitzjohn, S. M., Morton, R. A., Collingridge, G. L., and Seabrook, G. R. (2000). Reduced long-term potentiation in hippocampal slices prepared using sucrose-based artificial cerebrospincal fluid. *Journal of Neuroscience Methods*, 100:117–22.

Kurahashi, H. and Hirose, S. (2002). Autosomal dominant nocturnal frontal lobe epilepsy. GeneReviews [Internet].

Lachowicz, J. E. and Sibley, D. R. (1997). Molecular characteristics of mammalian dopamine receptors. *Pharmacology and Toxicology*, 81:105–13.

Lagerlund, T. D., Sharbrough, F. W., and Busacker, N. E. (1997). Spatial filtering of multichannel electroencephalographic recordings through principal component analysis by singular value decomposition. *J Clin Neurophysiol*, 14(1):73–82.

Lakatos, P., Shah, A. S., Knuth, K. H., Ulbert, I., Karmos, G., and Schroeder, C. E. (2005). An oscillatory hierarchy controlling neuronal excitability and stimulus processing in the auditory cortex. *J Neurophysiol*, 94(3):1904–11.

Laurie, D. J., Seeburg, P. H., and Wisden, W. (1992). The distribution of 13 gabaa receptor subunit mrnas in the rat brain. ii. olfactory bulb and cerebellum. *J Neurosci*, 12(3):1063–76.

Lazarova, M., Bendotti, C., and Samanin, R. (1983). Studies on the role of serotonin in different regions of the rat central nervous system on pentylenetetrazol-induced seizures and the effect of di-n-propyl-acetate. *Archive of Pharmacology*, 322:147–152.

Le Moine, C. and Gaspar, P. (1998). Subpopulations of cortical gabaergic interneurons differ by their expression of d1 and d2 dopamine receptor subtypes. *Molecular Brain Research*, 58:231–6.

Le Van Quyen, M., Staba, R. J., Bragin, A., Dickson, C., Valderrama, M., Fried, I., and Engel Jr, J. (2010). Large-scale microelectrode recrdings of high-frequency gamma oscillations in human cortex during sleep. *The Journal of Neuroscience*, 30(23):7770–82.

Lee, K., Massia, S., and He, J. (2005). Biocompatible benzocyclobutene-based intracortical neural implant with surface modification. *Journal of Micromechanics and Microengineering*, 15(11):2149.

Lee, S., Hjerling-Leffler, J., Zagha, E., Fishell, G., and Rudy, B. (2010a). The largest group of superficial neocortical gabaergic interneurons expresses ionotropic serotonin receptors. *J Neurosci*, 30(50):16796–808.

Lee, S.-H., Földy, C., and Soltesz, I. (2010b). Distinct endocannabinoid control of gaba release at perisomatic and dendritic synapses in the hippocampus. *J Neurosci*, 30(23):7993–8000.

Leech, P., Reeves, G., and Holland, A. (2001). Reactive ion etching of diamond in cf4, o2, o2 and ar-based mixtures. *Journal of materials science*, 36(14):3453–3459.

Lena, I., Parrot, S., Deschaux, O., Muffat-Joly, S., Sauvinet, V., Renaud, B., Suaud-Chagny, M., and Gottesmann, C. (2005). Variations in extracellular levels of dopamine,

noradrenaline, glutamate and asparate across the sleep-wake cycle in the medial prefrontal cortex and nucleus accumbens of freely moving rats. *Journal of Neuroscience Research*, 81(6):891–9.

Leresche, N., Parri, H. R., Erdemli, G., Guyon, A., Turner, J. P., Williams, S. R., Asprodini, E., and Crunelli, V. (1998). On the action of the anti-absence drug ethosuximide in the rat and cat thalamus. *J Neurosci*, 18(13):4842–53.

Lesca, G., Rudolf, G., Labalme, A., Hirsch, E., Arzimanoglou, A., Genton, P., Motte, J., de Saint Martin, A., Valenti, M.-P., Boulay, C., De Bellescize, J., Kéo-Kosal, P., Boutry-Kryza, N., Edery, P., Sanlaville, D., and Szepetowski, P. (2012). Epileptic encephalopathies of the landau-kleffner and continuous spike and waves during slow-wave sleep types: genomic dissection makes the link with autism. *Epilepsia*, 53(9):1526–38.

Li, K. and Xu, E. (2008). The role and the mechanism of gamma-aminobutyric acid during central nervous system development. *Neurosci Bull*, 24(3):195–200.

Lin, H., Vicini, S., Hsu, F.-C., Doshi, S., Takano, H., Coulter, D. A., and Lynch, D. R. (2010). Axonal 7 nicotinic ach receptors modulate presynaptic nmda receptor expression and structural plasticity of glutamatergic presynaptic boutons. *Proc Natl Acad Sci U S A*, 107(38):16661–6.

Liu, F., Wan, Q., Pristupa, Z. B., Yu, X. M., Wang, Y. T., and Niznik, H. B. (2000). Direct protein-protein coupling enables cross-talk between dopamine d5 and gamma-aminobutyric acid a receptors. *Nature*, 403(6767):274–80.

Livingstone, M. S. and Hubel, D. H. (1981). Effects of sleep and arousal on the processing of visual information in the cat. *Nature*, 291(5816):554–61.

Llinas, R. (1988). The intrinsic electrophysiological properties of mammalian neurons: Insights into central nervous system function. *Science*, 242:1654–64.

Loddenkemper, T., Fernández, I. S., and Peters, J. M. (2011). Continuous spike and waves during sleep and electrical status epilepticus in sleep. *J Clin Neurophysiol*, 28(2):154–64.

Lorincz, M., Bao, Y., Crunelli, V., and Hughes, S. (2007). Number 881.19. Society of Neuroscience.

Lorincz, M., Bao, Y., Crunelli, V., and Hughes, S. (2008). Number 41.6. Society of Neuroscience.

Lu, L., Chou, T., and Saper, C. B. (2006). Identification of wake-active dopaminergic neurons in the ventral periaqueductal gray matter. *Journal of Neuroscience*, 26(1):193–202.

Luo, S., Kulak, J. M., Cartier, G. E., Jacobsen, R. B., Yoshikami, D., Olivera, B. M., and McIntosh, J. M. (1998). α-conotoxin auib selectively blocks $\alpha 3\beta 4$ nicotinic acetylcholine receptors and nicotine-evoked norepinephrine release. *The Journal of neuroscience*, 18(21):8571–8579.

Lüttjohann, A., Schoffelen, J.-M., and van Luijtelaar, G. (2013). Peri-ictal network dynamics of spike-wave discharges: phase and spectral characteristics. *Exp Neurol*, 239:235–47.

Lydic, R. and Biebuyck, J., editors (1988). *Clinical Physiology of Sleep*, chapter 1. Central regulation of sleep and autonomic physiology by R. Lydic, pages 1–19. American Physiological Society, Bethesda.

Mahmoodi, M. and Ghazanfari, L. (2011). Fundamentals of biomedical applications of biomorphic sic. *Properties and App lications of Silicon Carbide. In-Tech*, pages 297–345.

Manning, J. P. A., Richards, D. A., Leresche, N., Crunelli, V., and Bowery, N. G. (2004). Cortical-area specific block of genetically determined absence seizures by ethosuximide. *Neuroscience*, 123(1):5–9.

Mansvelder, H. D., van Aerde, K. I., Couey, J. J., and Brussaard, A. B. (2006). Nicotinic modulation of neuronal networks: from receptors to cognition. *Psychopharmacology (Berl)*, 184(3-4):292–305.

Marescaux, C., Vergnes, M., and Depaulis, A. (1992). Genetic absence epilepsy in rats from strasbourg–a review. *J Neural Transm Suppl*, 35:37–69.

Maricq, A., Peterson, A., Brake, A., Myers, R., and Julius, D. (1991). Primary structure and functional expression of the 5ht3 receptor, a serotonin-gated ion channel. *Science*, 254(5030):432–7.

Marini, C. and Guerrini, R. (2007). The role of the nicotinic acetylcholine receptors in sleep-related epilepsy. *Biochemical Pharmacology*, 74:1308–1314.

McClelland, J., McNaughton, B., and O'Reilly, R. (1995). Why there are complementary learning systems in the hippocampus and neocortex: insights from the successes and failures of connectionist models of learning and memory. *Psychology Review*, 102:419–57.

McCormick, D. and Pape, H. (1990). Properties of a hyperpolarization-activated cation current and its role in rhythmic oscillation in thalamic relay neurones. *Journal of Physiology*, 431:291–318.

McCormick, D. A., Connors, B. W., Lighthall, J. W., and Prince, D. A. (1985). Comparative electrophysiology of pyramidal and sparsely spiny stellate neurons of the neocortex. *Journal of Neurophysiology*, 54(4):782–806.

McEntee, W. J. and Crook, T. H. (1993). Glutamate: its role in learning, memory, and the aging brain. *Psychopharmacology*, 111(4):391–401.

McKeown, M. J., Humphries, C., Iragui, V., and Sejnowski, T. J. (1999). Spatially fixed patterns account for the spike and wave features in absence seizures. *Brain Topogr*, 12(2):107–16.

McKernan, R. M. and Whiting, P. J. (1996). Which gabaa-receptor subtypes really occur in the brain? *Trends Neurosci*, 19(4):139–43.

McTague, A. and Cross, J. H. (2013). Treatment of epileptic encephalopathies. *CNS Drugs*, 27(3):175–84.

Medvedev, A., Mackenzie, L., Hiscock, J. J., and Willoughby, J. O. (1996). Frontal cortex leads other brain structures in generalised spike-and-wave spindles and seizure spikes induced by picrotoxin. *Electroencephalogr Clin Neurophysiol*, 98(2):157–66.

Meldrum, B. S. (1994). The role of glutamate in epilepsy and other cns disorders. *Neurology*, 44(11 Suppl 8):S14–23.

Mena-Segovia, J., Sims, H., Magill, P., and Bolam, J. (2008). Cholinergic brainstem neurons modulate cortical gamma activity during slow oscillations. *Journal of Physiology*, 586:2947–60.

Merica, H. (2000). Fast and slow frequency spindles in sleep: two generators? *Clinical Neurophysiology*, 111(9):1704–5.

Metz-Lutz, M.-N. and Filippini, M. (2006). Neuropsychological findings in rolandic epilepsy and landau-kleffner syndrome. *Epilepsia*, 47(S2):71–75.

Michelucci, R., Rubboli, G., and Plasmati, R. (1987). Clinical relevance of various eeg features of electrical status epilepticus during slow sleep. In *Book of Abstracts*, Jerusalem. 17th Epilepsy International Congress.

Midzianovskaia, I. S., Kuznetsova, G. D., Coenen, A. M., Spiridonov, A. M., and van Luijtelaar, E. L. (2001). Electrophysiological and pharmacological characteristics of two types of spike-wave discharges in wag/rij rats. *Brain Res*, 911(1):62–70.

Misulis, K. E. and Head, T. C. (2003). *Essentials of Clincial Neurophysiology*. Garland Science, 3rd edition.

Mitchell, S. and Ranck, J. J. (1980). Generation of theta rhythm in medial entorhinal cortex of freely moving rats. *Brain Research*, 189(1):49–66.

Molle, M., Marchall, L., Gais, S., and Born, J. (2002). Grouping of spindle activity during slow oscillations in human non-rapid eye movement sleep. *The Journal of Neurocience*, 22(24):10941–7.

Montgomery, S. M. (2002). Extracellular electrophysiology.

Monti, J., Hawkins, M., and Jantos, H. a. (1988a). Biphasic effects if dopamine d-2 receptor agonist on sleep and wakefulness in the rat. *Psychopharmacology*, 95:395–400.

Monti, J., Jantos, H., and Fernandez, M. (1988b). Effects of the selective deopamine d-2 receptor agaonist, quinpirole on sleep and wakefulness in the rat. *European Journal of Pharmacology*, 169:61–6.

Monti, J., Monti, D., Jantos, H., and Ponzoni, A. (1995). Effects of selective activitation of the 5-ht1b receptor with cp-94,253 on sleep and wakfulness in the rat. *Neuropharmacology*, 34:1647–51.

Monti, J. M. (2011). Serotonin control of sleep-wake behaviour. *Sleep Medicine Reviews*, 15:269–81.

Monti, J. M., Fernandez, M., and Jantos, H. (1990). Sleep during acute dopamine d1 agonist skf38393 or d1 antagonist sch23390 administration in rats. *Neuropsychopharmacology*, 3:153–62.

Monti, J. M. and Jantos, H. (1992). Dose dependent effects of the 5-ht1a receptor agonist 8-oh-dpat on sleep and wakefulness in the rat. *Journal of Sleep Research*, 1(3):169–175.

Monti, J. M., Leopoldo, M., and Jantos, H. (2008). The serotonin 5-ht7 agonist lp-44 microinjected into the dorsal raphe nucleus suppresses rem sleep in the rat. *Behavioural Brain Research*, 191:184–9.

Monti, J. M. and Monti, D. (2007). The involvement of dopamine in the modulation of sleep and waking. *Sleep Medicine reviews*, 11(2):113–33.

Morikawa, T., Seino, M., Watanabe, M., et al. (1995). *Continuous Spikes and Waves During Slow Sleep, Electrical Status Epilepticus During Slow Sleep: Acquired Epileptic Aphasia and Related Conditions*, chapter Long-term outcome of CSWS syndrome, pages 27–36. John Libbey.

Moulard, B., Picard, F., le Hellard, S., Agulhon, C., Weiland, S., Favre, I., Bertrand, S., Malafosse, A., and Bertrand, D. (2001). Ion channel variation causes epilepsies. *Brain Res Brain Res Rev*, 36(2-3):275–84.

Mount, D. B., Mercado, A., Song, L., Xu, J., Jr., A. L. G., Delpire, E., and Gamba, G. (1999). Cloning and characterization of kcc3 and kcc4, new members of the cation-chloride cotransporter gene family. *The Journal of Biological Chemistry*, 274(23):16355–62.

Murrin, L. and Zeng, W. (1990). Ontogeny of dopamine d1 receptors in rat forebrain: a quantitative autoradiographic study. *Developmental Brain Research*, 57(1):7–13.

Musumeci, S., Hagerman, R., Ferri, R., Bosco, P., Dalla Bernadino, B., Tassarini, C., DeSarro, G., and Elia, M. (1999). Epilepsy and eeg findings in males with fragile x syndrome. *Epilepsia*, 40:1092–9.

Musumecia, S., Ferri, R., Elia, M., Colognola, R., Bergonzi, P., and Tassinari, C. (1991). Epilepsy and fragile x syndrome: a follow-up study. *American Journal of Medical Genetics*, 38:511–13.

Muthuswamy, J., Okandan, M., Jain, T., and Gilletti, A. (2005). Electrostatic microactuators for precise positioning of neural microelectrodes. *Biomedical Engineering, IEEE Transactions on*, 52(10):1748–1755.

Nadasdy, A., Hirase, H., Czurko, A., Csicsvari, J., and Buzsaki, G. (1999). Replay and time compression of recurring spike sequences in the hippocampus. *Journal of Neuroscience*, 9:9497–507.

Nai, Q., McIntosh, J. M., and Margiotta, J. F. (2003). Relating neuronal nicotinic acetylcholine receptor subtypes defined by subunit composition and channel function. *Mol Pharmacol*, 63(2):311–24.

Nass, R. and Gross, A. (2001). *Epilepsy and Developmental Disabilities*, chapter Landau-Kleffner suyndromme and its variants, pages 72–92. Butterworth-Heinemann, Boston.

Neubauer, B. A. (2000). The genetics of rolandic epilepsy. *Epilepsia*, 41(8):1061–62.

Neubauer, B. A., Fiedler, B., Himmelein, B., Kampfer, F., Lassker, U., Schwabe, G., Spanier, I., Tams, D., Bretscher, C., Moldenhauer, K., Kurlemann, G., Weise, S., Tesroff, K., Eeg-Olofsson, O., Wadelius, C., and Stephani, U. (1998). Centrotemporal spikes in families with rolandic epilepsy - linkage to chromosome 15q14. *Neurology*, 51:1608–12.

Neubauer, B. A., Moises, H., Lassker, U., Waltz, S., Diebold, U., and Stephani, U. (1997). Benign childhood epilepsy with centrotemporal spikes and electroencephalography trait are not linked to ebn1 and ebn2 of benign famial convulsions. *Epilepsia*, 38:782–7.

Neumann, A., Reske, T., Held, M., Jahnke, K., Ragoss, C., and Maier, H. (2004). Comparative investigation of the biocompatibility of various silicon nitride ceramic qualities in vitro. *Journal of Materials Science: Materials in Medicine*, 15(10):1135–1140.

Ngomba, R. T., Ferraguti, F., Badura, A., Citraro, R., Santolini, I., Battaglia, G., Bruno, V., De Sarro, G., Simonyi, A., van Luijtelaar, G., and Nicoletti, F. (2008). Positive allosteric modulation of metabotropic glutamate 4 (mglu4) receptors enhances spontaneous and evoked absence seizures. *Neuropharmacology*, 54(2):344–54.

Niedermeyer, E. and da Silva, F. L. (2004a). *Electroencephalography: Basic Principles, Clinical Applications, and Related Fields*, chapter 13. Abnormal EEG Patterns: Epileptic and Paroxysmal, pages 255–280. Lippincott Williams and Wilkins.

Niedermeyer, E. and da Silva, F. L. (2004b). *Electroencephalography: Basic Principles, Clinical Applications, and Related Fields*, chapter 27. Epileptic Seizure Disorders, pages 476–585. Lippincott Williams and Wilkins.

Niedermeyer, E. and Sakkubai, N. (1990). Further eeg observations in children with the rett syndrome. *Brain and Development*, 12(1):53–4.

NISBET, H. I. (1959). Status epilepticus treated with d-tubocurarine and controlled respiration. *Br Med J*, 1(5114):95–6.

Nishida, M., Asano, E., Juhász, C., Muzik, O., Sood, S., and Chugani, H. T. (2008). Cortical glucose metabolism correlates negatively with delta-slowing and spike-frequency in epilepsy associated with tuberous sclerosis. *Hum Brain Mapp*, 29(11):1255–64.

Normann, R., Campbell, P., and Jones, K. (1993). Three-dimensional electrode device.

Normann, R. A., Maynard, E. M., Rousche, P. J., and Warren, D. J. (1999). A neural interface for a cortical vision prosthesis. *Vision Research*, 39:2577–2587.

Olandi, A., Zucconi, M., Asselta, R., Modugno, M., Bonati, M. T., Dalpra, L., Malcovati, M., Tenchini, M. L., Smirne, S., and Ferini-Strambi, L. (1998). Autosomal dominant nocturnal frontal lobe epilepsy : A video-polysomnographic and genetic appraisal of 40 patients and delineation of the epileptic syndrome. *Brain*, 121:205–223.

Olsson III, R. H., Buhl, D. L., Sirota, A. M., Buzsaki, G., and Wise, K. D. (2005). Band-tunable and multiplexed integrated circuits for simultaneous recording and stimulation with microelectrode arrays. *Biomedical Engineering, IEEE Transactions on*, 52(7):1303–1311.

Ongini, E., Caporali, M., and Massotti, M. (1985). Stimulation of dopamine d-1 receptors by kf 38393 induces eeg desynchronization and behavioral arousal. *Life Sciences*, 37(24):2327–33.

Orcutt, J. A., Michaelson, S. M., and Prytherch, J. P. (1963). The inhibition of nicotine-induced convulsions in the rat. *Arch Int Pharmacodyn Ther*, 146:238–44.

Osborne, J. (1849). Tending to prove that the choroid plexus is the organ of sleep. *Journal of Practical Medicine*, pages 977–82.

Ostojić, Z. S., Ilić, T. V., Vesković, S. M., and Andjus, P. R. (2013). Gabab receptors as a common target for hypothermia and spike and wave seizures: Intersecting mechanisms of thermoregulation and absence epilepsy. *Neuroscience*, 238C:39–58.

Palma, E., Bertrand, S., Binzoni, T., and Bertrand, D. (1996). Neuronal nicotinic alpha 7 receptor expressed in xenopus oocytes presents five putative binding sites for methyllycaconitine. *J Physiol*, 491 (Pt 1):151–61.

Pan, A., Gupta, A., Wyllie, E., Lüders, H., and Bingaman, W. (2004). Benign focal epileptiform discharges of childhood and hippocampal sclerosis. *Epilepsia*, 45(3):284–8.

Panayiotopoulos, C. P. (2008). Autosomal dominant nocturnal frontal lobe epilepsy, adapted from the epileptic syndromes.

Parisi, P., Bruni, O., Villa, M. P., Verrotti, A., Miano, S., Luchetti, A., and Curatolo, P. (2010). The relationship between sleep and epilepsy: the effect on cognitive functioning in children. *Developmental Medicine and Child Neurology*, 52:805–10.

Parrino, L., Halasz, P., Tassinari, C., and Terzano, M. (2006). Cap, epilepsy and motor events during sleep: the unifying role of arousal. *Sleep Medicine Reviews*, 10(4):267–85.

Pavone, P., Bianchini, R., Trifiletti, R., Incorpora, G., Pavone, A., and Parano, E. (2001). Neuropsychological assessment in children with absence epilepsy. *Neurology*, 56:1047–51.

Paxinos, G. and Watson, C. (1998). *The Rat Brain in stereotaxic coordinates*. Academic Press.

Pedersen, S. and Cohen, J. (1990). d-tubocurarine binding sites are located at alpha-gamma and alpha-delta subunit interfaces of the nicotinic acetylcholine receptor. *Proceedings of the National Academy of Sciences of the USA*, 87(7):2785–9.

Peled, N., Shorer, Z., Peled, E., and Pillar, G. (2001). Melatonin effect on seizures in children with severe neurological deficit disorders. *Epilepsia*, 42(9):1208–1210.

Pellegrini, A., Musgrave, J., and Gloor, P. (1979). Role of afferent input of subcortical origin in the genesis of bilaterally synchronous epileptic discharges of feline generalized penicillin epilepsy. *Experimental neurology*, 64(1):155–173.

Penfield, W. L. B., Erickson, T. C., Jasper, H. H., and Harrower-Erickson, M. R. (1942). Epilepsy and cerebral localization. *American Journal of Medical Sciences*, 203(3):431.

Perry, E. and Perry, R. (1995). Acetylcholine and hallucinations - disease-related compared to drug-induced alterations in human consciousness. *Brain and Cognition*, 28(3):240 – 258.

Perry, E., Walker, M., Grace, J., and Perry, R. (1999). Acetylcholine in mind: a neurotransmitter correlate of consciousness? *Trends in Neuroscience*, 22:273–80.

Peters, J. A., Malone, H. A., and Lambert, J. J. (1990). Antagonism of 5-ht3 receptor mediated currents in murine n1e-115 neuroblastoma cells by (+)-tubocurarine. *Neuroscience Letters*, 110(1-2):107–112.

Picard, F., Bruel, D., Servent, D., Saba, W., Fruchard-Gaillard, C., and Schollhorn-Peyronneau, M. A. (2006). Alteration of the in vivo nicotinic receptor density in adnfle patients: a pet study. *Brain*, 129(8):2047–60.

Picard, F., Pegna, A., Arntsberg, V., Lucas, N., Kaczmarek, I., Todica, O., Chiriaco, C., Seeck, M., and Brodtkorb, E. (2009). Neuropsychological disturbances in frontal lobe epilepsy due to mutated nicotinic receptors. *Epilepsy Behaviour*, 14:354–9.

Pinault, D., Vergnes, M., and Marescaux, C. (2001). Medium-voltage 5-9-hz oscillations give rise to spike-and-wave discharges in a genetic model of absence epilepsy: in vivo dual extracellular recording of thalamic relay and reticular neurons. *Neuroscience*, 105(1):181–201.

Pinton, F., Ducot, B., Motte, J., Arbues, A.-S., Barondiot, C., Barthez, M.-A., Chaix, Y., Cheminal, R., Livet, M.-O., Penniello, M.-J., Peudenier, S., de Saint-Martin, A.,

and Billard, C. (2006). Cognitive functions in children with benign childhodd epilepsy with centrotemporal spikes (bects). *Epileptic Disorders*, 8(1):11–23.

Pivik, R. and Harman, K. (1995). A reconceptualization of eeg alpha activity as an index of arousal during sleep: all alpha activity is not equal. *Journal of Sleep Research*, 4(3):131–7.

Plihal, W. and J, B. (1997). Effects of early and late nocturnal sleep on declarative and procedural memory. *Journal of Cognitive Neuroscience*, 9:534–547.

Ponzoni, A., Jaime, M. M., and Jantos, H. (1993). The effects of selective activation of the 5-ht3 receptor with m-chlorophenylbiguanide on sleep and wakefulness in the rat. *European Journal of Pharmacology*, 249:259–64.

Ponzoni, A., Monti, J., Jantos, H., Altier, H., and Monti, D. (1995). Increased waking after intra-accumbens injection of m-chlorophe- nylbiguanide: prevention with serotonin or dopamine receptor an- tagonists. *European Journal of Pharmacology*, 278:111–5.

Popesko, P., Rajtova, V., and Horak, J. (1990). *Colour atlas of anatomy of small laboratory animals: rat, mouse, golden hamster*, volume 2. Saunders Ltd.

Porri, S. and Korff, C. M. (2010). Epilepsy in fragile x suyndrome: an illustrative case report. *Epileptologie*, 27:178–181.

Pugh, P., Corriveau, R., Conroy, W., and Berg, D. (1995). Novel subpopulation of neuronal acetylcholie receptors among those beinding alpha-bungarotoxin. *Molecular Pharmacology*, 47:717–25.

Queiroz, C. M. and Mello, L. E. (2007). Synaptic plasticity of the ca3 commissural projection in epileptic rats: an in vivo electrophysiological study. *European Journal of Neuroscience*, 25(10):3071–3079.

Rabow, L. E., Russek, S. J., and Farb, D. H. (1995). From ion currents to genomic analysis: recent advances in gabaa receptor research. *Synapse*, 21(3):189–274.

Raggenbass, M. and Bertrand, D. (2002). Nicotinic receptors in circuit excitability and epilepsy. *J Neurobiol*, 53(4):580–9.

Rauchs, G., Bertran, F., Guillery-Girard, B., Desgranges, B., Kerrouche, N., Denise, P., Foret, J., and Eustache, F. (2004). Consolidation of strictly episodic memories mainly requires rapid eye movement sleep. *Journal of Sleep and sleep disorders research*, 27(3):395–401.

Rauchs, G., Desgranges, B., Foret, J., and Eustache, F. (2005). The relationships between memory systems and sleep stages. *Journal of Sleep research*, 14:123–140.

Reiner, P. and Kamondi, A. (1994). Mechanisms of antihistamine-induced sedation in the human brain: H1 receptor activation reduces a background leakage potassium current. *Neuroscience*, 59:59–588.

Richardson, R., Miller, J., and Reichert, W. (1993). Polyimides as biomaterials: preliminary biocompatibility testing. *Biomaterials*, 14(8):627–635.

Rigas, P. and Castro-Alamancos, M. A. (2007). Thalamocortical up states: different eggects of intrinsic and extrinsic cortical inputs on persistent activity. *Journal of Neuroscience*, 27:4261–72.

Roediger, H., Dudai, Y., and Fitzpatrick, S. (2007). *Science of Memory Concepts*. Science of Memory. Oxford University Press, USA.

Roopun, A., Kramer, M., Carracedo, L., and Kaiser, M. (2008). Temporal interactions between cortical rhythms. *Frontiers in Neuroscience*, 2(2):145–154.

Roopun, A. K., Simonotto, J. D., Pierce, M. L., Jenkins, A., Nicholson, C., Schofield, I. S., Whittaker, R. G., Kaiser, M., Whittington, M. A., Traub, R. D., and Cunningham, M. O. (2010). A nonsynaptic mechanism underlying interictal discharges in human epileptic neocortex. *Proc Natl Acad Sci U S A*, 107(1):338–43.

Roth, C., Achermann, P., and Borbely, A. (1999). Alpha activity in the human rem sleep eeg: topography effect of rem sleep deprivation. *Clinical Neurophysiology*, 110(4):632–5.

Rousche, P. J. and Normann, R. A. (1998). Chronic recording capability of the utah intracortical electrode array in cat sensory cortex. *Journal of Neuroscience Methods*, 82:1–15.

Sakai, K. (1991). Physiological properties and afferent connections of the locus coeruleus and adjacent tegmental neurons involved in the generation of paradoxical sleep in the cat. *Progress in Brain Research*, 88:31–45.

Salas, R., Cook, K. D., Bassetto, L., and De Biasi, M. (2004). The 3 and 4 nicotinic acetylcholine receptor subunits are necessary for nicotine-induced seizures and hypolocomotion in mice. *Neuropharmacology*, 47(3):401–7.

Sanchez-Vives, M. V. and McCormick, D. A. (2000). Cellular and network mechanisms of rhythmic recurrent activity in neocortex. *Nature Neuroscience*, 3(10):1027–34.

Sanei, D. S. and Chambers, J. A. (2007). *EEG Signal Processing*. John Wiley and Sons Ltd.

Saper, C. B., Scammell, T. E., and Lu, J. (2005). Hypothalamic regulation of sleep and circadian rhythms. *Nature*, 437:1257–1263.

Schofield, P. R., Darlison, M. G., Fujita, N., Burt, D. R., Stephenson, F. A., Rodriguez, H., Rhee, L. M., Ramachandran, J., Reale, V., and Glencorse, T. A. (1987). Sequence and functional expression of the gaba a receptor shows a ligand-gated receptor superfamily. *Nature*, 328(6127):221–7.

Schulz, M. (1999). The end of the road for silicon? *Nature*, 399(6738):729–730.

Schwindt, P. C., Spain, W. J., and Crill, W. E. (1988). Influence of anomalous rectifier activation on afterhyperpolarizations of neurons from cat sensorimotor cortex in vitro. *J Neurophysiol*, 59(2):468–81.

SCS. Speciality coating systems: Electronics coatings data sheet. PDF.

Seifritz, E., Moore, P., Trachsel, L., Bhatti, T., Stahl, S., and Gillin, J. (1996). The 5-ht1a agonisr ipsapirone enhances eeg slow wave activity in human sleep and produces a power spectrum similar to 5-ht2 blockade. *Neuroscience Letters*, 209:41–4.

Shah, M. M., Migliore, M., and Brown, D. A. (2011). Differential effects of kv7 (m-) channels on synaptic integration in distinct subcellular compartments of rat hippocampal pyramidal neurons. *J Physiol*, 589(Pt 24):6029–38.

Shen, H., Sabaliauskas, N., Sherpa, A., Fenton, A. A., Stelzer, A., Aoki, C., and Smith, S. S. (2010). A critical role for alpha4betadelta gabaa receptors in shaping learning deficits at puberty in mice. *Science*, 327(5972):1515–8.

Shen, J.-x. and Yakel, J. L. (2009). Nicotinic acetylcholine receptor-mediated calcium signaling in the nervous system. *Acta Pharmacol Sin*, 30(6):673–80.

Shu, Y., Hasenstaub, A., and McCormick, D. (2003). Turning on and off recurrent balanced cortical activity. *Nature*, 423:288–93.

Siapas, A. G. and Wilson, M. A. (1998). Coordinated interactions between hippocampal ripples and cortical spindles during slow-wave sleep. *Neuron*, 21(5):1123–8.

Siddiqui, K. A., Siddiqui, I., Ali, R., and Benamer, H. (2007). Genes and epilepsy. *Pakistan Journal of Neurological Sciences*, 2(2):106–110.

Siebler, M., Köller, H., Schmalenbach, C., and Müller, H. W. (1988). Gaba activated chloride currents in cultured rat hippocampal and septal region neurons can be inhibited by curare and atropine. *Neurosci Lett*, 93(2-3):220–4.

Siegel, J. M. (2001). The rem sleep-memory consolidation hypothesis. *Science*, 294(5544):1058–63.

Singer, W. (2009). Distributed processing and temporal codes in neuronal networks. *Cognitive Neurodynamics*, 3:189–196.

Sirota, A., Csicsvari, J., Buhl, D., and Buzsáki, G. (2003). Communication between neocortex and hippocampus during sleep in rodents. *Proc Natl Acad Sci U S A*, 100(4):2065–9.

Sitnikova, E. and van Luijtelaar, G. (2005). Reduction of adrenergic neurotransmission with clonidine aggravates spike-wave seizures and alters activity in the cortex and the thalamus in wag/rij rats. *Brain Res Bull*, 64(6):533–40.

Sloviter, R. S. (1991). Permanently altered hippocampal structure, excitability, and inhibition after experimental status epilepticus in the rat: the "dormant basket cell" hypothesis and its possible relevance to temporal lobe epilepsy. *Hippocampus*, 1(1):41–66.

Smeets, E. E. J., Pelc, K., and Dan, B. (2011). Rett syndrome. *Molecular Syndromology*, 2:113–27.

Smith, R. (1985). Revovery and tissue repair. *Biritish Medical Bulletin*, 41(3):295–301.

Smith, S. (2005). Eeg in the diagnosis, classification, and management of patients with epilepsy. *Journal of Neurology, Neurosurgery and Psychiatry with practical neurology*, 76(s2):ii2–ii7.

Sommerfelt, L. and Ursin, R. (1993). The 5-ht2 antagonist ritanserin decreases sleep in cats. *Sleep*, 16:15–22.

Son, C. D., Moss, F. J., Cohen, B. N., and Lester, H. A. (2009). Nicotine normalizes intracellular subunit stoichiometry of nicotinic receptors carrying mutations linked to autosomal dominant nocturnal frontal lobe epilepsy. *Molecular pharmacology*, 75(5):1137–1148.

Soria-Jasso, L., Bahena-Trujillo, R., and Arias-Montano, J. (1997). Histamine h1 receptors and inositol phosphate formation in rat thalamus. *Neuroscience Letters*, 225:11–120.

Spain, W. J., Schwindt, P. C., and Crill, W. E. (1987). Anomalous rectification in neurons from cat sensorimotor cortex in vitro. *J Neurophysiol*, 57(5):1555–76.

Srejic, L. R., Valiante, T. A., Aarts, M. M., and Hutchison, W. D. (2013). High-frequency cortical activity associated with postischemic epileptiform discharges in an in vivo rat focal stroke model: Laboratory investigation. *Journal of neurosurgery*, pages 1–9.

Staba, R. J., Wilson, C. L., Bragin, A., Fried, I., and Engel Jr, J. (2002). Quantitative analysis of high frequency oscillations recored in human epileptic hippocampus and entorhinal cortex. *Journal of Neurophysiology*, 88:1743–52.

Stark, N. (1996). Literature review: biological safety of parylene c. *Medical Plastic and Biomaterials*, 3:30–35.

Statnick, M., Dailey, J., Jobe, P., and Browning, R. (1996). Abnormalities in brain serotonin concentration, high-affinity uptake, and tryptophan hydroxylase activity in severe-seizure genetically epilepsy-prone rats. *Epilepsia*, 37:311–21.

Steinlein, O., Hoda, J., Bertrand, S., and Bertrand, D. (2012). Mutations in familial nocturnal frontal lobe epilepsy might be associated with distinct neurological phenotypes. *Seizure*, 21(2):118–23.

Steinlein, O., Mulley, J., Propping, P., Wallace, P., Phillips, H., and Sutherland, G. (1995). A missense mutation in the neuronal nicotinic acetylcholine receptor alpha 4 subunit is associated with autosomal cominant nocturnal frontal lobe epilepsy. *National Genetics*, 11(2):201–3.

Steriade, M. (1994). Sleep oscillations and their blockage by activating systems. *Journal of Psychiatric Neuroscience*, 19(5):354–58.

Steriade, M. (2003). The cortticothalamic system in sleep. *Frontiers in Bioscience*, 8:878–99.

Steriade, M. (2006). Grouping of brain rhythms in corticothalamic systems. *Neuroscience*, 137(4):1087–106.

Steriade, M. and Amzica, F. (1996). Intracortical and corticothalamic coherency of fast spontaneous oscillations. *Proc Natl Acad Sci U S A*, 93(6):2533–8.

Steriade, M., Amzica, F., and Contreras, D. (1996). Synchronization of fast (30-40hz) spontaneous cortical rhythms during brain activation. *Journal of Neuroscience*, 16:392–417.

Steriade, M., Curro Dossi, R., and Nunez, A. (1991). Network modulation of a slow intrinsic oscillation of cat thalamocortical neurons implicated in sleep delta waves: cortically induced synchronization and brainstem cholinergic suppression. *The Journal of Neurocience*, 11(10):3200–17.

Steriade, M., McCormick, D. A., and Sejnowski, T. J. (1993a). Thalamocortical oscialltions in the sleeping and aroused brain. *Science*, 262(5134):679–85.

Steriade, M., Nunez, A., and Amzica, F. (1993b). Intracellular analysis of relations between the slow (¡1hz) neocortical oscillations and other sleep rhythms of electroencephalogram. *The Journal of Neuroscience*, 13:3266–83.

Steriade, M., Nunez, A., and Amzica, F. (1993c). A novel slow (¡1 hz) oscillation ofneocortical neurons in vivo: depolarizing and hyperpolarizing components. *The Journal of Neuroscience*, 13(8):3252–65.

Stevens, T. R., Krueger, S. R., Fitzsimonds, R. M., and Picciotto, M. R. (2003). Neuroprotection by nicotine in mouse primary cortical cultures involves activation of calcineurin and l-type calcium channel inactivation. *J Neurosci*, 23(31):10093–9.

Stickgold, R. and Walker, M. (2009a). *The Neuroscience of Sleep*, chapter 4.6 Acetylcholine by Jones, B.E. Academic Press.

Stickgold, R. and Walker, M. (2009b). *The Neuroscience of Sleep*, chapter 4.7 Dopamine by Fuller, P. M. and Lu, J. Academic Press.

Stickgold, R. and Walker, M. (2009c). *The Neuroscience of Sleep*, chapter 4.3 Histamine by Haas, H.L. and Selbach, O. and Sergeeva, O.A. Academic Press.

Stickgold, R. and Walker, M. (2009d). *The Neuroscience of Sleep*, chapter 4.5 Locus Coeruleus and Raphe Nucleus by Jones, B.E. Academic Press.

Stickgold, R. and Walker, M. (2009e). *The Neuroscience of Sleep*, chapter 2.1 Sleep Architecture by Pace-Scott, E.F. Academic Press.

Stickgold, R. and Walker, M. (2009f). *The Neuroscience of Sleep*, chapter PET Activation Patterns by Dang-Vu, T.T., Desseilles, M., Peigneux, P., Laureys, S. and Maquet, P., pages 30–36. Academic Press.

Stickgold, R. and Walker, M. (2009g). *The Neuroscience of Sleep*, chapter Thalamic Regulation of Sleep by A. Destexhe and T.J. Sejnowski, pages 87–90. Academic Press.

Stitzel, J. A., Jimenez, M., Marks, M. J., Tritto, T., and Collins, A. C. (2000). Potential role of the 4 and 6 nicotinic receptor subunits in regulating nicotine-induced seizures. *The Journal of Pharmacology and Experimental Therapeutics*, 293(1):67–74.

Strumwasser, F. (1958). Long-term recording from single neurons in brain of unrestrained mammals. *Science*, 127(3296):469–470.

Szabo, S. I., Zelles, T., Vizi, E. S., and Lendvai, B. (2008). The effect of nicotine on spiking activity and ca2+ dynamics of dendritic spines in rat ca1 pyramidal neurons. *Hippocampus*, 18(4):376–85.

Tabarean, I., Klein, I., Korn, H., and Bartfai, T. (2007). Bidirectional effects of histamine in preoptic/anterior hypothalamic neurons. *Society of Neuroscience Abstr*, 676:22.

Tanaka, S., Rajanna, K., Abe, T., and Esashi, M. (2001). Deep reactive ion etching of silicon carbide. *Journal of Vacuum Science & Technology B: Microelectronics and Nanometer Structures*, 19(6):2173–2176.

Tang, A.-H., Karson, M. A., Nagode, D. A., McIntosh, J. M., Uebele, V. N., Renger, J. J., Klugmann, M., Milner, T. A., and Alger, B. E. (2011). Nerve terminal nicotinic acetylcholine receptors initiate quantal gaba release from perisomatic interneurons by activating axonal t-type (cav3) ca channels and ca release from stores. *J Neurosci*, 31(38):13546–61.

Tao, J. X., Chen, X.-J., Baldwin, M., Yung, I., Rose, S., Frim, D., Hawes-Ebersole, S., and Ebersole, J. S. (2011). Interictal regional delta slowing is an eeg marker of epileptic network in temporal lobe epilepsy. *Epilepsia*, 52(3):467–76.

Tassinari, C. A., Rubboli, G., Volpi, L., Meletti, S., d'Orsi, G., Franca, M., Sabetta, A. R., Riguzzi, P., Gardella, E., Zaniboni, A., and Michelucci, R. (2000). Encephalopathy with electrical status epilepticus during slow sleep or eses syndrome including the acquired aphasia. *Clin Neurophysiol*, 111 Suppl 2:S94–S102.

Thorpy, M. J. and Yager, J. (2001). *The encyclopedia of sleep and sleep disorders*. Facts on File. Inc, 132 West 31st Street, New York NY 10001, 2nd edition edition.

Tiberi, M., Nash, S., Bertrand, L., Lefkowitz, R., and Caron, M. G. (1996). Differential regulation of dopamine d1a receptor responsiveness by various g protein-coupled receptor kinases. *Journal of Biological Chemistry*, 271:3771–8.

Tissier, M.-H., Lainey, E., Fattaccini, C.-M., Hamon, M., and Adrien, J. (1993). Effects of ipsaprione, a 5-ht1a agonist, on sleep/wakefulness cycles: probable post-synaptic action. *Journal of Sleep Research*, 2:103–9.

Touchon, J., Baldy-Moulinier, M., Billiard, M., Besset, A., and Cadilhac, J. (1991). Sleep organization and epilepsy. *Epilepsy Research Supplement*, 2:73–81.

Tracton, A. A. (2007). *Coatings materials and surface coatings*. CRC Press Llc, Taylor and Francis group, 1st edition.

Traub, R. D. (1979). Neocortical pyramidal cells: a model with dendritic calcium conductance reproduces repetitive firing and epileptic behavior. *Brain Res*, 173(2):243–57.

Treiman, D. M. (2001). Gabaergic mechanisms in epilepsy. *Epilepsia*, 42 Suppl 3:8–12.

Tronson, N. C. and Taylor, J. R. (2007). Molecular mechanisms of memory reconsolidation. *Nat Rev Neurosci*, 8(4):262–75.

Tsai, M.-L. and Hung, K.-L. (1998). Topographic mapping and clincial analysis of benign childhood epilepsy with centrotemporal spikes. *Brain and Development*, 20(1):27–32.

Tsuneki, H., Salas, R., and Dani, J. (2003). Mouse muscle denervation increases expression of an alpha7 nicotinic receptor with unusual pharmacology. *The Journal of Physiology*, 547(1):169–79.

Turban, G. and Rapeaux, M. (1983). Dry etching of polyimide in o2-cf4 and o2-sf6 plasmas. *Journal of the Electrochemical Society*, 130(11):2231–2236.

Turski, W. A., Cavalheiro, E. A., Schwarz, M., Czuczwar, S. J., Kleinrok, Z., and Turski, L. (1983). Limbic seizures produced by pilocarpine in rats: behavioural, electroencephalographic and neuropathological study. *Behav Brain Res*, 9(3):315–35.

Uhlhaas, P., Haenschel, C., Nikolic, D., and Singer, W. (2008). The role of oscillations and synchrony in cortical networks and their putative relevance for the pathophysiology of schizophrenia. *Schizophrenia Bulletin*, 34(5):927–43.

Ursin, R. (2002). Serotonin and sleep. *Sleep Medicine Reviews*, 6(1):57–69.

Uteshev, V., Meyer, E., and Papke, R. (2002). Activation and inhibition of native neuronal alpha-bungarotoxin-sensitive nicotinic ach receptors. *Brain Research*, 948:33–46.

Valderrama, M., Crepon, B., Botella-Soler, V., Martinerie, J., Hasboun, D., Alvarado-Rojas, C., Baulas, M., Adam, C., Navarro, V., and Quyen, M. L. V. (2012). Human gamma oscillations during slow wave sleep. *PLoS one*, 7(4):1–14.

Van Hese, P., Martens, J.-P., Waterschoot, L., Boon, P., and Lemahieu, I. (2009). Automatic detection of spike and wave discharges in the eeg of genetic absence epilepsy rats from strasbourg. *IEEE Trans Biomed Eng*, 56(3):706–17.

Van Luijtelaar, E. L. and Coenen, A. M. (1988). Circadian rhythmicity in absence epilepsy in rats. *Epilepsy Res*, 2(5):331–6.

van Luijtelaar, G., Hramov, A., Sitnikova, E., and Koronovskii, A. (2011). Spike-wave discharges in wag/rij rats are preceded by delta and theta precursor activity in cortex and thalamus. *Clin Neurophysiol*, 122(4):687–95.

Vanderwolf, C. (1969). Hippocampal electrical activity and voluntary movement in the rat. *Electroencephalography and Clinical Neurophysiology*, 26:407–18.

Veggiotti, P., Pera, M. C., Teutonico, F., Brazzo, D., Balottin, U., and Tassinari, C. A. (2012). Therapy of encephalopathy with status epilepticus during sleep (eses/csws syndrome): an update. *Epileptic Disord*, 14(1):1–11.

Vergnes, M., Marescaux, C., Depaulis, A., Micheletti, G., and Warter, J. (1987). Spontaneous spike and wave discharges in thalamus and cortex in a rat model of genetic petit mal-like seizures. *Experimental neurology*, 96(1):127–136.

Wagner, R. (1844). *Handworterbuch der Physiologie*, volume 2, chapter Wachen, schlaf, traum und verwandte zustande by J.E. Purkinje, pages 412–480. Braunschweig. F. Vieweg und sohn, 3rd edition edition.

Walker, M. P. (2008). Cognitive consequences of sleep and sleep loss. *Sleep Medicine*, 9(S1):S29–S34.

Warburton, D. M. and Rusted, J. M. (1993). Cholinergic control of cognitive resources. *Neuropsychobiology*, 28(1-2):43–6.

Watts, D. J. and Strogatz, S. H. (1998). Collective dynamics of 'small-world' networks. *Nature*, 393(1):440–2.

Wenger, G., Stitzel, R., and Craig, C. (1973). The role of biogenic amines in the reserpine-induced alteration of minimal electroshock seizure thresholds in the mouse. *Neuropharmacology*, 12:693–703.

Whitehouse, W., Diebold, U., Ress, M., Parker, K., Doose, H., and Gardiner, R. (1993). Exclusive of linkage of genetic focal sharp waves to the hla region on the chromosome 6p in families with benign partial epilepsy with centrotemporal sharp waves. *Neuropediatrics*, 24:208–10.

Whittington, M. A., Traub, R. D., and Jefferys, J. G. (1995). Erosion of inhibition contributes to the progression of low magnesium bursts in rat hippocampal slices. *J Physiol*, 486 (Pt 3):723–34.

Whittington, M. A., Traub, R. D., Kopell, N., Ermentrout, B., and Buhl, E. H. (2000). Inhibition-based rhythms: experimental and mathematical observations on network dynamics. *Int J Psychophysiol*, 38(3):315–36.

Williams, K. R., Gupta, K., and Wasilik, M. (2003). Etch rates for micromachining processing-part ii. *Microelectromechanical Systems, Journal of*, 12(6):761–778.

Willoughby, J. O., Pope, K. J., and Eaton, V. (2003). Nicotine as an antiepileptic agent in adnfle: an n-of-one study. *Epilepsia*, 44(9):1238–40.

Wilson, M. A. and McNaughton, B. L. (1994). Reactivation of hippocampal ensemble memories during sleep. *Science*, 265(5172):676–9.

Wise, K. D., Angell, J. B., and Starr, A. (1970). An integrated circuit approach to extracellular microelectrodes. *IEEE Transactions on Biomedical Engineering*, 17:238–247.

Wonnacott, S. and Barik, J. (2007). Nicotinic ach receptors. *Tocris Reviews*, (28):1–20.

Wotring, V. E. and Yoon, K. W. (1995). The inhibitory effects of nicotinic antagonists on currents elicited by gaba in rat hippocampal neurons. *Neuroscience*, 67(2):293–300.

Wright, N. and Horsfall, A. (2007). Sic sensors: a review. *Journal of Physics D: Applied Physics*, 40(20):6345.

Xanthopoulos, P., Liu, C., Zhang, J., Miller, E., Nair, S., Uthman, B., Kelly, K., and Pardalos, P. (2009). A robust spike and wave algorithm for detecting seizures in a genetic absence seizure model. *Conf Proc IEEE Eng Med Biol Soc*, pages 2184–7.

Yan, D., Pedersen, S., and White, M. (1998). Interaction of d-tubocurarine analogs with the 5-ht3 receptor. *Neuropharmacology*, 37(2):251–7.

Yan, D., Schulte, M. K., Bloom, K. E., and White, M. M. (1999). Structural features of the ligand-binding domain of the serotonin 5ht3 receptor. *The Journal of Biological Chemistry*, 274(9):5537–41.

Yan, D. and White, M. (2002). Interaction of d-tubocurarine analogs with mutant 5-ht(3) receptors. *Neurpharmacology*, 43(3):367–73.

Yasuhara, A., Yoshida, H., Hatanaka, T., Sugimoto, T., Kobayashi, Y., and Dyken, E. (1991). Epilepsy with continuous spike-waves during slow sleep and its treatment. *Epilepsia*, 32(1):59–62.

Zerem, A., Nishri, D., Yosef, Y., Blumkin, L., Lev, D., Leshinsky-Silver, E., Kivity, S., and Lerman-Sagie, T. (2013). Resolution of epileptic encephalopathy following treatment with transdermal nicotine. *Epilepsia*, 54(1):e13–5.

Zimmerman, A., Nidermeyer, E., and Hodges, F. (1977). Lennox-gastaut syndrome and computerized axial tomography. *Epilepsia*, 18:463–64.